Features of Thermohaline Structure and Circulation in the Gulf of Riga

MARIS SKUDRA

TALLINN UNIVERSITY OF TECHNOLOGY
Marine Systems Institute

Dissertation was accepted for the defence of the degree of Doctor of Philosophy in Earth Sciences on December 19, 2016.

Supervisors: Prof. Urmas Lips, Marine Systems Institute at Tallinn University of Technology, Estonia

Dr. Victor Zhurbas, Marine Systems Institute at Tallinn University of Technology, Estonia; Shirshov Institute of Oceanology, Moscow, Russia

Opponents: Dr. Lars Arneborg, Swedish Meteorological and Hydrological Institute, Sweden

Dr. Erko Jakobson, Tartu Observatory, Estonia.

Defence of the thesis: January 25, 2017 at the Marine Systems Institute, Tallinn University of Technology, Akadeemia tee 15a, Tallinn, Estonia.

Declaration:

Hereby I declare that this doctoral thesis, my original investigation and achievement, submitted for the doctoral degree at Tallinn University of Technology has not been submitted for doctoral or equivalent academic degree.

/Maris Skudra/

Termohaliinse struktuuri ja tsirkulatsiooni mustrid Liivi lahes

MARIS SKUDRA

TABLE OF CONTENTS

LIST OF ORIGINAL PUBLICATIONS

I   Skudra, M., Lips, U. (2016). Characteristics and inter-annual changes in temperature, salinity and density distribution in the Gulf of Riga. *Oceanologia*, in press, doi: 10.1016/j.oceano.2016.07.001.

II   Lips, U., Zhurbas, V., Skudra, M., Väli, G. (2016). A numerical study of circulation in the Gulf of Riga, Baltic Sea. Part I: Whole-basin gyres and mean currents. *Continental Shelf Research*, 112, 1–13, doi: 10.1016/j.csr.2015.11.008.

III   Lips, U., Zhurbas, V., Skudra, M., Väli, G. (2016). A numerical study of circulation in the Gulf of Riga, Baltic Sea. Part II: Mesoscale features and freshwater transport pathways. *Continental Shelf Research*, 115(1), 44–52, doi: 10.1016/j.csr.2015.12.018.

IV   Liblik, T., Skudra, M., Lips, U. (2016). On the buoyant sub-surface salinity maxima in the Gulf of Riga. *Oceanologia*, in press, doi: 10.1016/j.oceano.2016.10.001.

AUTHOR'S CONTRIBUTION

I   The author participated in the field measurements and was responsible for data collection, data analysis and writing of the manuscript.

II   The author processed and analyzed vertical profiles of salinity and temperature, contributed to the model setup, data analysis and writing of the manuscript.

III   The author processed and analyzed vertical profiles of salinity and temperature, contributed to the model setup, data analysis and writing of the manuscript.

IV   The author participated in the field measurements and contributed to the data analysis and writing of the manuscript.

APPROBATION OF THE RESULTS

1. ICES Annual Science Conference 2013, Reykjavik, Iceland, 23–27th of September, 2013. Long-term changes in the temperature and salinity distribution patterns in the gulf of Riga (with U. Lips).

2. IEEE/OES Baltic International Symposium, Tallinn, Estonia, 27–29th of May, 2014. Features of summertime circulation in the Gulf of Riga (A numerical simulation) (with U. Lips, V. Zhurbas and G. Väli).

3. 10th Baltic Sea Science Congress, Riga, Latvia, 15–19th of June, 2015. Inter-annual changes in temperature, salinity and density distribution in the Gulf of Riga (with U. Lips).

4. 1st Baltic Earth Conference, Nida, Lithuania, 13–17th of June, 2016. High-resolution view on the sub-surface salinity maxima in the Gulf of Riga (with T. Liblik and U. Lips).

INTRODUCTION

The Baltic Sea is a semi-enclosed and brackish sea consisting of several sub-basins, including the Gulf of Riga which is connected to the open Baltic Sea through two shallow straits – Irbe Strait and Suur Strait. Thus, the thermohaline structure and internal dynamics of the basins are of great importance for the biogeochemical processes responsible for the ecosystem functioning in the Baltic Sea and its sub-basins.

The present knowledge about the characteristics of the thermohaline structure of the Gulf of Riga is based on the previous studies which mostly cover the period until mid-nineties. Although the main principles are well known, there is still a gap of knowledge regarding the hydrography and thermohaline dynamics of the gulf. The whole-basin circulation patterns in the Gulf of Riga have not been studied yet, and the existence and characteristics of these circulation patterns have been suggested or predicted based on a few available case studies. Similarly as with the whole-basin circulation patterns, there is a gap of knowledge regarding the mesoscale features and variability to which a proper attention has not been devoted before. Moreover, the variability of the thermohaline characteristics during the last 20 years has not been described although the regular monitoring has been in place in the gulf.

In this thesis, the thermohaline structure was described on both the long-term and short-term scale using the available CTD (conductivity, temperature, depth) profiles collected during research and monitoring cruises since 1993 and by an autonomous buoy profiler in summer 2015. Numerical models nowadays provide a valuable tool to study different processes with high-resolution in cases where spatial and temporal distribution of observations is not sufficient to come up with meaningful analysis and conclusions. Such a model approach was also used in the present thesis to study the main circulation patterns as well as characteristics of the mesoscale features in the Gulf of Riga.

The main scientific questions studied in the present Ph.D. thesis were related to the hydrography of the Gulf of Riga during a period of 20 years – characteristics and variability of the vertical thermohaline structure, whole-basin circulation and mesoscale features. The main results include the significant influence of river runoff in spring to the stratification strength in summer (August); the change of the whole-basin circulation pattern from cyclonic in the cold period of the year to anticyclonic in the summer; the existence of well detectable sub-surface salinity intrusions and mesoscale features like meanders and eddies related to the Daugava River plume and thermohaline circulation.

1. BACKGROUND

1.1 Knowledge on the Gulf of Riga hydrography

The Gulf of Riga is an almost regularly shaped basin in the eastern part of the Baltic Sea with the surface area of approximately 17913 km^2 and volume of 405 km^3 (Leppäranta and Myrberg 2009). It is rather isolated from the open Baltic Sea as it has two shallow straits – the Irbe Strait (sill depth of 25 m and cross-section of 0.4 km^2) in the western part and the Suur Strait (sill depth of 5 m and cross-section of 0.04 km^2) in the northern part of the gulf (Berzinsh 1995). The majority (70-80%) of the water exchange occurs via the Irbe Strait (Petrov 1979). The mean depth of the Gulf of Riga is 26 m which is about two times less than in the Baltic Sea. The deepest regions (depth reaches 56 m) of the gulf are located near the Ruhnu Island but the deepest spot in the whole Gulf of Riga reaches 66 m (Stiebrins and Väling 1996).

The overall hydrography of the gulf during 1920-1990 was thoroughly described by Berzinsh (1995). Several studies have been performed on the shorter time scales describing, for example, stratification characteristics (Stipa et al. 1999), hydrographic structures and characteristics in specific years (Lips et al. 1995; Kõuts and Håkansson 1995) or inter-annual and seasonal variations of temperature and salinity (Berzinsh 1980; Raudsepp 2001).

The catchment area of the Gulf of Riga consists of 134000 km^2 and there are five major rivers discharging into the gulf – Daugava, Lielupe, Gauja, Pärnu and Salaca with approximately 86% of all river runoff discharging into the southern part of the gulf (Berzinsh 1995). Annual mean runoff to the gulf in 1950-2012 has been stated as 1013.5 m^3 s^{-1} (Kronsell and Andersson 2014). In addition to the substantial amount of freshwater from rivers, precipitation exceeds evaporation by 82 m^3 s^{-1} (379.4 and 297.4 m^3 s^{-1}, respectively) based on the data from 1981-1994 (Omstedt et al. 1997). Due to the specific distribution of the freshwater inputs and limited water exchange through the shallow straits, the surface water salinity decrease from the Irbe Strait (6.0 PSU – units according to the Practical Salinity Scale 1978) to the southern part of the gulf (2.0 PSU) close to the mouth of Daugava and Lielupe exists (see e.g. Berzinsh 1980; Berzinsh 1995; Stipa et al. 1999). A slight surface salinity difference (about 1.0-1.5 PSU) has also been acknowledged across the gulf from west (saltier) to east (fresher) in April (Stipa et al. 1999) as spring is the season when river discharge is at its maximum in the Gulf of Riga. Regarding the long-term salinity trends in the Gulf of Riga two periods with opposite tendencies have been detected – from the beginning of the 1960s till 1977 average salinity increased (average rate of 0.035 PSU per year), whereas, from 1977 till the early 1990s salinity decreased (0.041 PSU per year). It has been suggested that these changes were mainly related to the dynamics of long-term river runoff. Raudsepp (2001) concluded that the corresponding decline of salinity was observed in the whole water column as well.

Water temperature in the Gulf of Riga has a seasonal pattern with cooling phases occurring during September-October (starting from surface layers) and November-February (whole water column) and warming phases in spring-summer with the maximum surface layer temperature in August (Berzinsh 1995). Seasonal changes in thermal stratification are consistent with the annual cycle of air-sea heat exchange (Raudsepp 2001). Due to this cycle, the whole water column in the Gulf of Riga is thermally well mixed during December-March, whereas, seasonal thermocline starts to develop in April with the strongest stratification observed in August (see e.g. Stipa et al. 1999; Raudsepp 2001). Based on the remote sensing data from 1990-2008, an increase in the sea surface temperature (SST) of about 0.8-1.0 °C per decade was indicated in the Gulf of Riga. The temperature increase was similar or slightly higher only in two other basins of the Baltic Sea – the Gulf of Finland and Bothnian Bay (BACC 2015).

Since the Irbe Strait has a vital role in the water exchange between the gulf and the Baltic Proper it has been a center of attention in different studies describing, for example, the flow regime (Lilover et al. 1998; Laanearu et al. 2000), water exchange and its volumes (Kõuts and Håkansson 1995; Otsmann et al. 1997; Raudsepp 2001) or hydrographic structures and characteristics (Lips et al. 1995) in it. More recently the numerical models have been used to study the Daugava River plume dynamics in the southern part of the Gulf of Riga (Soosaar et al. 2014; Soosaar et al. 2016) which is heavily affected by the freshwater discharge.

The general circulation in the surface layers of the Baltic Sea and its main basins has a cyclonic pattern (Leppäranta and Myrberg 2009), although, a possible anticyclonic circulation pattern has been suggested in the Gulf of Riga in summer based on salinity measurements (Lips et al. 1995). Circulation in the deep layers of the Gulf of Riga is different from that observed in the Baltic Sea as the gulf is rather isolated from the open part of the Baltic Sea and water masses from the lower layer of the Baltic Sea cannot enter the gulf through the Irbe Strait. Instead, waters from the surface layer of the Baltic Sea enter the gulf and penetrate into the lower layer of the Gulf of Riga due to the increased salinity and corresponding density if compared to the ambient water in the gulf. More saline and dense waters flow further in the Gulf of Riga deep layers along the western coast (Lilover et al. 1998) suggesting that cyclonic circulation could be evident in the deep layers as well. Whole-basin circulation patterns in the Gulf of Riga have also been studied based on the basin-scale topographic wave analysis (Raudsepp et al. 2003).

The knowledge of mesoscale processes and features in the Gulf of Riga is rather limited. Karimova (2012) reported of eddies in the Gulf of Riga captured by the satellite radar data in 2009-2010. To study the dynamics in the Irbe Strait a model experiment was carried out by Raudsepp and Elken (1999) although the authors concluded that the resolution of the model was not good enough to reproduce the mesoscale variability. Nevertheless, the mesoscale features in the Baltic Sea have been studied since the 1970s with the start of CTD

measurements at a high enough resolution (Aitsam and Elken 1982). Since then many mesoscale features have been described throughout the Baltic Sea e.g. intrapycnocline anticyclonic lenses, sub-surface cyclonic eddies or surface layer cyclonic and anticyclonic eddies (Reißmann 2005, 2006). These mesoscale features have been found in many parts of the Baltic Sea like the Eastern Gotland Basin (e.g. Elken 1996; Zhurbas and Paka 1997), Bornholm Basin and Słupsk Furrow (Piechura 2007), Arkona Basin (Lass and Mohrholz 2003) and Gulf of Finland (Zhurbas et al. 2008; Laanemets et al. 2011). More detailed insight and a list of numerous studies regarding the mesoscale eddies in the Baltic Sea region can be found in an overview by Leppäranta and Myrberg (2009).

1.2 Motivation and objectives

Changes in temperature, salinity and corresponding variations in density together with the main circulation patterns and mesoscale dynamics are factors of great importance influencing the hydrography of the Gulf of Riga and consequently having a potential to affect the whole ecosystem of the gulf. For example, it has been reported that the temperature increase would affect the phytoplankton community in the Gulf of Riga suggesting a shift from dinoflagellates to chlorophytes in summer (Jurgensone et al. 2011). The reduction in salinity has had negative consequences for most of the benthic invertebrate species referring to their salinity tolerance (Kotta et al. 2009). In general, the dynamics of zooplankton, zoobenthos, and fish in the Gulf of Riga primarily relies on climatic conditions.

The general motivation of the thesis is to improve the present knowledge of the Gulf of Riga in different time scales. The collected CTD dataset over 20 years was used and analyzed to link the long-term and inter-annual changes to different forcing factors in order to characterize the thermohaline structure, compare it to the previously observed results and describe the present state of the Gulf of Riga. The CTD profiles with high temporal resolution gave an opportunity to look into details of the vertical thermohaline structure in summer and to determine the main factors influencing it. Finally, numerical experiments revealed the main whole-basin circulation patterns which were linked to the observation data and the simulated mesoscale features allowed to understand the dynamics related to the freshwater discharge in the southern part of the gulf.

In comparison to the earlier studies about the hydrographic conditions in the Gulf of Riga (e.g. Berzinsh 1995; Stipa et al. 1999; Raudsepp 2001 etc.), the present work also includes the years after mid-nineties. The collected dataset is a valuable source to characterize the overall thermohaline structure and its features as well as describe the changes in the Gulf of Riga over the last two decades.

The main objectives of the study are:

- to describe the vertical structure of salinity, temperature and density in the Gulf of Riga in summer (May-August) based on the CTD data collected in 1993-2012;
- to relate the inter-annual variations of salinity, temperature, density and stratification strength to the atmospheric forcing (Baltic Sea Index - BSI) and river runoff;
- to describe the main circulation patterns and their governing factors in the Gulf of Riga using numerical experiments;
- to describe the freshwater transport pathways in the gulf;
- to characterize mesoscale features in the Gulf of Riga, including their scales and occurrence associated with the Daugava River plume and main currents;
- to show the dynamics of vertical thermohaline structure in the Gulf of Riga using high-resolution autonomous profiler;
- to reveal the possible mechanisms and origin of the sub-surface salinity intrusions observed in the Gulf of Riga in summer;
- to suggest the possible future changes in the vertical thermohaline structure due to the climate change and their consequences.

2. MATERIAL AND METHODS

2.1 Observational data and calculations

Present thesis analyzed the CTD data collected in 1993-2015 during various monitoring programs and research projects conducted by Latvian Institute of Aquatic Ecology, Marine Systems Institute at Tallinn University of Technology and Institute of Food Safety, Animal Health and Environment (Latvia) and their predecessors. Vertical profiles of different parameters were acquired with multiple CTD profilers – AROP 500, SBE 19plus SeaCAT, SBE 19 SeaCAT, Neil Brown Mark III, Idronaut OS316plus and Idronaut OS320plus.

The CTD profiles used in the thesis can be divided into three sub-sets:

- profiles collected onboard different research vessels throughout the Gulf of Riga (Paper **I**); in total 3558 CTD casts were processed and 863 CTD casts were used from the period of May-August, 1993-2012; the Gulf of Riga borders were set along 58°N latitude and 22.6°E longitude and only stations with depth > 20 m were used (Fig. 1);
- profiles collected by an autonomous vertical profiler (12 h profiling interval) in the western part of the Gulf of Riga (Paper **IV**); in total 202 CTD casts were processed and used from the period of May-September, 2015 (Fig. 1);
- profiles collected throughout the Gulf of Riga from May to August 2012 were used to compare and validate the model output regarding the vertical distribution of temperature and salinity (Paper **II**).

CTD profiles were processed and analyzed with the vertical resolution of 0.5 m (constant for all profiles). The salinity values were expressed as absolute salinity (g kg^{-1}) and derived from CTD measured salinity values (on Practical Salinity Scale) following TEOS-10 (Thermodynamic Equation Of Seawater - 2010) guidelines and Feistel et al. (2010). Density values were expressed as density anomaly in kg m^{-3} (Paper **I**) and as potential density anomaly (a reference pressure of 0 dbar was used; σ_0; kg m^{-3}, Paper **IV**).

Mean values of studied CTD parameters in May-August, 1993-2012 were estimated as simple arithmetic means of every month in each year. These values were further used to obtain the monthly mean values for the whole research period of 1993-2012, from which finally one mean value was derived for each parameter. For a more detailed analysis, only data from May and August with the number of CTD casts equal or exceeding 5 casts with acceptable spatial distribution were used. The estimates of the upper mixed layer (UML) from August 1993, 1994 and 2008 should be regarded with caution regarding the mean conditions in the gulf because the spatial distribution of the stations in these years was not homogeneous - in 1993 and 1994 the data only from the northern and northwestern part and in 2008 only from the southern part of the Gulf of Riga were available. The same principle applies to the deep layer (DL) results from May 1993 with stations available only in the northwestern part (Paper **I**).

The correlation coefficient *r* and only significant correlations ($p<0.05$) are provided throughout the thesis. In order to analyze the dynamics of various parameters in different parts of the Gulf of Riga ten "main" stations (102A, 135, 142, 111, 119, 120, 121, 137A, 121A, 107) were chosen determined by the data availability (Fig. 1).

In addition, the following data sets were used in the thesis:

- monthly mean flow rates ($m^3 s^{-1}$) of four biggest rivers in Latvia discharging into the Gulf of Riga – Daugava, Gauja, Lielupe and Salaca (Paper **I**);
- wind data from Sõrve, Ruhnu, Kihnu and Pärnu meteorological stations (Papers **I**, **IV**);
- monthly-averaged Baltic Sea Index (BSI), which is the difference of normalized sea level pressures between Szczecin in Poland and Oslo in Norway (Lehmann et al. 2002); values provided by Andreas Lehmann (Paper **I**);
- temperature and salinity data from thermosalinograph (SBE45 MicroTSG, Sea-Bird Electronics; included in the flow-through system) installed on board the RV "Salme" (Paper **IV**);
- HELCOM data (http://ocean.ices.dk/helcom, 25 February 2016) was used to evaluate the occurrence of the sub-surface salinity maxima in the past (Paper **IV**);
- coastal temperature measurements at Ruhnu, Häädemeeste, and Roomassaare (Paper **IV**);
- the level 3 SST (sea surface temperature) product over European Seas by Copernicus Marine Environment Monitoring Service (http://marine.copernicus.eu/) (Paper **IV**).
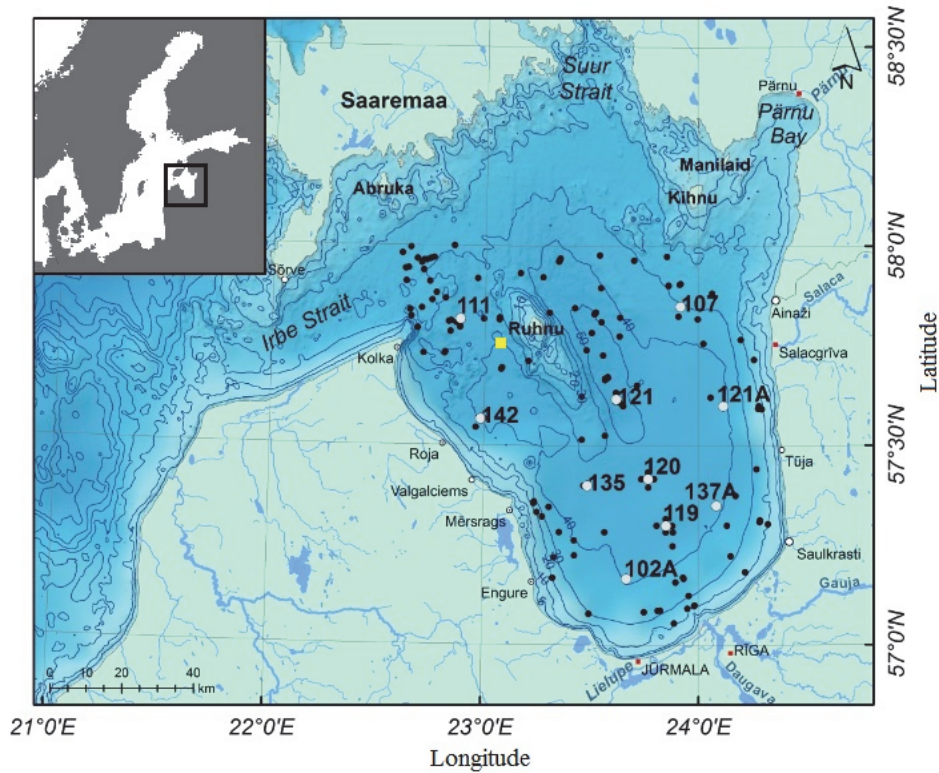
Figure 1. Bathymetric map of the Gulf of Riga with CTD cast locations indicated with black dots (all stations) and white dots (10 main stations with station labels). Yellow rectangle shows the location of the autonomous vertical profiler (buoy station).

In order to characterize the vertical thermohaline structure in the Gulf of Riga the subsequent parameters were defined or calculated:

- the UML depth which also marks the start of the thermocline (Papers **I**, **IV**);
- the UML and deep layer (DL) temperature, salinity and density, as well as their differences between the DL and UML (Paper **I**);
- relative contributions of temperature (ST_T) and salinity (ST_S) to the vertical stability (ST) of the water column and UML (Paper **IV**);
- intrusion index (I) was calculated in order to estimate the intensity of interleaving (Paper **IV**).

The exact calculation process of the respective parameters is provided in material and methods section in Papers **I** and **IV**, respectively.

2.2 Model setup and numerical experiments

To simulate hydrodynamics of the Gulf of Riga the Princeton Ocean Model, POM (Blumberg and Mellor 1983) was used. The POM is a sigma co-ordinate, free surface, hydrostatic model equipped with a 2.5 moment turbulence closure

scheme by Mellor and Yamada (1982). It uses a traditional central differencing advection scheme; the time step was 6 and 180 sec for the external and internal modes, respectively. The model domain includes the whole Baltic Sea closed at the Danish Straits, and digital topography is taken from (Seifert and Kayser 1995). The grid cell size along the latitudes and longitudes, Δx and Δy, is varying spatially from $\Delta x = (1/60)°$ between 21°–24.6°E and $\Delta y = (1/120)°$ between 56.933°–59.333°N (or $\Delta x \approx \Delta y = 0.5$ nautical miles = 926 m) in the Gulf of Riga and its vicinity to $\Delta x = (1/15)°$ and $\Delta y = (1/30)°$ elsewhere. There are 20 sigma layers in the vertical direction. The model is eddy resolving in the region under investigation since the baroclinic Rossby radius of about 2–5 km (e.g. Fennel et al. 1991) is well above the grid cell size. The model setup does not include any sea-ice module.

Two rivers inflowing to the Gulf of Riga were included in the model - the Daugava River and the Pärnu River with the annual mean volume rates of 660 m^3 s^{-1} and 48 m^3 s^{-1}, respectively (Leppäranta and Myrberg 2009). Since the Lielupe and Gauja (second and third largest rivers) that contribute to the Gulf of Riga freshwater inflow, have their mouths within a 20–km vicinity of the Daugava mouth, the three rivers can be considered as a single source with the volume rate of 818 m^3 s^{-1}. The latter volume rate is the mean runoff of Latvian rivers into the Gulf of Riga for 1921-1990, May–October, taken from http://www.modlab.lv/publications/1998/publ3.htm. Therefore, one may consider 660 m^3 s^{-1} and 818 m^3 s^{-1} as the lower and upper limits for the Daugava River mean flow rate. The seasonal variations of river runoff were not considered in the model setup and each river was incorporated into the model using an addition of some amount of freshwater to a grid cell corresponding to the position of the river mouth at each time step. Freshwater supply related to the precipitation and rivers inflowing to the Baltic Sea outside the Gulf of Riga were not included in the model.

The basic model run comprised a one-year period from May 1, 2012 to April 30, 2013. For the initial temperature conditions, a 1 n.m. grid output of the High Resolution Operational Model for the Baltic (HIROMB, see http://www.smhi.se/en/Research/Research-departments/Oceanography/hiromb-1.8372) was interpolated to the spatially-varying grid, whereas, the initial salinity fields were constructed from the measurement data collected in the Data Assimilation System (DAS) coupled with the Baltic Environmental Database (see http://nest.su.se/das) and supplemented with the CTD data collected in the Gulf of Riga during 1996-2013 (788 CTD profiles from April 15 to May 15).

Atmospheric forcing parameters (wind stress and total heat fluxes) were formulated based on the output of the numerical weather prediction forecast system HIRLAM (High Resolution Limited Area Model; see www.hirlam.org). The output data from a version of HIRLAM applied at the Estonian Meteorological and Hydrological Institute (Männik and Merilain 2007) providing meteorological parameters on an approximately 10 km horizontal grid with 3 h time step were used by bilinear interpolation to the model grid.

To estimate the relative importance of various mechanisms responsible for the formation of large-scale circulation patterns in the Gulf of Riga, the basic one-year model run was complemented with a number of scenario studies or numerical experiments (Paper **II**):

- a model run with modified bottom topography;
- a model run with zero heat flux;
- a model run with zero atmospheric forcing (no heat flux and no wind stress);
- a model run with uniform initial temperature/salinity distribution with no atmospheric forcing.

The basic one-year model run was extended to the three-year period (May 1, 2012 to April 30, 2015) with modified initial temperature-salinity fields outside the Gulf of Riga to study the reliability of revealed circulation patterns (Paper **II**).

In order to separate the intrinsic buoyant plume dynamics and the effects related to the thermohaline circulation and atmospheric forcing, three numerical experiments were performed (Paper **III**):

- intrinsic propagation of the Daugava River plume (spatially uniform density distribution, no atmospheric forcing);
- propagation of the Daugava River plume driven by buoyant plume dynamics and thermohaline circulation (real initial fields of temperature and salinity, no atmospheric forcing);
- basic model run (real initial fields of temperature and salinity and real atmospheric forcing).

The full details of the model setup and numerical experiments are provided in material and methods section in Papers **II** and **III**, respectively.

3. RESULTS AND DISCUSSION

3.1 Thermohaline structure and general circulation in the Gulf of Riga

3.1.1 General thermohaline characteristics and stratification

The overall UML mean depth based on the all available CTD casts in the Gulf of Riga during 1993-2012 (May-August) was 10.7 m. On average, the shallowest UML depth was in May, it was deeper in June and July and the deepest in August (Paper **I**). The spatial distribution of the UML mean depth in August was not uniform throughout the gulf – the shallowest UML mean depth (12.3-13.3 m) was found along the western part of the Gulf of Riga, whereas, the deepest UML mean depth – along the eastern part of the gulf (14.6-15.4 m). Consequently, there is a thermocline slope and corresponding sea level slope between the two coasts which is, most probably, determined by the prevailing WSW winds in the study period and mutual relationship between the wind stress and sea level fluctuations in the region (Suursaar et al. 2002). Slightly higher mean sea level in the eastern part than that of the western part of the Gulf of Riga was observed during 1978-1982 (Raudsepp et al. 1999).

The UML mean salinity and temperature in the whole period (May-August) were 5.17 g kg^{-1} and 14.5 °C, while those in May were 4.90 g kg^{-1} and 8.0 °C, in June - 5.14 g kg^{-1} and 12.5 °C, in July - 5.28 g kg^{-1} and 18.7 °C, in August - 5.38 g kg^{-1} and 18.6 °C, respectively. The spatial distribution of the UML mean temperature in August did not reveal any notable differences between various parts or north-south/west-east directions of the Gulf of Riga and temperature mainly varied around 19.0 °C. On the contrary, the spatial distribution of the UML mean salinity in August was not uniform and salinity increased from 5.10 g kg^{-1} in the southern part to around 5.4-5.5 g kg^{-1} in the northern part of the gulf (Paper **I**). The freshwater influence on the surface salinity in the southern part of the Gulf of Riga has been acknowledged in many previous studies (e.g. Berzinsh 1980; Stipa et al. 1999; Raudsepp 2001). In addition, the UML mean salinity (August) in the Gulf of Riga during the whole study period was found to be about 0.1 g kg^{-1} higher in the eastern part than the western part which is not evident, for example, in some earlier studies (Berzinsh 1980; Kõuts and Håkansson 1995). Nevertheless, a case study by Lips et al. (1995) also noted lower salinity in the western part of the gulf and suggested that it was due to the anticyclonic circulation during August 1994. This observational feature is in accordance with the model simulation (Paper **II**) suggesting that the existing anticyclonic circulation in the Gulf of Riga during summers could transport fresher waters from the southern gulf along the western shore of the gulf.

The DL mean salinity and temperature based on the all available CTD casts in the Gulf of Riga during 1993-2012 (May-August) was 5.99 g kg^{-1} and 2.2 °C, respectively. Monthly mean salinity in May, June, July and August was about 6.0 g kg^{-1} in each month, and it varied only by 0.06 g kg^{-1} between the months,

whereas, DL mean temperature increased almost linearly from 1.4 °C in May to 3.0 °C in August (Paper **I**). On average, the DL mean salinity and temperature during 1993-2012 slightly increased in May and August from the southern part of the gulf towards the Irbe Strait along the western coast of the gulf (by about 0.35 g kg^{-1} and 2.1 °C in May and 0.20 g kg^{-1} and 2.6 °C in August) which is the main pathway how the more saline and warmer water from the Baltic Proper enters the Gulf of Riga through the Irbe Strait (Berzinsh 1995; Lilover et al. 1998; Laanearu et al. 2000). A high correlation (r = 0.88) was detected between the DL mean salinity in the Irbe Strait and the DL mean salinity in the Gulf of Riga in August 1993-2012. The highest correlation was near the Irbe Strait and in the western part of the gulf (r = 0.93-0.95), whereas, towards the southern, southeastern part the correlation steadily decreased and was the lowest (in some cases not significant) in the central and eastern parts of the gulf. Due to the partially developed stratification in May, the same correlation between the DL mean salinity in the Irbe Strait and the DL mean salinity in the Gulf of Riga was significant (r = 0.67-0.70) only in the region close to the Irbe Strait and the correlation was not significant elsewhere in the gulf.

Based on the UML mean depth in the Gulf of Riga the weakest stratification was in the May during the whole study period. The whole gulf was partially stratified in May as only 1/3 of the CTD casts had distinctly developed UML. During June and July, the stratification strengthened and reached its maximum in August when the deepest UML mean depth was observed (Paper **I**). This result is in accordance with the previous studies in the Gulf of Riga (Stipa et al. 1999; Raudsepp 2001) and other sub-basins of the Baltic Sea (Omstedt and Axell 2003; Liblik and Lips 2011). In August, when the strongest stratification was observed, the mean salinity and temperature difference between the UML and the DL was 0.62 g kg^{-1} and 15.5 °C, respectively, whereas, the mean vertical structure of temperature showed typical two-layer formation with thermocline situated approximately at 10-30 m depth (Fig. 2). In some cases, three-layer stratification can occur in the western region of the Gulf of Riga caused by the strong water inflow from the Baltic Proper (denser and warmer water) in the bottom layers (Berzinsh 1995).
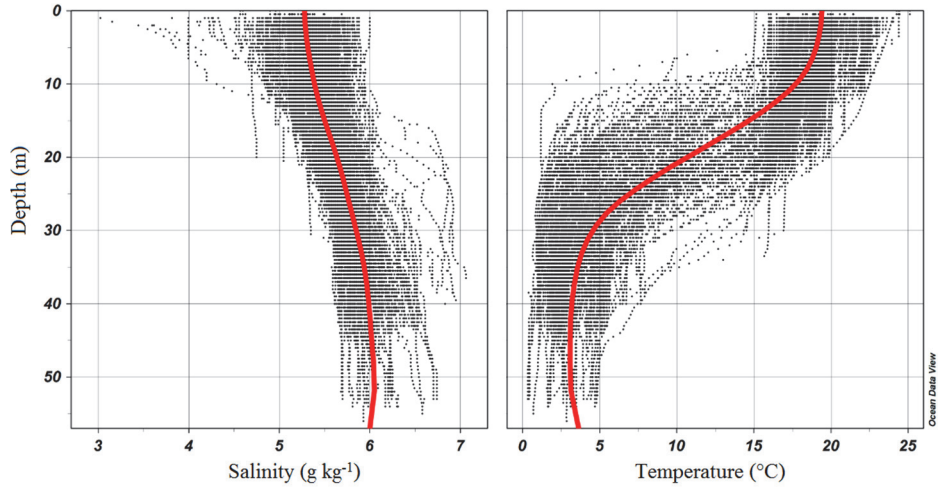
Figure 2. Scatter plot of vertical profiles of salinity and temperature in August 1993-2012. The red line represents the mean vertical profile for the whole period.

It has been reported earlier that the mean salinity difference between the surface and the bottom layers in the Gulf of Riga in 1973-1995 was 1 PSU (Raudsepp 2001) which is considerably higher than we obtained despite analyzing only the period of the strongest stratification. The explanation for this is most probably the DL salinity which was higher in 1973-1995 than in 1993-2012. The mean density difference between the surface and deep waters in the middle of the summer has been reported as 1.5-2 kg m^{-3} in years 1993-1995 (Stipa et al. 1999) which is similar, although, a bit lower than we found out (2.2 kg m^{-3}) using considerably longer period of 1993-2012 (August).

3.1.2 General circulation, main currents and governing factors

To determine the possible causes that form large-scale circulation pattern in the Gulf of Riga a vorticity balance equation (e.g. Ezer and Mellor 1994; Schwab and Beletsky 2003) was used highlighting the effects of wind stress curl and bottom topography on the current vorticity generation (Paper **II**). From the equation, it follows that positive or clockwise (negative or counter-clockwise) wind stress curl generates the positive (negative) current curl. As for the topography effect, equation states that in the case of uniform wind stress the positive (negative) current curl is generated when the sea depth increases to the left (right) when looking downwind. Regarding the topography effect, in the Gulf of Riga case (northern part), the negative current curl should be generated by a westerly wind blowing over a water area whose depth increases to the south.

Time series of current curl, wind stress curl and wind stress components from May 1, 2012 to April 30, 2013 (Fig. 3) showed that current curl changes the sign from negative in the summer season to mostly positive in the rest of the

year (except for a calm period from mid-February to mid-April, 2013). Similarly as current curl the wind stress curl also was negative for the summer period and positive for the fall–early winter period and there was an increase of positive correlation between current curl and wind stress curl in the fall–early winter period from September 15, 2012 to January 15, 2013 when winds were relatively strong (Paper **II**).
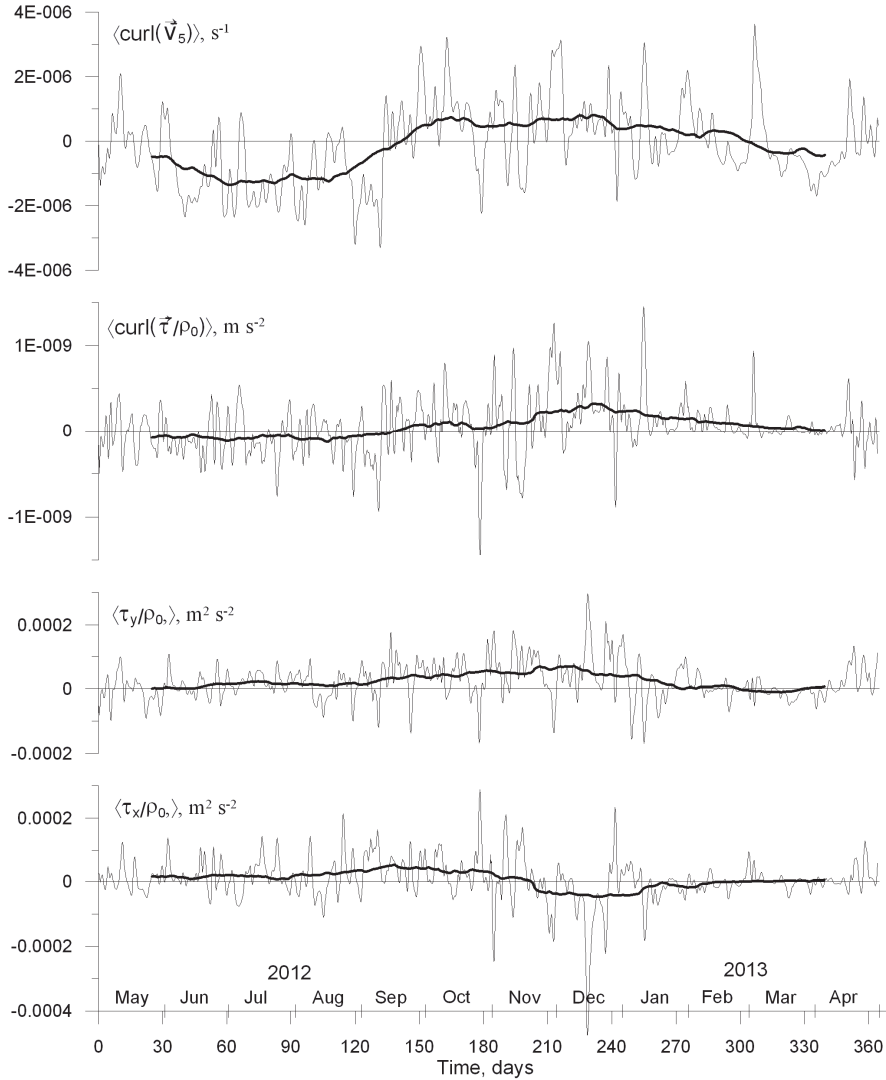

Figure 3. Thin curves: time series of the 28.2 hour averages of the current curl, $\langle \text{curl}(\vec{V}_5) \rangle$, wind stress curl, $\langle \text{curl}(\vec{\tau} / \rho_0) \rangle$, and wind stress components, $\langle \tau_x / \rho_0 \rangle$ and $\langle \tau_y / \rho_0 \rangle$, averaged over a deep part of the Gulf of Riga where $H > 20\,\text{m}$, for

21

the modeling period from May 1, 2012 to April 30, 2013. Bold curves are the same as thin ones but low-pass filtered (50 day window running mean).

For the entire modeling period of one year, the correlation coefficient between the current curl and wind stress curl was relatively high (r = 0.72) which suggests that the wind stress curl is the main contributor to the current curl in the Gulf of Riga. Moreover, the correlation was even higher (r = 0.79) in the fall–early winter season. Nevertheless, the correlation between the current curl and wind stress curl decreased (r = 0.61) and the regression coefficient (intercept) was negative and relatively far from zero in summer (Paper **II**) which implies that in the summer season, a relatively large negative value of the current curl in the Gulf of Riga was observed at zero wind stress curl. Consequently, this means that some other effect besides the wind stress curl contributed to the current vorticity generation in the summer. Conducting several additional model runs besides the basic model run (see Paper **II**) allowed us to conclude that stratification contributes substantially to anticyclonic circulation in the Gulf of Riga during summer. As summer was the only season within the modeling period when the westerly winds prevailed, the topographic characteristics of the gulf also had a role in the generation of negative values of the current curl in summer in the Gulf of Riga. The model run with no atmospheric and heat flux showed that the value of current curl for a one-year period was negative (Paper **II**) which might partially explain the appearance of anticyclonic circulation (negative current curl) in the Gulf of Riga during calm weather from mid-February to mid-April 2013.

To acquire the mean circulation patterns in the different seasons the main model run output was averaged in time over the periods from June 15 to September 15, 2012 when the seasonal thermocline was present in the Gulf of Riga and from November 1 to December 31, 2012 when the seasonal pycnocline was already destroyed by the fall/winter convective mixing but the sea was still ice free (Paper **II**). The overall circulation pattern during summer in the Gulf of Riga (in the presence of stratification and prevalence of westerly winds) was characterized by a whole-basin anticyclonic gyre with enhanced intensity of currents in the western half-basin where a jet-like alongshore northward current was clearly identified (Fig. 4a). The map of surface salinity shows two low salinity tongues originated from the Daugava River mouth – one is extended along the western shoreline of the Gulf of Riga and the other is attached to the eastern coast of the gulf representing the two pathways of riverine water transport during the summer season. On contrary, the cold period of the year, when stratification was absent and southerly winds prevailed, was characterized by a cyclonic gyre with more intense currents in the eastern half of the gyre (Fig. 4b).
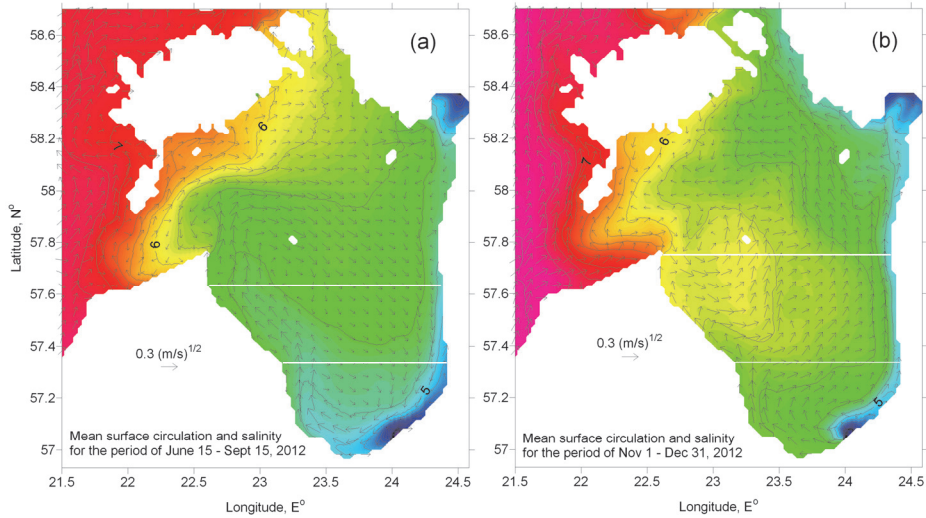
Figure 4. (a) The mean summertime circulation and salinity in the surface layer of the Gulf of Riga (an average of the simulation results over a period from June 15 to September 15, 2012 interpolated to 5 m depth). (b) The same as in (a) but for the late fall–early winter period of November 1–December 31, 2012.

As it was mentioned before the change of the mean surface circulation in the Gulf of Riga from anticyclonic in summer to cyclonic in late fall–early winter (during the basic model run of one year) was primarily caused by the respective change of the mean wind stress curl in the area. Nevertheless, the extended three year model run (1 May 2012–30 April 2015) demonstrated that the alteration between the cyclonic and the anticyclonic gyre was not a consistent feature observed every year, and it could be violated due to the inter-annual variability of wind forcing. The anticyclonic circulation in summer was observed in 2012, it was less pronounced in 2013, but it was not observed in 2014 (Fig. 5). Such outcome is correspondent with the wind stress curl time series – wind stress curl was negative in summer 2012, mostly negative in summer 2013 (for a shorter period from mid-June to mid-August) and close to nil in summer 2014. Despite the changes in anticyclonic circulation during 2012-2015, cyclonic circulation in the Gulf of Riga was observed in every cold season accompanied with positive (cyclonic) wind stress curl.

On the longer time scales (2006-2014) the annual cycle of monthly mean wind forcing confirms that negative wind stress curl under prevailing westerly-south-westerly wind stress in the warm season (May-September) changes for positive wind stress curl under prevailing southerly wind stress in the cold season (November-March), thus, we can conclude that the mean seasonal cycle of the wind stress curl contributes to the prevailing anticyclonic circulation pattern in the summer and prevailing cyclonic pattern in the cold season, but in some years this might change due to the inter-annual variability of wind forcing (see Paper **II**).
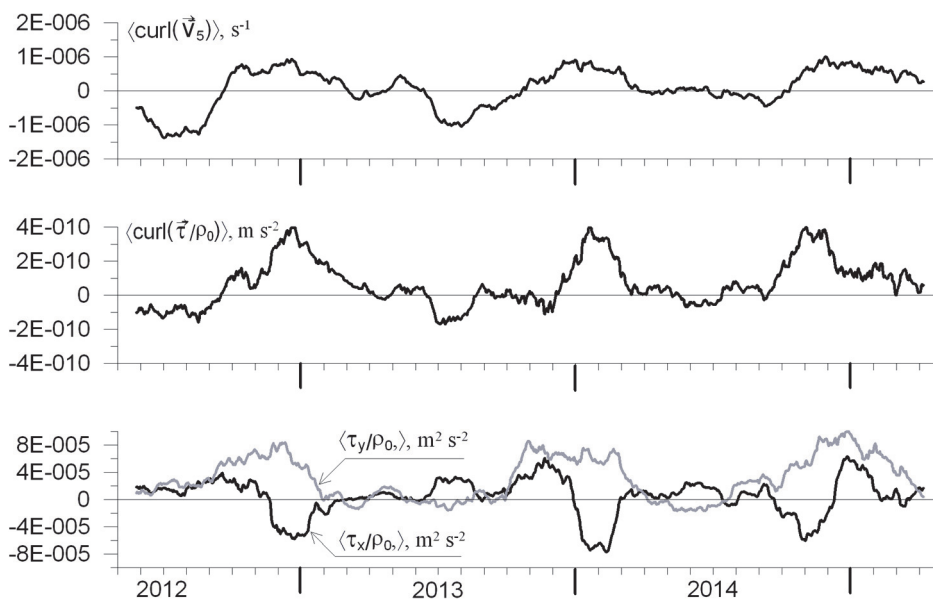
Figure 5. Low-pass filtered (50 day window running mean) time series of $\left\langle \mathrm{curl}(\vec{V}_5) \right\rangle$, $\left\langle \mathrm{curl}(\vec{\tau}/\rho_0) \right\rangle$, $\left\langle \tau_x/\rho_0 \right\rangle$ and $\left\langle \tau_y/\rho_0 \right\rangle$ for the extended modeling period from May 1, 2012 to April 30, 2015.

The existence of an anticyclonic gyre in the southern Gulf of Riga in spring driven, primarily by the estuarine type density field and strongly affected by wind forcing was reported based on a model study by Soosaar et al. (2014). Nevertheless, it might also be considered as a river plume bulge during the season of large runoff modified by wind forcing. Taking into account that the mean value of wind stress curl in April was close to zero, it could explain why Soosaar et al. (2014) found neither cyclonic nor anticyclonic whole-basin gyre in the Gulf of Riga but a double gyre pattern instead. The suggestion of the present study that the whole-basin circulation pattern in the Gulf of Riga is mainly determined by a combined effect of wind stress curl, seasonal stratification and bottom topography is in accordance with the large-scale circulation results in the Lake Michigan (Schwab and Beletsky 2003).

In a recent overview of the Baltic Sea physical oceanography (Omstedt et al. 2014) it was concluded that strong and stable cyclonic gyres exist in the Baltic Proper and Bothnian Sea (e.g. Meier 2007), whereas, in the Gulf of Riga, Gulf of Finland and Bothnian Bay the strength and persistence of currents are lower. The recent results in the Gulf of Riga (Soosaar et al. 2014; Paper **II**) show that the circulation pattern is mainly influenced by the wind forcing and its seasonal and inter-annual variations. Several model studies in the Gulf of Finland have

shown that the classical cyclonic circulation pattern (e.g. Andrejev et al. 2004) may differ depending on the chosen study period (e.g. Elken et al. 2011; Soomere et al. 2011). Also the current measurements in the surface layer of the Gulf of Finland have shown the existence of average westward flow at the southern slope (Suhhova et al. 2015) suggesting the occurrence of anticyclonic circulation cells predicted by the numerical experiments (Lagemaa 2012; Elken et al. 2011).

From the model output some major currents were detected in relation to the whole-basin circulation gyres in the summer and late fall-early winter periods (Paper **II**). First of all, a coastal jet-like current along the eastern shore of the Gulf of Riga was observed in both seasons (Fig. 4). This buoyant coastal current can also be distinguished as a reduced salinity along the eastern coast as it transports the freshwater from the southeastern part of the gulf where an excessive amount of freshwater is supplied by rivers (especially, Daugava River). Due to the cyclonic circulation during the cold period of the year, the buoyant coastal current is more pronounced if compared to the anticyclonic circulation during the summer (Fig. 4). The buoyant coastal current along the eastern shore has also been detected in other recent model studies about Daugava River plume evolution and dynamics (Soosaar et al. 2014; Soosaar et al. 2016).

During summer when anticyclonic circulation pattern is dominating another major current was detected – a jet-like alongshore northward current (NLC – the Northward Longshore Current) which can be regarded as a manifestation of the anticyclonic gyre in the Gulf of Riga (Fig 4a). Similarly to the buoyant coastal current along the eastern shore, the NLC can also be seen as extended low-salinity tongue originated from the southeastern part of the gulf. Note that due to the alteration of the whole-basin gyres, the NLC was not detected in the cold period of the year when cyclonic gyre is prevailing in the Gulf of Riga. The existence of the anticyclonic circulation and NLC in summer was also confirmed by the observation data from August (see sub-chapters 3.1.1, 3.1.4 and Paper **I**). The two vertical sections (see Paper **II**) displayed the NLC as a narrow, 10–km wide flow with the maximum surface velocity of 0.08-0.13 m s^{-1}.

The NLC and coastal buoyant current along the eastern coast are surface currents which can be easily detected in the map of mean surface circulation (Fig. 4). Nevertheless, the vertical sections (see Paper **II**) showed the existence of a sub-surface jet-like southward current along the eastern shore of the Gulf of Riga with the maximum value of the seasonally averaged velocity of 0.06 m s^{-1} at approximately 15 m depth (hereafter the SSLC – Southward Sub-surface Longshore Current). The SSLC was more pronounced in summer and the submergence of it is likely caused by the influence of the above-lying coastal buoyant plume of riverine waters, which has a tendency to flow northwards along the eastern coast of the gulf. More detailed information regarding the vertical structure with sections of the currents is provided in Papers **II** and **III**.

3.1.3 Inter-annual changes of thermohaline characteristics in summer

Apart from 1993 and 1994 when the maximum and minimum values of UML mean depth were observed the UML mean depth during 1993-2012 varied mostly between 10-20 m in the Gulf of Riga (Fig. 6). The UML mean salinity during 1993-2012 varied between 5.0-5.5 g kg^{-1} and three years stood out from the whole period. Two salinity peaks were observed in years 2003 and 2006 when UML mean salinity was 5.58 g kg^{-1} and 5.63 g kg^{-1}, respectively, whereas, the lowest UML mean salinity was 5.01 g kg^{-1} in 2010 (Paper **I**). Salinity in the Gulf of Riga depends strongly on the river runoff as well as water exchange through the straits (Irbe and Suur straits). The lowest UML mean salinity observed in 2010 corresponds well to the second largest (19.0 km^3) river runoff in spring during 1993-2012 which was only slightly less than that observed in 1994 (19.6 km^3). Nevertheless, there was no reduced salinity detected in 1994 one would expect based on the highest river runoff in this year, most probably, since in 1994 only the data from northern part of the gulf were available. The influence of freshwater can also be seen in inter-annual variations of density where density in years 1994 and 2010 was considerably lower (1.68 kg m^{-3} and 1.53 kg m^{-3}, respectively) than in other years when density most of the time fluctuated around 2.5 kg m^{-3}. In addition, two salinity peaks observed in the surface layer in 2003 and 2006 correspond to the lowest river runoff in spring (7.2 km^3 and 7.1 km^3, respectively) during the study period. Years 1994 and 2010 stood out again when looking at inter-annual variations of the UML mean temperature (Fig. 6). During 1993-2012 the temperature mainly varied between 17.5-20.0 °C, whereas, in 1994 and 2010 it was considerably higher – 22.4 °C and 21.8 °C, respectively. Although, the data distribution from 1994 was not homogeneous in our study, a considerably higher surface layer temperature in August 1994 (23 °C) was reported in the Gulf of Riga earlier (Raudsepp 2001) which was, by far, the highest during 1970-1998. The reason for elevated temperatures in 1994 and 2010 might be the combined effect of previously mentioned increased river runoff in these years and following intensification of stratification (described further below) enabling an excessive warm up of the thin surface layers.

The estimated UML mean parameters (depth, salinity, temperature and density) in August were correlated with the BSI to explore the possible influence of atmospheric forcing (see sub-chapter 3.1.4 and Paper **I**).
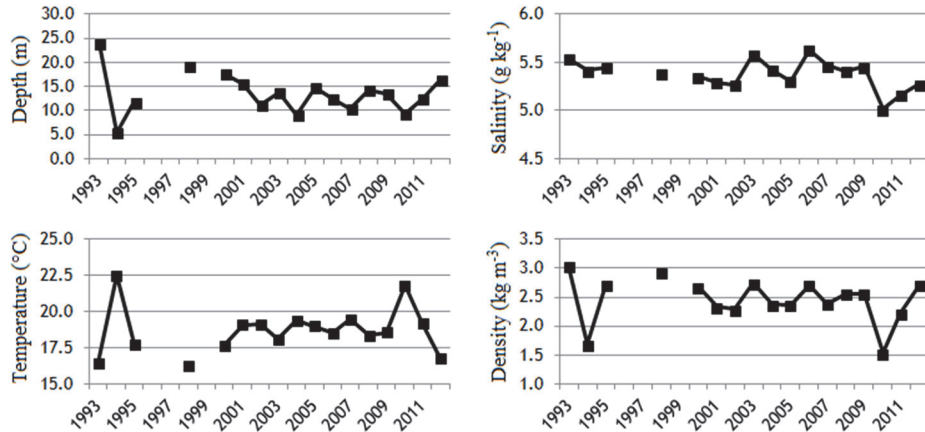
Figure 6. Inter-annual variability of mean characteristics of upper mixed layer in August, 1993-2012.

Despite the considerable inter-annual variations of UML mean depth, salinity, temperature, and density in August no clear tendency or trend was detected in the period 1993-2012 which is in contrast to what has been observed and reported earlier, for example, about the salinity increase during 1960-1977 (e.g. Berzinsh 1980; Berzinsh 1995) and decrease from the end of 1970s till the start of 1990s (Raudsepp 2001; Berzinsh 1995). Moreover, Jurgensone et al. (2011) reported a general increase in water temperature in the central and southern part of the Gulf of Riga during 1976-2008 (summer). The satellite data during 1990-2004 showed a positive trend in the yearly mean SST of the Baltic Sea with summer and autumn dominating this trend and positive summer trend being highest in the northern Baltic Sea (Siegel et al. 2006) and remote sensing data during 1990-2008 showed an increase of SST specifically in the Gulf of Riga by about 1.0 °C per decade (BACC 2015).

The inter-annual variability of the DL mean salinity in May and August is somewhat similar (Fig. 7). The highest salinity in May and August was observed in 2010 when the DL mean salinity was 6.48 g kg^{-1} and 6.39 g kg^{-1}, respectively. Similar but fairly lower salinity peak in both months was observed in 2006. In May an additional salinity peak was also observed in 1996 (6.40 g kg^{-1}), whereas, in August there was no data from 1996. The DL salinity peaks are usually associated with the more saline water inflow through the Irbe Strait along the western coast of the gulf (Berzinsh 1995; Lilover et al. 1998). It has to be noted that the salinity peak in 2003 was evident in August (6.20 g kg^{-1}) but was absent in May (5.89 g kg^{-1}) suggesting of more saline water inflow at some point between these two months, whereas, in 2006 and 2010 the more saline water inflow happened already in May or before that. The inter-annual variations of the DL mean density followed the salinity pattern in both respective months and density most of the time varied between 4.5-5.0 kg m^{-3} (Fig. 7). Finally, the inter-annual variations of the DL mean temperature in May

and August were also rather high and temperature was different in both months, although, there were also some similarities in the pattern of the temperature variations. In May during 1993-2012 the DL mean temperature varied mostly between 0.0-2.0 °C, whereas, in August – between 2.0-4.0 °C. The more saline water inflow at some point before May in 1996, 2006 and 2010 was probably the reason for the lowered DL mean temperatures in May also observed in these years. It has to be noted that the DL mean temperature in August was still remarkably low in 2010 (1.6 °C) if compared to 2006 when temperature reached 3.6 °C (Paper **I**). The reason behind this feature could be explained by a strong stratification observed already in May 2010 which is not typical in the Gulf of Riga.

Similarly to the UML dynamics, inter-annual variations of mean temperature, salinity and density were evident but no clear tendency or trend could be detected in May or August during 1993-2012.
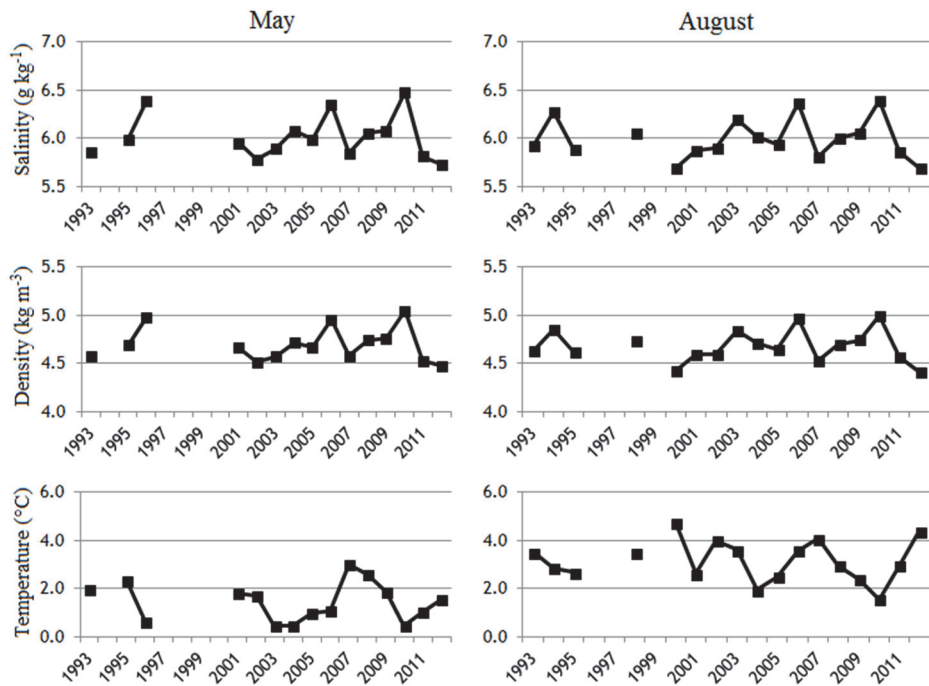

Figure 7. Inter-annual variability of mean characteristics of the deep layer in May (left column) and August (right column), 1993-2012.

The strongest stratification (expressed as salinity difference (ΔS) and density difference (ΔD) between the DL and UML and temperature difference (ΔT) between the UML and DL) during the study period was observed in years 1994 and 2010 (Fig. 8). In 2010, it was slightly stronger and ΔS was approximately two times higher (1.38 g kg^{-1}) than the average difference between the DL and

UML during 1993-2012 with ΔD and ΔT substantially exceeding (3.46 kg m^{-3} and 20.2 °C, respectively) the average values. In 1994, ΔD and ΔT were fairly similar (3.18 kg m^{-3} and 19.6 °C, respectively) to those values found in 2010, whereas, ΔS was substantially lower (0.86 g kg^{-1}) than in 2010. This discrepancy in ΔS was due to the spatial distribution of the data in 1994 (see material and methods). The main reasons for the strong stratification in 1994 and 2010 were the increased river runoff in spring and substantially higher UML mean temperature in both years as was already described before.

BSI and river runoff was used to see whether any correlation could be found between the inter-annual changes in vertical stratification and forcing factors (Paper **I**). There was no significant correlation between BSI mean values and stratification parameters (see sub-chapter 3.1.4 and Paper **I**). On the contrary, significant positive correlation was found between the river runoff in spring (March-May) and corresponding ΔS, ΔD and ΔT with coefficient r = 0.52, 0.62 and 0.65, respectively (n = 17, $p < 0.05$). This positive correlation supports the suggestion that elevated UML temperatures (August) in 1994 and 2010 might be the combined effect of increased river runoff and following intensification of stratification.
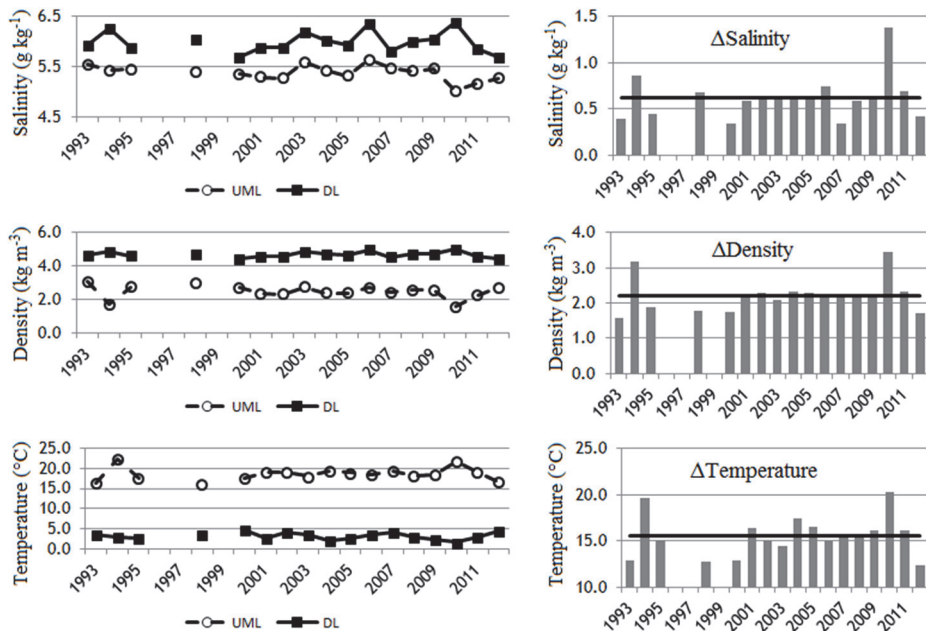

Figure 8. Mean salinity, density (sigma-t) and temperature in the upper mixed layer and deep layer in August 1993-2012 (left column) and their differences between the two layers (right column). Differences are given as deep layer minus upper mixed layer for salinity and density, and opposite for temperature; solid line represents the mean difference during 1993-2012.

Latest projections of the future climate change (BACC 2015) continue to predict a significant water temperature increase in the Baltic Sea region similarly as it was stated before (BACC 2008). Based on the results from long-term CTD data (Paper **I**) it can be suggested that if the water temperature will continue to increase then the warming would generate stronger stratification conditions in the Gulf of Riga in summer. Furthermore, stronger stratification is likely to favor the oxygen depletion in the deeper parts of the gulf. Thus, the previously detected parts with low oxygen concentration or no oxygen at all (Hansson et al. 2009) in the Gulf of Riga could expand in wider areas. It has been stated before that the temperature increase by itself will worsen the oxygen conditions throughout the Baltic Sea area as elevated nutrient levels will amplify this effect due to elevated primary production (Skogen et al. 2014). The same source predicted that eutrophication status in the Gulf of Riga would change from potential problem area to problem area in the future due to the declining oxygen conditions and increasing phytoplankton biomass.

While precipitation and evapotranspiration were projected to increase in the Gulf of Riga region, the mean annual river runoff was projected to decrease. However, strong seasonal changes with a shift of the maximum river runoff from spring to winter were also projected (BACC 2015). Due to the factors mentioned above, the salinity minimum usually observed (in the surface layers) starting from the spring in the southern part of the gulf could also shift in accordance with the changes in the river runoff seasonal dynamics. An earlier maximum of river runoff together with water temperature increase could benefit for the faster development of the seasonal stratification in the Gulf of Riga. Strong stratification could be observed already in May or even earlier

3.1.4 Influence of freshwater and atmospheric forcing

The average yearly river runoff in the Gulf of Riga during 1950-2012 was reported as 32 km^3 (Bergström et al. 2001; Kronsell and Andersson 2014) while during the study period of 1993-2012 it was 27.7 km^3 based on only four biggest Latvian rivers (Pärnu in Estonia and smaller rivers were left out). By far the largest river runoff occurred in spring (12.2 km^3, March-May) almost doubling the observed river runoff in winter (6.5 km^3, December-February), whereas, the river runoff in summer (June-August) and autumn (September-November) was rather similar – 3.9 km^3 and 4.5 km^3, respectively. The seasonal pattern of the river runoff during 1993-2012 is similar to what has been reported earlier in the Gulf of Riga (Leppäranta and Myrberg 2009).

The most evident freshwater influence is the reduced salinity in the surface layers in the southern part of the gulf. Despite the fact that the strongest freshwater influence was observed in spring, a correlation between the UML mean salinity in August and the mean river runoff in spring (March-May) was detected in the Gulf of Riga during 1993-2012. The correlation was rather high ($r = -0.66$, $n = 17$, $p < 0.05$) using all available data but it increased even more ($r = -0.82$, $n = 14$, $p < 0.05$) when three years were excluded from the calculations

due to the unsatisfactory spatial data coverage (Paper **I**). As expected, the highest correlation was observed in the southern, southwestern part of the gulf. Despite the persistent but relatively narrow coastal current carrying the fresher waters from the southern part along the eastern coast of the gulf (Soosaar et al. 2016; Papers **II** and **III**), the lowest correlation was observed in the eastern part of the gulf and it steadily decreased further away from the southern shore. More surprising was the fact that correlation between the UML mean salinity in August and the mean river runoff in spring stayed high in the central part as well as western and northwestern parts of the gulf close to the Irbe Strait (r was between -0.76 and -0.77). This feature could be explained by the previously mentioned anticyclonic circulation in the Gulf of Riga during summers (see Fig. 4a and Paper **II**).

Atmospheric forcing was characterized by monthly-averaged Baltic Sea Index (BSI) during 1993-2012, which is the difference of normalized sea level pressures between Szczecin in Poland and Oslo in Norway (Lehmann et al. 2002). The changes in BSI were related to the inter-annual variations of UML and DL mean parameters as well as stratification strength during the same period.

No significant correlation was found between the UML mean salinity, temperature and density and BSI. Nevertheless, a bit surprisingly significant positive correlation was found between the inter-annual changes in the UML mean depth in the Gulf of Riga and BSI in 1993-2012 (Paper **I**). The best correlation (r = 0.71, $n = 14$, $p < 0.05$) was found using mean BSI values from the period of June-August. With the increase in the BSI, the westerlies are dominating over the Baltic Sea (Lehmann et al. 2002) and becoming stronger which would benefit the mixing of the surface layers, thus, increasing the UML mean depth in the gulf.

The DL mean parameters in May and August, as expected, did not reveal any significant correlation with BSI. Nevertheless, at some special occasions in May the correlation was evident when using BSI averaged over May and March-May (Paper **I**). A similar absence of significant correlation was detected between BSI and mean parameters characterizing stratification (ΔS, ΔD and ΔT) despite the fact that BSI values from August, June-August and July-August were tested (Paper **I**).

3.2 Mesoscale features and freshwater transport pathways

3.2.1 Mesoscale features and formation of eddies

The water balance of the Gulf of Riga is determined by the saltwater inflow from the Baltic Proper mainly through the Irbe Strait in the northwestern part, freshwater inflow mainly in the southeastern part and compensating mixed water outflow mainly through the Irbe Strait. These processes and variable wind forcing have a potential to form mesoscale structures such as cyclonic eddies related to the saltwater inflow, freshwater plumes, intrusions and buoyant

coastal jets. The model used (POM) to study these mesoscale features is eddy resolving as the grid size of the model is below the mean Rossby radius in May (1.6 km) and August (3.2 km) calculated from the available CTD casts (Paper **I**).

The model run of thermohaline circulation (no atmospheric forcing) in the Gulf of Riga revealed the formation of salinity front and a gravitational (density) current in the Irbe Strait (see Paper **III**) due to the salinity difference between the Baltic Proper and the Gulf of Riga (approximately 1.5 g kg^{-1}). The gravitational flow that transports saltwater eastward from the Baltic Proper to the Gulf of Riga is attached to the southern shore between the Irbe Strait and the Cape Kolka as geostrophic flow. The flow is highly unstable and creates a chain of mesoscale cyclonic eddies with a core of increased salinity/density. Eddies are generated at the Irbe Strait sill and move eastwards along the southern shore to the Cape Kolka with translation velocity of ~0.03 m s^{-1} (Paper **III**). While propagating along the Irbe Strait towards the Cape Kolka, the eddy size (diameter) increased from approximately 10 km to 15 km which is in accordance to what has been reported before regarding the size of the eddies in the Baltic Sea and the Gulf of Riga based on the satellite data (Karimova 2012). On the beam of the Cape Kolka, the cyclonic eddy splits into two smaller cyclonic eddies with one eddy moving to northeastern and the other to southeastern part (Paper **III**).

As it was discussed before the anticyclonic gyre dominates the general circulation in the Gulf of Riga in summer (Paper **II**). This circulation pattern is determined by a combined effect of the prevailing negative wind curl, thermohaline stratification and bottom topography. Note that similar conclusion about the anticyclonic circulation in the upper layer in the southern Gulf of Riga due to the three-dimensional estuarine type density field was drawn by Soosaar et al. (2014). Thus, such general thermohaline circulation in the gulf could cause substantial modification of the Daugava River plume. As a result, the low saline riverine water from the anticyclonic bulge can propagate along the shore to the left as far as two-thirds of the alongshore distance from the Daugava mouth to the Cape Kolka (see Paper **III**). At that point, the low saline riverine water meets the high saline water that came from the Baltic Proper in the form of cyclonic eddies. Due to the convergence of water masses, the water mass of riverine origin turns right to the open sea and ultimately finds its way further to the north in the form of multiple low-saline squirts leaking between the high-saline cyclones. Note that along with the left-hand propagation of riverine waters, some fraction of Daugava River runoff is still involved in the right-hand coastal jet caused by intrinsic buoyant plume dynamics in rotating media.

3.2.2 Daugava river plume and meandering of coastal buoyant jet

To simulate intrinsic propagation of the Daugava River plume, a model run with spatially uniform initial fields of temperature and salinity ($T_0 = 10$ °C and $S_0 = 5.6$ g kg^{-1}) and without atmospheric forcing was performed (Fig. 9a).

The Daugava River plume consists of an anticyclonic bulge of riverine water attached to the river mouth and a coastal jet-like current carrying part of the riverine waters to the north along the eastern coast of the Gulf of Riga. A transition zone between the bulge and the northward coastal jet displayed wave-like disturbances with a wavelength of approximately 8 km (Fig. 9a). The shape of the observed plume confirms the diagnostics made based on the conceptual model by Yankovsky and Chapman (1997) – the Daugava River plume is the surface-advected plume. Note that the observed offshore extension of the bulge of 20-25 km (Paper **III**) is somewhat larger than the theoretical estimate of it (14.9 km). The discrepancy is not surprising because the theoretical expression for y_s (offshore extension) was derived by assuming that the plume is in a steady state. However, in the present model experiment, the bulge appeared to grow in time as it has also been shown in several other studies, e.g. by Fong and Geyer (2002).

Results from freshwater transport of the coastal jet-like current across a zonal section (see Paper **III** for details) showed that the ratio of the freshwater transport by the coastal jet to the Daugava River volume flux, after approximately 80-day transition period, was established at $V_{freshwater} / Q_{Daugava} =$ 0.4–0.5 with the mean value of 0.46. The last estimate coincides with the estimates by Fong and Geyer (2002) who reported 0.40–0.48 for the ratio of freshwater transport by the coastal jet to the river volume flux in their model experiments. It shows that, in the case of the absence of other forcing components like atmospheric forcing and saltwater inflows, more than half of the river discharge would feed the growing anticyclonic bulge.
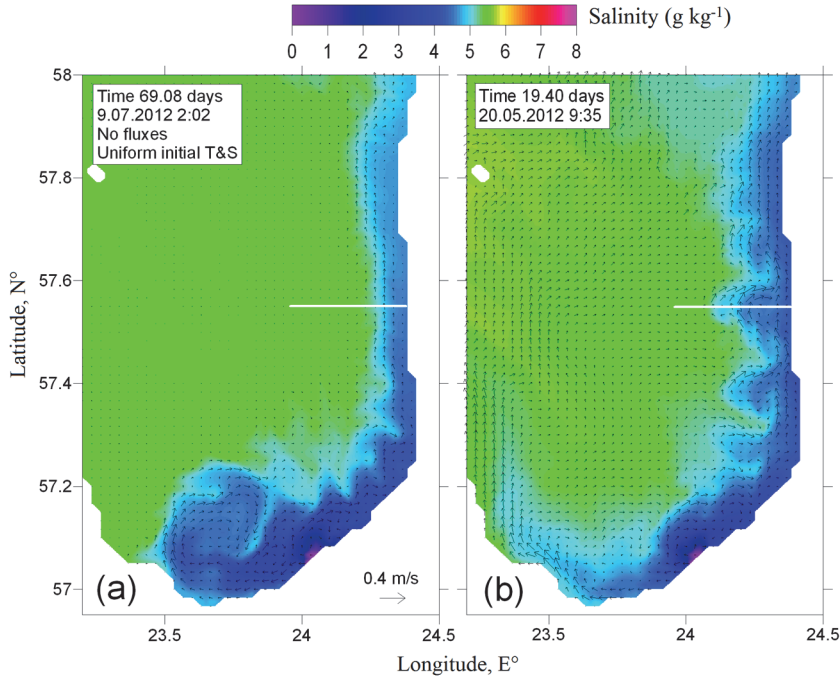
Figure. 9. Plan views of simulated salinity and current velocity in the surface layer (at 1 m depth) of the south-eastern part of the Gulf of Riga: (a) – a numerical experiment with uniform initial temperature and salinity fields and no atmospheric forcing, results after 69 days from the model run onset; (b) – the basic run on 20.05.2012 at 9:35.

Despite the anticyclonic circulation pattern in summer when the NLC transports a significant part of the riverine water along the western coast (see Fig. 4a and Paper **II**) a buoyant coastal current is still persistent transporting the freshwater to the north along the eastern coast. Being adjoined to the lateral boundary, such a current is expected to be stable (Zhurbas et al. 2006). However, at some circumstances due to the wind forcing this jet-like current and related salinity front can detach from the shore and fall into baroclinic instability where the buoyant coastal plume being relatively wide displays vigorous meandering with a wavelength of $\lambda = 12$–15 km (Fig. 9b). Rossby radius (R_{bc}) calculations confirmed baroclinic instability as a possible cause for the meanders since R_{bc} was found to be approximately 5 km in the meanders (Paper **III**) indicating that the prevailing wavelength of meanders ($\lambda = (2.4 \div 3)R_{bc}$) is in accordance with the expression for the wavelength of the fastest growing mode (Eady 1949). Similar meandering pattern was previously modeled and also observed on infrared images of the Po River plume (Cushman-Roisin et al. 2007), whereas, Magaldi et al. (2010) showed that the meandering of the current could be related to the baroclinic instability. Thus, the wind forcing influences both, the bulge and the coastal current jet and plays a major role in mixing and transport of the river discharge (see also Jurisa and Chant 2012; Horner-Devine et al. 2008).

3.2.3 Convergence of water masses

As mentioned above the summer season is characterized by a whole-basin anticyclonic circulation in the Gulf of Riga (Paper **II**) which means that the Daugava River plume water can be partially involved in the anticyclonic circulation and transported to the north along the western coast by the NLC. In some cases, the related tongue of reduced salinity of riverine origin can be identified as far as at 58°N (almost reaching the Saaremaa Island) due to the intensification of the NLC resulting from favorable winds (Paper **III**). The NLC is associated with a baroclinic (density) front, which is supposed to be a zone of flow convergence (e.g. Fedorov 1986). Due to the convergence, the low salinity riverine water sinks and spreads seaward occupying an intermediate layer and forming an intrusion with salinity inversion of approximately 0.1 g kg^{-1} (Paper **III**). This circumstance might explain the reduced salinity in the sub-surface layers registered by the autonomous buoy profiler (see Fig. 10b and Paper **IV**). Transport of riverine waters by the NLC, their sinking and spreading within an intermediate layer ultimately works for effective mixing of the river runoff with the Gulf of Riga waters.

3.3 Features of vertical stratification related to lateral water exchange

3.3.1 High-resolution view on the vertical thermohaline structure in summer

A high-resolution view on the vertical structure of the water column was obtained using autonomous buoy profiler located to the west from the Ruhnu Island during May-September 2015 (Fig. 10)

In general, the obtained high-resolution temperature data during May-September 2015 revealed the well-known seasonal pattern of temperature described before in the Gulf of Riga (Raudsepp 2001) as well as in other basins of the Baltic Sea (Liblik and Lips 2012). Nevertheless, the high-resolution salinity data from autonomous profiler captured the fresher (e.g. first week of the July) and more saline sub-surface water patches (e.g. end of July) which cannot be detected analyzing the mean monthly characteristics of salinity.

Time series of the water column stability (see Paper **IV**) showed that the pycnocline is situated deeper starting from the August than in the first part of the study period. The existence of the strongest stratification in the Gulf of Riga in August has been shown earlier for 1973-1995 (Raudsepp 2001) and 1993-2012 (Paper **I**).

The seasonal thermocline was the main contributor to the stability of the water column if compared to the salinity contribution (Paper **IV**). Negative stability values occurred in July and August (especially in the second part of July) due to the vertical salinity gradient. Those layers were located in the thermocline and were connected to the existence of sub-surface buoyant saltier

water intrusions. Nevertheless, the layer with the inversed salinity gradient was always situated between the layers with common salinity gradient when salinity increased with the depth.

The integrated stability over the whole water column (Paper **IV**) showed that the thermal buoyancy dominated while salinity had a minor importance in the strength of stratification at the buoy location. Similarly, the UML was also mainly stabilized by the temperature, but occasionally salinity (at the beginning of July) had an opposite effect while at the beginning of August salinity and temperature had a similar contribution to the stability of the UML. Nevertheless, it was showed that river runoff in the Gulf of Riga also plays an important role creating the vertical stratification in spring, mostly in the southern part with high freshwater influence (Stipa et al. 1999). Moreover, it was found that there is still a significant correlation between the river runoff in spring and stratification in August (see sub-chapter 3.1.3 and Paper **I**), thus, emphasizing the influence of river runoff to the stratification dynamics in the Gulf of Riga.
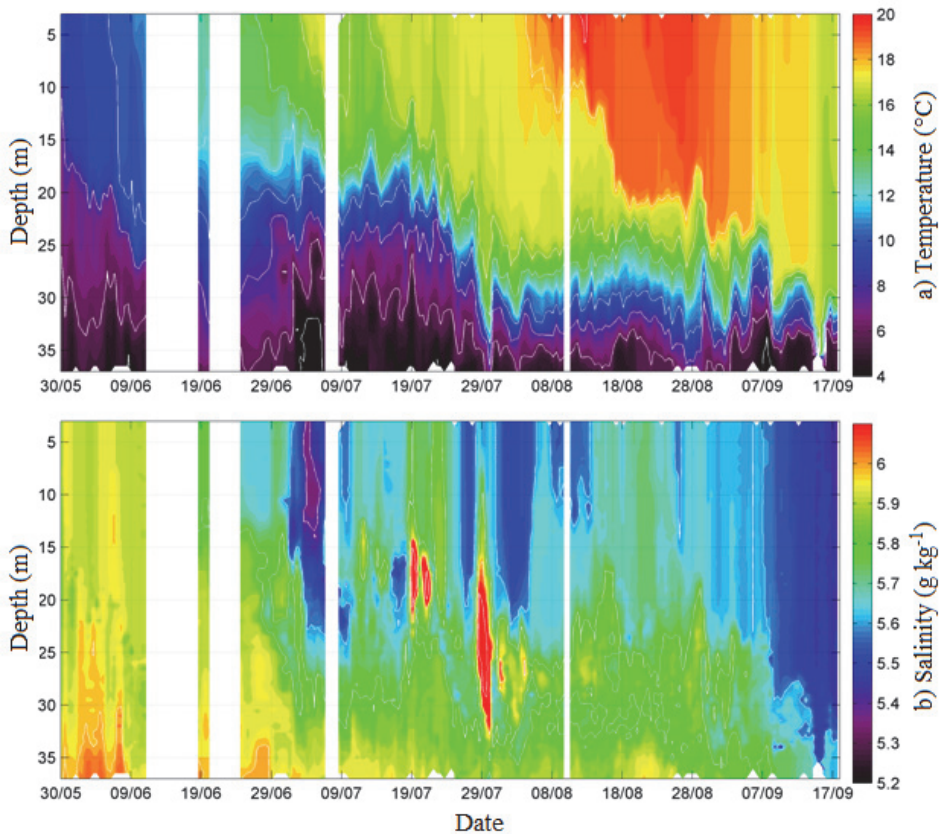

Figure 10. Time series of a) temperature (°C) and b) absolute salinity (g kg^{-1}) at the buoy station from 30 May 2015 to 18 September 2015.

3.3.2 Sub-surface intrusions of saltier waters and their possible origin

It is interesting that just before the first notable appearance of saltwater patches a clear signature of fresher water was registered at the 15-20 m depth (Fig. 11, 19 Jul 12:00). The core of this fresher layer had the salinity of 5.55-5.60 g kg^{-1} and it was situated between the upper layer with the salinity of 5.75-5.80 g kg^{-1} and deep layer with the salinity of 5.95 g kg^{-1}. Further on, the fresher water in the sub-surface layer was replaced by the salinity maximum in 12 h (the profiling interval; Fig. 11, 20 Jul 00:00). This saltier sub-surface layer was located in the depth range of 11 to 25 m and its core with the salinity of 6.45 g kg^{-1} was located at 17 m depth. The sub-surface salinity maximum disappeared on 22 July (Paper **IV**).

The saltier water reappeared in the sub-surface layer on 29 July (Fig. 11, 29 July 12:00). The core of the sub-surface layer was located at 22 m depth and had salinity of 6.30 g kg^{-1}. The sub-surface salinity maximum also occurred until the end of August, although, it was much weaker than events described before (Fig. 10b).

The spatial distribution of previously mentioned sub-surface salinity maximum layers is difficult to determine due to the sparse dataset. Despite that, three available CTD profiles (not shown here) from July to August revealed the occurrence of salt maxima in the Ruhnu Deep which means that sub-surface salinity maximum can reach at least the central part of the gulf and, based on the rapid disappearance of maximum layer, this is a result of the advection process. Thus, it can be assumed that the patches of sub-surface salt maxima only occasionally reached or passed the profiling station.

The only evidence of similar sub-surface salt maximum in the Gulf of Riga has been reported at two stations in the eastern part of the Irbe Strait on 29 August–1 September 1993 (Stipa et al. 1999), whereas, the existence of fresher sub-surface waters found at the buoy station has also been predicted by the numerical modeling (see sub-chapter 3.2.3 and Paper **III**). Regarding the Baltic Sea exceptionally warm and saline inflows embedded in the halocline of the Bornholm Basin were reported in 2002 and 2003 (Mohrholz et al. 2006).
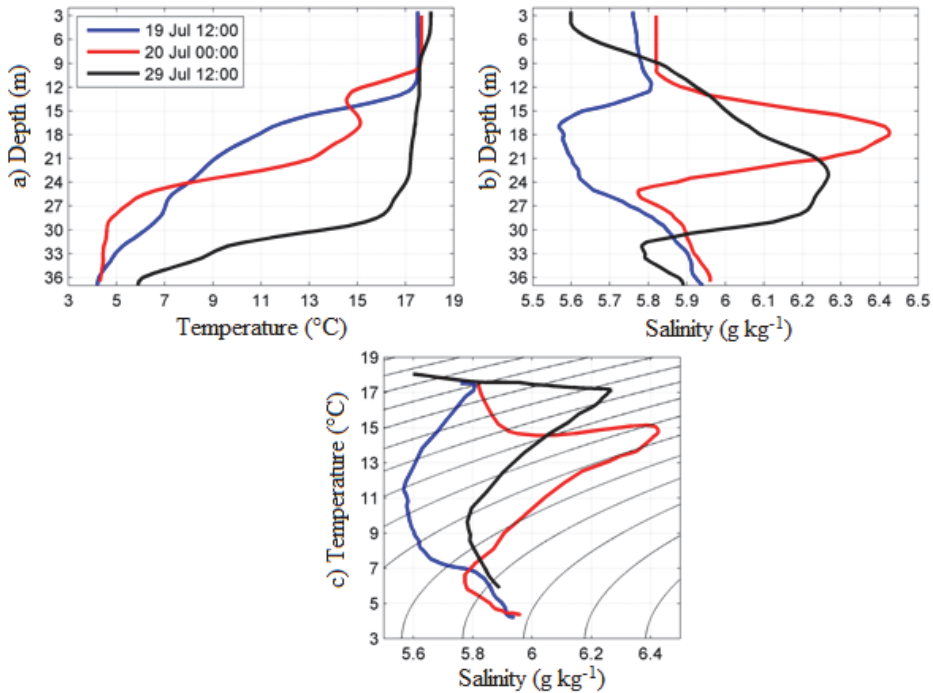
Figure 11. Selected profiles of temperature (°C, a) and salinity (g kg^{-1}, b) and respective temperature-salinity diagram with density anomaly (kg m^{-3}, c) as contour lines in profiling station (the location is shown as a yellow rectangle in Fig. 1).

Based on the configuration of the Gulf of Riga there are two ways how more saline waters from the Baltic Proper can enter the gulf – either through the Suur Strait in the northern part or Irbe Strait in the western part. Unfortunately, there were no continuous measurements available in the straits to be able to capture the entering process of the saltier waters directly. Despite the fact that majority of the water exchange occurs through the Irbe Strait (Petrov 1979) the sub-surface salt maximum formation via the Suur Strait cannot be excluded, although it is very unlikely as very strong and long-lasting northerly wind impulse is needed (see Otsmann et al. 2001 and Paper **IV**).

Using a few available shipborne CTD profiles in the Irbe Strait as well as autonomously recorded temperature and salinity by thermosalinograph during the surveys conducted on 14-15 July and 7-9 August surprisingly cold water in the upper layer of the Irbe Strait was observed during the former survey. The temperature of the upper layer was around or exceeding 17 °C in the Baltic Proper and the gulf, but below 13 °C inside of this cold patch (Paper **IV**). Such a feature in the surface layer suggests of the upwelling event. During the period from 5 to 10 July strong SW winds (>10 m s^{-1}) prevailed which is a good precondition for the upwelling in the Gulf of Riga along the coast of the Saaremaa Island. The satellite-derived sea surface temperature complemented

with temperature measurements at the coastal stations and by the onboard thermosalinograph indicated that, indeed, the upwelling occurred in the NW part of the Gulf of Riga in mid-July (Fig. 12). Results from the statistical analysis based on three-dimensional modeling during the summers of 1979-1988 (Myrberg and Andrejev 2003) and analysis of satellite data for 1990-2009 (Lehmann et al. 2012) also approved that NW part (along the coast of the Saaremaa Island) is one of the main upwelling regions in the Gulf of Riga.
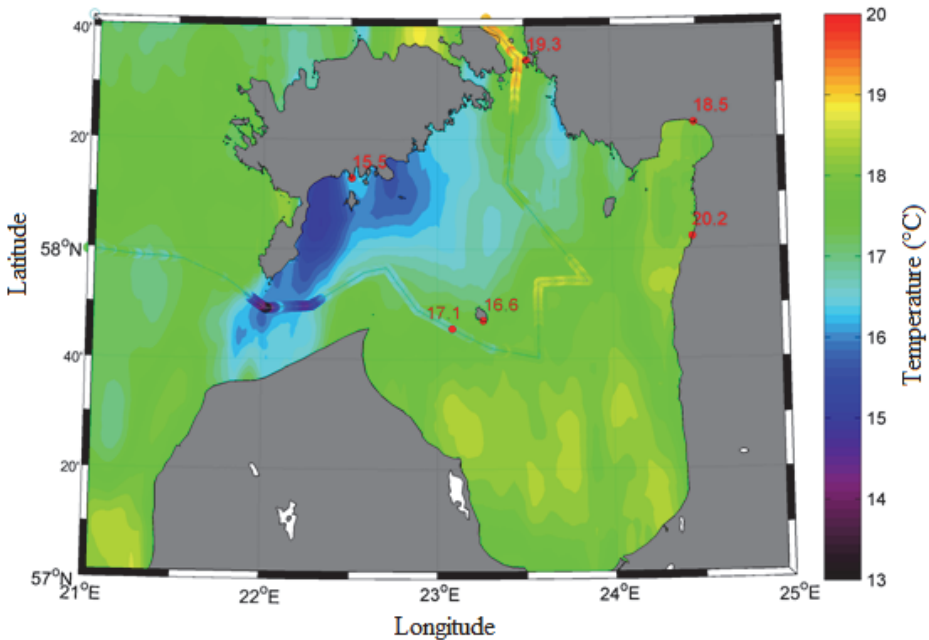

Figure 12. Satellite-derived sea surface temperature; upper layer temperature registered along the RV SALME track by thermosalinograph, at the buoy station and selected coastal stations on 15 July 2015.

The only available profile in the Irbe Strait on 14-15 July was acquired eastward from the core of the upwelling and it revealed three layers - upper layer (15.00 °C and 5.90 g kg^{-1}), deep layer (4.70 °C and 5.95 g kg^{-1}) and salt maximum layer (12.15 °C and 6.35 g kg^{-1}) between the former two. Similar structure of salt intrusion was found in the central part of the Irbe Strait on 9 August as well (Figs. 13c and 13d) and the structure of the salt maximum in July and August was similar to the one observed at the buoy station, which suggests that the salt impulse entered the gulf via the Irbe Strait. Moreover, the most recent profile from the central part of the Irbe Strait on August 2016 also had a sub-surface salinity intrusion.

On 9 August high saline (> 6.7 g kg^{-1}) and warm water was observed in the upper layer in the southern part of the strait (see the green curve in Fig. 13d and Paper **IV**). The temperature-salinity curves suggest that the salt maximum layer

observed in the central part of the strait was a mixture of high saline warm water and thermocline water of the Gulf of Riga. The process that could initiate such a mixing event was the downwelling along the southern coast of the Irbe Strait which appeared simultaneously with the upwelling along the coast of the Saaremaa Island promoted by the SW winds. Moreover, the SW wind likely creates a coastal boundary current along the eastern coast of the Baltic Proper. It can be seen that at the station marked in green in Fig. 13d, this warm, salty water has pushed over the fresher water probably causing some vertical mixing as well.

Since the Irbe Strait is relatively narrow and shallow, the downwelled waters (originated from the Baltic Proper) reached the seabed quite fast. We suggest that the upwelled water was (at least partly) compensated by this warm and saltier downwelling water in the Irbe Strait. This hypothesis is supported by the TS-curves - one source water (see the green curve in 13d and Paper **IV**) for the salt maximum layer observed in the central strait on 9 August (blue curve in Fig. 13d) had almost the same TS-characteristics as the warm and saltier water more to the east along the southern part of the Irbe Strait (see the magenta curve in Fig. 13d and Paper **IV**).
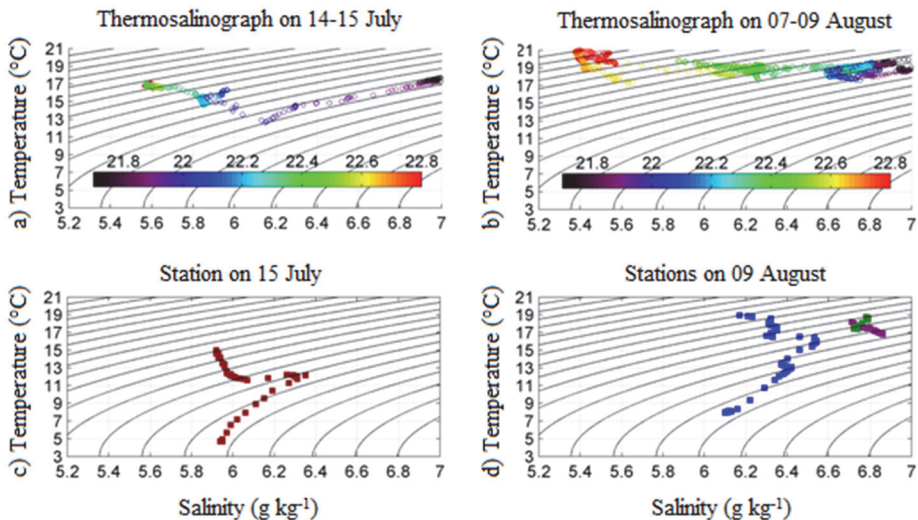

Figure 13. Temperature-salinity (TS) curves on 14-15 July and 7-9 August. TS curves along the vessel track acquired by the thermosalinograph (a, b) and at selected CTD stations (c, d) during the two analyzed surveys. The thermosalinograph tracks and locations of CTD stations are shown in Paper **IV** (station dots on the map have same colors as TS dots here). Color bars in the uppermost panel show the longitude.

The period of upwelling coincided with the period of strongest salt maxima observed at the buoy station (see intrusion index in Paper **IV**). This coincidence supports the suggestion that the salt intrusions entered the gulf during the simultaneous upwelling in the northwestern gulf (along the shore of the

Saaremaa Island) and downwelling along the southern coast of the Irbe Strait. Similar suggestion was made by Stipa et al. (1999) stating that downwelling depresses the seasonal pycnocline on the Baltic Proper side of the strait and creates a baroclinic pressure gradient along the strait, which might drive the Baltic Sea surface water, instead of the water below the seasonal pycnocline, into the Gulf of Riga. It was suggested that downwelling occurred in the Baltic Proper along the Latvian coast in 1993 (Stipa et al. 1999) when the salinity maxima in the area were registered. More frequent water column profiling should be carried out in order to check if only the baroclinic pressure gradient is needed (Stipa et al. 1999) for the maxima layer generation, or also the cross-strait downwelling plays a significant role as suggested in the present study.

3.3.3 Water exchange regimes and their impact

In the previous sub-chapter, it was suggested that the sub-surface saltwater maxima originated from the upper layer of the Baltic Proper and likely entered the gulf via the Irbe Strait. For the sub-surface saltwater intrusions to originate from the upper layer of the Baltic Proper and enter the Gulf of Riga through the Irbe Strait, specific conditions are required regarding the water density in the two basins. The inflowing saltier water must be lighter than the deep layer water and denser than the upper layer water in the gulf to locate in between them (Paper **IV**). The upper layer density in the Baltic Proper in January-April (1979-2014) was in a range of 5.5-6.0 kg m^{-3}, whereas, water density at the 32-38 m depth in the Gulf of Riga was mostly below 5.0 kg m^{-3} throughout the year (Fig. 14a). As the water cools down to the temperature of maximum density (2.6-2.7 °C) every winter in the Gulf of Riga, the salinity over 6.9 g kg^{-1} (at the temperature of 2.6-2.7 °C) would be necessary to reach the density of 5.5 kg m^{-3}. Despite that, salinity in the deepest layers of the gulf does not typically exceed 6.5 g kg^{-1} (Raudsepp 2001) which means that if the Baltic Proper water enters the Gulf of Riga in January-April, it must sink to the near-bottom layer of the gulf and cannot form a sub-surface salinity maximum during this period. In Autumn and early winter the situation is rather similar - although during the autumn-winter cooling period the temperature in the Gulf of Riga drops faster than in the Baltic Proper, the Baltic Proper still has heavier upper layer water which means that it cannot lie above the Gulf of Riga water and form any salt intrusions in the sub-surface layer.
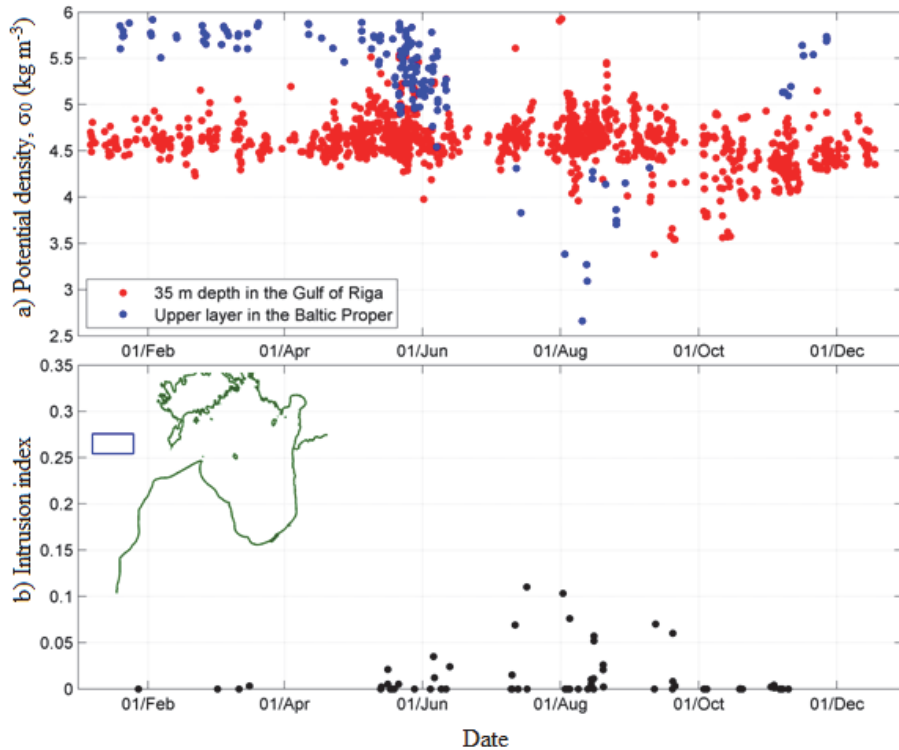
Figure 14. (a) Annual cycle of average density anomalies [σ_0; kg m^{-3}] in the 0-5 m layer of the Baltic Proper (1979-2014) and at the 32-38 m depth in the Gulf of Riga. (b) Intrusion index in the Gulf of Riga at ≥35 m deep stations (1993-2015); only high-resolution profiles were included. The blue box indicates the location of the analyzed profiles from the Baltic Proper. In the Gulf of Riga, all available deep enough measurements were included.

Nevertheless, the upper layer water in the Baltic Proper tends to be lighter than water in the Gulf of Riga at 32-38 m depth from mid-July to the beginning of September (Fig. 14a). Thus, if the Baltic Proper water flows into the gulf during that time, it likely does not reach the bottom layers of the gulf and can potentially form sub-surface salinity maxima. The temporal variability of the intrusion index (based on the CTD casts during 1993-2014) confirms latter and shows that the saltwater intrusions have been observed from mid-July to mid-September (Fig. 14b). Moreover, it has to be noted that at the autonomous buoy location the saltwater intrusions, as well as higher intrusion index, were also detected during this time of the year (see Paper **IV**).

Buoyant intrusions of inflowing waters are well-known features in the Western Baltic Sea. It is the water that has flown through the Danish Straits to the Baltic and which is not dense (light) enough to reach the bottom layers (to stay in the surface layer) of the Baltic. If the baroclinic inflows occur during summer in the Western Baltic (Feistel et al. 2004), buoyant temperature maxima

can develop at the depths of the halocline. Since maxima formation can be influenced by wind forcing, one might expect that the salt and water balance in the gulf could be impacted by the suggested wind regime changes in the future (Christensen et al. 2015).

Previously described buoyant inflow regime might occur in many semi-enclosed basins where a sill restricts the water exchange with the neighbouring water basin which has higher salinity/density. For now, such regime is well known only in fjords (e.g. Belzile et al. 2016). In summer when the seasonal thermocline is present, certain forcing conditions could cause deepening of the upper mixed layer and the inflowing water originating from the surface (or thermocline) layer forms a buoyant salinity maximum in a basin.

To ascertain the possible role of the sub-surface salinity maxima, for example, in the salt balance of the Gulf of Riga, more frequent and dense measurements should be carried out also involving the advantages of the high-resolution modeling. Nevertheless, it seems that it is not an easy task for the operational models to detect the sub-surface salinity maxima as, for example, the existing operational model HIROMB-EST (Lagemaa 2012) and the HBM (Berg and Poulsen 2012) did not capture the salt maxima formation and constantly underestimated salinity (on average by 0.6 g kg^{-1}) at the buoy location in the present study.

The apparent oxygen utilization (AOU) and salinity curves (see Paper **IV**) suggested that source water for the salt intrusion had almost saturated oxygen content as the water was originating from the upper layer of the Baltic Proper. The Gulf of Riga has a high production (Seppälä and Balode 1999) and high oxygen consumption (HELCOM 2009) due to decomposition of organic material in the near-bottom layer. Lateral advection might be an important source of oxygen for the deep layers in the gulf, especially in summer, when strong stratification impedes vertical mixing. However, if the inflowing saltier water does not reach the deeper bottom layers, the bottom remains isolated from this lateral advection of oxygen. Thus, the oxygen conditions in the near-bottom layer of the gulf strongly depend on the water exchange regime in the Irbe Strait. In summer 2015, the regime resulting in buoyant sub-surface saltwater intrusions prevailed, and the near-bottom layer of the gulf did not receive additional oxygen through the lateral advection. This suggestion can be confirmed by dissolved oxygen content and AOU profiles (see Paper **IV**) acquired from the Ruhnu Deep from April to August 2015.

In conclusion, it can be suggested that two types of Baltic Proper inflow regimes exist in the gulf. The near-bottom layer salt wedge regime is the only inflow pattern from October to May/June. In summer, from June/July to September, the regime leading to the formation of the buoyant salt intrusion (or saltier water patches) if the inflowing water originates from the upper layer or the regime resulting in the near-bottom salt wedge if the inflowing water originates from the layer beneath the seasonal thermocline can occur.

CONCLUSIONS

The main aim of the thesis was to improve the present knowledge about the thermohaline structure in the Gulf of Riga in summer and ascertain the main factors and processes influencing it. Additional attention was devoted to the characterization and description of the vertical thermohaline structure based on the shorter and longer time scales. Important role was allocated to the mesoscale processes and circulation in the Gulf of Riga using the approach of numerical experiments.

In comparison with other studies in the Gulf of Riga, the present thesis provided the long-term results based on rather long historical CTD dataset obtained from 1993 to 2012. Together with different forcing factors this dataset allowed to describe the recent state of the Gulf of Riga regarding thermohaline variability and compare it to what has been observed and suggested before. Autonomous buoy profiler was used for the first time in the Gulf of Riga in order to acquire a high temporal resolution profiles which allowed to detect the sub-surface salinity intrusions which were just suggested and not thoroughly described before due to the limited resolution of the data. Until now, there have been only a few model studies devoted particularly to the Gulf of Riga, but not much attention has been paid to describe both the whole-basin circulation patterns and mesoscale features like eddies and meanders.

The main results of the present thesis can be concluded as follows:

- The vertical thermohaline structure in the Gulf of Riga in summer (August) is characterized by the average salinity and temperature of 5.38 g kg^{-1} and 18.6 °C in the UML, 6.0 g kg^{-1} and 3.2 °C in the DL, and resulting overall vertical density difference between the UML and DL of 2.2 kg m^{-3}.
- During summer, a whole-basin anticyclonic gyre with enhanced intensity of currents in the western half-basin was dominating governed by a combined effect of the wind stress curl, seasonal stratification and bottom topography, whereas, during the cold period of the year, a whole-basin cyclonic gyre with enhanced intensity of currents in the eastern half-basin was dominating primarily governed by the wind stress curl and bottom topography.
- The anticyclonic circulation pattern in summer was confirmed by the long-term observational data (lower salinity in the western part of the gulf) during August.
- River runoff in spring proved to be a major driving force for the salinity dynamics in the UML and a substantial contributor to enhancing the strength of the stratification in summer (August). The strongest stratification in 2010 was related to the highest river runoff in spring and second largest temperature during 1993-2012.
- It is shown that the Daugava River discharge forms a freshwater plume consisting of an anticyclonic bulge and buoyant jet along the eastern coast. In summer, a substantial fraction of freshwater can be involved into the anticyclonic whole-basin circulation leading to the bimodal freshwater transport pathways.

- Multiple mesoscale features, with the horizontal scales consistent with the Rossby radius estimates, were detected. Due to the wind forcing, the coastal buoyant current and related salinity front fell into baroclinic instability and displayed meanders along the eastern coast.
- Thermohaline circulation (the no atmospheric forcing case) revealed the formation of the chain of mesoscale cyclonic eddies generated in the Irbe Strait (with a core of increased salinity/density).
- Occasionally (during summer), the intrusions with strong salinity maxima were observed in the sub-surface layer of the Gulf of Riga originating from the Baltic Proper and formed, likely, through simultaneous upwelling and downwelling events along the two opposite coasts of the Irbe Strait.
- Due to the density characteristics in the Gulf of Riga and Baltic Proper, the sub-surface salinity maxima existence/creation is feasible only in summer. Such a water exchange regime might isolate the near-bottom layer of the Gulf of Riga from the lateral flows (containing more saline and oxygen rich waters from the Baltic Proper).
- The increase of water temperature and earlier occurrence of maximum river runoff as suggested by the climate change scenarios would generate a stronger stratification conditions in the Gulf of Riga in summer which, in turn, might lead to the increase of the hypoxic areas in the bottom layers of the Gulf of Riga.

REFERENCES

Aitsam, A., Elken, J., 1982. Synoptic scale variability of hydrophysical fields in the Baltic Proper on the basis of CTD measurements. In: Nihoul, J.C.J. (ed.), Hydrodynamics of semienclosed seas. Elsevier, Amsterdam, 433-468.

Andrejev, O., Myrberg, K., Alenius, P., Lundberg, P.A., 2004. Mean circulation and water exchange in the Gulf of Finland – a study based on three-dimensional modeling. *Boreal Environment Research*, 9, 1-16.

BACC Author Team, 2008. Assessment of climate change for the Baltic Sea basin. Springer Verlag, Berlin, 35-221 pp.

BACC II Author Team, 2015. Second assessment of climate change for the Baltic Sea basin. SpringerOpen, Geesthacht, 69-263 pp.

Belzile, M., Galbraith, P.S., Bourgault, D., 2016. Water renewals in the Saguenay Fjord. *Journal of Geophysical Research*, 121(1), 638-657.

Berg, P., Poulsen, J.W., 2012. Implementation details for HBM. DMI Technical Report No. 12-11, ISSN: 1399-1388, Copenhagen.

Bergström, S., Alexandersson, H., Carlsson, B., Josefsson, W., Karlsson, K.G., Westring, G., 2001. Climate and hydrology of the Baltic basin. In: Wulff, F., Rahm, L., Larsson, P. (Eds.), A systems analysis of the Baltic Sea. Springer, Berlin, 75-112 pp.

Berzinsh, V., 1980. Interannual and seasonal changes of water salinity in the Gulf of Riga. In: Rybokhozyaistvennye issledovaniya (BaltNIIRKH), Avots, Riga, Issue 15, 3-12 pp. (in Russian).

Berzinsh, V., 1995. Hydrology. In: Ojaveer, O. (Ed.), Ecosystem of the Gulf of Riga between 1920 and 1990. Tallinn, 7-32 pp.

Blumberg, A.F., Mellor, G.L., 1983. Diagnostic and prognostic numerical calculation studies of the South Atlantic Bight. *Journal of Geophysical Research*, 88(C8), 4579-4592.

Christensen, O.-E., Kjellström, E., Zorita, E., 2015. Projected change - atmosphere. In: The BACC II Author Team (Eds.), Second Assessment of Climate Change for the Baltic Sea Basin, Regional Climate Studies. SpringerOpen, Geesthacht, 217-233 pp.

Cushman-Roisin, B., Korotenko, K.A., Galos, C.E., Dietrich, D.E., 2007. Simulation and characterization of the Adriatic Sea mesoscale variability. *Journal of Geophysical Research*, 112, C03S14, doi:10.1029/2006JC003515.

Eady, E.T., 1949. Long waves and cyclone waves. *Tellus*, 1(3), 33-52.

Elken, J., Nõmm, M., Lagemaa, P., 2011. Circulation patterns in the Gulf of Finland derived from the EOF analysis of model results. *Boreal Environment Research*, 16(A), 84-102.

Elken J., 1996. Deep water overflow, circulation and vertical exchange in the Baltic Proper. Estonian Marine Institute Report Series No. 6, Tallinn, 1-91 pp.

Ezer, T., Mellor, G.L., 1994. Diagnostic and prognostic calculations of the North Atlantic circulation and sea level using a sigma coordinate ocean model. *Journal of Geophysical Research*, 99(C7), 14159-14171.

Fedorov, K.N., 1986. The physical nature and structure of oceanic fronts. Springer Verlag, Germany, 333 pp.

Feistel, R., Nausch, G., Heene, T., Piechura, J., Hagen, E., 2004. Evidence for a warm water inflow into the Baltic Proper in summer 2003. *Oceanologia*, 46(4), 581-598.

Feistel, R., Weinreben, S., Wolf, H., Seitz, S., Spitzer, P., Adel, B., Nausch, G., Schneider, B., Wright, D.G., 2010. Density and Absolute Salinity of the Baltic Sea 2006-2009. *Ocean Science*, 6(1), 3-24.

Fennel, W., Seifert, T., Kayser, B., 1991. Rossby radii and phase speeds in the Baltic Sea. *Continental Shelf Research*, 11(1), 23-36.

Fong D.A., Geyer W.R., 2002. The alongshore transport of freshwater in a surface-trapped river plume. *Journal of Physical Oceanography*, 32(3), 957-972.

Hansson, M., Axe, P., Andersson, L., 2009. Extent of anoxia and hypoxia in the Baltic Sea, 1960-2009. SMHI Report Mo 2009-214, http://www.smhi.se/polopoly_fs/1.10354!Oxygen_timeseries_1960_20 09.pdf

HELCOM (Helsinki Commission), 2009. Eutrophication in the Baltic Sea: an integrated thematic assessment of the effects of nutrient enrichment in the Baltic Sea region. In: Baltic Sea Environment Proceedings, 115B, Helsinki Commission. 148 pp.

Horner-Devine, A.R., Fong, D.A., Monismith, S.G., 2008. Evidence for the inherent unsteadiness of a river plume: Satellite observations of the Niagara River discharge. *Limnology and Oceanography*, 53(6), 2731-2737.

Jurgensone, I., Carstensen, J., Ikauniece, A., Kalveka, B., 2011. Long-term changes and controlling factors of phytoplankton community in the Gulf of Riga (Baltic Sea). *Estuaries and Coasts*, 34(6), 1205-1219.

Jurisa, J.T., Chant, R., 2012. The coupled Hudson River estuarine-plume response to variable wind and river forcings. *Ocean Dynamics*, 62(5), 771-784.

Karimova, S., 2012. Spiral eddies in the Baltic, Black and Caspian seas as seen by satellite radar data. *Advances in Space Research*, 50(8), 1107-1124.

Kotta, J., Kotta, I., Simm, M., Põllupüü, M., 2009. Separate and interactive effects of eutrophication and climate variables on the ecosystem elements of the Gulf of Riga. *Estuarine, Coastal and Shelf Science*, 84(4), 509-518.

Kõuts, T., Håkansson, B. (Eds), 1995. Observations of water exchange, currents, sea levels and nutrients in the Gulf of Riga. SMHI RO Series No. 23, Norrköping.

Kronsell, J., Andersson, P., 2014. Total and regional runoff to the Baltic Sea. HELCOM Baltic Sea Environment Fact Sheets. Online. 11.11.2015, http://www.helcom.fi/baltic-sea-trends/environment-fact-sheets/

Laanearu, J., Lips, U., Lundberg, P., 2000. On the application of hydraulic theory to the deep-water flow through the Irbe Strait. *Journal of Marine Systems*, 25(3-4), 323-332.

Laanemets J., Väli, G., Zhurbas, V., Elken, J., Lips, I., Lips, U., 2011. Simulation of mesoscale structures and nutrient transport during summer upwelling events in the Gulf of Finland in 2006. *Boreal Environment Research*, 16(A), 15-26.

Lagemaa, P., 2012. Operational forecasting in Estonian marine waters (Ph.D. thesis). Tallinn University of Technology, TUT Press.

Lass, H.-U., Mohrholz, V., 2003. On dynamics and mixing of inflowing saltwater in the Arkona Sea. *Journal of Geophysical Research*, 108, 3042, doi: 10.1029/2002JC001465, C2.

Lehmann, A., Krauss, W., Hinrichsen, H.-H., 2002. Effects of remote and local atmospheric forcing on circulation and upwelling in the Baltic Sea. *Tellus*, 54(3), 299-316.

Lehmann, A., Myrberg, K., Höflich, K., 2012. A statistical approach to coastal upwelling in the Baltic Sea based on the analyses of satellite data for 1990-2009. *Oceanologia*, 54(3), 369-393.

Leppäranta, M., Myrberg, K., 2009. Physical Oceanography of the Baltic Sea. Praxis Publishing Ltd., Chichester, 94-98 pp.

Liblik, T., Lips, U., 2011. Characteristics and variability of the vertical thermohaline structure in the Gulf of Finland in summer. *Boreal Environment Research*, 16(suppl. A), 73-83.

Liblik, T., Lips, U., 2012. Short-term variations of thermohaline structure in the Gulf of Finland. *Ocean Science Discussions*, 9(2), 877-908.

Lilover, M.J., Lips, U., Laanearu, J., Liljebladh, B., 1998. Flow regime in the Irbe Strait. *Aquatic Sciences*, 60(3), 253-265.

Lips, U., Lilover, M.J., Raudsepp, U., Talpsepp, L., 1995. Water renewal processes and related hydrographic structures in the Gulf of Riga. In: Toompuu, A., Elken, J. (Eds.), Hydrographic studies within the Gulf of Riga Project, 1993-1994. Estonian Marine Institute, Report series, No. 1, Tallinn, 1-34 pp.

Magaldi, M.G., Özgökmen, T.M., Griffa, A., Rixen, M., 2010. On the response of a turbulent coastal buoyant current to wind events: the case of the Western Adriatic Current. *Ocean Dynamics*, 60(1), 93-122.

Männik, A., Merilain, M., 2007. Verification of different precipitation forecasts during extended winter-season in Estonia. HIRLAM Newsletter, No. 52, July 2007, 65-70.

Mellor, G.L., Yamada, T., 1982. Development of a turbulence closure model for geophysical fluid problems. *Reviews of Geophysics and Space Physics*, 20(4), 851-875.

Meier, H.E.M., 2007. Modeling the pathways and ages of inflowing salt- and freshwater in the Baltic Sea. *Estuarine, Coastal and Shelf Science*, 74(4), 610-627.

Myrberg, K., Andrejev, 2003. Main upwelling regions in the Baltic Sea – a statistical analysis based on three-dimensional modelling. *Boreal Environment Research*, 8(2), 97-112.

Mohrholz, V., Dutz, J., Kraus, G., 2006. The impact of exceptional warm summer inflow events on the environmental conditions in the Bornholm Basin. *Journal of Marine Systems*, 60(3-4), 285-301.

Omstedt, A., Axell, L.B., 2003. Modeling the variations of salinity and temperature in the large Gulfs of the Baltic Sea. *Continental Shelf Research*, 23(3-4), 265-294.

Omstedt, A., Elken, J., Lehmann, A., Leppäranta, M., Meier, H.E.M., Myrberg, K., Rutgersson, A., 2014. Progress in physical oceanography of the Baltic Sea during the 2003-2014 period. *Progress in Oceanography*, 128, 139-171.

Omstedt, A., Meuller, L., Nyberg, L., 1997. Interannual, seasonal and regional variations of precipitation and evaporation over the Baltic Sea. *Ambio*, 26(8), 484-492.

Otsmann, M., Astok, V., Suursaar, Ü., 1997. A model for water exchange between the Baltic Sea and the Gulf of Riga. *Hydrology Research*, 28(4-5), 351-364.

Otsmann, M., Suursaar, Ü., Kullas, T., 2001. The oscillatory nature of the flows in the system of straits and small semienclosed basins of the Baltic Sea. *Continental Shelf Research*, 21(15), 1577-1603.

Petrov, V.S., 1979. Water balance and water Exchange between the Gulf of Riga and the Baltic Proper. In: Sbornik rabot rizhskoj gidrometeorologicheskoj observatorii, 18, Riga, 20-40 pp. (in Russian).

Piechura, J., 2007. A mesoscale structure in the Baltic Sea deep waters. BSSC 2007 Rostock, Abstracts, p. 16. (http://www2008.io-warnemuende.de/bssc2007/ downloads/pdf/Abstract_volume_lectures.pdf).

Raudsepp, U., 2001. Interannual and seasonal temperature and salinity variations in the Gulf of Riga and corresponding saline water inflow from the Baltic Proper. *Nordic Hydrology*, 32(2), 135-160.

Raudsepp, U., Beletsky, D., Schwab, D.J., 2003. Basin-scale topographic waves in the Gulf of Riga. *Journal of Physical Oceanography*, 33, 1129-1140.

Raudsepp, U., Elken, J., 1999. Application of the Bryan-Cox-type ocean model to reproduce synoptic and mesoscale variability of the Irbe Strait salinity front. *German Journal of Hydrography*, 51(4), 477-488.

Raudsepp, U., Toompuu, A., Kõuts, T., 1999. A stochastic model for the sea level in the Estonian coastal area. *Journal of Marine Systems*, 22(1), 69-87.

Reißmann, J.H., 2005. An algorithm to detect isolated anomalies in three-dimensional stratified data fields with an application to density fields

from four deep basins of the Baltic Sea. *Journal of Geophysical Research*, 110, C12018, doi:10.1029/2005JC002885.

Reißmann, J.H., 2006. On the representation of regional characteristics by hydrographic measurements at central stations in four deep basins of the Baltic Sea. *Ocean Science*, 2, 71-86.

Schwab, D.J., Beletsky, D., 2003. Relative effects of wind stress curl, topography, and stratification on large-scale circulation in Lake Michigan. *Journal of Geophysical Research*, 108(C2), 3044, doi:10.1029/2001JC001066.

Seifert, T., Kayser, B., 1995. A high resolution spherical grid topography of the Baltic Sea. Meereswissenschaftliche Berichte (Marine Science Reports), No. 9, 72-88.

Seppälä, J., Balode, M., 1999. Spatial distribution of phytoplankton in the Gulf of Riga during spring and summer stages. *Journal of Marine Systems*, 23(1), 51-67.

Siegel, H., Gerth, M., Tschersich, G., 2006. Sea surface temperature development of the Baltic Sea in the period 1990-2004. *Oceanologia*, 48(S), 119-131.

Skogen, M.D., Eilola, K., Hansen, J.L.S., Meier, H.E.M., Molchanov, M.S., Ryabchenko, V.A., 2014. Eutrophication status of the North Sea, Skagerrak, Kattegat and the Baltic Sea in present and future climates: A model study. *Journal of Marine Systems*, 132, 174-184.

Soomere, T., Delpeche, N., Viikmäe, B., Quak, E., Meier, H.E.M., Döös, K., 2011. Patterns of current-induced transport in the surface layer of the Gulf of Finland. *Boreal Environment Research*, 16(A), 49-63.

Soosaar, E., Maljutenko, I., Raudsepp, U., Elken, J., 2014. An investigation of anticyclonic circulation in the southern Gulf of Riga during the spring period. *Continental Shelf Research*, 78, 75-84.

Soosaar, E., Maljutenko, I., Uiboupin, R., Skudra, M., Raudsepp, U., 2016. River bulge evolution and dynamics in a non-tidal sea – Daugava River plume in the Gulf of Riga, Baltic Sea. *Ocean Science*, 12(2), 417-432.

Stiebrins, O., Väling, P., 1996. Bottom sediments of the Gulf of Riga. Geological survey of Latvia, Riga, 4 pp.

Stipa, T., Tamminen, T., Seppälä, J., 1999. On the creation and maintenance of stratification in the Gulf of Riga. *Journal of Marine Systems*, 23(1-3), 27-49.

Suhhova, I., Pavelson, J., Lagemaa, P., 2015. Variability of currents over the southern slope of the Gulf of Finland. *Oceanologia*, 57(2), 132-143.

Suursaar, Ü., Kullas, T., Otsmann, M., 2002. A model study of the sea level variations in the Gulf of Riga and the Väinameri Sea. *Continental Shelf Research*, 22(14), 2001-2019.

Yankovsky, A.E., Chapman, D.C., 1997. A simple theory for the fate of buoyant coastal discharges. *Journal of Physical Oceanography*, 27(7), 1386-1401.

Zhurbas, V., Laanemets, J., Vahtera, E., 2008. Modeling of the mesoscale structure of coupled upwelling/downwelling events and the related input of nutrients to the upper mixed layer in the Gulf of Finland, Baltic Sea. *Journal of Geophysical Research*, 113, C05004, doi:10.1029/2007JC004280.

Zhurbas, V., Oh, I.S., Park, T., 2006. Formation and decay of a longshore baroclinic jet associated with transient coastal upwelling and downwelling: A numerical study with applications to the Baltic Sea. *Journal of Geophysical Research*, 111, C04014, doi:10.1029/2005JC003079.

Zhurbas, V.M., Paka, V.T., 1997. Mesoscale thermohaline variability in the Eastern Gotland Basin following the 1993 major Baltic inflow. *Journal of Geophysical Research*, 102(C9), 20917-20926, doi:10.1029/97JC00443.

PUBLICATIONS

Paper I

Skudra, M., Lips, U. (2016). Characteristics and inter-annual changes in temperature, salinity and density distribution in the Gulf of Riga. *Oceanologia*, in press, doi: 10.1016/j.oceano.2016.07.001.

ORIGINAL RESEARCH ARTICLE

Characteristics and inter-annual changes in temperature, salinity and density distribution in the Gulf of Riga

Maris Skudra [a,b,*], Urmas Lips [a]

[a] Marine Systems Institute, Tallinn University of Technology, Tallinn, Estonia
[b] Latvian Institute of Aquatic Ecology, Riga, Latvia

Summary   Available CTD profiles from the Gulf of Riga (May—August, 1993—2012) were analyzed to study inter-annual and long-term changes in temperature, salinity and density in relation to river runoff and atmospheric forcing (e.g. Baltic Sea Index). To describe temporal changes in vertical stratification, the upper mixed layer (UML) and deep layer (DL) parameters were estimated. On average the UML depth increases from 8.7 m in May to 9.0, 11.5 and 13.7 m in June, July and August, respectively, and the UML temperature increases from 8.0°C to 12.5, 18.7 and 18.6°C (May, June, July and August) while the UML salinity increases from 4.90 g kg^{-1} to 5.14, 5.28 and 5.38 g kg^{-1}, respectively. High correlation ($r = -0.82$) was found between the inter-annual changes in river runoff (spring) and mean salinity in the UML in August as well as between DL mean salinity ($r = 0.88$) and density ($r = 0.84$) in the Irbe Strait and DL mean salinity and density in the Gulf of Riga. Inter-annual changes in the UML depth as well as in DL salinity and density had a significant correlation with the changes in Baltic Sea Index. The strongest stratification (August) can be observed in the years with the highest UML temperature and the highest river run-off in spring. We suggest that the predicted increase in water temperature and changes in river run-off due to the climate change would result in faster development of the seasonal thermocline in spring and stronger vertical stratification in summer.
© 2016 Institute of Oceanology of the Polish Academy of Sciences. Production and hosting by Elsevier Sp. z o.o. This is an open access article under the CC BY-NC-ND license (http://creativecommons.org/licenses/by-nc-nd/4.0/).

* Corresponding author at: Marine Systems Institute, Tallinn University of Technology, Akadeemia Rd. 15A, 12618 Tallinn, Estonia. Tel.: +371 28740641; fax: +372 620 4301.
    E-mail address: maris.skudra@msi.ttu.ee (M. Skudra).

1. Introduction

The Gulf of Riga (GoR) is a relatively closed basin in the eastern part of the Baltic Sea with surface area of 17,913 km^2 and volume 405 km^3 (Leppäranta and Myrberg, 2009). It has two openings — the Irbe Strait (sill depth of 25 m and cross-section of 0.4 km^2) in the western part and the Suur Strait (sill depth of 5 m and cross-section of 0.04 km^2) in the northern part of the gulf with 70—80% (Petrov, 1979) of the water exchange occurring through the Irbe Strait. The mean depth of the GoR is 26 m which is about two times less than in the Baltic Sea. The deepest regions of the gulf are situated to the east and southeast from Ruhnu Island where depth reaches about 56 m, although, the deepest spot in the whole GoR is Mersraga Trough (width about 50 m and length 4.5 km) with the depth of 66 m (Stiebrins and Väling, 1996) situated approximately 13 km to the north from the village of Mersrags.

The catchment area of the GoR consists of 134,000 km^2 with five major rivers discharging into the GoR — Daugava, Lielupe, Gauja, Pärnu and Salaca. First three are located in the southern part of the gulf where approximately 86% of all river run-off occurs (Berzinsh, 1995) and latter two in the eastern part. Annual mean run-off to the gulf in 1950—2012 has been stated as 1013.5 $m^3 s^{-1}$ (Kronsell and Andersson, 2014) or approximately 32 km^3 which is about 7.9% of the volume of the gulf. It has been showed that river run-off together with the limited water exchange are the main reasons for the observed horizontal salinity difference in the surface layer — salinity decreases from the Irbe Strait to the southern part of the gulf (see e.g. Berzinsh, 1980, 1995; Stipa et al., 1999). The strongest difference can be observed in April and May when the influence of the river discharge is at its maximum and salinity decreases from about 6.0 PSU (Practical Salinity Scale) in the Irbe Strait to 2.0 PSU and less close to the mouths of Daugava and Lielupe. Slight surface salinity difference (about 1.0—1.5 PSU) can be observed also across the gulf from west to east during April (Stipa et al., 1999).

Water temperature in the GoR has a seasonal pattern — during November—February cooling of the whole water column occurs, March—April marks the start of the water column warming from surface layers which intensifies and reaches maximum during May—August and is again followed by a steady cooling during September—October. Data analysis during 1963—1990 revealed that mean temperature for the whole water column in winter, spring, summer and autumn was 0.0, 2.8, 12.0 and 9.0°C, respectively (Berzinsh, 1995). It was reported (Raudsepp, 2001) that seasonal changes in thermal stratification are consistent with the annual cycle of air-sea heat exchange. Due to these seasonal characteristics the whole water column in the GoR is thermally well mixed during December—March, whereas, seasonal thermocline starts to develop in April and the strongest stratification can be observed in August. More detailed analysis on stratification in the GoR is described in the research by Stipa et al. (1999).

According to the previous studies (Berzinsh, 1980, 1995) there have been two periods with opposite tendencies regarding salinity — from beginning of 1960s till 1977 average salinity increased (average rate of 0.035 PSU per year), whereas, from 1977 till early 1990s salinity decreased

(0.041 PSU per year) which was mainly related to the dynamics of long-term river run-off. Similar decline of salinity was also observed within different layers (expressed as mean values at 0, 10, 20, 30, 40 and 50 m) of the GoR (Raudsepp, 2001). Remote sensing data for 1990—2008 has showed a strong increase of the sea surface temperature (SST) in the GoR — about 0.8—1.0°C per decade with similar or slightly higher values only in the Gulf of Finland and Bothnian Bay (BACC, 2015). Long-term changes in both, temperature and salinity, not only influence the physical characteristics of the GoR but they can have an impact to the whole ecosystem of the gulf. For example, Jurgensone et al. (2011) reported that the temperature increase would affect the phytoplankton community in the GoR suggesting a shift from dinoflagellates to chlorophytes in summer. Kotta et al. (2009) stated that the reduction in salinity had negative consequences for most of the benthic invertebrate species referring to their salinity tolerance. In general, the dynamics of zooplankton, zoobenthos and fish in the GoR primarily relies on climatic conditions.

The main goal of the present study was to describe the vertical characteristics of temperature, salinity and density fields and their inter-annual variability in the GoR based on the CTD data collected during 1993—2012 (May—August) as well as possible connection of revealed changes with different forcing factors. Previous studies have mainly focused on short-term analysis of temperature and salinity data (Kõuts and Håkansson, 1995; Stipa et al., 1999) and/or covered only the time period until 1995 (Raudsepp, 2001). In addition, present research aimed to estimate the baroclinic Rossby radius on the basis of the existing CTD profiles with a similar approach as used by Alenius et al. (2003) for the Gulf of Finland. Based on the results of this analysis and taking into account the latest climate change predictions we also suggest what could happen in the future.

2. Material and methods

Present paper analyzed the CTD data collected in 1993—2012 during various monitoring programmes and research projects conducted by Latvian Institute of Aquatic Ecology, Marine Systems Institute at Tallinn University of Technology and Institute of Food Safety, Animal Health and Environment (Latvia) and their predecessors. Vertical profiles of different parameters were acquired with following CTD profilers — AROP 500, SBE 19plus SeaCAT, SBE 19 SeaCAT, Neil Brown Mark III and Idronaut OS320plus.

In total 3558 CTD casts were processed and 863 CTD casts were used in the present study from the period of May—August, 1993—2012 with Gulf of Riga borders set along 58°N latitude and 22.6°E longitude (Fig. 1). CTD profiles were processed and analyzed with vertical resolution of 0.5 m (constant for all profiles) and only stations with depth over 20 m were used. Availability of CTD profiles differed widely between the years and months (Table 1).

Upper mixed layer (UML) depth was estimated using smoothed (2.5 m moving average) vertical profiles of density and the UML depth was defined at each vertical profile as the shallowest depth where the density difference between consecutive data points was equal or exceeded 0.05 $kg m^{-3}$. The latter value was derived empirically as a value which best reflects the start of pycnocline and, thus,

Table 1 The available CTD casts by year and month.

Year	May	June	July	August	Total
1993	15	—	—	11	26
1994	6	5	10	12	33
1995	19	17	15	15	66
1996	15	—	—	3	18
1997	—	3	—	—	3
1998	4	3	—	12	19
1999	2	—	9	—	11
2000	—	—	—	18	18
2001	29	—	8	20	57
2002	31	7	17	19	74
2003	31	9	10	30	80
2004	23	5	3	13	44
2005	11	9	—	12	32
2006	14	—	10	18	42
2007	29	—	17	23	69
2008	31	4	6	9	50
2009	28	—	3	24	55
2010	40	—	6	31	77
2011	20	—	6	15	41
2012	7	10	5	26	48
Total	355	72	125	311	863

obtained only from profiles deeper than 35 m. The salinity in the present study was expressed as absolute salinity [g kg^{-1}] and derived from CTD measured salinity values (on Practical Salinity Scale) using freely available software "Ocean Data View" (Schlitzer, 2010) and following TEOS-10 (Thermodynamic Equation Of Seawater — 2010) guidelines and Feistel et al. (2010).

River run-off data were calculated from monthly mean flow rates [m^3 s^{-1}] of four biggest rivers in Latvia discharging into the Gulf of Riga — Daugava, Gauja, Lielupe and Salaca (data provided by Latvian Environment, Geology and Meteorology Centre). The mouths of Daugava, Gauja and Lielupe are located in southern part, whereas, the mouth of Salaca in eastern part of the Gulf of Riga.

Available wind data were acquired from Sõrve (1995—2012), Ruhnu (2003—2012), Kihnu (1993—2011) and Pärnu (1993—2012) meteorological stations provided by Estonian Environment Agency. To characterize the atmospheric forcing conditions over the Gulf of Riga we analyzed the monthly-averaged Baltic Sea Index (BSI), which is the difference of normalized sea level pressures between Szczecin in Poland and Oslo in Norway (Lehmann et al., 2002; values provided by Andreas Lehmann).

Mean values of studied CTD parameters in May—August were estimated at the beginning as a simple arithmetic means of every month in each year. These values were further used to obtain the monthly mean values for the whole research period of 1993—2012 from which finally one mean value was derived for each parameter. For more detailed CTD parameter analyses we used only data from May and August and only those monthly mean values where available amount of CTD casts was equal or exceeded 5 casts in a month.
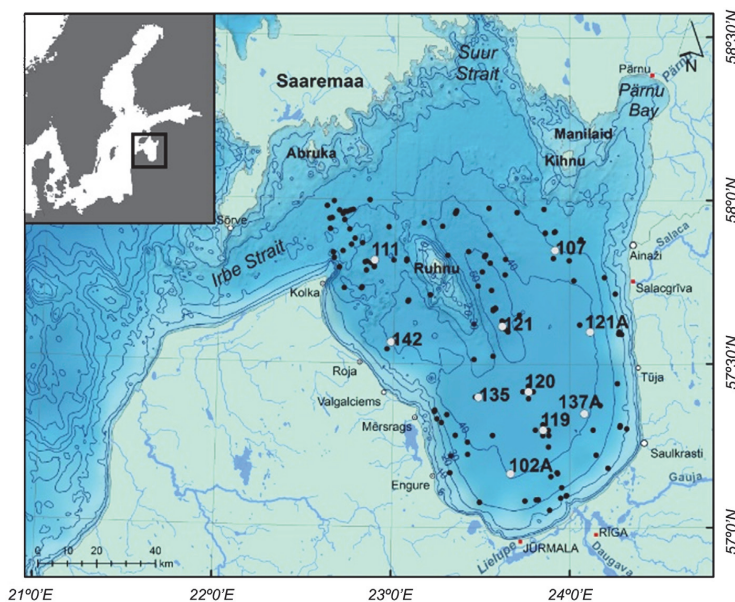
the depth of UML. Smoothed vertical profiles of density were used to avoid possible fluctuations which might mislead the correct distinction of the UML by exceeding the selected density difference (0.05 kg m^{-3}) between consecutive data points. Deep layer (DL) was defined as a layer with depth >35 m and all estimated parameter characteristics of DL were

Figure 1 Bathymetric map of the Gulf of Riga with CTD cast locations indicated with black dots (all stations) and white dots (10 main stations with station labels).

Rossby radius was calculated numerically solving eigen-value problem using Runge—Kutta scheme combined with trial-and-error approach. See Chelton et al. (1998) for more detailed information about definition and calculation of Rossby radius.

In order to analyze the dynamics of various parameters in different parts of the GoR ten "main" stations (102A, 135, 142, 111, 119, 120, 121, 137A, 121A, 107) were chosen determined by the data availability from these stations (Fig. 1).

3. Results

3.1. Upper mixed layer

From analyzed 863 CTD casts we were able to define UML in 533 of them. Regarding monthly distribution of defined UML, from 356 CTD casts in May we defined UML in 133 (37%) of them and from 75 (June), 125 (July) and 311 (August) casts we defined UML in 35 (48%), 98 (78%) and 267 (85%) of them, respectively.

The mean UML depth derived from all available CTD casts in the Gulf of Riga in the period of 1993—2012 (May—August) was 10.7 m. The shallowest mean UML depth in the research period was found in May (8.7 m), it was deeper in June (9.0 m) and July (11.5 m) but the deepest UML was detected in August (13.7 m) (Fig. 2).

The UML mean salinity and temperature in the whole period were 5.17 g kg^{-1} and 14.5°C, whereas density (expressed as sigma-t which is seawater density, where density value of 1000 kg m^{-3} has been subtracted) — 2.95 kg m^{-3}. Salinity and temperature increased from 4.90 g kg^{-1} and 8.0°C in May to 5.14 g kg^{-1} and 12.5°C in June, to 5.28 g kg^{-1} and 18.7°C in July and 5.38 g kg^{-1} and 18.6°C in August, respectively. Mean UML density in May, June, July and August was 3.59, 3.32, 2.39 and 2.48 kg m^{-3}, respectively (Fig. 2).

3.1.1. August
Greater amount of CTD casts in August allowed us to make more detailed inter-annual and long-term analysis of UML characteristics and suggest probable factors which may have impact on different UML parameters. The mean vertical

structure of salinity in the GoR during 1993—2012 showed that salinity was about 5.3 g kg^{-1} at the surface and around 6.0 g kg^{-1} in the bottom layer, whereas, the mean vertical structure of temperature showed typical two-layer formation with thermocline situated approximately at 10—30 m depth (Fig. 3).

During the period of 1993—2012, the UML mean depth varied between different parts (10 main stations) of the GoR. Results showed that the UML mean depth was shallower in the western (W) part of the gulf ranging between 12.3 and 13.3 m (stations 111, 142, 135 and 102A), whereas, in the eastern (E) part the UML mean depth was deeper ranging between 14.6 and 15.4 m (stations 107, 121A and 137A). When looking at the section from the W to the E part of the GoR (stations 142-121-121A), an increase of the UML mean depth (start of the thermocline) can be observed (12.3, 14.2 and 14.6 m, respectively), thus, suggesting occurrence of differences between the two coastal areas in the gulf. The UML mean salinity also varied spatially during the research period. Results from 10 main stations revealed that on average the UML mean salinity was higher in the E part of the GoR (5.53, 5.42 and 5.37 g kg^{-1} at stations 107, 121A and 137A, respectively) and slightly lower values were observed in the W part of the gulf (5.36, 5.31, 5.31 and 5.29 g kg^{-1} at stations 111, 142, 135 and 102A, respectively). As expected, the UML mean salinity decreased towards the southern (S) part of the GoR where influence of river run-off is more pronounced than in the northern (N) part of the gulf.

The inter-annual variations of UML mean depth, temperature, salinity and density in August were noticeable but no clear tendency or trend could be detected in the period 1993—2012 (Fig. 4). Results from years 1993, 1994 and 2008 should be regarded with caution regarding the mean conditions in the gulf because of spatial distribution of stations in these years — in 1993 and 1994 the data only from the N and northwestern (NW) part and in 2008 only from the S part of the Gulf of Riga were available. This circumstance might explain rather big peaks in 1993 (UML mean depth) and 1994 (UML mean depth, temperature, density). Apart from that, the UML mean depth varied mainly between 10 and 20 m in the whole study period. Regarding the mean salinity, temperature and density, years 2003, 2006 and 2010 stand out from the whole period of inter-annual variability. Two salinity peaks were observed in 2003 (5.58 g kg^{-1})
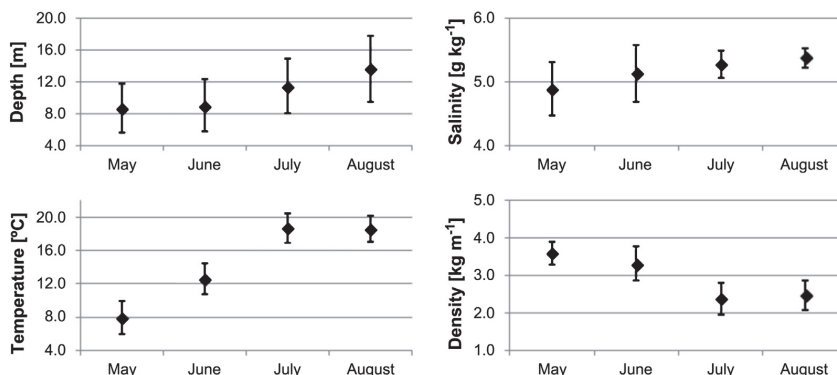

Figure 2   Mean characteristics of upper mixed layer between 1993 and 2012 (May—August) with standard deviations.
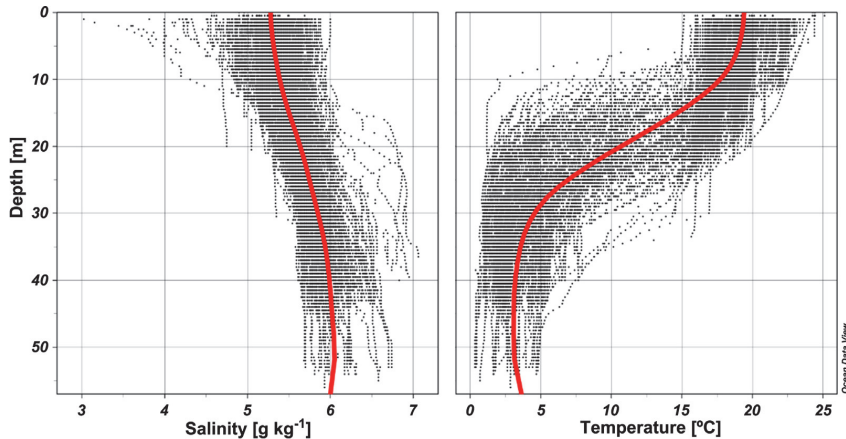
Figure 3 Scatter plot of vertical profiles of salinity and temperature in August, 1993—2012. The red line represents the mean vertical profile for the whole period. (For interpretation of the references to colour in this figure legend, the reader is referred to the web version of this article.)
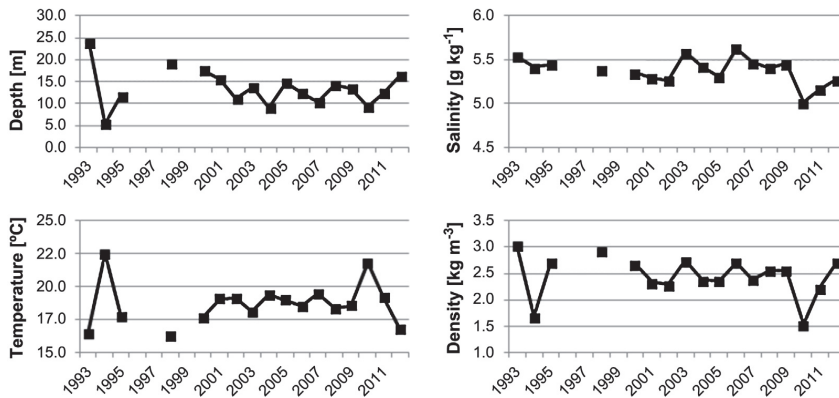

Figure 4 Inter-annual variability of mean characteristics of upper mixed layer in August, 1993—2012.

and 2006 (5.63 g kg⁻¹), respectively. However, year 2010 stood out as a year with the lowest salinity (5.01 g kg⁻¹) and density (1.53 kg m⁻³) as well as with the second largest UML mean temperature (21.8°C) in the whole period. In addition, correlation was found between the UML mean temperature and UML mean depth ($r = -0.84$, $n = 17$, $p < 0.05$). Correlation remained significant (r values ranging from -0.58 to -0.8, $p < 0.05$) throughout the GoR when looking at specific parts (ten main stations).

A rather high correlation ($r = -0.66$, $n = 17$, $p < 0.05$) during 1993—2012 was found between the UML mean salinity (August) and mean river run-off in spring (March—May). Correlation increased even more ($r = -0.82$, $n = 14$, $p < 0.05$) when years 1993, 1994 and 2008 were taken out of calculations due to the insufficient data in regard of their spatial distribution. The above mentioned correlation remained high almost throughout the whole GoR when looking at specific parts/stations (Table 2) — the highest correlation was found in the S and southwestern (SW) part of the GoR at stations 119 ($r = -0.85$, $n = 13$, $p < 0.05$), 102A ($r = -0.80$,

$n = 15$, $p < 0.05$) and 135 ($r = -0.81$, $n = 13$, $p < 0.05$), respectively. The lowest correlation was found in the E part of GoR at the stations 137A ($r = -0.66$, $n = 15$, $p < 0.05$), 121A ($r = -0.63$, $n = 14$, $p < 0.05$) and 107 ($r = -0.49$, $n = 14$, $p > 0.05$), respectively, with correlation decreasing further away from the S part of the GoR. A remarkably high correlation was still observed at the stations 121 ($r = -0.77$, $n = 17$, $p < 0.05$), 142 ($r = -0.77$, $n = 14$, $p < 0.05$) and 111 ($r = -0.76$, $n = 18$, $p < 0.05$), respectively, despite being relatively far away from the freshwater sources mostly located in the S part of the GoR.

The estimated UML parameters in August were correlated with the Baltic Sea Index and significant correlation was found between inter-annual changes of the UML mean depth and BSI in 1993—2012. The best correlation ($r = 0.71$, $n = 14$, $p < 0.05$) was found using mean BSI values from the period of June—August and excluding years 1993, 1994 and 2008 from the calculations as it was done before. Correlation was somewhat scattered when looking at specific parts/stations of the GoR (Table 2) — the highest correlation was found along

Table 2 Correlation between the upper mixed layer characteristics and various forcing factors in the Gulf of Riga during 1993—2012. Bold numbers indicate significant correlation ($p < 0.05$), n shows the number of years used in the analysis and "All stations" row shows the correlation between the average upper mixed layer characteristics over all stations and forcing factors.

Station	n	UML salinity (August) and river runoff (March—May)	UML depth (August) and Baltic Sea Index (June—August)	UML depth (August) and wind speed (August)
111	18	**−0.76**	**0.71**	**0.64**
142	14	**−0.77**	0.43	0.51
135	13	**−0.81**	**0.88**	0.37
102A	15	**−0.80**	**0.74**	0.51
119	13	**−0.85**	**0.56**	0.34
120	13	**−0.71**	0.18	0.13
121	17	**−0.77**	0.41	0.37
137A	15	**−0.66**	0.40	0.41
121A	14	**−0.63**	**0.66**	**0.56**
107	14	**−0.49**	**0.55**	0.01
All stations	14	**−0.63**	**0.71**	**0.59**

SW and W part of the GoR at stations 102A ($r = 0.74$, $n = 15$, $p < 0.05$), 135 ($r = 0.88$, $n = 13$, $p < 0.05$) and 111 ($r = 0.71$, $n = 18$, $p < 0.05$), respectively. Lower correlation was obtained at stations 107 ($r = 0.55$, $n = 14$, $p < 0.05$) and 121A ($r = 0.66$, $n = 14$, $p < 0.05$) in the E part of the GoR and at station 119 ($r = 0.56$, $n = 13$, $p < 0.05$) in the S part of the gulf but no significant correlation was found in the remaining stations — 137A, 120, 121 and 142. In addition, a probable link between the UML mean depth and wind speed (measured at the Sõrve meteorological station) was searched from the same period. Significant correlation was found ($r = 0.59$, $n = 14$, $p < 0.05$) between the UML mean depth in August and average wind speed (August). However, if we look at the specific parts/stations of the GoR then significant correlation was obtained only at two stations — 111 ($r = 0.64$, $n = 16$, $p < 0.05$) in the NW part and 121A ($r = 0.56$, $n = 14$, $p < 0.05$) in the E part of the GoR (Table 2).

3.2. Deep layer

Altogether, 558 CTD casts during the period of May—August, 1993—2012 with depth >35 m were available for deep layer analysis. The mean salinity, temperature and density derived for the whole period was 5.99 g kg^{-1}, 2.2°C and 4.68 kg m^{-3}, respectively.

Monthly mean salinity and density for the whole period showed negligible variations in the DL during May—August when the mean salinity and density fluctuated only by 0.06 g kg^{-1} and 0.04 kg m^{-3} between the months. Monthly mean DL temperature increased steadily from 1.4°C (May) to 1.9°C (June), 2.5°C (July) and 3.0°C (August), respectively (Fig. 5).

Greater amount of CTD casts in May and August allowed us to make more detailed inter-annual and long-term analysis about DL characteristics. Similarly to UML dynamics, inter-annual variations of mean temperature, salinity and density were evident but no clear tendency or trend could be detected in May or August during the period of 1993—2012 (Fig. 6). Results from years 1993 (stations only in NW part) in May and 1993, 1994 and 2008 in August should be regarded with caution regarding the mean conditions in the gulf because of spatial distribution of stations in these years (see Section 3.1.1). This might explain rather big salinity peak in 1994 (August). Apart from 1994, the peaks of DL mean salinity in August, 2006 and 2010 coincided well with similar peaks in May (seen also in density), whereas, the salinity peak
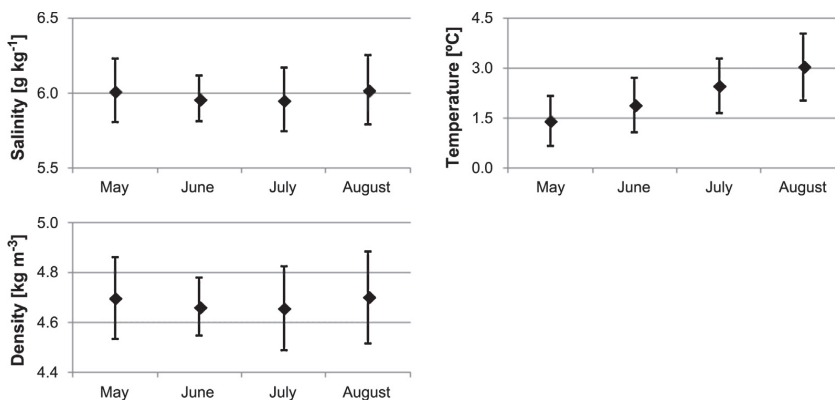

Figure 5 Mean characteristics of deep layer between 1993 and 2012 (May—August) with standard deviations.
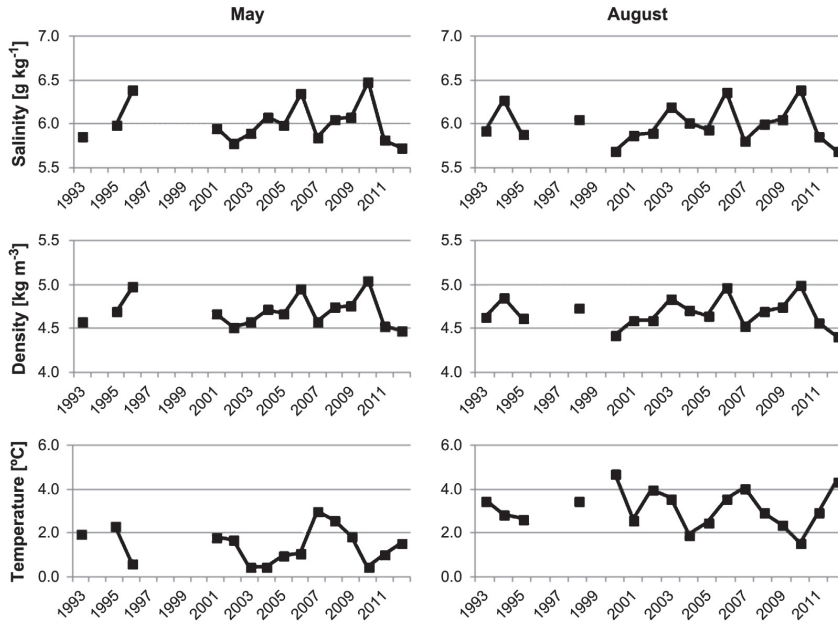
Figure 6 Inter-annual variability of mean characteristics of deep layer in May (left column) and August (right column), 1993—2012.

in 2003 was more pronounced in August (6.20 g kg^{-1}) than in May (5.89 g kg^{-1}) suggesting of more saline water inflow sometime between May and August. In May 1996 the second largest (6.40 g kg^{-1}) mean salinity was observed from the whole study period, whereas, in August only data from one station (121) was available with mean salinity of 6.46 g kg^{-1}.

As majority of water exchange between the GoR and Baltic Sea takes place through the Irbe Strait a possible connection was expected between DL characteristics in the Irbe Strait and DL in the GoR. High correlation ($r = 0.88$, $n = 12$, $p < 0.05$) during 1993—2012 was found in August between DL mean salinity in the Irbe Strait and DL mean salinity in the GoR. Similar correlation ($r = 0.84$, $n = 12$, $p < 0.05$) was observed regarding the DL mean density in both locations. Correlation between the previously mentioned DL mean salinity in the Irbe Strait and GoR was slightly different when looking at specific parts/stations of the GoR — the highest correlation was observed at the stations near the Irbe Strait and along the W coast of the gulf (stations 111, 142 and 135 with $r = 0.94$, 0.95 and 0.93, respectively, $p < 0.05$). Towards the S and southeastern (SE) part of the GoR correlation steadily decreased ($r = 0.83$, 0.76 and 0.71 at stations 102A, 119 and 137A, respectively, $p < 0.05$) whereas correlation was even lower in the central and E part of the gulf (stations 120, 121 and 121A with $r = 0.68$, 0.49 and 0.59, respectively, correlation not being significant at latter 2 stations). Analyzing all the data from May, the previously described connection between the DL mean parameters in the Irbe Strait and GoR was not significant regarding salinity and density. Nevertheless, when looking at specific stations significant correlation was still observed regarding salinity at 2 stations closest to the Irbe strait (111 and 142 with $r = 0.70$ and 0.67, respectively, $n = 10$, $p < 0.05$). Regarding

density, the correlation was significant ($r = 0.72$, $n = 10$, $p < 0.05$) only at station 111.

The DL characteristic parameters in May and August were also correlated with the Baltic Sea Index. As expected, neither in May nor in August significant correlation was detected between BSI and any parameter characterizing DL when analyzing mean values from the whole GoR. Nevertheless, at some occasions in May the correlation was evident when using BSI averaged over May and March—May. In both cases significant negative correlation was found in S part of the gulf (station 119) between BSI (May and March—May) and salinity ($r = -0.55$ and -0.61, respectively) as well as density ($r = -0.58$ and -0.65, respectively, $n = 16$, $p < 0.05$). Similar negative correlation was observed at station 137A between averaged BSI (March—May) and salinity as well as density ($r = -0.57$ and -0.59, respectively). This negative correlation tendency between BSI and salinity and density was evident in other stations as well, although, it was not significant ($p > 0.05$).

3.3. Vertical stratification in August

Inter-annual and long-term variability of different parameters in May and August was analyzed in previous sections. To study the vertical stratification and its variability we used the month of August which had the best data coverage during the whole study period (Fig. 7). The average salinity, density (sigma-t) and temperature difference between the UML and DL during 1993—2012 was 0.62 g kg^{-1}, 2.22 kg m^{-3} and 15.5°C, respectively. Year 2010 remarkably stood out as a year where difference between the UML and DL characteristics was the greatest — difference in salinity, density and
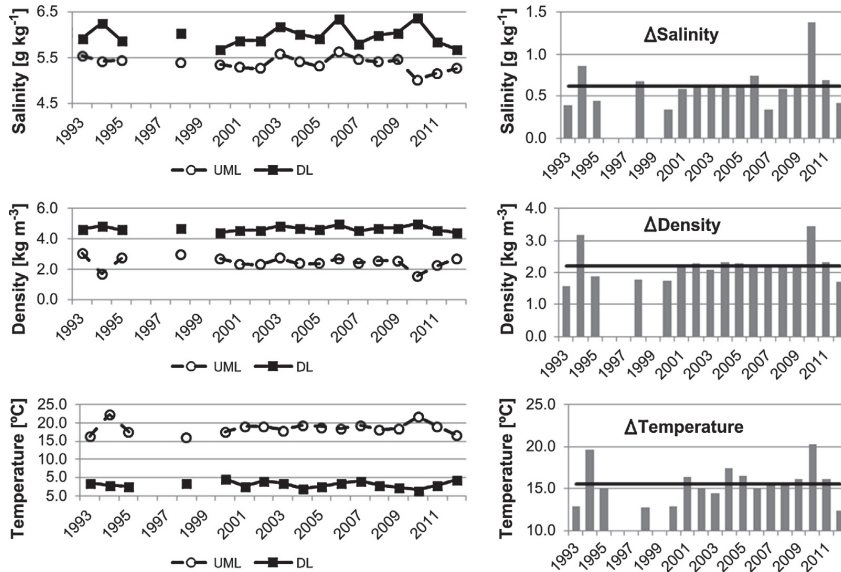
Figure 7   Mean salinity, density (sigma-t) and temperature in the upper mixed layer and deep layer in August 1993—2012 (left column) and their differences between the two layers (right column). Differences are given as deep layer minus upper mixed layer for salinity and density, and opposite for temperature; solid line represents the mean difference during 1993—2012.

temperature was 1.38 g kg^{-1}, 3.46 kg m^{-3} and 20.2°C, respectively. Salinity in the UML was the lowest (5.01 g kg^{-1}), whereas, in DL the highest (6.39 g kg^{-1}) from the whole period. Similar situation was observed regarding density — UML was characterized with the lowest (1.53 kg m^{-3}) and DL with the highest density (4.99 kg m^{-3}) in the whole period. The lowest DL mean temperature (1.6°C) was also observed in 2010 but the highest UML mean temperature (22.5°C) was observed in 1994 with the UML mean temperature in 2010 slightly lower at 21.8°C. In 1994 there was also observed rather high difference in mean salinity and density between UML and DL but this result should be treated with caution as in 1994 the data was available only from the N and NW part of the GoR.

Baltic Sea Index and river run-off was used to see whether any correlation could be found between the inter-annual changes of vertical stratification (expressed as salinity difference (ΔS) and density difference (ΔD) between the DL and UML and temperature difference (ΔT) between the UML and DL) and forcing factors. Results showed that there was no significant correlation between BSI mean values (values from August, June—August and July—August were tested) and any mentioned parameters (ΔS, ΔD and ΔT). On contrary, significant positive correlation was found between the river run-off in spring and corresponding ΔS, ΔD and ΔT with coefficient $r = 0.52$, 0.62 and 0.65, respectively ($n = 17$, $p < 0.05$).

3.4. Rossby radius

To estimate the characteristic values of Rossby radius in the GoR and, thus, corresponding scales of mesoscale features (eddies etc.) and to see whether there are some trends evident, we calculated Rossby radius in May and August using all available CTD profiles from ten main stations during 1993—2012.

The overall mean Rossby radius in May was roughly 2 times less than in August — 1.6 and 3.2 km, respectively. Inter-annual variability of mean Rossby radius was characteristic for both months but no conclusive trend could be observed in neither of them (Fig. 8). Although in August, in the beginning of 1990s the two lowest values of Rossby radius were observed (1993 and 1996), data only from 3 out of 10 stations were available and, thus, these results should be treated with caution. Similar situation was in August 1994 and in May 1993, 1994, 1998 and 1999. Nevertheless, August 2001, 2005 and 2010 stood out as years with the highest Rossby radius with values exceeding 3.5 km, whereas, in May, on the contrary, the lowest Rossby values in 2003 (0.9 km) and 2007 (1.2 km) were more distinguishable from the whole period.

During 1993—2012 the mean Rossby radius in May varied from 0.9—1.9 km, whereas, in August from 2.2—3.9 km. Although the mean Rossby radius is definitely higher in August than in May also some similarities and differences can be detected when looking at the spatial distribution of mean
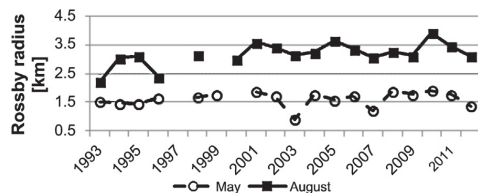

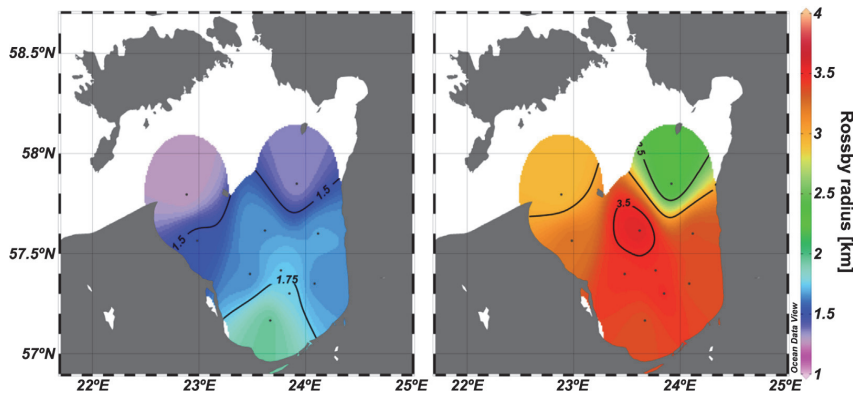**Figure 8**   Mean Rossby radius in May and August during 1993—2012.

Figure 9   Mean Rossby radius in May (left) and August (right) at 10 main stations in the Gulf of Riga during 1993—2012.

Rossby radius in both months (Fig. 9). The lowest mean Rossby radius values can be observed at stations 111, 142 and 107 in both months — 1.3, 1.5 and 1.3 in May and 2.9, 3.2 and 2.3 km in August, respectively. In May the highest mean Rossby radius values can be seen in the S part of the GoR at stations 102A and 119 (2.0 and 1.8 km, respectively), whereas, in August the maximum value was found in the central part of the gulf at station 121 (3.6 km). In August the mean Rossby radius in the E part (3.4 km at stations 121A and 137A) and SW part (3.4 km at station 102A) was also somewhat lower (0.1 km on average) than at other stations situated more in the central (120 and 119) part of the GoR.

4. Discussion

Estimation of UML depth from CTD profiles, to our knowledge, has not been done before in the GoR with similar approach as in the present study. Although Stipa et al. (1999) and Tamminen and Seppälä (1999) concluded before that mixed layer depth increases from spring to late summer, both studies relied on the data from 4 surveys during 1993—1995 and referred to the data from one section when talking about mixed layer depth. Consequently, we needed to compare our findings with some other regions than GoR. Resembling research in the Gulf of Finland (GoF) by Liblik and Lips (2011) using CTD profiles and analyzing the vertical structure of the water column showed that the UML mean depth in the GoF (12.8 m) during 1987—2008 (June—August) is about 1.4 m deeper than in our findings about the GoR (using also June—August). The UML mean salinity in the GoR during 1993—2012 (May—August) was practically identical to those findings in the GoF (although they used Practical Salinity Scale as opposed to Absolute Salinity in our case), whereas, the UML mean temperature in June, July and August was about 0.7—1.8°C higher in the GoR, probably, due to the fact that the GoR is a shallower water basin accumulating and releasing the heat more rapidly. If the UML characteristics are quite similar in both water basins mentioned before, then substantial differences can be seen in the DL characteristics, mainly, due to the fact that both water basins are hydrographically diverse — GoR is a rather shallow, semi-enclosed sub-basin of the Baltic Sea as opposed to the GoF which is much more deeper and has an open access to the Baltic Sea.

Thus, the DL mean salinity is about 2.5 g kg^{-1} higher in the GoF than in the GoR and mean temperature is lowest in the cold intermediate layer (as opposed to the DL) which, on the other hand, is not typical in the GoR where the lowest temperatures occur in the DL itself.

Analyzing the temperature and salinity values in the GoR at standard depths from 1973—1995 Raudsepp (2001) concluded that the mean salinity difference between surface and bottom is about 1 PSU which is substantially higher than what we obtained (0.62 g kg^{-1}) analyzing the month of August when the strongest stratification is expected. Comparing both studies we suggest that this difference between the surface and bottom layers is basically due to the increased bottom layer salinity during 1973 to 1995. In our study we had almost identical mean salinity (6.0 g kg^{-1}) in the DL (average from 35 m till bottom of the profile) from May to August in 1993—2012, whereas, in the results reported by Raudsepp (2001) at approximately 35 m depth salinity was around 6.1 PSU and increased more in the DL (about 6.5 PSU at the bottom). In addition, Raudsepp (2001) used Practical Salinity Scale for salinity, so each salinity value in his work is even higher if compared to Absolute Salinity, which is used in the present study. On the other hand, Stipa et al. (1999) reported of the density difference between the surface and deep waters in the middle of the summer being 1.5—2 kg m^{-3} using years 1993—1995 in their study. This is somewhat similar, although, a bit lower than we found out (2.2 kg m^{-3}) in our research during 1993—2012 (August).

Obtained mean Rossby radius values in May during 1993—2012 (0.9—1.9 km) were on average 2—2.5 times smaller than in the study where Rossby radius values from the model results were presented (Lips et al., 2016b). Such a discrepancy is caused by the different approaches used to calculate the Rossby radius. It has been showed before that in the whole Baltic Sea (Fennel et al., 1991) as well as in specific parts as the Gulf of Finland (Alenius et al., 2003) the Rossby radius has seasonal characteristics with minimum values during the autumn and winter and maximum values occurring in the summer mainly due to the strong stratification. Our results from the August correspond to these maximum Rossby radius values quite well exceeding the values in May almost two times. The stratification is strongest during the August in the GoR and the highest UML mean depth in August served as

a good indicator for this in our research. In May, on the other hand, the GoR is partially stratified with mainly shallow UML but in approximately 2/3 of the CTD casts we were not able to detect distinctly developed UML in May. Strength of the stratification in the GoR is the main reason for Rossby radius differences in May and August. In August the Rossby radius was larger in the deeper parts (smaller in shallower parts) of the GoR which is in accordance to what has been found in the GoF (Alenius et al., 2003) and worldwide (Chelton et al., 1998). Nevertheless, in May the largest Rossby radius was observed in the S part of the gulf rather than in the central, deeper part. We suggest that this could be related to maximum river run-off occurring in spring and strongly influencing the surface layers starting from the S part of the gulf, thus, promoting stratification as well.

Seasonal changes in the UML mean depth in the GoR (May—August) showed similar characteristics as reported by Tamminen and Seppälä (1999) on the basis of data from 1993—1995 in the GoR and by Liblik and Lips (2011) using long-term data in the GoF, with depth increasing with each consecutive month. Estimated UML mean depth in the GoR in summer was shallower and mean temperature was warmer than that of the GoF, mainly because GoR is a shallower water basin than the GoF. The UML mean temperature also increased during May—August following the air temperature raise and, in general, this temperature dynamics corresponds well with previous studies (e.g. Berzinsh, 1995; Raudsepp, 2001) about seasonal variations of temperature in the GoR. Finally, the UML mean salinity during May—August increased steadily as well in the GoR and this dynamics is in accordance with previously mentioned study by Raudsepp (2001) where it was described that lower surface salinity in May is due to the maximum river run-off in the spring. A bit older studies by Berzinsh (1980, 1987) covering the periods 1963—1976 and 1971—1982, respectively, showed that mean salinity in June can be as low as in May and that the surface layer (0—10 m) mean salinity continued to slightly decrease also after May in June and the following increase started again from July. In these last two studies one can observe that the mean surface salinity is about 1.0 g kg^{-1} higher than we found in our results during 1993—2012. Seasonal changes in the DL characteristics are minor mainly due to the fact that there is no direct influence from the atmosphere.

Inter-annual variability dominated in our results during 1993—2012 and they did not reveal any unequivocal trends or tendencies in the UML or DL characteristics as opposed to previous studies where it was reported, for example, that salinity increased during 1960—1977 (e.g. Berzinsh, 1980, 1995) and decreased from the end of 1970s till the start of 1990s (Berzinsh, 1995; Raudsepp, 2001). Based on the data from 1976—2008 at four monitoring stations (standard depths) in the central and S part of the GoR, Jurgensone et al. (2011) reported about general increase of water temperature in the summer (June—September). Based on the satellite data during 1990—2004, Siegel et al. (2006) showed a positive trend in the yearly mean SST of the Baltic Sea with summer and autumn dominating this trend and positive summer trend being highest in the northern Baltic Sea. Similar analysis of remote sensing data from 1990—2008 (BACC, 2015) showed an increase of SST specifically in the GoR by about 1.0°C per decade. However, our results based on the CTD data in August did not show similar pattern with

unequivocal temperature increase in the GoR during 1993—2012, although, apart from 1994, in general the UML mean temperature has increased from 1993—2010. Jurgensone et al. (2011) also noticed a salinity decrease before 1993 and a slight increase afterwards, whereas, there was no apparent trend in the stratification strength expressed as density difference between the surface (0—10 m) and subsurface layer. The latter corresponds well to our findings about the stratification strength (expressed as difference between the UML and DL) in August, whereas, we did not find any pronounced increase (or decrease) in the mean salinity in August during 1993—2012. Nevertheless, our results from August show that the mean salinity in last 3 years of the research period has been fairly lower compared with the values from the beginning of the 1990s.

Spatial distribution of the UML mean salinity from ten main stations in August showed higher salinity in the E coast than the W coast. In addition, the UML mean depth in August showed shallower UML depth in the W coast than in the central and E part of the gulf (UML mean depth in E part only slightly exceeded that in the central part). Therefore, it allows us to suggest that in the summer there is evident thermocline slope and corresponding sea level slope (opposite to the thermocline slope) between the two coasts and it is steeper in the W part of the GoR. Prevailing winds from WSW during the research period also indicate higher sea level in the E coast of the GoR. Thus, due to the average sea level gradient the general northward flow is dominating in the western part of the open gulf. This type of water flow is in accordance with the recent model results (Lips et al., 2016a) where it was reported that anticyclonic circulation exists in the GoR during summer forming a water tongue with lower salinity in the W part of the GoR.

High correlation found between the UML mean salinity (August) and the river run-off in spring during 1993—2012 confirmed the results of previous studies in the GoR (e.g. Berzinsh, 1995; Raudsepp, 2001) where it was shown that river run-off is the main factor for the salinity variations. A bit unexpected was the fact that high connection between these two factors was found not only in the S part of the gulf (majority of the freshwater discharges in this part) but, basically, throughout the gulf (10 main stations) and, especially, in the stations near the Irbe Strait. However, the mentioned model study by Lips et al. (2016a) also showed that during summer the anticyclonic (clockwise) circulation pattern dominates in the GoR, thus, transporting fresher surface waters from the south to north along the W coast of the gulf. Taking into account that our results showed also weaker correlation between the UML mean salinity and river run-off in spring on the E coast of the gulf, we feel that this general anticyclonic circulation (in the summer during stratified conditions) fits well with our findings and helps to explain them.

During the research period BSI (June—August) was found to be related ($r = 0.71$) to the UML mean depth (August) in the GoR. A positive BSI corresponds to an anomalous sea level pressure difference between Szczecin in Poland and Oslo in Norway (north-south distance of approximately 600 km) which means that the westerlies are prevailing over the Baltic Sea. If the BSI increases the winds from west are dominating and becoming stronger and, in general, stronger influence from the atmosphere should initiate more mixing in

the UML and, thus, make it deeper. Obtained significant correlation between the average wind speed (August) and UML mean depth ($r = 0.59$) also adds up to this relation. Nevertheless, the results from 10 main stations showed that not always this correlation between the BSI and UML mean depth (as well as wind speed and UML mean depth) is significant and that it varies in different parts of the gulf which might be due to, for example, upwelling and downwelling events (e.g. Lehmann and Myrberg, 2008; Lehmann et al., 2012; Lips et al., 2009) or other factors which might have local influence on the water masses (mesoscale structures like eddies, filaments etc.). We suggest that, although atmospheric forcing undoubtedly plays an important role affecting the UML depth, it is only a part of explanation and more detailed research should be carried out in this direction to come up with more justified conclusions which are based on the data with better spatial and temporal resolution as we had.

At some occasions in May a connection (negative correlation) was found between the BSI (March—May) and DL mean salinity and density. We suggest that this is caused by the stronger winds and corresponding more intense vertical mixing. Although this negative correlation was not significant in all parts of the GoR (the overall correlation and correlation at some main stations was just over the chosen significance level of $p < 0.05$), it still was evident as a common tendency in all main stations. Taking into account that in May, on average, the GoR is not characterized by fully developed and permanent stratification, this might as well serve as a factor favouring water column mixing and transferring the impact of the atmosphere to the deep layers.

Inter-annual variations of the DL mean salinity in the GoR (August) are related to the DL mean salinity in the Irbe Strait (August). Best correlation was found in the W part of the gulf close to the Irbe Strait with correlation steadily decreasing towards the S part of the GoR, thus, suggesting that the inflow through the Irbe Strait continues anticlockwise along the W coast and penetrating deeper in the GoR. This corresponds well to what was previously reported regarding saline water inflow through Irbe Strait and further movement of saline deep waters into the GoR (e.g. Berzinsh, 1995; Lilover et al., 1998).

For numerical modelling purposes in order to resolve mesoscale processes it is important to estimate the Rossby radius in the GoR. Our estimates of the Rossby radius in May and August showed that numerical models with horizontal grid spacing 1 km or less should be applied. Nevertheless, our temporal and spatial resolution of the CTD data did not allow us to determine Rossby radius in winter when the Rossby radius values are usually the lowest. Alenius et al. (2003) showed that the Rossby radius summer values are approximately 1.75 times the winter values in the centre of the Gulf of Finland. However, they also emphasized that the analysis is somewhat biased due to temporal distribution of the observations. Taking into account that the GoR is a shallower water basin than GoF and the water column is usually thoroughly mixed from the end of autumn till early spring, we speculate that Rossby radius in winter and early spring should be even lower than 1 km.

As previously discussed river run-off plays a major role affecting the salinity dynamics in the whole GoR. In addition to that, we also found a significant connection (positive correlation) between the mean river run-off in spring and stratification in August (expressed as difference between the temperature, salinity and density in the UML and DL) during 1993—2012. As river run-off increases it increases not only the salinity difference between the UML and DL but strengthens temperature and density difference as well. It means that river run-off in the GoR serves as instantaneous source of changes but it can also have further impact on the whole water column after some time. Maximum stratification found in 2010 serves as a good example for previously mentioned connection — in 2010 the second largest (after 1994) river run-off in spring was observed from the whole research period with following maximum strength of stratification observed later in August. Similar pattern can be observed in 1994 which was characterized by the largest river run-off in spring from the whole period. Although salinity difference between the UML and DL is considerably lower than in 2010 we suggest that this is due to the rather poor spatial distribution of the data (data available only from the N part of the gulf which is not affected by river run-off at the same level as the S part) and, judging by differences in temperature and density, the stratification in 1994 was at least as strong as in 2010.

Latest projections of the future climate change (BACC, 2015) continue to predict a significant water temperature increase in the Baltic Sea region similarly as it was stated before (BACC, 2008). Current study and results obtained using the CTD profiles from 20 years allows us to foresee the possible situation and changes in the GoR. We suggest that if the water temperature will continue to increase then the warming would generate a stronger stratification conditions in the GoR in summer. Furthermore, stronger stratification is likely to favour the oxygen depletion in the deeper parts of the gulf and following hypoxic or, at some cases, even anoxic conditions. Thus, the previously detected parts with low oxygen concentration or no oxygen at all (Hansson et al., 2009) in the GoR could expand in wider areas. Due to the projected strong decrease in sea-ice extent (BACC, 2015) the spring bloom could start earlier with possible shifts in dominating species characteristics as it was already suggested by Jurgensone et al. (2011). Moreover, with projected increase in the river run-off in winter (BACC, 2015), the nutrient amounts will also increase suggesting longer spring blooms with higher biomass.

Since 1977 there is an evident salinity decrease in the Baltic Proper and the GoR. Although it is not so pronounced since the beginning of the 1990s, most of the studies about future scenarios (see BACC, 2015) predict further salinity decrease. If so, then increase of freshwater species in the coastal areas is likely to occur.

While precipitation and evapotranspiration were projected to increase in the GoR region, the mean annual river run-off was projected to decrease. However, strong seasonal changes with shift of the maximum river run-off from spring to winter were also projected. We suggest that, due to the above mentioned factors, the salinity minimum usually observed (in the surface layers) starting from the spring in the S part of the gulf will also shift in accordance to changes in the river run-off seasonal dynamics. Earlier maximum river run-off together with water temperature increase could benefit for the faster development of permanent stratification in the GoR. Strong stratification could be observed already in May or even earlier as opposed to only partially

stratified conditions (May) shown in the present study. Due to the stronger and earlier stratification in spring which hinders the vertical mixing, riverine water discharging mainly into the S part of the gulf could be transported for longer distances away from the coast. Such freshwater dynamics would have an impact on surrounding water masses by, for example, bringing more nutrient-rich water in the surface layers and increasing total suspended matter content in the areas where it was previously not observed or the effect was minor.

In conclusion, we showed that relatively large inter-annual variations dominated in the temporal variability of different UML and DL parameters and no clear long-term trend could be detected in the GoR during 1993—2012. The UML mean depth was found to be related to the Baltic Sea Index. River run-off proved to be a major driving force for the salinity dynamics and a substantial contributor to enhancing the strength of the stratification in summer. The analysis of inter-annual variations in density difference between the UML and DL revealed that the strongest stratification was observed in the years with the highest UML mean temperature and highest river run-off during spring. We suggest that the predicted water temperature increase and seasonal changes in river run-off will result in a stronger stratification in the GoR.

Acknowledgements

References

Alenius, P., Nekrasov, A., Myrberg, K., 2003. Variability of the baroclinic Rossby radius in the Gulf of Finland. Cont. Shelf Res. 23 (6), 563—573.

BACC, 2008. Assessment of Climate Change for the Baltic Sea Basin. Springer Verlag, Berlin, 35—221.

BACC, 2015. Second Assessment of Climate Change for the Baltic Sea Basin. SpringerOpen, Geesthacht, 69—263.

Berzinsh, V., 1980. Interannual and seasonal changes of water salinity in the Gulf of Riga. Rybokhozyaistvennye issledovaniya (Balt-NIIRKH), vol. 15Avots, Riga, pp. 3—12,, (in Russian).

Berzinsh, V., 1987. Hydrological dividing of the open part of the Gulf of Riga. In: Andrusaitis, G.P., Laganovska, R.Y., Apine, S.O. (Eds.), Hydrochemical and Hydrobiological Characteristics and Dividing of the Coastal Part of the Baltic Sea, Gulf of Riga and Gulf of Finland, Zinatne, Riga, 7—20, (in Russian).

Berzinsh, V., 1995. Hydrology. In: Ojaveer, O. (Ed.), Ecosystem of the Gulf of Riga Between 1920 and 1990. Estonian Acad. Publ., Tallinn, 7—32.

Chelton, D.B., DeSzoeke, R.A., Schlax, M.G., Naggar, K.E., Siwertz, N., 1998. Geographical variability of the first baroclinic Rossby radius of deformation. J. Phys. Oceanogr. 28 (3), 433—460.

Feistel, R., Weinreben, S., Wolf, H., Seitz, S., Spitzer, P., Adel, B., Nausch, G., Schneider, B., Wright, D.G., 2010. Density and absolute salinity of the Baltic Sea 2006—2009. Ocean Sci. 6 (1), 3—24.

Fennel, W., Seifert, T., Kayser, B., 1991. Rossby radii and phase speeds in the Baltic Sea. Cont. Shelf Res. 11 (1), 23—36.

Hansson, M., Axe, P., Andersson, L., 2009. Extent of anoxia and hypoxia in the Baltic Sea, 1960—2009. SMHI Report Mo 2009-214, http://www.smhi.se/polopoly_fs/1.10354!Oxygen_timeseries_1960_2009.pdf.

Jurgensone, I., Carstensen, J., Ikauniece, A., Kalveka, B., 2011. Long-term changes and controlling factors of phytoplankton community in the Gulf of Riga (Baltic Sea). Estuaries Coasts 34 (6), 1205—1219.

Kotta, J., Kotta, I., Simm, M., Põllupüü, M., 2009. Separate and interactive effects of eutrophication and climate variables on the ecosystem elements of the Gulf of Riga. Estuar. Coast. Shelf Sci. 84 (4), 509—518.

Kõuts, T., Håkansson, B. (Eds.), 1995. Observations of Water Exchange, Currents, Sea Levels and Nutrients in the Gulf of Riga. SMHI RO Series No. 23, Norrköping. 141 pp.

Kronsell, J., Andersson, P., 2014. Total and regional runoff to the Baltic Sea. HELCOM Baltic Sea Environment Fact Sheets, http://www.helcom.fi/baltic-sea-trends/environment-fact-sheets/ (accessed: 11 November 2015).

Lehmann, A., Krauss, W., Hinrichsen, H.-H., 2002. Effects of remote and local atmospheric forcing on circulation and upwelling in the Baltic Sea. Tellus A 54 (3), 299—316.

Lehmann, A., Myrberg, K., 2008. Upwelling in the Baltic Sea — a review. J. Marine Syst. 74 (Suppl.), S3—S12.

Lehmann, A., Myrberg, K., Höflich, K., 2012. A statistical approach to coastal upwelling in the Baltic Sea based on the analyses of satellite data for 1990—2009. Oceanologia 54 (3), 369—393, http://dx.doi.org/10.5697/oc.54-3.369.

Leppäranta, M., Myrberg, K., 2009. Physical Oceanography of the Baltic Sea. Praxis Publ. Ltd., Chichester, 46 pp.

Liblik, T., Lips, U., 2011. Characteristics and variability of the vertical thermohaline structure in the Gulf of Finland in summer. Boreal Environ. Res. 16 (Suppl. A), 73—83.

Lilover, M.J., Lips, U., Laanearu, J., Liljebladh, B., 1998. Flow regime in the Irbe strait. Aquat. Sci. 60 (3), 253—265.

Lips, I., Lips, U., Liblik, T., 2009. Consequences of coastal upwelling events on physical and chemical patterns in the central Gulf of Finland (Baltic Sea). Cont. Shelf Res. 29 (15), 1836—1847.

Lips, U., Zhurbas, V., Skudra, M., Väli, G., 2016a. A numerical study of circulation in the Gulf of Riga, Baltic Sea. Part I: Whole-basin gyres and mean currents. Cont. Shelf Res. 112, 1—13.

Lips, U., Zhurbas, V., Skudra, M., Väli, G., 2016b. A numerical study of circulation in the Gulf of Riga, Baltic Sea. Part II: Mesoscale features and freshwater transport pathways. Cont. Shelf Res. 115 (1), 44—52.

Petrov, V.S., 1979. Water balance and water exchange between the Gulf of Riga and the Baltic Proper. In: Sbornik rabot rizhskoj gidrometeorologicheskoj observatorii, 18, Riga. 20—40, (in Russian).

Raudsepp, U., 2001. Interannual and seasonal temperature and salinity variations in the Gulf of Riga and corresponding saline water inflow from the Baltic Proper. Hydrol. Res. 32 (2), 135—160.

Schlitzer, R., 2010. Ocean Data View, http://odv.awi.de.

Siegel, H., Gerth, M., Tschersich, G., 2006. Sea surface temperature development of the Baltic Sea in the period 1990—2004. Oceanologia 48 (S), 119—131.

Stiebrins, O., Väling, P., 1996. Bottom Sediments of the Gulf of Riga. Geological Survey of Latvia, Riga, 4 pp.

Stipa, T., Tamminen, T., Seppälä, J., 1999. On the creation and maintenance of stratification in the Gulf of Riga. J. Marine Syst. 23 (1—3), 27—49.

Tamminen, T., Seppälä, J., 1999. Nutrient pools, transformations, ratios, and limitation in the Gulf of Riga, the Baltic Sea, during four successional stages. J. Marine Syst. 23 (1—3), 83—106.

Paper II

Lips, U., Zhurbas, V., Skudra, M., Väli, G. (2016). A numerical study of circulation in the Gulf of Riga, Baltic Sea. Part I: Whole-basin gyres and mean currents. *Continental Shelf Research*, 112, 1–13, doi: 10.1016/j.csr.2015.11.008.

Research papers

A numerical study of circulation in the Gulf of Riga, Baltic Sea. Part I: Whole-basin gyres and mean currents

Urmas Lips [a,*], Victor Zhurbas [a,b], Maris Skudra [a,c], Germo Väli [a]

[a] Marine Systems Institute, Tallinn University of Technology, Akadeemia Road 15A, 12618 Tallinn, Estonia
[b] Shirshov Institute of Oceanology, 36 Nakhimovsky Avenue, 117997 Moscow, Russia
[c] Latvian Institute of Aquatic Ecology, Daugavgrivas Street 8, LV-1048 Riga, Latvia

ABSTRACT

A regional model of the Gulf of Riga (GoR) with horizontal grid spacing of 0.5 nautical miles was applied to study the features and driving forces of the whole-basin circulation in the GoR. The initial conditions and atmospheric forcing were taken from the operational models High Resolution Operational Model for the Baltic (HIROMB) and High Resolution Limited Area Model (HIRLAM), respectively. The wind stress curl is shown to be a major contributor to the whole-basin circulation pattern. An anticyclonic circulation pattern in the summer is determined by a combined effect of the negative wind stress curl, thermal density stratification and bottom topography. Positive values of the wind stress curl and a cyclonic circulation pattern prevail during the cold period of the year when seasonal thermocline is absent. During calm periods, the anticyclonic type of circulation is established due to a combined effect of the river runoff, saltier water inflow into and mixed water outflow from the GoR. Two seasonal baroclinic jet-like currents are identified in the summer: the Northward Longshore Current in the western GoR and Southward Subsurface Longshore Current in the eastern GoR. The alteration of the circulation pattern in the GoR from cyclonic in the cold period of the year to anticyclonic in the summer, and vice versa, was shown to be observed not every year due to inter-annual variability of wind forcing.

© 2015 Elsevier Ltd. All rights reserved.

1. Introduction

The Gulf of Riga (GoR) is a semi-enclosed basin in the eastern part of the Baltic Sea with the area of 17,913 km^2 and volume V_{GoR} =405 km^3 (Leppäranta and Myrberg, 2009). A specific feature of the GoR is the presence of two straits – the Irbe Strait (sill depth of 25 m and cross-section of 0.4 km^2) in the western part and the Muhu Strait (sill depth of 5 m and cross-section of 0.04 km^2) in the northern part of the GoR (Fig. 1). The average depth of the GoR is 26 m, which is approximately two times less than that of the Baltic Sea. The northern part of the GoR is quite shallow and contains many islands (e.g. Abruka, Kihnu, and Manilaid) and banks. The Ruhnu Island situated in the central part of the GoR is a continuation of a relatively large bank – Gretagrund – dividing the deep-water zone into the western and eastern regions. The deepwater zone reaches depths of about 56 m in the east of the Ruhnu Island, although, the deepest spot in the whole gulf is Mersraga trough (width about 50 m and length 4.5 km) with the depth of 66 m (Stiebrins and Väling, 1996) which is situated approximately

13 km to the north from the village of Mersrags.

The catchment area of the gulf covers 134,000 km^2 (Ojaveer (1995)) with five large rivers discharging into the GoR-Daugava, Lielupe, Gauja, Pärnu and Salaca. All these rivers are located in the southern and eastern part of the GoR. The annual freshwater runoff into the gulf varies between 17.2 and 55.1 km^3 (Yurkovskis et al., 1993) and the average runoff has been stated as Q_{Rivers}=30 km^3/yr, from which 86% fall into the southern part of the gulf (Berzinsh, 1995). The biggest contributor to the freshwater inflow is the Daugava River, which gives about 70% of the overall river input into the GoR (Yurkovskis et al., 1993).

Due to substantial river input to the GoR and relatively restricted water exchange with the Baltic Proper (BP), the mean salinity in the GoR (S_{GoR}=5.6 g/kg) is by 1.6 g/kg lower than the mean salinity in the adjacent region of the BP (S_{BP}=7.2 g/kg). If assuming the annual balance of water volume and salt content in the GoR in the form of $Q_{out} = Q_{in} + Q_{Rivers}$ and $Q_{out}S_{GoR} = Q_{in}S_{BP}$, where Q_{out} and Q_{in} are the annual outflow and inflow volume rates through the straits between the GoR and BP, one can obtain $Q_{out} = Q_{Rivers}S_{BP}/(S_{BP} - S_{GoR}) = 135$ km^3 yr and estimate the water renewal period for the GoR as $V_{GoR}/Q_{out} \approx 3$ yr (Lilover et al., 1998).

A general cyclonic type circulation scheme with southward

---

* Corresponding author.
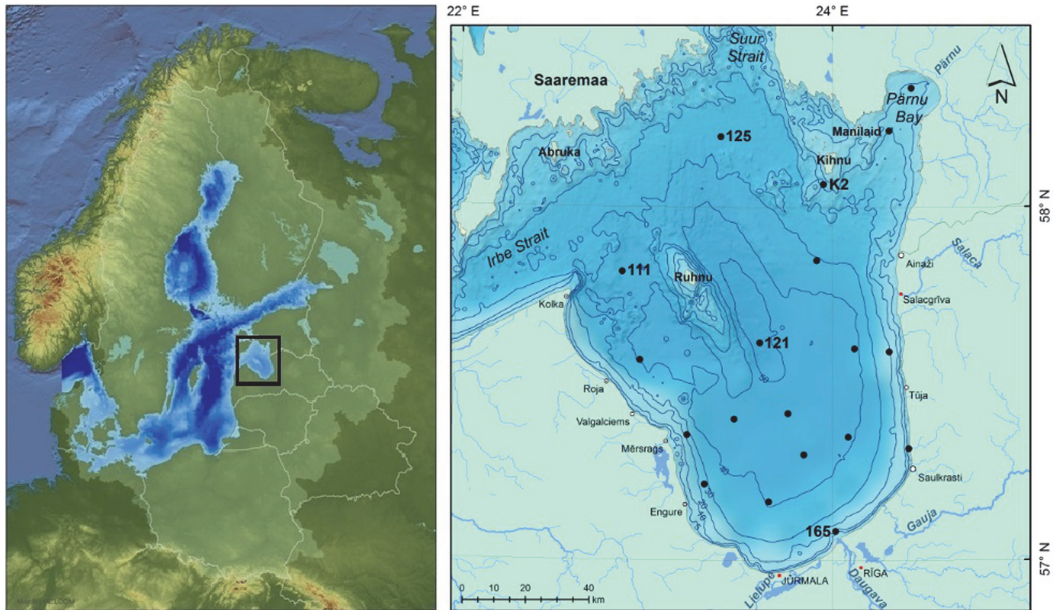*E-mail address:* urmas.lips@msi.ttu.ee (U. Lips).

Fig. 1. Map of the Baltic Sea region with the Gulf of Riga highlighted (left panel). Bathymetric map of the Gulf of Riga (right panel). The black dots are the positions of CTD measurements used for the model validation. Examples of temperature and salinity profiles from CTD stations 165, 111, 125, K2 and 121 are presented in Figs. 4 and 5.

flow at the western side and northward flow at the eastern side of the GoR has been described based on a rather limited number of direct measurements (Yurkovskis et al., 1993). This scheme is consistent with density-driven estuarine circulation in a wide non-tidal estuary (e.g. Elken et al., 2003). In accordance with this scheme, most of the freshwater supply in its south-eastern region propagates to the north along the gulf's eastern shore as a buoyant coastal plume, while the saltier water entering the gulf mostly through the Irbe Strait in the northwest corner propagates to the south along the gulf's western slope as a geostrophically balanced bottom gravity current.

On the other hand, in a closed, non-stratified basin of variable depth, the closed circulation loops of depth-averaged currents, which are called "topographic gyres", develop in response to spatially uniform wind impulse (Csanady, 1975). These loops are paired with downwind currents near the coasts and return flow in the center (deep part) of the basin. Note that the formation of "topographic gyres" is related to generation of potential vorticity by uniform wind forcing over sloping bottom and is not directly related to bottom friction and rotation. The dynamic effect of the earth's rotation manifests itself through the cyclonic propagation of the wind-generated basin-scale topographic wave that appears in cyclonic rotation of the current velocity vector with the period of 3–4 days (Raudsepp et al., 2003).

Some insight into the variations of the circulation in the northern part of the Gulf of Riga was obtained from synoptic CTD surveys performed on monthly basis from May to November, in 1994 (Lips et al., 1995). Using the dynamic topography at 5 dbar relative to 20 dbar, a northward flow was shown to dominate over the central part of the gulf in May and June with moderate winds mainly from NE and NW corresponding to the "topographic gyres". During calm weather in July and August, the flow was southward in the eastern gulf and northward in the western gulf corresponding to a whole-basin anticyclonic gyre. The ADCP transect performed on 17–18 July 1994, over the northern half of the gulf confirmed the described flow pattern. From September to

November, the flow was mainly northward again, while the wind was variable in direction, but weak. A presumably anticyclonic pattern of surface circulation in the GoR was reconstructed from aerial surveying of currents in August and September 1965 (Baranov, 1970), which corresponds to the findings by Lips et al. (1995). The reduced surface salinity in the western GoR in comparison to that in the eastern GoR was also reported by Berzinsh (1980) on the basis of measurements in August–September 1971–1975. It corresponds to the transport of the Daugava River runoff by a whole-basin anticyclonic gyre.

A study of the springtime water circulation in the southern GoR was recently conducted by Soosaar et al. (2014) based on the results of a 10-year simulation (1997–2006) using the General Estuarine Transport Model (GETM). Monthly mean currents in the surface layer of the GoR revealed a double gyre structure dominated either by an anticyclonic or cyclonic gyre in the near-river-mouth south-eastern part and by a corresponding cyclonic or anticyclonic gyre in the near-open-sea-exit north-western part of the gulf. The anticyclonic circulation pattern in the southern GoR was enhanced by easterly winds but blocked or even reversed by westerly winds. The authors suggested that such circulation pattern is different from the basic coastal ocean buoyancy-driven circulation where an anticyclonic bulge develops near the river mouth and a coastal current is established along the right hand coast (in the northern hemisphere; see a simple analytical model by Yankovsky and Chapman (1997)).

We argue that in relation to the whole-basin circulation patterns in the GoR the following open questions still exist: What kind of whole-basin circulation gyre (cyclonic or anticyclonic) is typical in the GoR in different seasons? What processes control the whole-basin circulation pattern in the GoR? Are there any quasi-permanent, at least in seasonal sense, currents in the GoR?

This work is an attempt to answer these questions based on numerical experiments with an eddy-resolving circulation model. In sense of methodology, our approach is similar to that of Schwab and Beletsky (2003) who, using different model scenarios, have
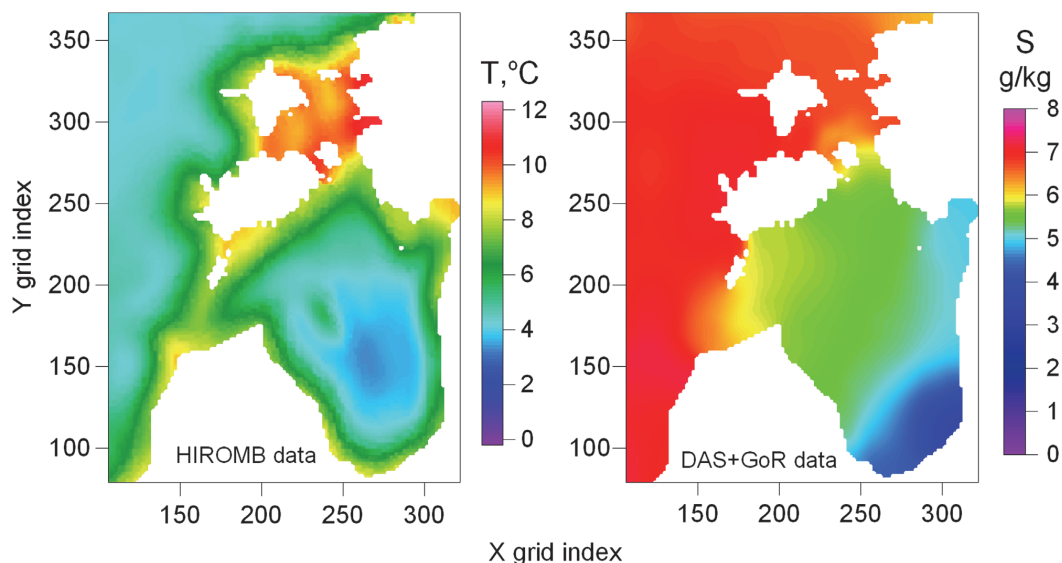
Fig. 2. The initial fields of surface layer temperature and salinity in the high-resolution part of the model domain compiled from HIROMB output for May 1, 2012, and from DAS+GoR data for the period from April 15 to May15, 1996–2012, respectively.

studied the relative importance of various mechanisms responsible for the large-scale circulation patterns in Lake Michigan by analyzing the vorticity balance in the lake on a monthly timescale.

2. Model setup

Here we use the Princeton Ocean Model POM (Blumberg and Mellor, 1983) to simulate hydrodynamics of the GoR. The POM is a sigma co-ordinate, free surface, hydrostatic model equipped with a 2.5 moment turbulence closure scheme by Mellor and Yamada (1982). It uses a traditional central differencing advection scheme; the time step was 6 and 180 s for the external and internal modes, respectively. The model domain includes the whole Baltic Sea closed at the Danish Straits. Digital topography is taken from (Seifert and Kayser, 1995). The grid cell size along the latitudes and longitudes, Δx and Δy, is varying spatially from $\Delta x = (1/60)°$ in the range of 21–24.6°E and $\Delta y = (1/120)°$ in the range of 56.933–59.333°N (or $\Delta x \approx \Delta y = 0.5$ nautical miles=926 m) in the GoR and its vicinity to $\Delta x = (1/15)°$ and $\Delta y = (1/30)°$ elsewhere; there are 20 sigma layers in the vertical direction. The model is eddy resolving in the region under investigation where the baroclinic Rossby radius of about 2–5 km (e.g., Fennel et al., 1991) is well above the grid cell size. The model setup does not include any sea-ice module.

Two rivers inflowing to the GoR are included to the model: the Daugava River and the Pärnu River with the annual mean volume rates of 660 m³/s and 48 m³/s, respectively (Leppäranta and Myrberg, 2009). Since the Lielupe and Gauja, the second and third largest rivers that contribute to the GoR freshwater inflow, have their mouths within a 20 km vicinity of the Daugava mouth, the three rivers can be considered as a single source with the volume rate of 818 m³/s. The latter volume rate is the mean runoff of Latvian rivers into the GoR for 1921–1990, May–October, taken from http://www.modlab.lv/publications/1998/publ3.htm. Therefore, one may consider 660 m³/s and 818 m³/s as the lower and upper limits for the Daugava River mean flow rate. The seasonal variations of river runoff are not considered in the model setup. Each river is incorporated into the model by means of addition of some amount of freshwater to a grid cell corresponding to the position of the river mouth at each time step. The added river water is first placed above the sea water and it is then mixed into the top layer(s) down to the inflow depth h_0, which was taken at $h_0 = 4$ m and 2 m in case of the Daugava and Pärnu River, respectively. Freshwater supply related to the precipitation and rivers inflowing to the Baltic Sea outside the GoR is not included to the model.

The basic model run comprised a one-year period from May 1, 2012 to April 30, 2013. For the initial conditions (temperature and salinity) we attempted to use 1 n.m. grid output of the High Resolution Operational Model for the Baltic (HIROMB, see http://www.smhi.se/en/Research/Research-departments/Oceanography/hiromb-1.8372) interpolated to our spatially-varying grid. However, it was found that the HIROMB output for May 1, 2012 gives surface layer salinity above 6 g/kg almost everywhere in the GoR, while all observations available in the GoR during the period of April–May 2012 showed surface layer salinity below 6 g/kg. Therefore, it was decided to construct the initial salinity field from measurements collected in the Data Assimilation System (DAS) coupled with the Baltic Environmental Database (established and maintained by Alexander Sokolov and Fredrik Wulff at the Stockholm University; see http://nest.su.se/das). The DAS data were supplemented with the CTD data collected in the GoR by Estonian and Latvian research institutes (788 CTD profiles from April 15 to May 15 in 1996–2013). The initial fields of surface layer temperature and salinity in the high-resolution part of the model domain compiled from HIROMB output and DAS+GoR data, respectively, are shown in Fig. 2.

The numerical integration in prognostic mode started from zero initial velocities and zero sea surface elevation without any spin-up period.

Boundary conditions (atmospheric forcing), such as wind stress that was calculated taking into account atmospheric stability and precipitation, and total heat flux including solar (short wave) radiation reduced by clouds, long wave (upward) radiation, latent

and sensible heat fluxes, were formulated based on the output of the numerical weather prediction forecast system High Resolution Limited Area Model (HIRLAM; see www.hirlam.org). The output data from a version of HIRLAM applied at the Estonian Meteorological and Hydrological Institute (Männik and Merilain, 2007) providing meteorological parameters on an approximately 10 km horizontal grid with 3 h time step were used by means of bilinear interpolation to the model grid.

In order to estimate the relative importance of various mechanisms responsible for the formation of large-scale circulation patterns in the GoR, the basic one-year model run was complemented with a number of scenario studies or numerical experiments. These experiments included model runs with modified (e.g. flat) bottom topography, zero heat flux, zero atmospheric forcing (no heat flux and no wind stress), and uniform initial temperature/salinity distribution with no atmospheric forcing.

The basic, one-year model run was extended to the three-year period from May 1, 2012 to April 30, 2015 to study the reliability of revealed circulation patterns. Modified initial TS fields outside the GoR were applied. Since the maximum depth of the Irbe Strait sill (approximately 25 m) is well above the permanent halocline level in the Eastern Gotland Basin (60–70 m), the saltier water overflow entering the GoR is fed by the Eastern Gotland Basin upper layer waters with salinity of approximately 7.2 g/kg. Therefore, to model the circulation in the GoR for a longer period, it is sufficient to apply a long-term supply of 7.2 g/kg salinity waters through the Irbe Strait. Such a salt water supply for a relatively long period, τ, can be granted if we consider constant salinity of $S_0 = 7.2$ g/kg everywhere in the Baltic Sea outside the GoR. Indeed, since the Baltic Sea volume is $V_{BS} = 21,205$ km^3 and the annual river runoff to the GoR is $Q_{GoR} = 30$ km^3/yr (Leppäranta and Myrberg, 2009), the mean salinity of the artificially closed Baltic Sea will be decreased due to the GoR rivers as $S(\tau) = S_0 V_{BS}/(V_{BS} + Q_{GoR}\tau)$, or only by 0.01 g/kg a year and 0.03 g/kg for a 3 year period. Based on these estimates, the above-described initial TS fields were modified to provide constant, 7.2 g/kg salinity and hydrostatically stable temperature outside the GoR in the closed Baltic Sea.

3. Validation of the model

Since the prognostic model runs started from motionless state and zero sea surface elevation, the spin-up time should be estimated before the comparison of simulated results with the observations. To estimate the spin-up time, the basic run started on May 1, 2012 was complemented by an additional test run started on June 1, 2012. In the test run, the simulated TS fields from the basic run on June 1, 2012 and zero velocities and surface elevation were used as the initial conditions. As seen from the simulated time series of the specific kinetic energy averaged in the whole GoR, which were calculated for the basic and test run (E_0 and E_1, respectively), a few days after the start of the test run, the E_1 time series became identical to that of E_0 within 10 percent accuracy (see Fig. 3). Note that the perfect identity cannot be achieved because the model is eddy-resolving. Therefore, one may conclude that the spin-up time of the GoR model under atmospheric forcing is estimated as a few days. Moreover, even if the atmospheric forcing is turned off the spin-up time forced by baroclinic density field will not exceed 10 days (it is shown in Section 4.1 where the results of the no atmospheric forcing run are presented).

Available CTD data collected from May to August 2012 allowed us to compare the observed vertical profiles of temperature and salinity in the GoR with the modeled profiles at the same place and time (Figs. 4 and 5). In general, the observational and model data matched well. However, as a rule, the modeled profiles revealed weaker vertical temperature gradient than the observations
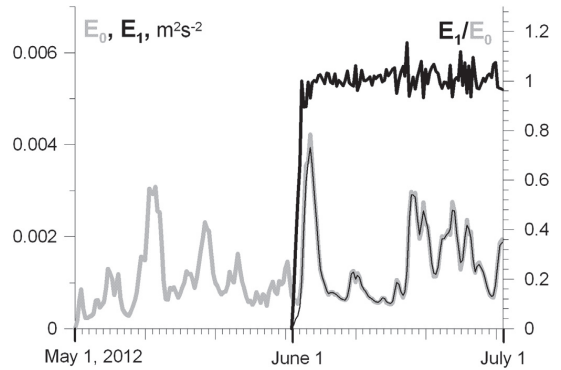

Fig. 3. Time series of the mean specific kinetic energy of GoR waters for the basic run started on May 1, 2012, from initial TS fields and zero velocities and surface elevation (E_0, the bold gray curve) and for the run started on June 1, 2012, from the TS fields obtained from the basic run and zero velocities and surface elevation (E_1, the thin black curve), as well as the ratio of E_1/E_0 (the bold black curve).

– the temperature difference between the surface and the bottom layer was almost the same in the model and observations, while the thermocline was clearly sharper in the observations than in the model output (Fig. 4). The modeled salinity almost always slightly exceeded the observed salinity in the GoR. The biggest differences between the modeled and observed salinity were found at the coastal stations in the eastern part of the GoR (e.g. station K2, Fig. 4). It can be attributed to the fact that not all rivers were included in the model. At the same time, the model simulates well the low salinity water patch near the Daugava River mouth (e.g. station 165, Fig. 4) and the vertical profiles of temperature and salinity in the western (e.g. station 111, Fig. 4) and north-eastern part of the open GoR (station 125, Fig. 4). The maximum salinity differences between the modeled and observed values exceeded 0.5 g/kg and the maximum temperature differences exceeded 3 °C at some stations and depths due to the mentioned discrepancy between the simulated and observed strength of the seasonal thermocline.

A characteristic development in time in regard of discrepancies between the model output and observational data can be noticed by comparison of modeled and observed vertical profiles in the central part of the GoR (Fig. 5). While in May the modeled surface layer salinity was close to the observed salinity, the difference did grow until July and August. At the same time, the difference between the modeled and observed deep layer salinity decreased from May to August. The difference between the vertical profiles of temperature increased in the course of the development of the seasonal thermocline.

Since the data presented in Fig. 5 show that with Daugava River runoff being at 660 m^3/s the simulated surface salinity displays growing positive excess relative to the observations, one may suggest that the growing salinity difference results from an underestimated runoff. However, a model run with the 818 m^3/s for the Daugava River runoff does not change the difference much; the simulated surface layer salinity in the central part of the GoR decreased only by approximately 0.02–0.03 g/kg, while in the eastern and northern parts of the GoR, i.e. within the pathway of intrinsic propagation of the Daugava River plume, the salinity decrease was larger, reaching approximately 0.1 g/kg.

The decrease of bottom salinity and increase of bottom temperature in the central part of the GoR for the period from May 17 to August 7, 2012 (see Fig. 5), was larger in the model (approximately 0.2 g/kg and 3 °C, respectively) than that from the observations (0.05 g/kg and 1 °C, respectively). This could probably
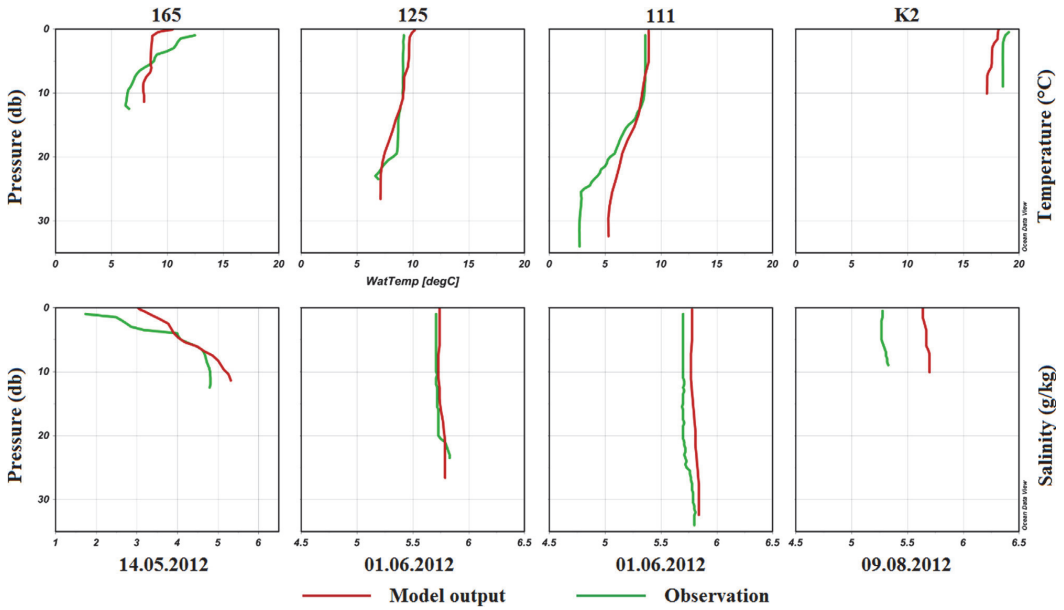
Fig. 4. Vertical profiles of temperature and salinity at station 165 in May, 125 and 111 in June and K2 in August (see locations of stations in Fig. 1). The red lines are the model output and the green lines are the observations. (For interpretation of the references to color in this figure legend, the reader is referred to the web version.)
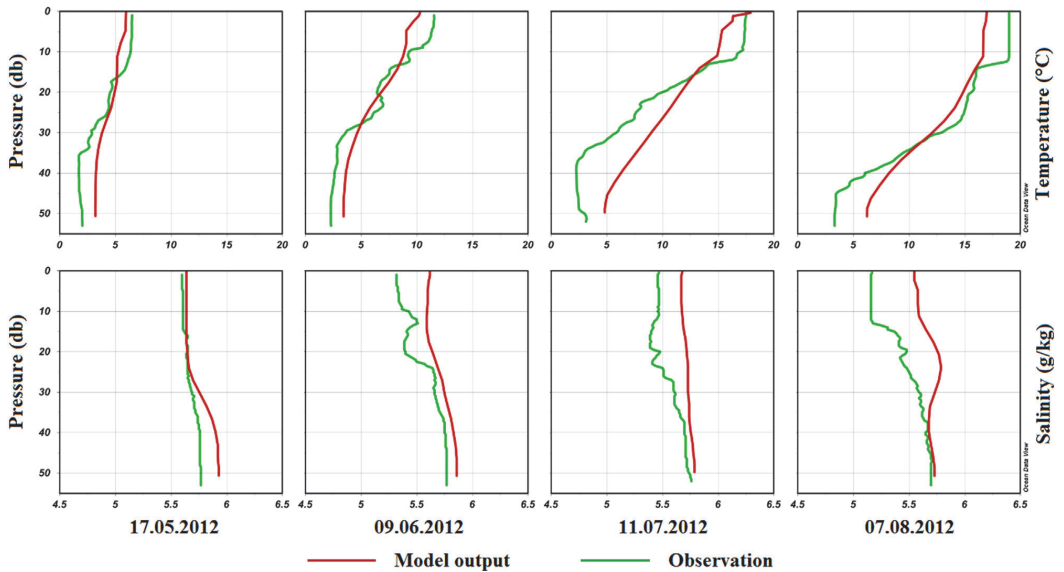

Fig. 5. Vertical profiles of temperature and salinity at station 121 in May, June, July and August 2012 (see location in Fig. 1). The red lines are the model output and the green lines are the observations. (For interpretation of the references to color in this figure legend, the reader is referred to the web version.)

be a result of overestimated vertical mixing (in relation to horizontal advection and mixing) in the model. Both the observed and modeled changes of the surface salinity, the former being larger than the latter, were irregular/non-monotonic within the study period, which could be caused by mesoscale variability.

4. Results

4.1. What governs the changes in circulation pattern in the GoR? (Mutual statistics of wind stress, wind stress curl and current curl)

An insight into possible causes that form large-scale circulation

pattern in the GoR can be provided by a vorticity balance equation (e.g., Ezer and Mellor, 1994; Schwab and Beletsky, 2003)

$$\frac{\partial \varsigma}{\partial t} = - \text{curl}\left(\frac{\vec{A}}{D}\right) - \text{div}(f\vec{v}) - \frac{1}{\rho_0} \text{curl}\left(\frac{1}{D}\nabla\Phi\right) + \text{curl}\left(\frac{\vec{\tau}}{\rho_0 D}\right)$$
$$- \text{curl}\left(\frac{\vec{\tau_b}}{\rho_0 D}\right), \tag{1}$$

where f is the Coriolis parameter, ρ_0 is the reference density, $\vec{v}$ is the depth-averaged current velocity vector, $\varsigma = \text{curl}(\vec{v})$ is the current vorticity, $\vec{A}$ is the vertically integrated transport vector, $\vec{\tau} = (\tau_x, \tau_y)$ and $\vec{\tau_b}$ are the surface (wind) stress and bottom stress vectors, respectively,

$$\Phi = \int_{-H}^{\eta} \rho g z \, dz \tag{2}$$

is potential energy, H is the still water depth, η is free surface elevation, $D = H + \eta$ is the water column depth, ρ is density, g is gravity acceleration, and z is the vertical coordinate directed upward. The terms in the right hand of (1) describe different effects on the current vorticity generation: the first term is responsible for a combined effect of nonlinear advection and horizontal diffusion, second term for flow divergence at the f-plane, third term for effect of baroclinicity, fourth term for effect of wind stress curl, and fifth term for bottom friction effect. The effect of bottom topography is included in the first, third, fourth and fifth terms. To qualitatively illustrate the effects of wind stress curl and bottom topography on the current vorticity generation, let us address Eq. (1) with the fourth term alone

$$\frac{\partial \varsigma}{\partial t} = \text{curl}\left(\frac{\vec{\tau}}{\rho_0 D}\right) = \frac{1}{D}\text{curl}\left(\frac{\vec{\tau}}{\rho_0}\right) - \frac{\tau_y}{\rho_0}\frac{1}{D^2}\frac{\partial D}{\partial x} + \frac{\tau_x}{\rho_0}\frac{1}{D^2}\frac{\partial D}{\partial y}. \tag{3}$$

It follows from (3) that the positive (negative) wind stress curl generates the positive (negative) current curl. As for the topography effect, Eq. (3) says that in the case of uniform wind stress the positive (negative) current curl is generated when the sea depth increases to the left (right) when looking downwind (e.g., the negative current curl is generated by a westerly wind blowing over a water area whose depth increases to the south – in accordance to Fig. 1, this topography configuration is typical for the northern part of the GoR).

To consider the relation between the wind stress curl and the current curl in the GoR, we calculated the mean values of the quantities, $\langle \text{curl}(\vec{\tau}/\rho_0) \rangle$ and $\langle \text{curl}(\vec{V_5}) \rangle$, as well as the mean values of wind stress components, $\langle \tau_x/\rho_0 \rangle$ and $\langle \tau_y/\rho_0 \rangle$, spatially averaged over a GoR part where $H > 20$ m. Keeping in mind further comparison of correlation between the wind stress curl and the current curl, the time series of $\langle \text{curl}(\vec{\tau}/\rho_0) \rangle$, $\langle \text{curl}(\vec{V_5}) \rangle$, $\langle \tau_x/\rho_0 \rangle$ and $\langle \tau_y/\rho_0 \rangle$, were preliminary low-pass filtered with the cut-off at the doubled inertial period, $4\pi/f = 28.2$ h. Looking at Fig. 1, one can see that the condition of $H > 20$ m is satisfied almost everywhere in the GoR except for a shallow coastal stripe. Note that the spatial average of the current curl over an entire closed basin is nil, and the GoR is almost a closed basin. The calculations of $\langle \tau_x/\rho_0 \rangle$, $\langle \tau_y/\rho_0 \rangle$, and $\langle \text{curl}(\vec{\tau}/\rho_0) \rangle$ were based on HIRLAM meteorology interpolated to the GoR model grid, while the calculation of $\langle \text{curl}(\vec{V_5}) \rangle$ was based on the model estimates of current velocity at every grid nodes interpolated to 5 m level below the sea surface.

Time series of $\langle \text{curl}(\vec{V_5}) \rangle$, $\langle \text{curl}(\vec{\tau}/\rho_0) \rangle$, $\langle \tau_x/\rho_0 \rangle$ and $\langle \tau_y/\rho_0 \rangle$ for the entire modeling period from May 1, 2012 to April 30, 2013, are shown in Fig. 6. The most striking feature seen in these time series
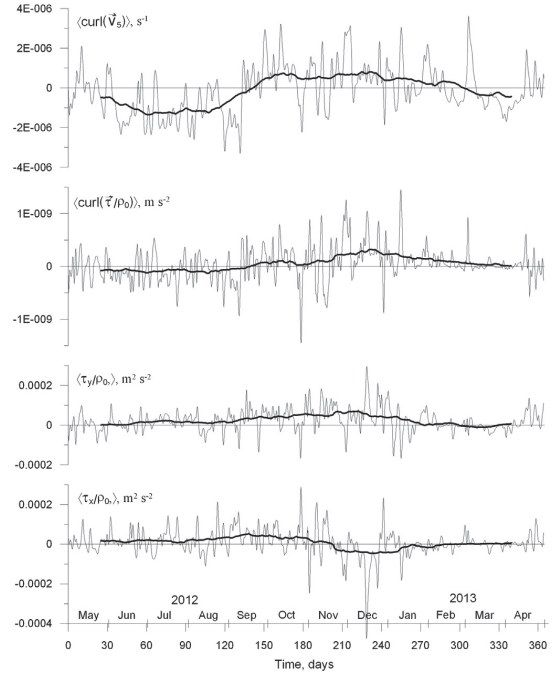

Fig. 6. Thin curves: time series of the 28.2 h averages of the current curl, $\langle \text{curl}(\vec{V_5}) \rangle$, wind stress curl, $\langle \text{curl}(\vec{\tau}/\rho_0) \rangle$, and wind stress components, $\langle \tau_x/\rho_0 \rangle$ and $\langle \tau_y/\rho_0 \rangle$, averaged over a deep part of the GoR where $H > 20$ m, for the modeling period from May 1, 2012 to April 30, 2013. Bold curves are the same as thin ones but low-pass filtered (50 day window running mean).

is the change of the sign of the current curl $\langle \text{curl}(\vec{V_5}) \rangle$ from negative in the summer season to mostly positive in the rest of the year except for a calm period from mid-February to mid-April, 2013, when $\langle \text{curl}(\vec{V_5}) \rangle$ was mostly negative again. The second feature seen with the unaided eye is the increase of positive correlation between $\langle \text{curl}(\vec{\tau}/\rho_0) \rangle$ and $\langle \text{curl}(\vec{V_5}) \rangle$ in the fall – early winter period from September 15, 2012 to January 15, 2013, the period when winds were relatively strong. Note that, like $\langle \text{curl}(\vec{V_5}) \rangle$, the average value of $\langle \text{curl}(\vec{\tau}/\rho_0) \rangle$ was negative for the summer period and positive for the fall – early winter period $\langle \text{curl}(\vec{\tau}/\rho_0) \rangle = -1.0 \times 10^{-10}$ m/s^2 and 1.7×10^{-10} m/s^2, respectively.

To quantitatively illustrate the above mentioned features scatter plots of $[\langle \text{curl}(\vec{\tau}/\rho_0) \rangle, \langle \text{curl}(\vec{V_5}) \rangle]$ drawn for the whole modeling period from May 1, 2012 to April 30, 2013, and separately for the fall – early winter and summer season are addressed (Fig. 7, a, b, and c, respectively). For the entire modeling period of one year, the correlation coefficient between $\langle \text{curl}(\vec{\tau}/\rho_0) \rangle$ and $\langle \text{curl}(\vec{V_5}) \rangle$ is relatively high ($r = 0.72$), so one may assert that the wind stress curl is the main contributor to the current curl in the GoR. In the fall – early winter season, the correlation coefficient between $\langle \text{curl}(\vec{\tau}/\rho_0) \rangle$ and $\langle \text{curl}(\vec{V_5}) \rangle$ is even higher ($r = 0.79$) and a regression coefficient $b = 3.0 \cdot 10^{-7}$ s^{-1} of the linear dependence of $\langle \text{curl}(\vec{V_5}) \rangle = b + a\langle \text{curl}(\vec{\tau}/\rho_0) \rangle$ is relatively small ($b/\text{rms}\langle \text{curl}(\vec{V_5}) = 0.27$). In the summer season, quite the opposite, the correlation coefficient between $\langle \text{curl}(\vec{\tau}/\rho_0) \rangle$ and $\langle \text{curl}(\vec{V_5}) \rangle$ is
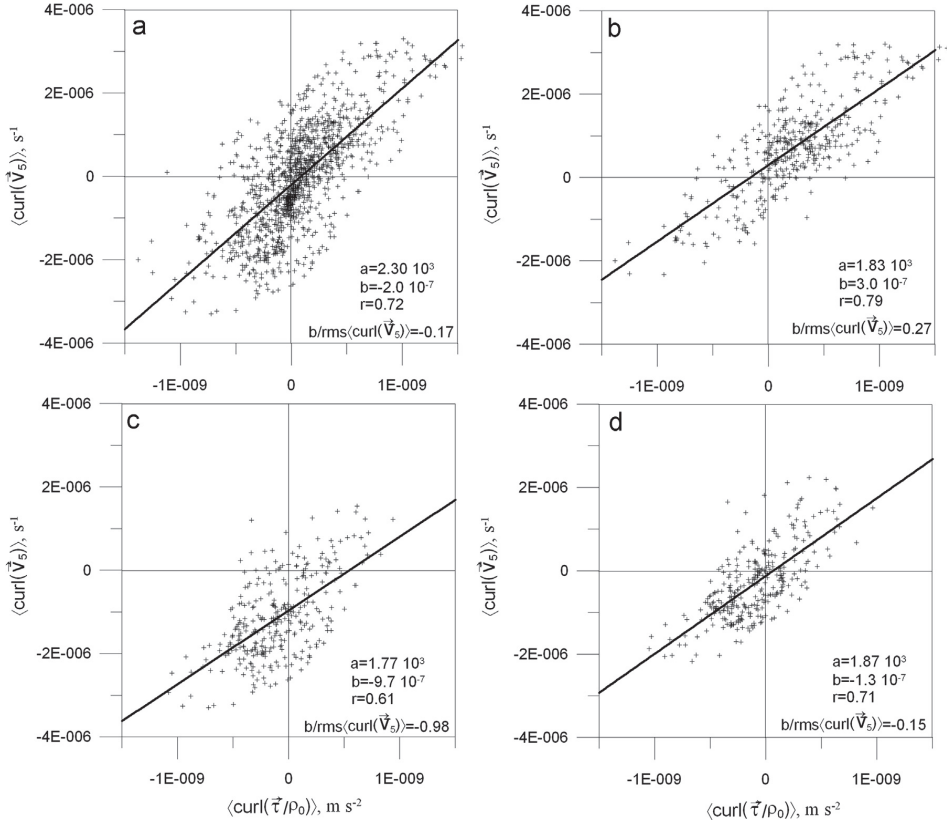
Fig. 7. Scatter plots of the 28.2 h averages of the wind stress curl versus the current curl in the GoR drawn for (a) the entire modeling period from May 1, 2012 to April 30, 2013, and separately for (b) the fall – early winter season from September 15, 2012 to January 15, 2013, and (c) for the summer season from June 15 to September 15, 2012. The panel (d) is the same as (c), but for the no heat flux run (Experiment 2). Values of a, b, and r given on the scatter plot panels are coefficients of the linear regression of $\langle \mathrm{curl}(V_5) \rangle = b + a \langle \mathrm{curl}(\vec{\tau}/\rho_0) \rangle$ and the correlation coefficient, respectively.

lower ($r = 0.61$) than that for the entire modeling period and the regression coefficient (intercept) $b = -9.7 \times 10^{-7}$ s^{-1} being negative is relatively far from zero ($b/\mathrm{rms}\langle \mathrm{curl}(\vec{V}_5) \rangle = -0.98$). Thus, in the summer season, a relatively large negative value of the current curl in the GoR was observed at zero wind stress curl, which means that some other effect, in addition to the wind stress curl, contributed to the current vorticity generation.

To identify this additional effect responsible for intensification of the whole-basin anticyclonic gyre in the GoR in summer we hypothesize the following possible contributing factors.

First, the summer season was the only season within the modeling period when the westerly (westerly and south-westerly) winds prevailed; the values of wind stress components, $\langle \tau_x/\rho_0 \rangle$ and $\langle \tau_y/\rho_0 \rangle$, averaged for the period from June 15 to September 15, 2012, were 2.7×10^{-5} m^2 s^{-2} and 1.5×10^{-5} m^2 s^{-2}, respectively. For comparison, during the fall – early winter period, southerly and south-easterly winds prevailed (see Fig. 6) with the mean values of $\langle \tau_x/\rho_0 \rangle$ and $\langle \tau_y/\rho_0 \rangle$ of -2.1×10^{-5} m^2 s^{-2} and 4.8×10^{-5} m^2 s^{-2}, respectively. According to the GoR topography (Fig. 1), the southern half of the gulf is relatively deep with $H = 40$–50 m, while the northern half displays a negative gradient of H in the northern–north-western direction with an almost uniform decrease of H from 50 m in the gulf's center to 20 m close to the southern shore of the Saaremaa Island. In accordance with Eq. (3),

the westerly–south-westerly wind under such topography configuration can generate negative (anticyclonic) vorticity.

Secondly, the summer season is characterized by a strong density stratification caused by the formation of seasonal thermocline, while in the rest of the year the density stratification is mostly determined by salinity and is relatively weak. Strong density stratification in combination with wind forcing implies the possibility of generation of alongshore baroclinic currents, which can intensify the whole-basin circulation.

Third, one may suggest that the circulation pattern in the GoR is governed by water transport through the Irbe Strait and river runoff.

Following Schwab and Beletsky (2003), we repeatedly reproduced the basic run of the GoR model for the period from May 1, 2012 to April 30, 2013, subsequently eliminating one or other of the abovementioned factors.

Experiment 1: elimination of the bottom topography asymmetry. The real topography of the GoR shown in Fig. 1 was replaced by a uniform sea depth of $H = 30$ m (the value close to the mean depth of GoR) in the offshore areas of the GoR and linear increase of the depth from the isobath of $H = 5$ m to $H = 30$ m within a 10 km wide region along the coast. The time series of monthly averaged values $\langle \mathrm{curl}(\vec{V}_5) \rangle$ for Experiment 1 are shown in Fig. 8 as the blue line. In accordance to the qualitative
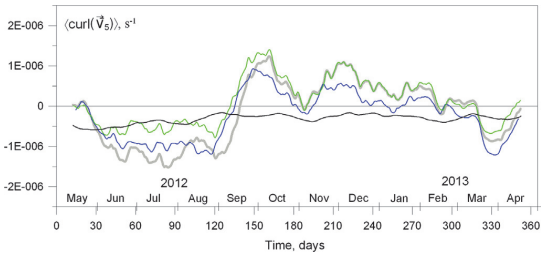
Fig. 8. Time series of the monthly averages of the current curl, $\langle \mathrm{curl}(\vec{V_5}) \rangle$, for the basic run (the bold gray line), flat bottom topography run (Experiment 1, the blue line), no heat flux run (Experiment 2, the green line), no wind and no heat flux run (Experiment 3, the black line).

interpretation of Eq. (3), it is seen that the replacement of real bottom topography in the GoR by the 30 m depth flat bottom results in an increase of $\langle \mathrm{curl}(\vec{V_5}) \rangle$ in the summer season (when the westerly–southwesterly winds prevail) relative to the basic run (the bold gray line). During cold seasons (when the westerly–southwesterly winds do not prevail), the flat bottom experiment gives some decrease of $\langle \mathrm{curl}(\vec{V_5}) \rangle$ relatively to the basic run. Therefore, Experiment 1 does bring some evidence for an importance of the topographic effect in generation of negative (positive) values of $\langle \mathrm{curl}(\vec{V_5}) \rangle$ in the summer (in cold periods of the year) in the GoR.

Experiment 2: elimination of seasonal thermocline. The basic prognostic run of the GoR model is performed with zero heat flux (the green line in Fig. 8). Negative values of $\langle \mathrm{curl}(\vec{V_5}) \rangle$ have become closer to zero (but still negative) during the summer season if compared to the results of the basic run. Removal of the seasonal thermocline results in some increase of the correlation coefficient between $\langle \mathrm{curl}(\vec{\tau}/\rho_0) \rangle$ and $\langle \mathrm{curl}(\vec{V_5}) \rangle$ for the period from June 15 to August 15, 2012 – it was $r = 0.71$ in Experiment 2 and $r = 0.61$ in the basic run. Moreover, the regression coefficient (intercept)

became much closer to zero – $b = -1.3 10^{-7}\,\mathrm{s}^{-1}$ and $b/\mathrm{rms}\langle \mathrm{curl}(\vec{V_5}) \rangle = -0.15$ in Experiment 2 versus $b = -9.7 10^{-7}\,\mathrm{s}^{-1}$ and $b/\mathrm{rms}\langle \mathrm{curl}(\vec{V_5}) \rangle = -0.98$ in the basic run (cf. Fig. 7, c and d). Therefore, effect of stratification contributes substantially to anticyclonic circulation in the GoR in the summer season.

Experiment 3: elimination of atmospheric fluxes (no wind stress, no heat flux). In this case, the large-scale circulation in the GoR is governed by freshwater inflow from rivers mostly in the southeast, saltwater inflow from the Irbe Strait, and compensating mixed water outflow through the Irbe Strait. Water transport through the Muhu Strait is small in comparison to that through the Irbe Strait. The saltwater inflow forms a gravitational near-bottom current contributing, in view of geostrophic equilibration, to cyclonic circulation. The freshwater inflow, on the one hand, forms an anticyclonic bulge, and, on the other hand, a coastal buoyant jet moving cyclonically, so a priori it is not clear whether the net contribution to $\langle \mathrm{curl}(\vec{V_5}) \rangle$ is positive or negative. The GoR model run with the duration of one year with zero wind stress and zero heat flux showed that the net contribution of freshwater inflow and water exchange through the straits is negative: the mean value of $\langle \mathrm{curl}(\vec{V_5}) \rangle$ for a one-year period is $\langle \mathrm{curl}(\vec{V_5}) \rangle = -3.2 \times 10^{-7}\,\mathrm{s}^{-1}$ (see Fig. 8, the black line). This result explains partially the appearance of anticyclonic circulation (negative $\langle \mathrm{curl}(\vec{V_5}) \rangle$) in the GoR during calm weather in the period from mid-February to mid-April 2013. Note that in the no atmospheric forcing case the $\langle \mathrm{curl}(\vec{V_5}) \rangle$ rises from zero (not seen in Fig. 8 due to running averaging of the time series) to some negative asymptotic value during the first 10 days of the simulation time. Therefore, one may conclude that the spin-up time does not exceed 10 days in the case without atmospheric forcing.

4.2. The mean currents in the summer and late fall – early winter seasons

To obtain the seasonally mean fields for the warm and cold seasons, the main model run output including 3D fields of
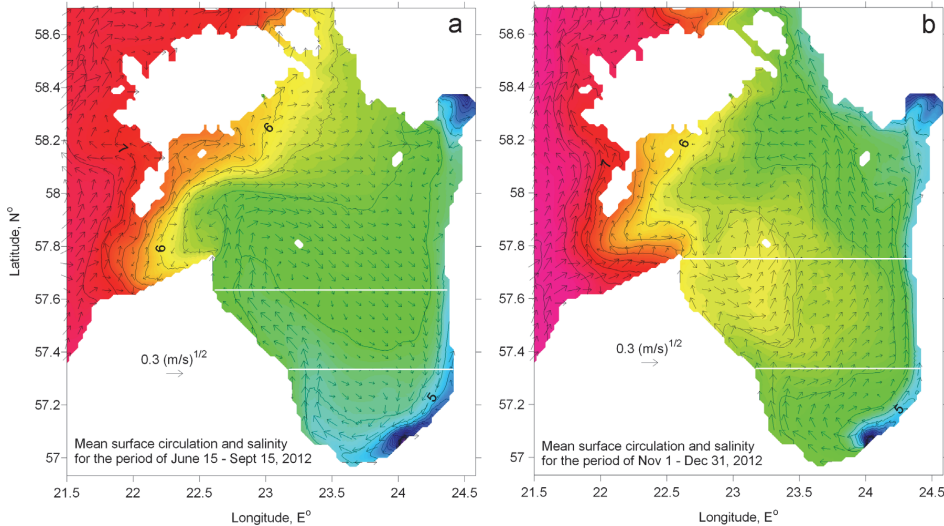

Fig. 9. (a) The mean summertime circulation and salinity in the surface layer of the GoR (an average of the simulation results over a period from June 15 to September 15, 2012 interpolated to 5 m depth). (b) The same as in (a) but for the late fall – early winter period of November 1–December 31, 2012. White horizontal lines across the GoR are the position of vertical sections presented in Figs. 10 and 11.

temperature, salinity, density, and x and y components of current velocity (U and V, respectively) was averaged in time over the periods from June 15 to September 15, 2012 (when the seasonal thermocline was present) and from November 1 to December 31, 2012 (when the seasonal pycnocline was already destroyed by the fall/winter convection but the sea was still ice free). The mean circulation and salinity in the surface layer (interpolated to 5 m depth) are presented in Fig. 9a for the summer season and Fig. 9b for the late fall – early winter season. Current velocities in Fig. 9 are presented in units of $(m/s)^{1/2}$ to visualize the gyres better.

The overall pattern of summertime surface currents in the GoR is characterized by a whole-basin anticyclonic gyre with enhanced intensity of currents in the western half-basin where a jet-like alongshore northward current (for brevity it will be addressed hereafter as NLC – the Northward Longshore Current) is clearly identified. The map of surface salinity displays two low salinity tongues originated from the Daugava River mouth; one is

extended along the western shoreline of the GoR, and the other is attached to the eastern coast of the GoR. The two low salinity tongues indicate the two pathways of riverine water transport in the GoR in summer season.

Fig. 9a displays a low-salinity bulge in the southeast corner of the gulf where the Daugava, Lielupe and Gauja mouths are located and two low-salinity tongues originated from the bulge and extended to the north along the eastern and western coasts; the latter (the western tongue) is a manifestation of the anticyclonic circulation. In contrast, the salinity pattern in the surface layer of the GoR compiled from the observations for the beginning of the ice-free season (see Fig. 2, the right panel) does not display the low-salinity tongue along the western coast and one may suggest that the anticyclonic gyre is not typical in the cold period of the year. To prove this, we plotted simulated fields of the mean surface layer currents and salinity averaged for the period from November 1 to December 31, 2012 (Fig. 9b). The result is quite clear: in the
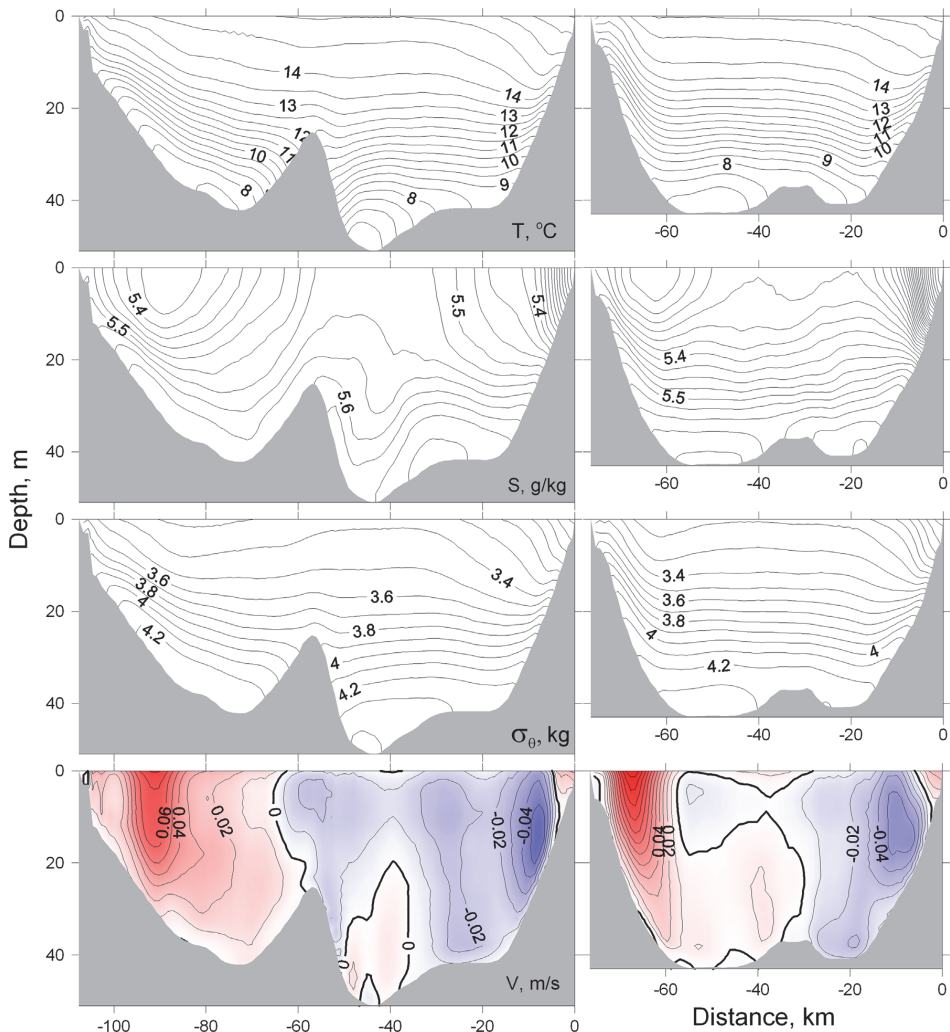

Fig. 10. Vertical sections of temperature T, salinity S, potential density anomaly , and meridional component of velocity V across the GoR at the latitudes of 57.33°N (right panels) and 57.63 °N (left panels) averaged over the summertime period from June 15 to September 15, 2012. Position of the sections is shown in Fig. 9a.

cold period of the year when the seasonal pycnocline is absent, the summertime anticyclonic gyre in the GoR was replaced by a cyclonic gyre with more intense currents in the eastern half of the gyre. Note that in the late fall – early winter the center of the whole-basin cyclonic gyre almost coincides with a salinity maximum formed east of the Cape Kolka by the saline water inflow from the Baltic Proper. Thus, the center of the whole-basin cyclonic gyre coincides with the mean position of a quasi-permanent mesoscale cyclonic eddy of the inflow origin, which therefore can be considered as a part of the gyre. In contrast, there is no such coincidence in summer when the mean position of a quasi-permanent mesoscale cyclonic eddy is located 14 km north of the Cape Kolka.

The vertical sections of summer mean temperature T, salinity S, potential density anomaly σ_θ and meridional component of velocity V across the GoR at the latitudes of 57.33°N and 57.63°N

(Fig. 10) display the NLC as a narrow, 10-km wide flow with maximum surface velocity of 0.13 m/s and 0.08 m/s, respectively. The NLC extends vertically as deep as the base of the seasonal thermocline. Note that the instant current speed in the NLC (not shown here) can reach 0.30–0.35 m/s (Lips et al., 2015). A new feature which was not displayed in the map of mean surface circulation (Fig. 9a) is a subsurface jet-like southward current along the eastern shore of the GoR with the maximum value of seasonally averaged velocity of 0.06 m/s at approximately 15 m depth (hereafter the SSLC – Southward Subsurface Longshore Current). Submergence of the SSLC is likely caused by the influence of the above-lying coastal buoyant plume of riverine waters, which has a tendency to flow northwards along the eastern coast of the GoR. The NLC is characterized by reduced salinity with the position of salinity minimum somewhat shifted seaward relative to the velocity maximum; another (stronger) salinity minimum is attached
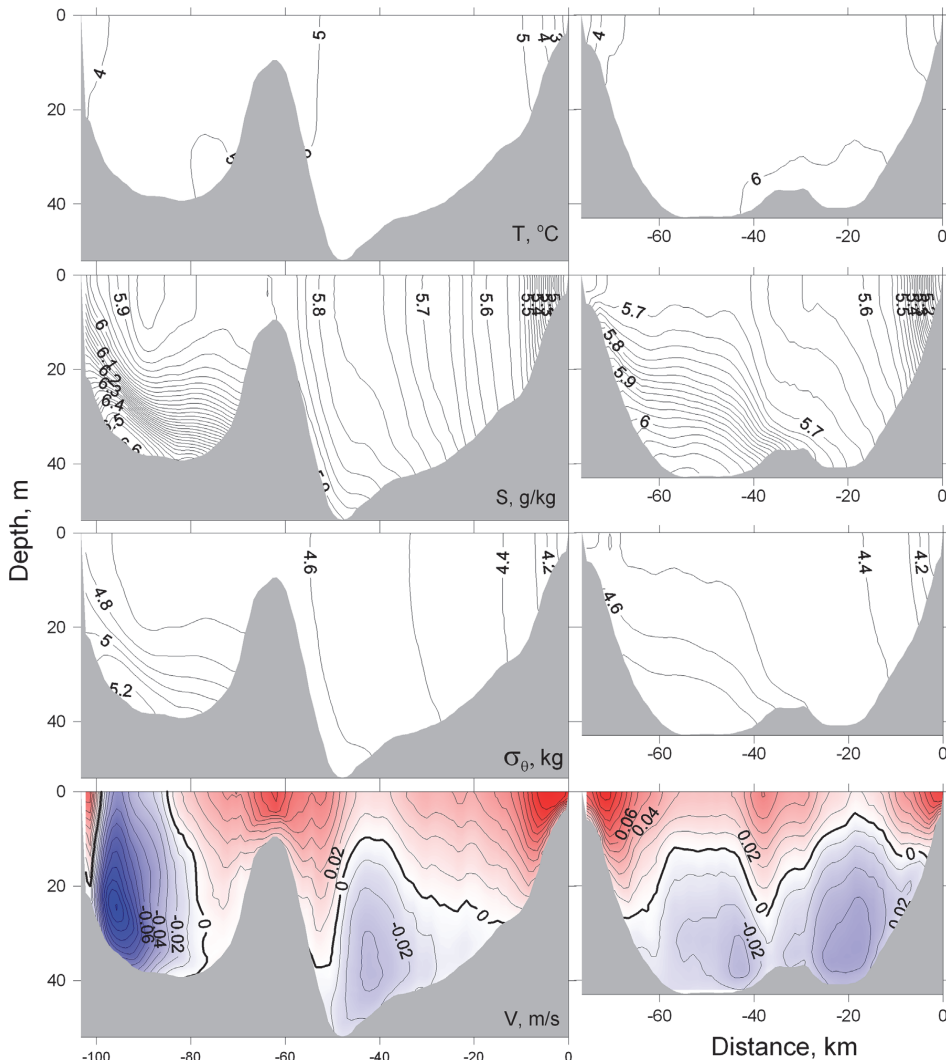

Fig. 11. The same as in Fig. 10 but at the latitudes of 57.33°N (right panels) and 57.75°N (left panels) for the late fall – early winter period from November 1 to December 31, 2012. Position of the sections is shown in Fig. 9b.

to the eastern shore and is obviously related with the coastal buoyant plume of riverine waters.

The vertical sections of temperature T, salinity S, potential density anomaly and meridional component of velocity V across the GoR at the latitudes of 57.33°N and 57.75°N, averaged for the period of November 1–December 31, 2012 (Fig. 11), display a tongue of overflow saline water moving to the south in the bottom layer along the western slope of the gulf and the quasi-permanent mesoscale cyclonic eddy of the inflow origin east of the Cape Kolka occupying the whole western region. Note that during the late fall – early winter season the maximum salinity in the bottom layer of the western region exceeds that of the eastern region just in accordance with the cyclonic type of the whole-basin circulation. To the contrary, during the summer season the maximum salinity in the bottom layer of the western region is lower than that of the eastern region just in accordance with the anticyclonic type of the whole-basin circulation (cf. Figs. 10 and 11). One more prominent feature seen in Fig. 11 is the presence of strong northward currents along the western and eastern shores of the GoR caused by a combined effect of the coastal buoyant plume and coastal upwelling/downwelling formed due to the prevailed southerly winds during the late fall – early winter 2012.

4.3. Extension of the basic run to the 3 year period

To check whether the above described alteration from the cyclonic gyre in the cold period of the year to the anticyclonic gyre in the summer season is a consistent feature observed in the GoR every year or it can be violated in some years due to the inter-annual variability of wind forcing, the basic, one-year run was extended to the thee-year period of 1 May 2012–30 April 2015. Low-pass filtered simulated time series of $\langle \mathrm{curl}(\vec{V_5}) \rangle$, $\langle \mathrm{curl}(\vec{\tau}/\rho_0) \rangle$, $\langle \tau_x/\rho_0 \rangle$ and $\langle \tau_y/\rho_0 \rangle$ (Fig. 12) display cyclonic circulation in the GoR during every cold season of 2012, 2013 and 2014, accompanied with positive (cyclonic) wind stress curl. As to the anticyclonic circulation in summer, it is observed in 2012 and to some extent in 2013 (less pronounced), and not observed at all in 2014. Such outcome is correspondent with the wind stress curl time series: $\langle \mathrm{curl}(\vec{\tau}/\rho_0) \rangle$ is negative in summer 2012, mostly negative in summer 2013 (for a shorter period of mid June–mid August), and close to nil in summer 2014. Also, it is worth noting that negative values of $\langle \mathrm{curl}(\vec{V_5}) \rangle$ and $\langle \mathrm{curl}(\vec{\tau}/\rho_0) \rangle$ in summers 2012 and 2013 were accompanied with westerly and southwesterly winds, while close to nil values of $\langle \mathrm{curl}(\vec{V_5}) \rangle$ and $\langle \mathrm{curl}(\vec{\tau}/\rho_0) \rangle$ in summer 2014 were accompanied with northwesterly and southerly winds.
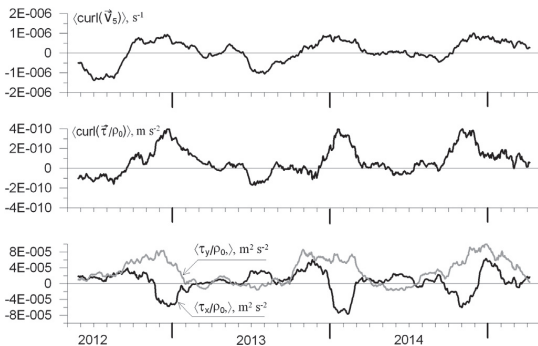

Fig. 12. Low-pass filtered (50 day window running mean) time series of $\langle \mathrm{curl}(\vec{V_5}) \rangle$, $\langle \mathrm{curl}(\vec{\tau}/\rho_0) \rangle$, $\langle \tau_x/\rho_0 \rangle$ and $\langle \tau_y/\rho_0 \rangle$ for the extended modeling period from May 1, 2012 to April 30, 2015.
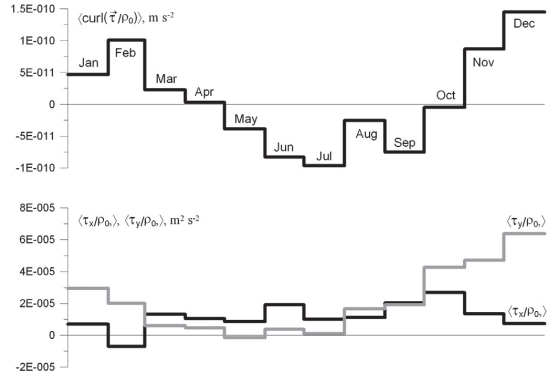

Fig. 13. Annual cycle of monthly mean values of wind stress curl and wind stress components averaged in the GoR area of $H > 20\,\mathrm{m}$ calculated from HIRLAM meteorology for the period of 2006–2014.

4.4. Inter-annual variability and the mean annual cycle of wind stress curl in the GoR area

Keeping in mind the revealed dependence of the current curl to the wind stress curl, the prevailing atmospheric forcing in the area on longer time scales needs to be analyzed with respect to the following questions: (1) What is the general wind stress curl in summer and winter? (2) To what extent is the seasonal alteration of the sign of $\langle \mathrm{curl}(\vec{\tau}/\rho_0) \rangle$ violated by the inter-annual variability? To answer the above questions, we addressed HIRLAM meteorology for the period 2006–2014 to calculate the mean seasonal cycle of monthly mean wind stress components and wind stress curl in the GoR area where $H > 20\,\mathrm{m}$ (Fig. 13), as well as the time series of the monthly mean values of $\langle \mathrm{curl}(\vec{\tau}/\rho_0) \rangle$, $\langle \tau_x/\rho_0 \rangle$ and $\langle \tau_y/\rho_0 \rangle$ (Fig. 14).

Fig. 13 clearly displays annual cycle of monthly mean wind forcing averaged in the area when negative wind stress curl under prevailing westerly–south-westerly wind stress in the warm season from May to September changes for positive wind stress curl under prevailing southerly wind stress in the cold season from November to March. Thus, we conclude that the mean seasonal cycle of the wind stress curl contributes to the prevailing anticyclonic circulation pattern in the summer and prevailing cyclonic pattern in the cold season.

Time series of monthly mean values of $\langle \mathrm{curl}(\vec{\tau}/\rho_0) \rangle$, $\langle \tau_x/\rho_0 \rangle$ and $\langle \tau_y/\rho_0 \rangle$ for the period of 2006–2014 calculated from HIRLAM meteorology dataset (Fig. 14) reveal that due to the inter-annual variability of wind forcing in the GoR area the typical pattern with positive (negative) $\langle \mathrm{curl}(\vec{\tau}/\rho_0) \rangle$ at southerly–southeasterly (westerly–southwesterly) winds in the cold (warm) seasons is observed
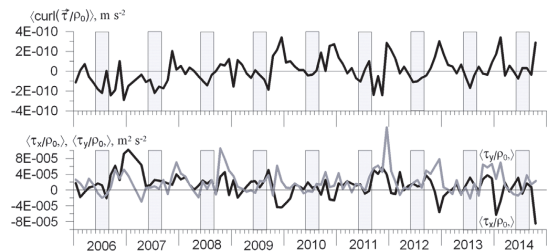

Fig. 14. Time series of the monthly mean values of wind stress curl and wind stress components averaged in the GoR area of $H > 20\mathrm{m}$ calculated from HIRLAM meteorology for the period of 2006–2014.

not every year. For example, winter 2006/2007 was characterized by negative $\langle \text{curl}(\vec{\tau}/\rho_0) \rangle$ at strong westerly winds while summers 2011 and 2014 were characterized by close to zero $\langle \text{curl}(\vec{\tau}/\rho_0) \rangle$ at southerly winds.

5. Discussion and conclusions

A regional, 0.5 nm and 20 sigma layer grid model of the Gulf of Riga (GoR) was implemented based on the Princeton Ocean Model code with initial TS fields and atmospheric forcing taken from HIROMB and HIRLAM output, respectively; the initial state started from a flat sea at rest. A basic run that covers a one-year period from May 1, 2012 to April 30, 2013, revealed the following results:

The current velocity curl $\langle \text{curl}(\vec{V_5}) \rangle$ and the wind stress curl $\langle \text{curl}(\vec{\tau}/\rho_0) \rangle$, both averaged over the deep part of the GoR where $H > 20$ m, are positively correlated with the correlation coefficient as high as 0.72; so the wind stress curl can be considered as a major contributor to the current velocity curl. In the cold period of the year when the seasonal thermocline is absent, the correlation coefficient between $\langle \text{curl}(\vec{\tau}/\rho_0) \rangle$ and $\langle \text{curl}(\vec{V_5}) \rangle$ increases to 0.79, while in the warm period of the year when the seasonal thermocline is developed, it decreases to 0.61. Weakening of the correlation between $\langle \text{curl}(\vec{\tau}/\rho_0) \rangle$ and $\langle \text{curl}(\vec{V_5}) \rangle$ in summer can be explained by the existence of relatively stable baroclinic currents – the NLC and SSLC, which are expected to be relatively insensible to the frequent (synoptic) changes of the wind stress curl. Negative value of $\langle \text{curl}(\vec{V_5}) \rangle$ in the summer season is determined by a combined effect of negative $\langle \text{curl}(\vec{\tau}/\rho_0) \rangle$, thermal density stratification and bottom topography. During calm periods (like one observed from mid-February to mid-April 2013) the negative value of $\langle \text{curl}(\vec{V_5}) \rangle$ (that characterizes anticyclonic circulation) is determined by a combined effect of the river runoff, saline/dense water inflow and mixed water outflow through the Irbe Strait.

The mean summertime surface circulation in the GoR being developed during the presence of seasonal thermocline and under the prevalence of westerly winds displays a whole-basin anticyclonic gyre with more intense currents in the western half of the gyre. Two seasonal baroclinic currents are identified: the Northward Longshore Current (NLC) in the western part of the GoR and the Southward Subsurface Longshore Current in the eastern part of the GoR.

In the cold season of the year (when seasonal pycnocline was absent and southerly winds prevailed), the anticyclonic gyre in the GoR was replaced by a cyclonic gyre with more intense currents in the eastern half of the gyre. As it was shown by the model run of one year duration the change of the mean surface circulation in the GoR from anticyclonic in summer to cyclonic in late fall – early winter was primarily caused by the respective change of the mean wind stress curl in the area.

In order to generalize the above-mentioned findings the basic run was extended to the three-year period of 1 May 2012–30 April 2015 and the mean annual cycle and inter-annual variability of the wind stress curl averaged over the GoR area was analyzed for the period of 2006–2015. It was shown that the anticyclonic (cyclonic) gyre in the GoR, being typical for the summer (winter) season, is probably not developed every summer (winter) depending on the inter-annual variability of the prevailing wind forcing. For example, negative values of $\langle \text{curl}(\vec{\tau}/\rho_0) \rangle$ were not typical in summer 2014 and, as a result, the mean anticyclonic gyre was not developed. To the contrary, winter 2006/2007 was characterized by mostly negative values of $\langle \text{curl}(\vec{\tau}/\rho_0) \rangle$ implying the appearance of anticyclonic gyre, which is atypical for the cold season.

A model study of the springtime circulation in the GoR was recently reported by Soosaar et al. (2014). The major finding of the study was the existence of an anticyclonic gyre in the southern GoR driven, according to the authors, primarily by the estuarine type density field and strongly affected by wind forcing (the gyre was strengthened by the easterly winds and weakened/blocked by the westerly winds). We argue that it may be considered as a river plume bulge during the season of large run-off modified by wind forcing. It is interesting to note that, in accordance with Fig. 13, the mean value of wind stress curl in April is close to zero, which would explain why Soosaar et al. (2014) did not find neither cyclonic nor anticyclonic whole-basin gyre in the GoR but a double gyre pattern instead.

In a recent overview of the Baltic Sea physical oceanography Omstedt et al. (2014) have concluded that strong and stable cyclonic gyres exist in both the Baltic Proper and Bothnian Sea (e.g. Meier, 2007) while the strength and persistence of currents are lower in the Gulf of Riga, Gulf of Finland (GoF), and Bothnian Bay. The results of the present study and by Soosaar et al. (2014) demonstrate that the circulation pattern in the GoR is largely influenced by the prevailing wind forcing in different seasons and years. Similarly, several recent model experiments have suggested that the circulation pattern in the GoF could differ from the classical cyclonic pattern (e.g. Andrejev et al., 2004) depending on the considered period (e.g. Elken et al., 2011; Soomere et al., 2011). Current measurements have confirmed the existence of an average westward flow in the GoF surface layer at the southern slope (Suhhova et al., 2015), which could be a sign of the existing anticyclonic circulation cells predicted by the numerical experiments (Lagemaa, 2012; Elken et al., 2011). Note that the wind stress curl as one of the possible mechanisms contributing to formation of general circulation patterns has not been analyzed in the GoF model experiments.

Omstedt et al. (2014) also suggested that one reason for varying model outcomes in regard of circulation patterns in the GoF and GoR could be the resolution of models, which often has been too coarse in comparison with the internal Rossby radius in those relatively shallow sub-basins of the Baltic Sea. In the present study, the grid spacing of 0.5 nautical miles was applied, which is less than the internal Rossby radius in the GoR. However, we noticed that the model overestimated the thickness of the seasonal thermocline. Although we assume that this drawback has no potential to affect the main dynamical features discussed in the paper, it has to be studied further what is causing this alteration of model results from the observations.

The brief summary of the present study is that the whole-basin circulation pattern in the GoR is primarily governed by the wind stress curl and bottom topography in the cold season and by a combined effect of the wind stress curl, seasonal stratification and bottom topography in the summer. This conclusion is in accordance with the results of Schwab and Beletsky (2003) in regard to the large-scale circulation in Lake Michigan.

References

Andrejev, O., Myrberg, K., Alenius, P., Lundberg, P.A., 2004. Mean circulation and water exchange in the Gulf of Finland – a study based on three-dimensional

modeling. Boreal Environ. Res. 9, 1–16.

Baranov, A.N., 1970. Currents in the Gulf of Riga and Irbe Strait. Collected articles of the Riga Hydrometeorology Observatory, No. 13, Riga, 86 p. (in Russian).

Berzinsh, V., 1995. Hydrology. In: Ojaveer, E. (Ed.), Ecosystem of the Gulf of Riga between 1920 and 1990. Estonian Academy Publishers, Tallinn, pp. 7–32.

Berzinsh, V., 1980. Interannual and seasonal changes of water salinity in the Gulf of Riga. Fishery Studies in the Baltic Sea Basin vol. 15. Avots, Riga, pp. 3–12.

Blumberg, A.F., Mellor, G.L., 1983. Diagnostic and prognostic numerical calculation studies of the South Atlantic Bight. J. Geophys. Res. 88, 4579–4592.

Csanady, G.T., 1975. Hydrodynamics of large lakes. Annu. Rev. Fluid Mech. 7, 357–386.

Ezer, T., Mellor, G.L., 1994. Diagnostic and prognostic calculations of the North Atlantic circulation and sea level using a sigma coordinate ocean model. J. Geophys. Res. 99, 14,159–14,171.

Elken, J., Nõmm, M., Lagemaa, P., 2011. Circulation patterns in the Gulf of Finland derived from the EOF analysis of model results. Boreal Environ. Res. 16, 84–102.

Elken, J., Raudsepp, U., Lips, U., 2003. On the estuarine transport reversals in deep layers of the Gulf of Finland. J. Sea Res. 49, 267–274.

Fennel, W., Seifert, T., Kayser, B., 1991. Rossby radii and phase speeds in the Baltic Sea. Cont. Shelf Res. 11, 23–36.

Lagemaa, P., 2012. Operational forecasting in Estonian marine waters (Ph.D. thesis). Tallinn University of Technology, TUT Press, pp. 45.

Leppäranta, M., Myrberg, K., 2009. Physical Oceanography of the Baltic Sea. Praxis Publishing Ltd, Chichester, UK, p. 370.

Lilover, M.-J., Lips, U., Laanearu, J., Liljebladh, B., 1998. Flow regime in the Irbe Strait. Aquat. Sci. 60, 253–265.

Lips, U., Lilover, M.-J., Raudsepp, U., Talpsepp, L., 1995. Water renewal processes and related hydrographic structures in the Gulf of Riga. In: Elken, J., Toompuu, A. (Eds.), Hydrographic studies within the Gulf of Riga Project, 1993–1994, EMI Report Series, pp. 1–34.

Lips, U., Zhurbas, V., Skurda, M., Väli, G., 2015. A numerical study of circulation in the Gulf of Riga, Baltic Sea. Part II: Mesoscale features and freshwater transport pathways. Cont. Shelf Res. (submitted for publication)

Männik, A., Merilain, M., 2007. Verification of different precipitation forecasts during extended winter-season in Estonia. HIRLAM Newsletter, No. 52, pp. 65–70.

Meier, H.E.M., 2007. Modeling the pathways and ages of inflowing salt- and freshwater in the Baltic Sea. Estuar. Coast. Shelf Sci. 74, 610–627.

Mellor, G.L., Yamada, T., 1982. Development of a turbulence closure model for geophysical fluid problems. Rev. Geophys. Space Phys. 20 (4), 851–875.

Ojaveer, O. (Ed.), 1995. Ecosystem of the Gulf of Riga between 1920 and 1990. Estonian Academy Publishers, Tallinn.

Omstedt, A., Elken, J., Lehmann, A., Leppäranta, M., Meier, H.E.M., Myrberg, K., Rutgersson, A., 2014. Progress in physical oceanography of the Baltic Sea during the 2003–2014 period. Prog. Ocean. 128, 139–171.

Raudsepp, U., Beletsky, D., Schwab, D.J., 2003. Basin scale topographic waves in the Gulf of Riga. J. Phys. Oceanogr. 33, 1129–1140.

Schwab, D.J., Beletsky, D., 2003. Relative effects of wind stress curl, topography, and stratification on large-scale circulation in Lake Michigan. J. Geophys. Res. 108 (C2), 3044. http://dx.doi.org/10.1029/2001JC001066.

Seifert, T., Kayser, B., 1995. A high resolution spherical grid topography of the Baltic Sea, Meereswissenschaftliche Berichte (Marine Science Reports), No. 9, pp. 72–88.

Soomere, T., Delpeche, N., Viikmäe, B., Quak, E., Meier, H.E.M., Döös, K., 2011. Patterns of current induced transport in the surface layer of the Gulf of Finland. Boreal Environ. Res. 16A, 49–63.

Soosaar, E., Maljutenko, I., Raudsepp, U., Elken, J., 2014. An investigation of anticyclonic circulation in the southern Gulf of Riga during the spring period. Cont. Shelf Res. 78, 75–84.

Stiebrins, O., Väling, P., 1996. Bottom Sediments of the Gulf of Riga. Geological Survey of Latvia, Riga.

Suhhova, I., Pavelson, J., Lagemaa, P., 2015. Variability of currents over the southern slope of the Gulf of Finland. Oceanologia 57, 132–143.

Yankovsky, A.E., Chapman, D.C., 1997. A simple theory for the fate of buoyant coastal discharges. J. Phys. Oceanogr. 27, 1386–1401.

Yurkovskis, A., Wulff, F., Rahm, L., Andrushaitis, A., Rodriguez-Medina, M., 1993. A nutrient budget of the Gulf of Riga; Baltic Sea. Estuar. Coast. Shelf Sci. 37 (2), 113–127.

Paper III

Lips, U., Zhurbas, V., Skudra, M., Väli, G. (2016). A numerical study of circulation in the Gulf of Riga, Baltic Sea. Part II: Mesoscale features and freshwater transport pathways. *Continental Shelf Research*, 115(1), 44–52, doi: 10.1016/j.csr.2015.12.018.

Research papers

A numerical study of circulation in the Gulf of Riga, Baltic Sea. Part II: Mesoscale features and freshwater transport pathways

Urmas Lips [a,*], Victor Zhurbas [a,b], Maris Skudra [a,c], Germo Väli [a]

[a] Marine Systems Institute, Tallinn University of Technology, Akadeemia Road 15A, 12618 Tallinn, Estonia
[b] Shirshov Institute of Oceanology, 36 Nakhimovsky Avenue, 117997 Moscow, Russia
[c] Latvian Institute of Aquatic Ecology, Daugavgrivas Street 8, LV-1048 Riga, Latvia

ARTICLE INFO

ABSTRACT

A regional eddy-resolving model is developed to study mesoscale processes in the Gulf of Riga in relation to river runoff, saltwater inflow, and atmospheric forcing. A number of mesoscale phenomena are simulated and discussed, such as meandering of coastal buoyant plume/current of riverine waters and formation and splitting of cyclonic eddies related to the saltwater inflow. It is shown that the Daugava River discharge forms a surface-advected plume (Yankovsky and Chapman, 1997) consisting of an anticyclonic bulge and coastal buoyant jet. In case of no saltwater inflow and no atmospheric forcing, the river runoff is distributed between the growing anticyclonic bulge and the coastal current in proportion of about 7:6. In the summer season, a substantial fraction of freshwater from the anticyclonic bulge can be transported to the north by the anticyclonic whole-basin circulation gyre leading to the bimodal transport pathways of the Daugava River plume.

© 2016 Elsevier Ltd. All rights reserved.

1. Introduction

Study of mesoscale processes in the Baltic Sea has a long history. It was started in the 1970s when regular eddy-resolving CTD surveys were introduced in the Baltic Proper (Aitsam and Elken, 1982). Since then, various mesoscale structures have been revealed in the Baltic Sea such as intrapycnocline anticyclonic lenses, sub-surface cyclonic eddies – negative lenses and "ordinary" upper layer cyclonic and anticyclonic eddies (Reißmann, 2005, 2006). The intrapycnocline anticyclonic lenses, which resemble Mediterranean water lenses (Meddies) in the Atlantic, were found in the East Gotland Basin (Elken et al., 1988; Kõuts et al., 1990; Elken, 1996; Zhurbas and Paka, 1997), Bornholm Basin and Słupsk Furrow (Piechura, 2007). The sub-surface cyclonic eddies – negative lenses usually formed during saline water inflows were observed in the Arkona Basin (Lass and Mohrholz, 2003), Bornholm Basin and Słupsk Furrow (Zhurbas et al., 2004, 2012; Piechura, 2007), Gdansk Basin (Zhurbas et al., 2004) and East Gotland Basin (Zhurbas and Paka, 1997). Lots of mesoscale eddies, both cyclonic and anticyclonic, were observed in infrared images of the Gulf of Finland during a relaxation period of upwelling/downwelling events (Zhurbas et al., 2008; Laanemets et al., 2011). Simulation of mesoscale eddies in the Baltic Sea in the framework of eddy-resolving

circulation models was performed by Zhurbas et al. (2003, 2004, 2006, 2008, 2012) and Laanemets et al. (2011).

The water balance of the Gulf of Riga (GoR), a semi-enclosed basin in the eastern part of the Baltic Sea, is determined by the saltwater inflow from the Baltic Proper mainly through the Irbe Strait in the northwest corner, freshwater inflow mainly in the southeast corner, and compensating mixed water outflow mainly through the Irbe Strait. These processes and variable wind forcing have a potential to form mesoscale structures such as cyclonic eddies related to the saltwater inflow, freshwater plumes and intrusions, and coastal buoyant jets. Modeling experiments have been conducted using eddy-permitting (or even eddy-resolving in most of the basins) models covering the entire Baltic Sea or part of it including the Gulf of Riga, however, specific studies on mesoscale variability in the GoR are almost absent. Raudsepp and Elken (1999) studied synoptic and mesoscale variability of the Irbe Strait salinity front revealed by an extensive measurement campaign in the area (Lips and Lilover, 1995). They concluded that the used model resolution of 2.5 nm was not enough to resolve mesoscale features, including the relative vorticity associated with the frontal dynamics.

In a recent study by Soosaar et al. (2014), the monthly circulation patterns in the Gulf of Riga were reproduced using General Estuarine Transport Model with the horizontal resolution of 2 nm. They found that the anticyclonic circulation pattern is more frequent in the southern GoR in the spring period and the spreading of Daugava River water along the eastern coast takes

---

* Corresponding author.
  E-mail address: urmas.lips@msi.ttu.ee (U. Lips).

place less frequently. Based on the measurements in 1993–1995, Stipa et al. (1999) have reported the presence of an almost ideal Daugava River plume bulge and an associated jet current along the eastern coast. A simple model of river plume dynamics has been developed by Yankovsky and Chapman (1997), and the influence of background circulation and topography to the plume dynamics has been studied in idealized conditions (e.g. Schiller and Kourafalou, 2010; Fong and Geyer, 2002). However, despite of the reported studies for many other coastal sea areas (e.g. Jurisa and Chant, 2012; Kourafalou, 2001), similar experiments have not been carried out to define the role of different forcing factors and processes to the spreading of Daugava River waters in the Gulf of Riga.

The objective of this work is as follows:

– to develop a local, high-resolution numerical model capable to adequately simulate the GoR hydrodynamics at the mesoscale and, in particular, the dynamics of the Daugava River plume;
– based on numerical experiments with different model scenarios, to investigate the role of different processes, such as intrinsic buoyant plume dynamics, thermohaline and wind-driven circulation, including coastal upwellings/downwellings, in formation of mesoscale structures and transport/mixing of the Daugava River plume.

2. Model setup and theoretical background

2.1. Model setup

Details of the model setup are given in the Part I (Lips et al., 2016); here only the basic features of the applied model are shortly described. The high-resolution numerical model of the GoR is based on the Princeton Ocean Model (POM) (Blumberg and Mellor, 1983), a sigma co-ordinate, free surface, hydrostatic model, where the subgrid-scale processes are parameterized using the 2.5 closure scheme by Mellor and Yamada (1982). The model domain includes the entire Baltic Sea closed at the Danish Straits; digital topography is taken from (Seifert and Kayser, 1995). The grid cell size along latitude and longitude, Δx and Δy, is varying spatially from $\Delta x = (1/60)°$ and $\Delta y = (1/120)°$ (or $\Delta x \approx \Delta y = 0.5$ nautical miles=926 m) in the GoR and its vicinity to $\Delta x = (1/15)°$ and $\Delta y = (1/30)°$ in distant parts of the Baltic Sea; there are 20 uniform sigma layers in the vertical direction.

Two rivers inflowing to the GoR are included to the model: the Daugava River and the Pärnu River with the annual mean volume fluxes of 660 m^3 s^{-1} and 48 m^3 s^{-1}, respectively. Since the Lielupe and Gauja, the second and third largest rivers that contribute to the freshwater inflow to the GoR, have their mouths within a 20-km vicinity of the Daugava mouth, the three rivers can be considered as a single source with the volume flux of 818 m^3 s^{-1}. The latter volume flux is the mean runoff of Latvian rivers into the GoR for 1921–1990, May–October, taken from http://www.modlab.lv/publications/1998/publ3.htm.

The basic model run comprised the period from May 1 to October 31, 2012. Initial conditions and atmospheric forcing were compiled from the output of operational models HIROMB (see http://www.smhi.se/en/Research/Research-departments/Oceanography/hiromb-1.8372) and HIRLAM (Männik and Merilain, 2007), with the inclusion of data collected in the Data Assimilation System (DAS) coupled with the Baltic Environmental Database (see http://nest.su.se/das). The DAS data were supplemented with the CTD data collected in the GoR by Estonian and Latvian research institutes in 1996–2013 (see Lips et al. (2016) for details).

In order to separate the intrinsic buoyant plume dynamics and the effects related to the thermohaline circulation and atmospheric forcing, three numerical experiments were performed:

(1) intrinsic propagation of the Daugava River plume (spatially uniform density distribution, no atmospheric forcing), (2) propagation of the Daugava River plume driven by buoyant plume dynamics and thermohaline circulation (real initial fields of temperature and salinity, no atmospheric forcing), and (3) the basic model run (real initial fields of temperature and salinity and real atmospheric forcing). Results of these three numerical experiments are addressed in the Sections 3.1, 3.2 and 3.3, respectively.

2.2. Predicted parameters of the Daugava River plume

Based on a simple analytical model developed by Yankovsky and Chapman (1997), the characteristic offshore width, y_s, and depth, h_b, of the buoyant plume can be expressed as follows:

$$y_s = 2(3g^*h_0 + v_i^2)/\left[(2g^*h_0 + v_i^2)^{1/2}f \right],$$ (1)

$$h_b = (2Qf/g^*)^{1/2},$$ (2)

where g^* is the reduced gravity based on the inflow density anomaly, h_0, v_i, L, and $Q \equiv v_i h_0 L$ are the inflow depth, velocity, width, and volume flux, respectively, and f is the Coriolis parameter. Offshore propagation of the buoyant fluid results from two competing mechanisms: (1) the radial spread of the lighter water over the ambient water, being deflected by the Coriolis force and producing an anticyclonic cyclostrophic plume, and (2) offshore transport of buoyant water in the frictional bottom boundary layer that moves the entire plume offshore while maintaining contact with the bottom (Yankovsky and Chapman, 1997). If $h_b < h_0$, then the bottom friction is of no importance and a purely surface-advected plume is formed. If $h_b > h_0$ and the h_b isobath is farer offshore than y_s, then a bottom-advected plume, trapped along the h_b isobath, is formed. Finally, if $h_b > h_0$ but the h_b isobath is shoreward of y_s, then an intermediate plume is formed. The purely surface-advected plume consists of an anticyclonic bulge of riverine water attached to the mouth and a coastal jet-like current of a smaller, nearly constant offshore width carrying a part of riverine waters rightwards (in the northern hemisphere). In the case of the bottom-advected plume, no anticyclonic bulge is formed.

In the case of the Daugava River, the mean annual runoff is 20.8 km^3 yr^{-1} (Leppäranta and Myrberg, 2009) or $Q = 660$ m^3 s^{-1}, $g^* = 0.043$ m s^{-2} (at the background salinity of 5.6 g kg^{-1} in the Gulf of Riga), and $f = 1.22 \times 10^{-4}$ s^{-1}, (at latitude of 57°N), which yields an estimate of the characteristic depth of the buoyant river plume as $h_b \approx 2$ m (see Eq. (2)). If taking into account that the average monthly discharges are ranging between 200 and 1600 m^3 s^{-1} (e.g. Klavins et al., 2002) then the estimate of h_b varies between 1.1 and 3.0 m, being still less than $h_0 = 4$ m (the average sea depth at the Daugava mouth). Thus, it can be concluded that the Daugava River plume is expected to be referred as the surface-advected plume since the inflow depth $h_0 = 4$ m is larger than the estimated characteristic depth of the buoyant plume. Stipa et al. (1999) made the same conclusion that the Daugava River discharge forms a surface-advected plume. Soosaar et al. (2014) suggested that the plume could exhibit a well-developed bulge at certain months; however, in the conditions of large discharge and low density anomaly it could be considered as a bottom-advected plume (maximum h_b of 7.5 m was estimated).

Since the large river discharge and small density anomaly could not coexist frequently, we assume that the Daugava River plume is a surface-advected plume. If taking $v_i = 0.25$ m s^{-1}, which corresponds to the inflow velocity in the case of the average volume flux and river channel parameters between the jetties, the characteristic offshore width of the bulge (y_s, see Eq. (1)) can be estimated as 14.9 km. This result is in accordance with the

estimate of the offshore extension of the bulge of 15 km made by Stipa et al. (1999). Note that the latter estimates are made under a steady state assumption while it has been shown that in the absence of any ambient current, the plume does not reach a steady state (Fong and Geyer, 2002). Furthermore, variable wind forcing largely influences the dynamics of river plumes that might lead to their inherent unsteadiness (e.g. Horner-Devine et al., 2008).

3. Results

3.1. Intrinsic propagation of Daugava River buoyant plume in the GoR

To simulate intrinsic propagation of the Daugava River plume, a model run with spatially uniform initial fields of temperature and salinity at $T_0 = 10\ ^\circ C$ and $S_0 = 5.6$ g/kg, respectively, and no atmospheric forcing was performed. Fig. 1a shows the simulated salinity and current velocity distributions in the surface layer of the GoR at 1 m depth at day 69 from the model run onset. The Daugava River plume is seen to consist of an anticyclonic bulge of riverine water attached to the river mouth and a coastal jet-like current carrying part of the riverine waters to the north along the eastern coast of the GoR. A transition zone between the bulge and the northward coastal jet displays wave-like disturbances with wavelength of ~8 km. Otherwise, the shape of the observed plume confirms the diagnostics made based on the conceptual model by Yankovsky and Chapman (1997) – the Daugava River plume is the surface-advected plume. Note that the observed offshore extension of the bulge of 20–25 km (at day 69; see Fig. 1a) is somewhat larger than the theoretical estimate of it (14.9 km). The discrepancy is not surprising because the theoretical expression for y_s was derived by assuming that the plume is in a steady state. However, in the present model experiment the bulge appeared to grow in time as it has also been shown in several other studies, e.g. by Fong and Geyer (2002).
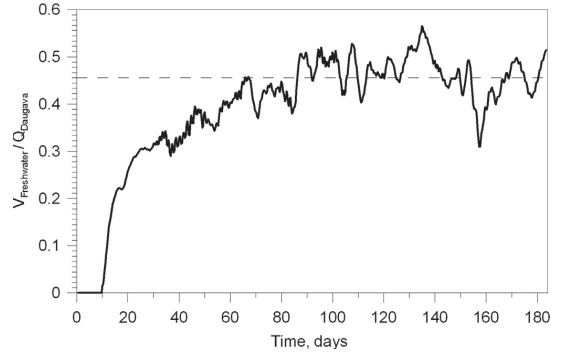
Fig. 2. Time series of the ratio of freshwater transport by the coastal jet-like current to the Daugava River runoff.

Freshwater transport of the coastal jet-like current across a zonal section $y = const$ can be calculated as

$$V_{freshwater} = \iint \frac{S_0 - S(x, y, z)}{S_0} v(x, y, z)\,dx\,dz \tag{3}$$

where integration is provided from the sea surface to the sea bottom and from the eastern shore of the GoR to a distance greater than the whole width of the buoyant coastal current. Calculations for $y = 57.56^\circ N$ (see a white line in Fig. 1) showed that the ratio of the freshwater transport by the coastal jet to the Daugava River volume flux, after approximately 80-day transition period, was established at $V_{freshwater}/Q_{Daugava} = 0.4$–$0.5$ with the mean value of 0.46 (see Fig. 2). The last estimate coincides with the estimates by Fong and Geyer (2002) who reported 0.40–0.48 for the ratio of freshwater transport by the coastal jet to the river volume flux in their model experiments. It shows that in case of the absence of other forcing components (atmospheric forcing and saltwater
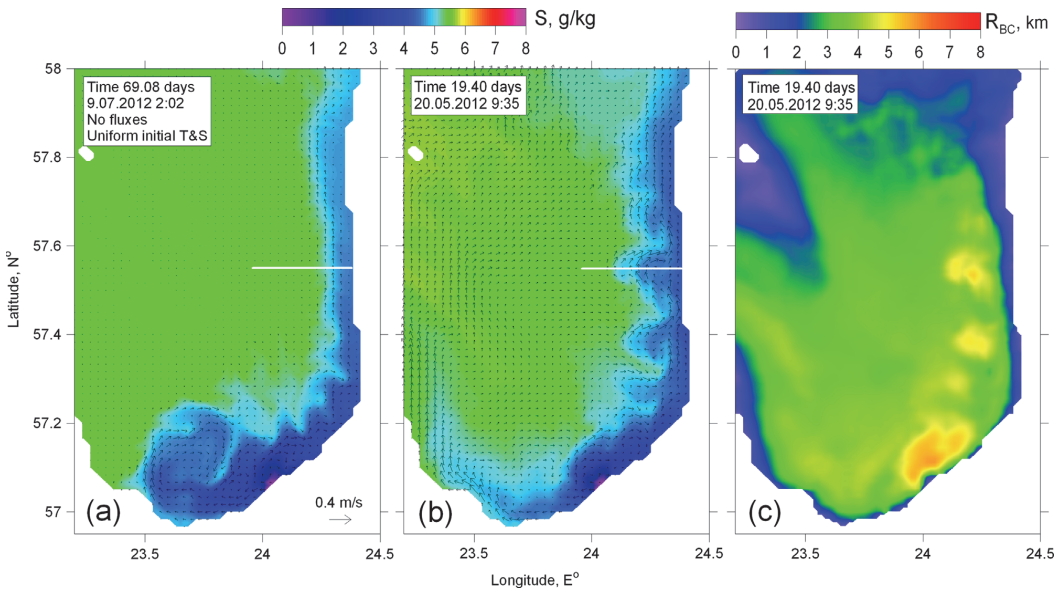
Fig. 1. Plan views of simulated salinity and current velocity in the surface layer (at 1 m depth) of the south-eastern part of the GoR: (a) – a numerical experiment with uniform initial temperature and salinity fields and no atmospheric forcing, results after 69 days from the model run onset; (b) – the basic run on 20.05.2012 at 9:35 and (c) – the same as (b) but for the baroclinic Rossby radius. A white-colored horizontal strait-line segment on (a) and (b) panels is the position of a vertical section shown in Fig. 7.
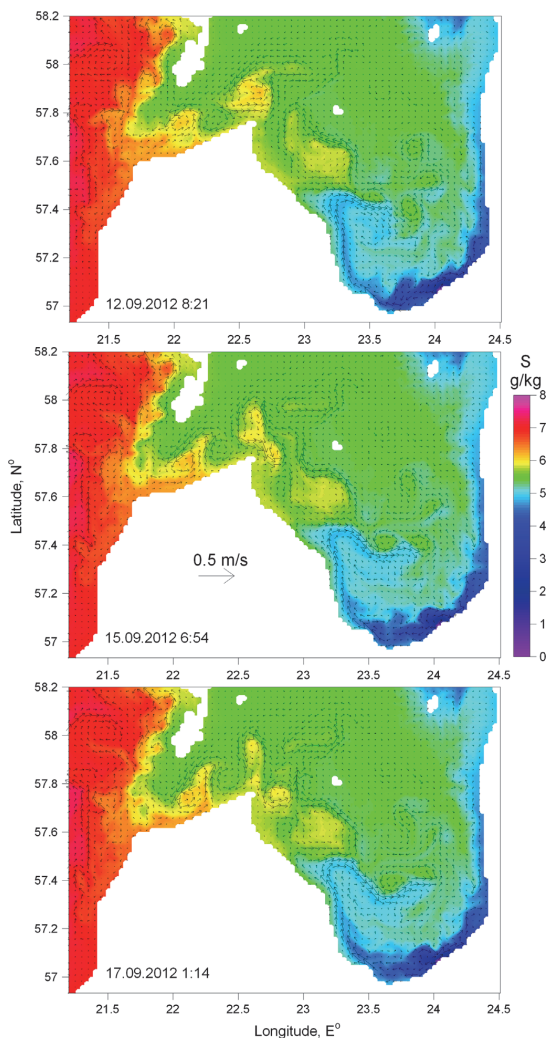
Fig. 3. Three successive plan views of surface layer salinity and current velocity vectors that demonstrate an event of splitting of haline cyclonic eddy on the beam of the Cape Kolka (numerical experiment with no atmospheric forcing).

Fig. 4. Plan views of simulated salinity and current velocity in the surface layer (at 5 m depth); the snapshots for the date of 25.07.2012.

inflows) more than half of the river discharge would feed the growing anticyclonic bulge.

3.2. Mesoscale features of thermohaline circulation (the no atmospheric forcing case)

Due to the salinity difference between the Baltic Proper and the Gulf of Riga of approximately 1.5 g kg^{-1}, a salinity front and a gravitational (density) current are formed in the Irbe Strait (Fig. 3). The gravitational flow that transports saltwater eastward from the Baltic Proper to the GoR is attached to the southern shore between the Irbe Strait and the Cape Kolka just in accordance with geostrophic equilibration. The flow is highly unstable and actually, presents a chain of mesoscale cyclonic eddies with a core of increased salinity/density. The eddies are generated at the Irbe Strait
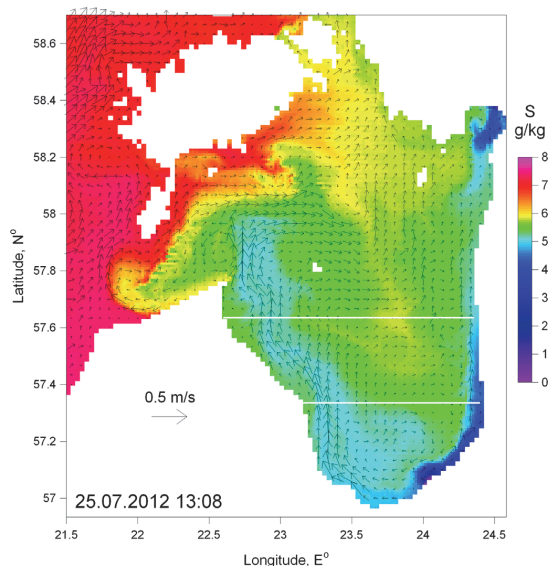
sill with the periodicity of 10–15 days and move eastwards along the southern shore to the Cape Kolka for the period of about 20–30 days with translation velocity of ~0.03 m s^{-1}. While propagating along the Irbe Strait towards the Cape Kolka, the eddy size (diameter) increases from approximately 10 km to 15 km. On the beam of the Cape Kolka, the cyclonic eddy splits into two smaller cyclonic eddies; one of these eddies travels to NE and the other to SE. Such an event of splitting of a cyclonic eddy is demonstrated in Fig. 3 by three successive plan views of surface layer salinity and current vectors.

As shown by Lips et al. (2016) the anticyclonic gyre dominates the general circulation in the GoR in summer. This circulation pattern is determined by a combined effect of the prevailing negative wind curl, thermohaline stratification and bottom topography. Note that similar conclusion about the anticyclonic circulation in the upper layer in the southern GoR due to the 3-dimensional estuarine type density field was drawn by Soosaar et al. (2014). Thus, such general thermohaline circulation in the gulf could cause substantial modification of the Daugava River plume. As a result, the low-saline riverine water from the anticyclonic bulge can propagate along the shore to the left as far as two thirds of alongshore distance from the Daugava mouth to the Cape Kolka (see Fig. 3). At that point, the low-saline riverine water meets the high-saline water that came from the Baltic Proper in the form of cyclonic eddies. Due to the convergence of water masses, the water mass of riverine origin turns right to the open sea and ultimately finds its way farther to the north in the form of multiple low-saline squirts leaking between the high-saline cyclones. Note that along with the left-hand propagation of riverine waters caused by thermohaline circulation, some fraction of Daugava River runoff is still involved in the right-hand coastal jet caused by intrinsic buoyant plume dynamics in rotating media. However, the width of the coastal jet and the volume flux involved in case of the background thermohaline circulation are considerably smaller than the width and volume flux in case of the pure buoyant plume.
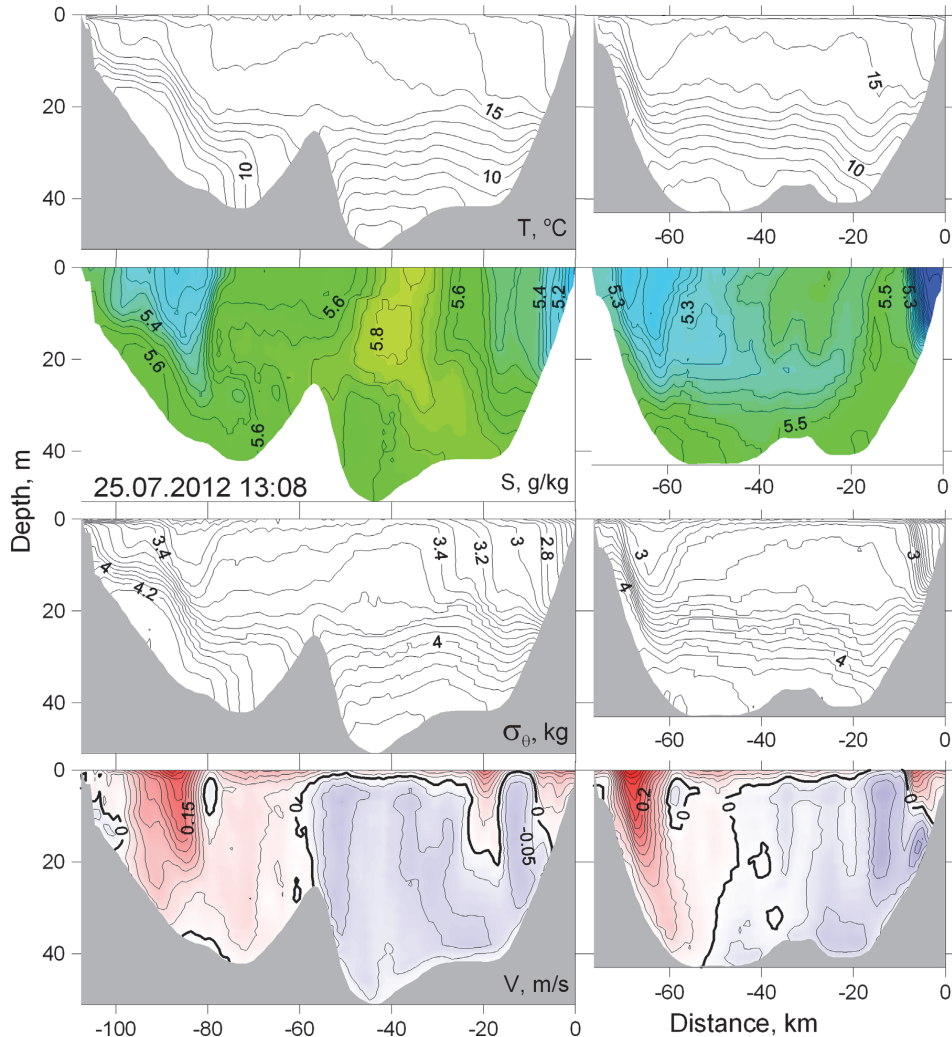
Fig. 5. Zonal–vertical transects of temperature *T*, salinity *S*, potential density anomaly σ_θ and meridional component of velocity *V* across GoR at latitude of 57.33°N (right panels) and 57.63°N (left panels); the snapshots for the date of 25.07.2012. Position of the transects is shown in Fig. 4 by the white lines.

3.3. Combined effects of forcing mechanisms on plume structure and transport

It was shown in Lips et al. (2016) that the summer season is characterized by whole-basin anticyclonic circulation in the GoR caused by the prevailing negative value of the wind stress curl, enhanced stratification due to the presence of seasonal thermocline, and bottom topography (see Lips et al. (2016) for details). The Daugava River plume water can be partly involved in the anticyclonic circulation and transported to the north along the western coast, whereas the rest of riverine waters goes to the north along the eastern coast as a buoyant coastal jet.

A plan view snapshot of simulated currents and salinity in the surface layer in the GoR for the date of 25.07.2012 is shown in Fig. 4. The overall circulation pattern is clearly characterized by a whole-basin anticyclonic gyre with enhanced intensity of currents in the western half-basin where a jet-like alongshore current can

be identified. In Lips et al. (2016), this seasonal current was named as the Northward Longshore Current (NLC). Vertical structure of the NLC is illustrated in Fig. 5 where two modeled zonal transects of temperature, salinity, density and meridional component of current velocity across the GoR are presented for the same date. The analyzed time period was characterized by a moderate SE wind of about 5 m s^{-1} followed by a 2-day period of SW gale with the wind speed of 15 m s^{-1}. These winds are favorable for a sea-level set-down/coastal upwelling along the western shore of the GoR and surges/coastal downwelling along the opposite, eastern shore of the GoR. As a result, the NLC has intensified to achieve instant velocity as high as 0.3–0.4 m s^{-1}, and the related tongue of reduced salinity of riverine origin was identified as far as at 58°N; thus, almost reaching the Saaremaa Island. It is important to note that the NLC is located in the area of maximum isopycnal slope and the lateral boundary of the jet has an inclination of the same sign as that of the isopycnals (i.e. the position of velocity
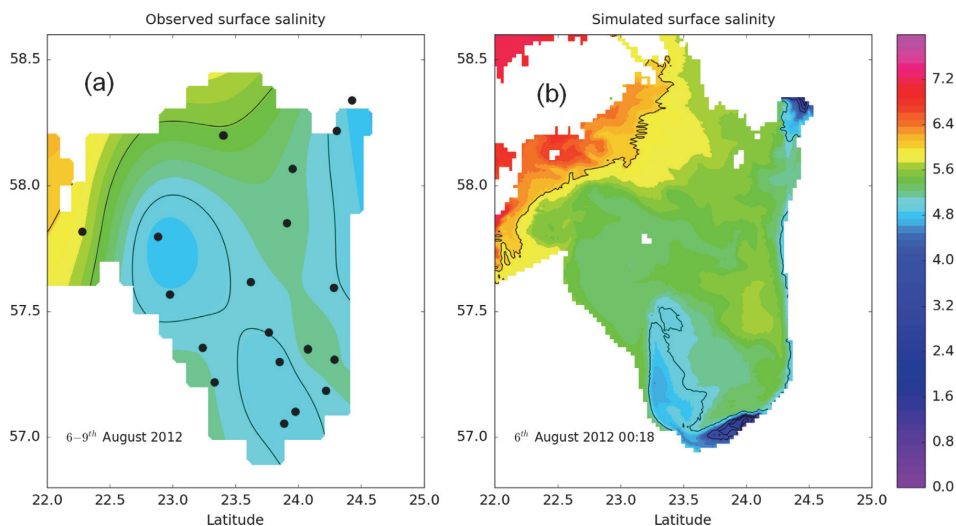
Fig. 6. (a) A plan view of surface layer salinity drawn using a very scarce set of CTD casts performed in the period of August 6–9, 2012, aboard Estonian R.V. SALME. (b) Modeled surface salinity for the date of August 6, 2012.

maximum shifts seaward with the depth). The NLC is associated with a baroclinic (density) front, which is supposed to be a zone of flow convergence (e.g. Fedorov, 1986). Due to the convergence, the low-salinity riverine water sinks down and spreads seaward occupying an intermediate layer and forming an intrusion with salinity inversion of approximately 0.1 g kg^{-1} (see Fig. 5). Transport of riverine waters by the NLC, their sinking and spreading within an intermediate layer ultimately works for effective mixing of the river runoff with the GoR waters.

Using modeled zonal transects of salinity and meridional component of current velocity shown in Fig. 5, one can roughly estimate the freshwater transport by the NLC, $V_{freshwater}$. In accordance with Fig. 5, $L_{NLC} = 10$ km, $H_{NLC} = 20$ m, $U_{NLC} = 0.1$ m s^{-1}, $\Delta S_{NLC} = 0.2$ g kg^{-1}, and $S_0 = 5.6$ g kg^{-1} are typical values of the width, depth and velocity of the NLC, salinity difference between the GoR background and the NLC, and background salinity, respectively, which yields $V_{freshwater} = L_{NLC} H_{NLC} U_{NLC} \Delta S_{NLC} / S_0 = 714$ m^3 s^{-1}. This rough estimate of the freshwater transport by the NLC (714 m^3 s^{-1}) is close to the river runoff to the GoR applied in the model ($Q_{Daugava} = const = 660$ m^3 s^{-1}). Therefore, one can conclude that the NLC has a potential to transport a substantial part of the river runoff, probably the whole river runoff in the periods favorable for the NLC intensification.

It is important to note that the existence of a long, almost reaching the Saaremaa Island, tongue of reduced salinity, forecasted by the model in the end of July 2012 (Fig. 4), was confirmed by in situ measurements. A map of the surface layer salinity drawn using a scarce set of CTD casts collected from 6 to 9 August 2012 onboard the R/V SALME displays a salinity value below 5 g kg^{-1} in the western GoR at the latitude of Cape Kolka (Fig. 6a). This is in accordance with the modeled salinity map shown in Figs. 4 and 6b.

Apart from riverine water transport by the NLC and despite of the anticyclonic pattern of mean circulation in the GoR in summer, some fraction of the Daugava River runoff makes its way to the north as a buoyant coastal plume – a jet-like current along the eastern shore of the GoR. Being adjoined to the lateral boundary, such a current is expected to be stable (Zhurbas et al., 2006). However, at some circumstances due to wind forcing this jet-like current and related salinity front can detach from the shore and

fall into baroclinic instability. Such an event of instability is demonstrated in Fig. 1b where the buoyant coastal plume being relatively wide displays vigorous meandering with wavelength of $\lambda = 12$–15 km. Our suggestion of baroclinic instability as a possible cause for the meanders is confirmed by rough estimates of the baroclinic Rossby radius $R_{bc} = (g^*H)^{1/2}/f$, where H is the sea depth. Value of R_{bc} in the meanders was found to be approximately 5 km (see Fig. 1c) indicating that the prevailing wavelength of meanders ($\lambda = (2.4 \div 3)R_{bc}$) is in accordance with the expression for the wavelength of the fastest growing mode in a theory by Eady (1949). Similar meandering pattern of the Po River plume was previously modeled and observed on infrared images by Cushman-Roisin et al. (2007).

This instability/meandering event in the GoR was preceded by a 10-day period of southerly winds prevalence (from May 8 to 18, 2012). Since the first half of May was characterized by weak temperature stratification in the GoR (the seasonal thermocline was not yet formed), the southerly, upwelling-favorable winds could not develop baroclinic longshore jet by the western shore of the GoR. At the same time, the northward baroclinic flow was developed along the eastern shore of the GoR where permanent density stratification is supported by the Daugava River discharge. As a result, the period was characterized by cyclonic type of circulation in the GoR, which is typical for the cold season (Lips et al., 2016), that swept off the riverine water bulge from the southern part of the GoR and distributed it within a relatively wide strip along the eastern shore. This wide riverine water plume ultimately became unstable.

Transverse structure of the buoyant coastal plume of riverine waters along the eastern shore of the GoR is illustrated by Fig. 7 where salinity and V-component of velocity versus depth and distance to the shore for a zonal transect at latitude of 57.55°N are drawn for different meteorological and hydrodynamic conditions. During and before the meandering event (Fig. 7b–d), the cross-section area filled with low-salinity water was considerably larger than that of the 'pure' coastal buoyant plume in a numerical experiment with uniform initial temperature and salinity fields and no atmospheric forcing (Fig. 7a). During strong downwelling event along the eastern coast, the offshore salinity/velocity front had a shape with the contours being almost vertical (Fig. 7c); posterior
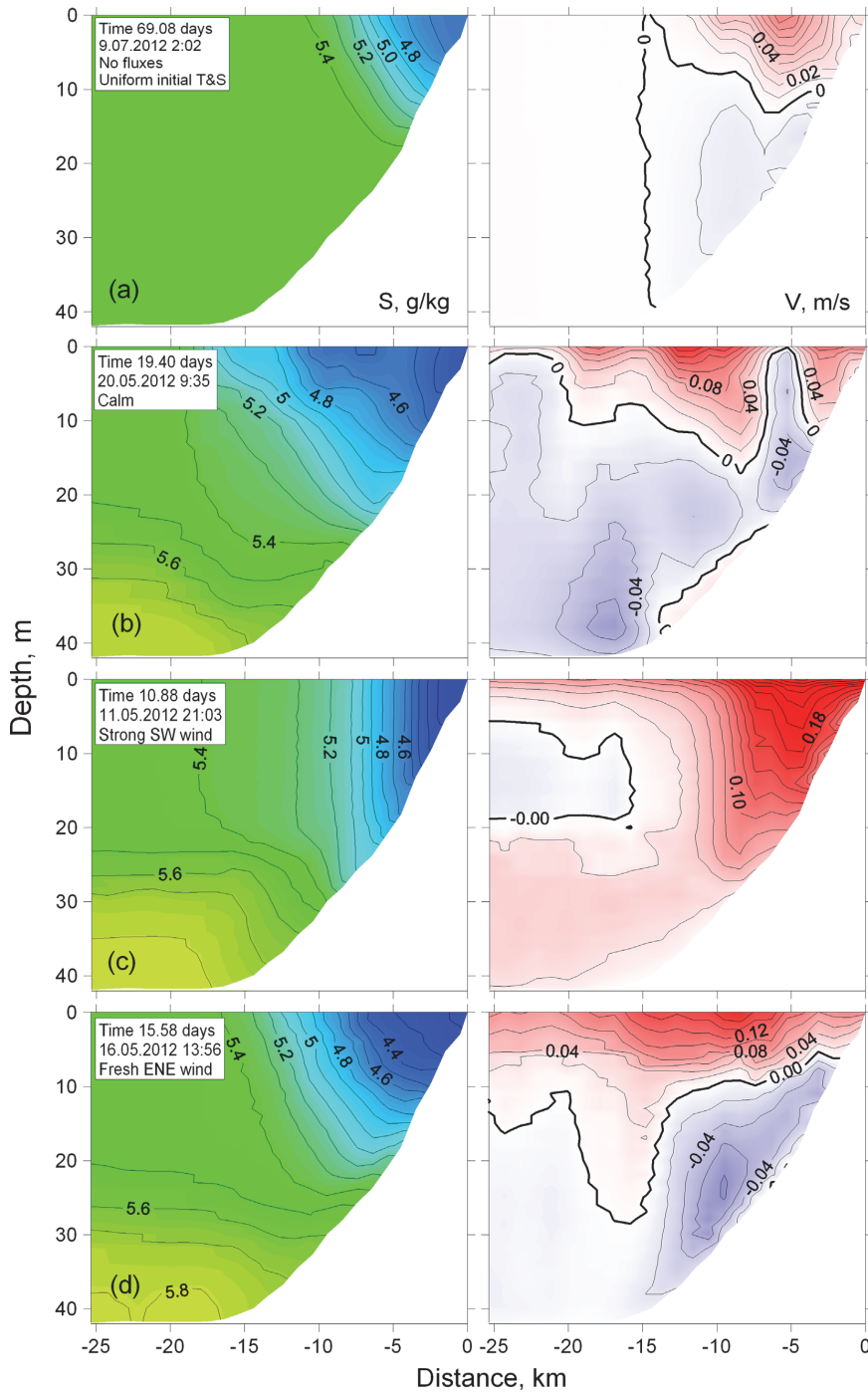
Fig. 7. Simulated salinity and V-component of velocity versus depth and distance to the eastern shore of GoR for zonal transect at latitude of 57.55°N (see Fig. 1a and b, for the position of the transect); (a) – a numerical experiment with uniform initial temperature and salinity fields and no atmospheric forcing (corresponds to Fig. 1a), (b) – intersection of a meander (corresponds to Fig. 1b); (c) – a case of strong downwelling-favorable wind 7 days before the meandering event; (d) – a case of westerly wind 2 days before the meandering event followed by downwelling relaxation.

relaxation of the downwelling was accompanied with thinning of the plume and spreading it offshore (Fig. 7d).

4. Discussion and conclusions

A regional, 0.5 n.m. and 20 sigma layer grid model of the Gulf of Riga (GoR) was implemented based on the Princeton Ocean Model code with initial conditions and atmospheric forcing taken from HIROMB and HIRLAM output and inclusion of the main rivers. Different scenario runs, including a basic run of a half-year period from May 1 to October 31, 2012, no atmospheric forcing run and no atmospheric forcing run combined with uniform initial thermohaline fields, brought the following results:

1. The Daugava River runoff forms a surface-advected plume (Yankovsky and Chapman, 1997) consisting of an anticyclonic bulge and coastal buoyant jet, i.e. a jet-like coastal current carrying a fraction of riverine waters rightwards. In the absence of other forcing factors, e.g. saltwater inflows through the Irbe Strait and atmospheric forcing, the anticyclonic bulge is growing in time in accordance with the results of earlier modeling studies, e.g. by Fong and Geyer (2002). In such no forcing conditions, the total river runoff is distributed between the bulge and the coastal current in proportion of about 7:6.
2. In some cases, depending on wind forcing history, the coastal current widens, detaches from the shore and eventually falls to instability, displaying vigorous meanders with the wave length of $\lambda = 12-15$ km or $\lambda = (2.4 \div 3)R_{bc}$, where R_{bc} is the baroclinic Rossby radius. Cushman-Roisin et al. (2007) have reported similar dynamics of a coastal buoyant current originating from the Po River outflow in the Adriatic Sea and Magdali et al. (2010) showed that the meandering of the current could be related to the baroclinic instability. Thus, the wind forcing influences both, the bulge and the coastal current jet and plays a major role in mixing and transport of the river discharge (see also Jurisa and Chant (2012) and Horner-Devine et al. (2008)).
3. In the no atmospheric forcing case, the saltwater inflow through the Irbe Strait displays vigorous instability; the gravity current consists of a chain of cyclonic eddies, slowly transported to the east. On the beam of the Cape Kolka, each cyclone splits into two smaller cyclones, the one goes to the northeast and the other to the south. Somewhere in between the Cape Kolka and Daugava River mouth, the cyclonic eddies meet the riverine waters carried with the prevailing anticyclonic circulation in the southern GoR and turn left towards the open gulf. In realistic, variable wind conditions such evolution of cyclonic eddies was not a regular process and their occurrence and role in the water exchange between the open Baltic Sea and the GoR has to be studied more closely in the future.
4. In the summer season, the anticyclonic type of whole-basin circulation in the GoR and related Northward Longshore Current (NLC) in the western GoR are formed (Lips et al., 2016). A substantial fraction of freshwater from the anticyclonic bulge of Daugava River waters is involved to the NLC and transported to the north almost reaching the southern shore of the Saaremaa Island. Due to the flow convergence, the low-salinity riverine water sinks down and spreads seaward occupying an intermediate layer and leading to the formation of a low-salinity intrusion. At the same time, part of the riverine water feeds the coastal buoyant current directed to the north along the eastern shore of the GoR. As a result, the coastal buoyant jet flowing to the right and the whole-basin anticyclonic gyre transporting the bulge water to the left form the bimodal transport pathways of the Daugava River plume in the summer. We suggest that in the cold season when the whole-basin cyclonic gyre prevails (Lips et al., 2016), most of the Daugava River discharge could be transported to the north along the eastern shore of the GoR.

References

Aitsam, A., Elken, J., 1982. Synoptic scale variability of hydrophysical fields in the Baltic Proper on the basis of CTD measurements. In: Nihoul, J.C.J. (Ed.), Hydrodynamics of Semienclosed Seas. Elsevier, Amsterdam, pp. 433–468.

Blumberg, A.F., Mellor, G.L., 1983. Diagnostic and prognostic numerical calculation studies of the South Atlantic Bight. J. Geophys. Res. 88, 4579–4592.

Cushman-Roisin, B., Korotenko, K.A., Galos, C.E., Dietrich, D.E., 2007. Simulation and characterization of the Adriatic Sea mesoscale variability. J. Geophys. Res. – Oceans 112, C03S14. http://dx.doi.org/10.1029/2006JC003515.

Eady, E.T., 1949. Long waves and cyclone waves. Tellus 1 (3), 33–52.

Elken, J., 1996. Deep Water Overflow, Circulation and Vertical Exchange in the Baltic Proper. Estonian Marine Institute, Tallinn, pp. 1–91, Report Series No 6.

Elken, J., Pajuste, M., Kõuts, T., 1988. On intrusive lenses and their role in mixing in the Baltic deep layers. In: Proceedings of the 16th Conference of Baltic Oceanographers, Kiel, pp. 367–376.

Fedorov, K.N., 1986. The Physical Nature and Structure of Oceanic Fronts. Springer Verlag, Germany, p. 333.

Fong, D.A., Geyer, W.R., 2002. The alongshore transport of freshwater in a surface-trapped river plume. J. Phys. Oceanogr. 32, 957–972.

Horner-Devine, A.R., Fong, D.A., Monismith, S.G., 2008. Evidence for the inherent unsteadiness of a river plume: satellite observations of the Niagara River discharge. Limnol. Oceanogr. 53, 2731–2737.

Jurisa, J.T., Chant, R., 2012. The coupled Hudson River estuarine-plume response to variable wind and river forcing. Ocean Dyn. 62, 771–784.

Kõuts, T., Elken, J., Lips, U., 1990. Late autumn intensification of deep thermohaline anomalies and formation of lenses in the Gotland Deep. In: Proceedings of the 17th Conference of Baltic Oceanogaphers, Norrköping, pp. 280–293.

Klavins, M., Briede, A., Rodinov, V., Kokorite, I., Frisk, T., 2002. Long-term changes of the river runoff in Latvia. Boreal Environ. Res. 7, 447–456.

Kourafalou, V.H., 2001. River plume dynamics in semi-enclosed Mediterranean regions: North Adriatic Sea and Northwestern Aegean Sea. J. Mar. Syst. 30, 181–205.

Laanemets, J., Väli, G., Zhurbas, V., Elken, J., Lips, I., Lips, U., 2011. Simulation of mesoscale structures and nutrient transport during summer upwelling events in the Gulf of Finland in 2006. Boreal Environ. Res. 16, 15–26.

Lass, H.-U., Mohrholz, V., 2003. On dynamics and mixing of inflowing saltwater in the Arkona Sea. J. Geophys. Res. – Oceans 108 (C2), 3042. http://dx.doi.org/10.1029/2002JC001465.

Leppäranta, M., Myrberg, K., 2009. Physical Oceanography of the Baltic Sea. Praxis Publishing Ltd., Chichester, UK, p. 370.

Lips, U., Lilover, M.-J., 1995. IRBEX-95 Data Report. Estonian Marine Institute, Tallinn, p. 122, Report Series No 2.

Lips, U., Zhurbas, V., Skurda, M., Väli, G., 2016. A numerical study of circulation in the Gulf of Riga, Baltic Sea. Part I: Whole-basin gyres and mean currents. Cont. Shelf Res. 112, 1–13.

Männik, A., Merilain, M., 2007. Verification of different precipitation forecasts during extended winter-season in Estonia. HIRLAM Newsl. No 52 4, 65–70, July 2007.

Magdali, M.G., Özgökmen, T.M., Griffa, A., Rixen, M., 2010. On the response of a turbulent coastal buoyant current to wind events: the case of the Western Adriatic Current. Ocean Dyn. 60, 93–122.

Mellor, G.L., Yamada, T., 1982. Development of a turbulence closure model for geophysical fluid problems. Rev. Geophys. Space Phys. 20 (4), 851–875.

Piechura, J., 2007. A mesoscale structure in the Baltic Sea deep waters. BSSC 2007 Rostock, Abstracts, p. 16. ⟨http://www2008.io-warnemuende.de/bssc2007/downloads/pdf/Abstract_volume_lectures.pdf⟩.

Raudsepp, U., Elken, J., 1999. Application of the Bryan-Cox-Type Ocean Model to reproduce synoptic and mesoscale variability of the Irbe Strait salinity front. Ger. J. Hydrogr. 51 (4), 477–488.

Reißmann, J.H., 2005. An algorithm to detect isolated anomalies in three-dimensional stratified data fields with an application to density fields from four deep basins of the Baltic Sea. J. Geophys. Res. 110, C12018. http://dx.doi.org/10.1029/2005JC002885.

Reißmann, J.H., 2006. On the representation of regional characteristics by hydrographic measurements at central stations in four deep basins of the Baltic Sea. Ocean Sci. 2, 71–86.

Schiller, R.V., Kourafalou, V.H., 2010. Modelling river plume dynamics with the Hybrid Coordinate Ocean Model. Ocean Model. 33, 101–117.

Seifert, T., Kayser, B., 1995. A high resolution spherical grid topography of the Baltic Sea. Meereswiss. Ber. (Mar. Sci. Rep.) 9, 72–88.

Soosaar, E., Maljutenko, I., Raudsepp, U., Elken, J., 2014. An investigation of anticyclonic circulation in the southern Gulf of Riga during the spring period. Cont. Shelf Res. 78, 75–84.

Stipa, T., Tamminen, T., Seppälä, J., 1999. On the creation and maintenance of stratification in the Gulf of Riga. J. Mar. Syst. 23, 27–49.

Yankovsky, A.E., Chapman, D.C., 1997. A simple theory for the fate of buoyant coastal discharges. J. Phys. Oceanogr. 27, 1386–1401.

Zhurbas, V., Oh, I.S., Park, T., 2006. Formation and decay of a longshore baroclinic jet associated with transient coastal upwelling and downwelling: a numerical study with applications to the Baltic Sea. J. Geophys. Res. – Oceans 111, C04014. http://dx.doi.org/10.1029/2005JC003079.

Zhurbas, V., Laanemets, J., Vahtera, E., 2008. Modeling of the mesoscale structure of coupled upwelling/downwelling events and the related input of nutrients to the upper mixed layer in the Gulf of Finland, Baltic Sea. J. Geophys. Res. – Oceans 113, C05004. http://dx.doi.org/10.1029/2007JC004280.

Zhurbas, V., Stipa, T., Mälkki, P., Paka, V., Golenko, N., Hense, I., Sklyarov, V., 2004. Generation of subsurface cyclonic eddies in the southeast Baltic Sea: observations and numerical experiments. J. Geophys. Res. – Oceans 109, C05033. http://dx.doi.org/10.1029/2003JC002074.

Zhurbas, V., Elken, J., Paka, V., Piechura, J., Väli, G., Chubarenko, I., Golenko, N., Shchuka, S., 2012. Structure of unsteady overflow in the Słupsk Furrow of the Baltic Sea. J. Geophys. Res. – Oceans 117, C04027. http://dx.doi.org/10.1029/2011JC007284.

Zhurbas, V.M., Paka, V.T., 1997. Mesoscale thermohaline variability in the Eastern Gotland Basin following the 1993 major Baltic inflow. J. Geophys. Res. – Oceans 102 (C9), 20917–20926.

Zhurbas, V.M., Oh, I.S., Paka, V.T., 2003. Generation of cyclonic eddies in the Eastern Gotland Basin of the Baltic Sea following dense water inflows: numerical experiments. J. Mar. Syst. 38, 323–336.

Paper IV

Liblik, T., Skudra, M., Lips, U. (2016). On the buoyant sub-surface salinity maxima in the Gulf of Riga. *Oceanologia*, in press, doi: 10.1016/j.oceano.2016.10.001.

Available online at www.sciencedirect.com

ScienceDirect

journal homepage: www.journals.elsevier.com/oceanologia/

ORIGINAL RESEARCH ARTICLE

On the buoyant sub-surface salinity maxima in the Gulf of Riga

Taavi Liblik [a,*], Maris Skudra [a,b], Urmas Lips [a]

[a] Marine Systems Institute, Tallinn University of Technology, Tallinn, Estonia
[b] Latvian Institute of Aquatic Ecology, Riga, Latvia

Summary   Thermohaline structure in the Gulf of Riga (GoR) was investigated by a multi-platform measurement campaign in summer 2015. Stratification of the water column was mainly controlled by the temperature while salinity had only a minor contribution. Buoyant salinity maxima with variable strength were observed in the intermediate layer of the Gulf of Riga. The salinity maxima were likely formed by a simultaneous upwelling—downwelling event at the two opposite sides of the Irbe strait. The inflowing salty water did not reach the deeper (> 35 m) parts of the gulf and, therefore, the near-bottom layer of the gulf remained isolated throughout the summer. Thus, the lateral water exchange regime in the near bottom layer of the Gulf of Riga is more complicated than it was thought previously. We suggest that the occurrence of this type of water exchange resulting in a buoyant inflow and lack of lateral transport into the near-bottom layers might contribute to the rapid seasonal oxygen decline in the Gulf of Riga.
© 2016 Institute of Oceanology of the Polish Academy of Sciences. Production and hosting by Elsevier Sp. z o.o. This is an open access article under the CC BY-NC-ND license (http://creativecommons.org/licenses/by-nc-nd/4.0/).

1. Introduction

The water exchange regime of semi-enclosed basins largely determines their physical and ecological nature. The classical estuarine circulation scheme in the estuaries with positive freshwater flux includes an outflow in the upper layer and inflow in the deep layer (Geyer and MacCready, 2014). The exact water exchange regime and faith of the inflowing denser water depends on the size and shape of the estuary as well as its mouth area (Valle-Levinson, 2010). Nevertheless, typically the inflowing water is in contact with the bottom of

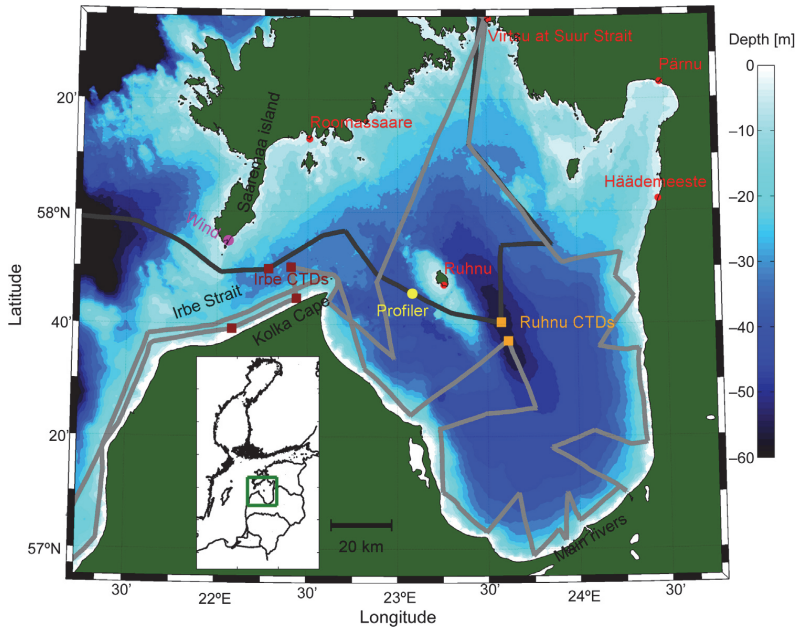ELSEVIER | **Production and hosting by Elsevier**

Figure 1 Map and topography of the Gulf of Riga. Color scale shows depth [m] of the study area. Lines show tracks of the RV Salme thermosalinograph surveys in July (darker gray) and August (brighter gray) 2015. Yellow circle represents the location of the moored profiler (buoy station), and red circles show locations where the coastal sea surface temperature time-series were acquired. Locations of Conductivity-Temperature-Depth (CTD) measurements at the Irbe Strait and Ruhnu Deep are shown as dark red and orange squares, respectively. The location of wind measurements at the Sõrve Cape station is shown as a magenta circle. The green box in the inlay map shows the location of the study area (Gulf of Riga) in the Baltic Sea.

the estuary. Exceptions might appear for the estuaries, which are separated from the adjacent sea basin by a sill. If the deeper layers of the estuary are filled with the saline water originating from the sporadic inflows, then the quasi-continuous water exchange over the sill involves inflowing water, which is too light to penetrate to the deepest layers of an estuary. Such regime can be found for several fjords (e.g. Belzile et al., 2016) and the Baltic Sea (Feistel et al., 2004). In the present study, we show that such water exchange regime can seasonally occur in a relatively large but shallow brackish estuary, the Gulf of Riga (GoR) as well.

The Gulf of Riga is a sub-basin of the eastern Baltic Sea. The gulf covers the area of 17 900 km², and its mean depth is 26 m. The deepest (> 50 m) area is in the central part of the gulf (Fig. 1). The gulf is connected to the Baltic Sea via two straits: the Irbe Strait in the west with the sill depth of 25 m, width of 28 km and cross-section of 0.4 km² and the Suur Strait in the north with the sill depth of 5 m, width of 6 km and cross-section of 0.04 km².

The water and salt budgets of the gulf are formed by the two sources: the saltier water from the open Baltic Sea (Baltic Proper) and the freshwater from the rivers and due to precipitation (e.g. Raudsepp, 2001; Skudra and Lips, 2016). The water from the open Baltic flows to the deep layer of the GoR (Laanearu et al., 2000) while the riverine water occupies the upper layer. Thus there is a vertical

salinity gradient present in the GoR (Skudra and Lips, 2016). The average river run-off to the gulf has been estimated approximately as 1000 m³ s⁻¹ (Berzinsh, 1995) while the average net precipitation to the gulf is about 80 m³ s⁻¹ (Omstedt and Axell, 2003). The 86% of the river run-off is discharged into the southern part of the gulf (Fig. 1, "Main rivers") from the Daugava, Lielupe and Gauja rivers (Berzinsh, 1995). This river discharge, in combination with the water exchange through the two straits in the northern part of the gulf, forms the latitudinal salinity gradient (e.g. Stipa et al., 1999). Due to the strong inter-annual variability and seasonality of the river run-off, salinity in the gulf varies remarkably at the same time-scales (e.g. Raudsepp, 2001; Skudra and Lips, 2016; Stipa et al., 1999). Due to the shallowness of the Irbe and Suur Strait, water from beneath the permanent halocline of the Baltic Sea (e.g. Reissmann et al., 2009) cannot penetrate into the GoR. There are strong salinity fronts at both straits, which change their position influenced by the wind forcing and sea level differences between the basins (Astok et al., 1999; Lilover et al., 1998).

The heat budget of the gulf (like the whole Baltic) is driven by the fluxes through the sea surface. The gulf is stratified during summers when the temperature exceeds 18°C in the upper mixed layer (Skudra and Lips, 2016). In autumn—winter, the water column is mixed down to the bottom due to the thermal convection. Further, temperature falls

below the temperature of maximum density (Raudsepp, 2001; Stipa et al., 1999), and the gulf is at least partly covered by ice (Seinä and Palosuo, 1996) during winters.

The available modeling studies have shown that the heat exchange with the atmosphere and the heat content of the water column can be estimated relatively well in the Baltic (e.g. Westerlund and Tuomi, 2016). However, to simulate correct salinity distributions (both, vertical and lateral) and estimate salt fluxes between the basins and between different layers using numerical models is much more complicated (Lips et al., 2016b; Omstedt et al., 2014). This difficulty might show that the internal processes responsible for transport and mixing are described not precisely enough in such stratified, but relatively shallow basins. In the present study, we analyze the observed salinity distributions and vertical structures and relate them to the forcing.

Oxygen consumption under conditions of developed vertical stratification in summer could result in poor oxygen conditions in the near-bottom layer of deep central areas of the gulf (Aigars et al., 2015; Eglite et al., 2014). It has been argued based on the analysis of seasonal dynamics of environmental parameters and biomarkers for instance that the clam *Macoma balthica* could be stressed in late summer due to lower oxygen levels in August in the near-bottom layer of the Gulf of Riga (Barda et al., 2013). Furthermore, hypoxia at the water-sediment interface alters the phosphorus flux between the water column and sediments as well as nitrogen removal due to denitrification (Yurkovskis, 2004). Due to the sediment release of phosphorus in hypoxic conditions, the main pathway of phosphorus removal from the gulf is its relatively slow export to the Baltic Proper (Müller-Karulis and Aigars, 2011). Thus, reoccurrence of such poor oxygen conditions and benthic nutrient release could counteract decreases in the external nutrient load to the gulf similarly to the deeper Baltic basins including the Gulf of Finland (Pitkänen et al., 2001).

The main aim of the present study is to present the high-resolution view on the stratification development in the Gulf of Riga. Available investigations include the data only from episodic ship surveys (Stipa et al., 1999) or are concentrated on the long-term changes in the gulf (Raudsepp, 2001; Skudra and Lips, 2016). Studies in other basins of the Baltic have shown that implementing a new type of in situ platforms, such as moored vertical profilers (Lips et al., 2016a), Argo floats (Purokoski et al., 2013; Westerlund and Tuomi, 2016) or underwater gliders (Alenius et al., 2014; Karstensen et al., 2014), can improve the understanding of thermohaline processes. High-resolution continuous temperature—salinity measurements have not been conducted so far in the Gulf of Riga. To fill this gap, an autonomous profiler was deployed in the northwestern part of the gulf from May to September 2015.

2. Material and methods

2.1. Data

The dataset analyzed in the present study was collected from May to September 2015. Altogether 202 temperature and salinity profiles were collected by an autonomous vertical profiler equipped with OS316plus CTD (Conductivity,

Temperature, Depth) probe (Idronaut S.r.l.). The profiler has been successfully applied in the Gulf of Finland for several years now (Lips et al., 2016a). The profiler was set to collect measurements in a depth range from 2 to 37 m twice a day. Initial vertical resolution of measurements was 0.1 m, but after the preliminary data processing, the profiles were stored for analysis purposes with a vertical resolution of 0.5 m. The CTD probe was calibrated by manufacturer right before the deployment, and the data quality was checked against shipborne CTD profiles several times during the study.

The shipborne CTD and dissolved oxygen data (OS320plus CTD, Idronaut S.r.l.) together with the thermosalinograph (SBE45 MicroTSG, Sea-Bird Electronics; included in the flow-through system) data were used to study the spatial thermohaline fields in the area (Section 3.2). The salinity data was checked against the water sample analyses using a salinometer 8410A Portasal (Guildline). The oxygen sensor was calibrated before each survey and was checked against water sample analyses using an OX 4000 L DO meter (WWR International, LLC).

The long-term CTD dataset 1993—2012 compiled by Skudra and Lips (2016), collected under Estonian and Latvian national monitoring programs, was extended to 2015. This dataset together with HELCOM data (http://ocean.ices.dk/helcom, 25 February 2016) was used to evaluate the occurrence of the sub-surface salinity maxima in the past (Section 3.3).

Coastal temperature measurements at Ruhnu, Häädemeeste, and Roomassaare, provided by the Estonian Environmental Agency, were included in data analysis. Likewise, the level 3 SST (sea surface temperature) product over European Seas by Copernicus Marine Environment Monitoring Service (http://marine.copernicus.eu/) was used as background information. Wind measurements at the Sõrve station were obtained from the Estonian Environmental Agency. The wind speed and direction, measured at 10 m height, were available every third hour as a 10 min average.

2.2. Calculations

The upper mixed layer (UML) depth was defined as the minimum depth where the criterion $\rho_z \geq \rho_3 + 0.15$ kg m^{-3} was satisfied (ρ_z is density at depth z, and ρ_3 is density at 3-m depth).

Relative contributions of temperature (ST_T) and salinity (ST_S) to the vertical stability of the water column were estimated as:

$$ST_T = \alpha \frac{dT}{dZ} \rho, \qquad (1)$$

$$ST_S = \beta \frac{dS}{dZ} \rho, \qquad (2)$$

where α is the thermal expansion coefficient, β is the saline contraction coefficient, ρ is the water density; dT/dZ and dS/dZ are the temperature and salinity gradients over the vertical distance dZ. Temperature and salinity profiles were both smoothed by 2.5 m window before the stability and intrusion index calculations. Stability (ST) of the water column was acquired by summation of ST_T and ST_S. Total

(contribution to) stability of the water column was calculated as vertically integrated ST_T, ST_S and ST. Likewise, the total contribution to the stability of the UML was calculated as vertically integrated ST_T, ST_S, and ST within the depth range of the UML.

In order to estimate the intensity of interleaving the intrusion index as the sum of negative salinity gradients [g kg^{-1} m^{-1}] was calculated same as by Lips et al. (2016a):

$$I = \sum_{z=h_1}^{z=h_2} \begin{cases} 0, & \text{if } \frac{dS}{dZ} \geq 0 \\ abs\left(\frac{dS}{dZ}\right), & \text{if } \frac{dS}{dZ} < 0 \end{cases}, \qquad (3)$$

where I is the intrusion index, h_1 and h_2 are the borders of the depth interval where the index was calculated. It means if salinity increases downwards throughout a profile, the index is zero. Contrary, if there is a strong sub-surface salinity maximum, the index has a higher value.

The apparent oxygen utilization (AOU) was used to show the difference between measured dissolved oxygen content and saturation level:

$$AOU = DO_{100} - DO_M, \qquad (4)$$

where DO_{100} is oxygen concentration at saturation level (Weiss, 1970), and DO_M is the measured oxygen concentration.

Salinity values are given as Absolute Salinity [g kg^{-1}], density as potential density anomaly to a reference pressure of 0 dbar [σ_0; kg m^{-3}] and the unit of oxygen values is mg L^{-1} in the present paper. Density values in Section 3.3 are presented as arithmetic averages at 0—5 m and 32—38 m depth ranges in the Baltic Proper and in the Gulf of Riga, respectively.

3. Results

3.1. Temperature, salinity, density and stratification time-series at mooring station

3.1.1. General description

Water column structure was determined by the seasonal thermocline at the beginning of the study period (Fig. 2). Temperature decreased almost linearly from the base of the upper layer (9.3—10.0°C) at 15—20 m depth to the near-bottom water (4.3—5.5°C). Vertical distribution of salinity was relatively even and ranged between 5.9 and 6.0 g kg^{-1}. Temporal development of the vertical thermohaline structure was characterized by a seasonal increase in temperature due to the atmospheric heat flux and a slight decrease in salinity in the upper layer in June. By the end of June, temperature (salinity) gradient from the upper layer to the near bottom (old winter water) layer was from 15.6 to 5.8°C and from 5.8 g kg^{-1} to 6.0 g kg^{-1}, respectively.

Advection of fresher water was observed at the buoy location in the upper 25 m in the first week of July. Salinity values below 5.4 g kg^{-1} were registered. At the same time, water temperature increased in the upper layer, which, however, cannot be related to the advection. First, the temperature maxima and salinity minima did not match exactly in time. Secondly, a simultaneous temperature increase and decrease after that were registered at all coastal stations around the gulf, which implies that the atmospheric heat flux was responsible for this temperature change.

Further developments in July included a general increase in the upper layer temperature and intermittent appearances of fresher and saltier patches in the sub-surface layer at the depth range from 14 to 24 m. Less saline water in the upper layer and thick sub-surface intrusion of saltier water after that were observed at the end of July. Upper layer temperature reached its seasonal maximum of 20.4°C in mid-August. Upper layer salinity varied around 5.5 g kg^{-1} in the first half of August and was close to 5.7 g kg^{-1} in the second half of the month.

Vertical structure in September was characterized by heat loss to the atmosphere and by advection of fresher water to the buoy location. A temperature and salinity decrease in the upper layer, as well as thickening of the mixed layer, were observed during that period. Thus, it was the advection of fresher water that dominated over the vertical transport of salt in the upper layer salt flux. Interestingly, temperatures below 4.5°C were occasionally registered at the deepest measured horizon of 37 m even in September.

3.1.2. Stratification

Time series of the water column stability are presented in Fig. 3a. The higher (red) values mark the location of the pycnocline while the dark blue color indicates that water is vertically homogeneous. The seasonal thermocline was the main contributor to the stability of the water column (Fig. 3b). There were only a few occasions when the temperature gradients had an opposite effect and caused weakening of the vertical stratification.

Negative stability values due to the vertical salinity gradient occurred in July and August, and they were especially strong in the second half of July (Fig. 3c). Those layers were located in the thermocline and were compensated by the vertical temperature gradient. It has to be noted that the layer with inverse salinity gradient was always surrounded by the layers above and below it where the salinity was increasing with the depth (Fig. 3c). The explanation for such salinity derived stability distribution was the existence of sub-surface buoyant saltier water intrusion. Starting from the sea surface, the following gradients/layers were associated with the salinity maxima and could be distinguished: (1) layer with positive salinity gradient from the ambient water in the thermocline to the core of maxima layer (red color); (2) values close to zero that show the location of the core (white color); (3) layer with negative salinity gradient between the core and ambient deep layer water (blue color); (4) values close to zero that show the point (range) where salt intrusion water merged with the ambient water (white color); (5) positive salinity gradient in deep water (red color).

The integrated stability over the water column (Fig. 3d) showed that the thermal buoyancy dominated while salinity had a minor importance in the strength of stratification at the buoy location. The minor role of salinity can be at least partly related to the fact that the highest salinity (intrusion) was located in the intermediate layer and not in the bottom layer. The salty water near the bottom would have increased the stability over the water column.
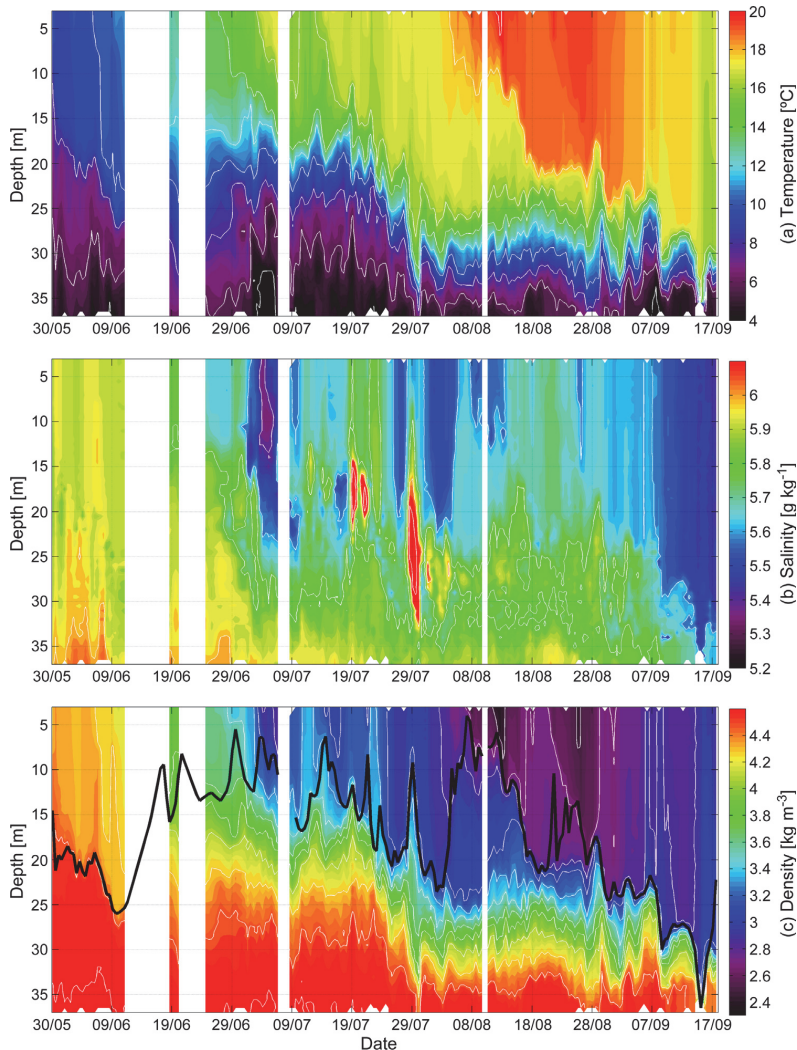
Figure 2   Time series of temperature [$^\circ$C], salinity [g kg^{-1}] and density anomaly [kg m^{-3}] at the buoy station from 30 May 2015 to 18 September 2015. Black line in the bottom panel is the upper mixed layer (*UML*) depth. The location of the mooring is shown as yellow circle in Fig. 1.

The *UML* depth ranged from a few meters to 35 m during the study period (Fig. 2c). The *UML* was mostly stabilized by the temperature while salinity had occasionally (at the beginning of July) an opposite effect (Fig. 3e). Salinity and temperature had a similar contribution to the stability at the beginning of August.

Time-series of intrusion index (Fig. 3f) show relatively low values (<0.05) until the beginning of July. It is noteworthy that intrusion index values differed from zero, most probably, due to the observed sub-surface freshwater patches (Fig. 2b). Occasional peaks of intrusion index up to 0.1 were observed until the beginning of September. The

highest values exceeded 0.2 and occurred in the second half of July.

3.1.3. Salinity fluctuations

The period with highest intrusion peaks is below described in more detail. It is noteworthy that immediately before the appearance of saltwater patches a clear signature of fresher water was registered at the 15—20 m depth (Fig. 4, 19 Jul 12:00). The core of this fresher layer had the salinity of 5.55—5.60 g kg^{-1}, and it lied in between the upper layer with the salinity of 5.75—5.80 g kg^{-1} and deep layer with the salinity of 5.95 g kg^{-1}.
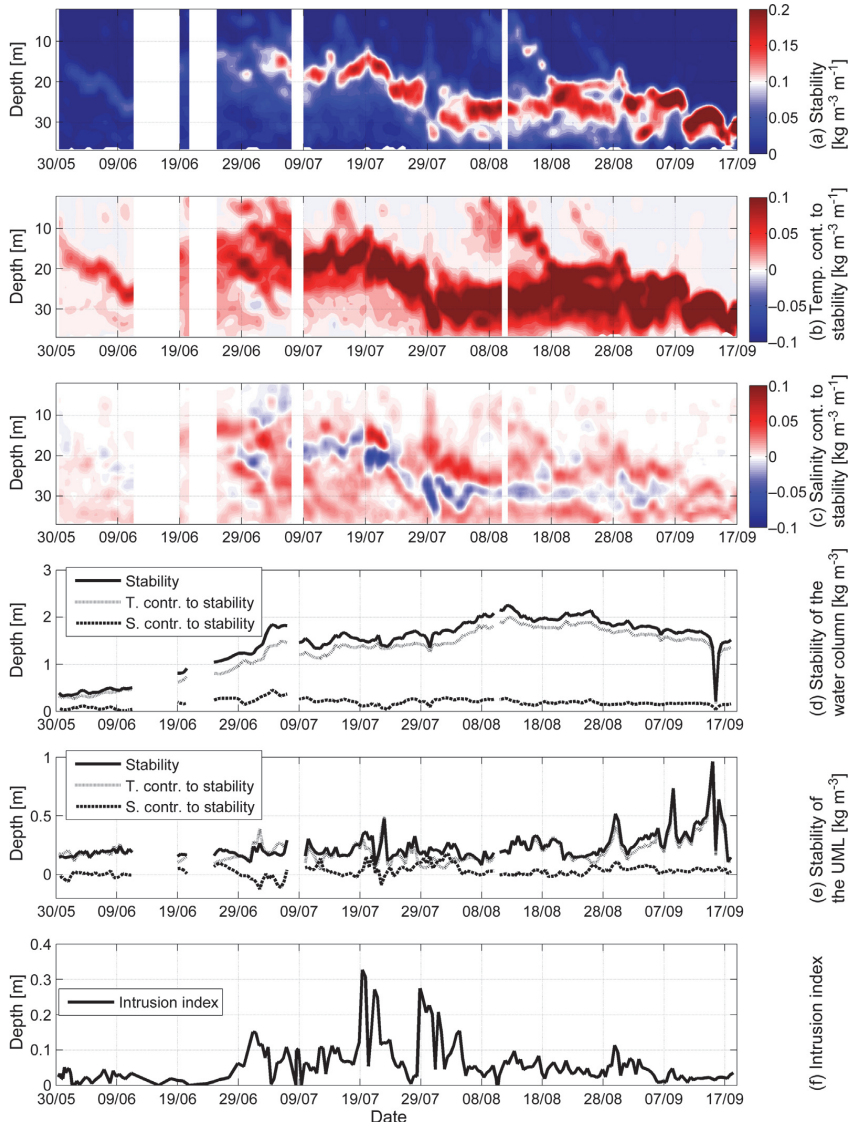
Figure 3 Temporal development of the following vertical stratification parameters at the buoy station from 30 May to 18 September 2015: stability (a; [kg m^{-3} m^{-1}]) and contribution of temperature (b) and salinity (c) to stability; integrated stability parameters [kg m^{-3}] for the whole water column (d) and for the upper layer (e); intrusion index (f).

Next, the saltier water (5.80 g kg^{-1}) appeared in the upper layer and rapidly (within our profiling interval of 12 h) the fresher water in the sub-surface layer was replaced by the salinity maximum (Fig. 4, 20 Jul 00:00). The saltier sub-surface layer was located in the depth range of 11—25 m and its core with the salinity of 6.45 g kg^{-1} was located at 17 m depth. The temperature of the core was 14.55°C while 3.5 m above the core it was 13.75°C. Thus, the salinity gradient above the core neutralized the negative buoyancy due to the vertical temperature distribution. It was opposite below the core: strong thermocline stabilized the water column despite the negative salinity gradient. The sub-surface salinity maximum disappeared on 22 July. Fresher sub-surface water was observed from 23 July to 28 July while salinity in the upper layer decreased from 5.80 to 5.55 g kg^{-1}. The saltier water reappeared in the sub-surface layer on 29 July (Fig. 4 29 July 12:00). The core of the sub-surface layer was located at 22 m depth and had salinity and
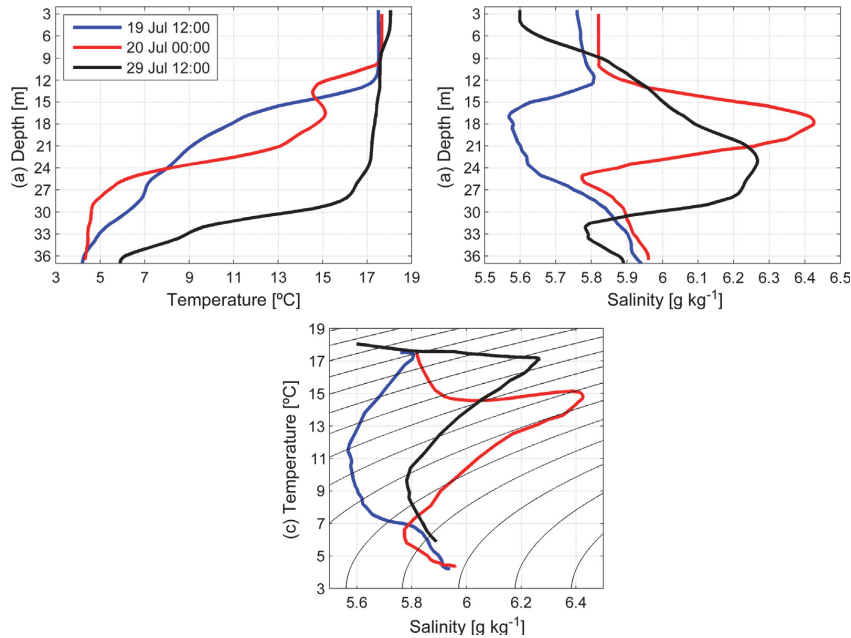
Figure 4 Selected profiles of temperature ([°C]; a) and salinity ([g kg^{-1}]; b) and respective temperature—salinity diagram with density anomaly ([kg m^{-3}]; c) as contour lines in profiling station (the location is shown as a yellow circle in Fig. 1).

temperature of 6.30 g kg^{-1} and 17.15°C, respectively. The core was only slightly (0.15°C) warmer than the layer above. That temperature change had a minor contribution to the vertical stratification as salinity increased from 5.70 g kg^{-1} to 6.30 g kg^{-1} in the same depth range. The sub-surface salinity maximum, though much weaker, was observable until the end of August.

3.2. Origin of the salt intrusion

The observed saltier water could potentially penetrate to the GoR from the Baltic Proper via either the Irbe Strait or Suur Strait. The core of the observed salt maxima layer had the salinity of 6.45, 6.30 g kg^{-1} and temperature of 14.55°C, 16.40°C on 20 July and 29 July, respectively. We can expect that if the source water has been modified, then it occurred because of mixing of it with the GoR ambient waters. The temperature—salinity curves (TS-curves) of the sub-surface salinity maxima cores indicate that this saltier water was slightly warmer than the surrounding GoR waters. Thus, if the observed core has been a subject of mixing, the source water of the salt maxima layers must have been saltier and slightly warmer than the observed core at the buoy station. Unfortunately, there were no continuous measurements available in the straits. Thus, we were not able to capture the entering process of the saltier waters directly. However, we collected some shipborne CTD profiles in the Irbe Strait area (Fig. 5). The other data source was made available by the thermo-salinograph that autonomously recorded temperature and salinity of the water pumped from 2 m depth during the

surveys on board RV SALME. The two surveys that were included in the analysis were conducted on 14—15 July and 7—9 August.

The first survey was conducted through the central part of the Irbe Strait on 14—15 July while the vessel visited more the southern part during the second survey; though, one station in the central part was sampled as well. During the second survey, the area was visited twice: the first passage on 7—8 August and the second passage on 9 August.

During the both surveys, a strong salinity front was found in the upper layer in the Irbe Strait area. The front was captured near the longitude of 22°E by the survey on 14—15 July (Fig. 5). Salinity values below 6.20 g kg^{-1} were observed toward east from the longitude of 22°E. The front was located further in the east on 7—9 August. However, due to different tracks of the two surveys (the latter was conducted along the southern coast) we cannot confirm, whether it was a spatial feature or temporal displacement of the front.

The most remarkable feature in the upper layer temperature dynamics was the colder water observed in the strait on 14—15 July survey. The temperature of the upper layer was around or exceeding 17°C in the Baltic Proper and the gulf, but below 13°C inside of this cold feature (Fig. 5). Since the Irbe Strait is a topographic barrier between the open Baltic and the gulf, upwellings in both basins can potentially bring cold water to the upper layer in the Irbe area. Strong SW winds (>10 m s^{-1}) occurred during the period from 5 to 10 July, i.e. favorable forcing for an upwelling in the GoR along the coast of the Saaremaa Island. Weaker winds from NW, i.e. from the favorable direction for the upwelling along

the Latvian coast in the Baltic Proper, prevailed from 11 to 15 July (Fig. 6). The satellite-derived sea surface temperature, as well as temperature measurements at the coastal stations and by the onboard thermosalinograph, indicated that the upwelling occurred in the NW part of the GoR in mid-July (Fig. 7). Since salinity in the whole water column was higher in the Baltic Proper than in the core of the upwelled cold water in the Irbe Strait (6.15 g kg^{-1}), this upwelled water cannot be a pure Baltic Proper water. On the other hand, the upwelled water was saltier than the GoR water. Thus, the upwelled water might be a mixture of waters from the both basins.

The only available profile in the Irbe Strait on 14—15 July was acquired eastward from the core of the upwelling (Fig. 5a). The profile revealed three layers: upper layer (15.00°C and 5.90 g kg^{-1}), deep layer (4.70°C and 5.95 g kg^{-1}) and salt maxima layer (12.15°C and 6.35 g kg^{-1}) between the former two (Fig. 8). The temperature profile, as

well as the satellite-derived sea surface temperature, showed that the station was in the upwelling zone but not in its coldest core area. Relatively low salinity of the upper layer (upwelled water) and deep layer at the station indicated that those waters originated from the gulf. The salt maxima layer at the station and coldest water in the upper layer observed by the thermosalinograph were similar. Though, the salt maxima water was slightly colder and saltier than in the upwelled water at the CTD station. Thus, the observed salt maxima layer water was likely mixed with warmer and fresher surface water before upwelled to the surface as registered by the thermosalinograph (Fig. 8).

The structure of the salt maximum was similar to the one observed at the buoy station, which suggests that the salt impulse entered the gulf likely via the Irbe Strait. The salt maxima at the thermocline were much saltier than the water below and above and the water in those layers was slightly
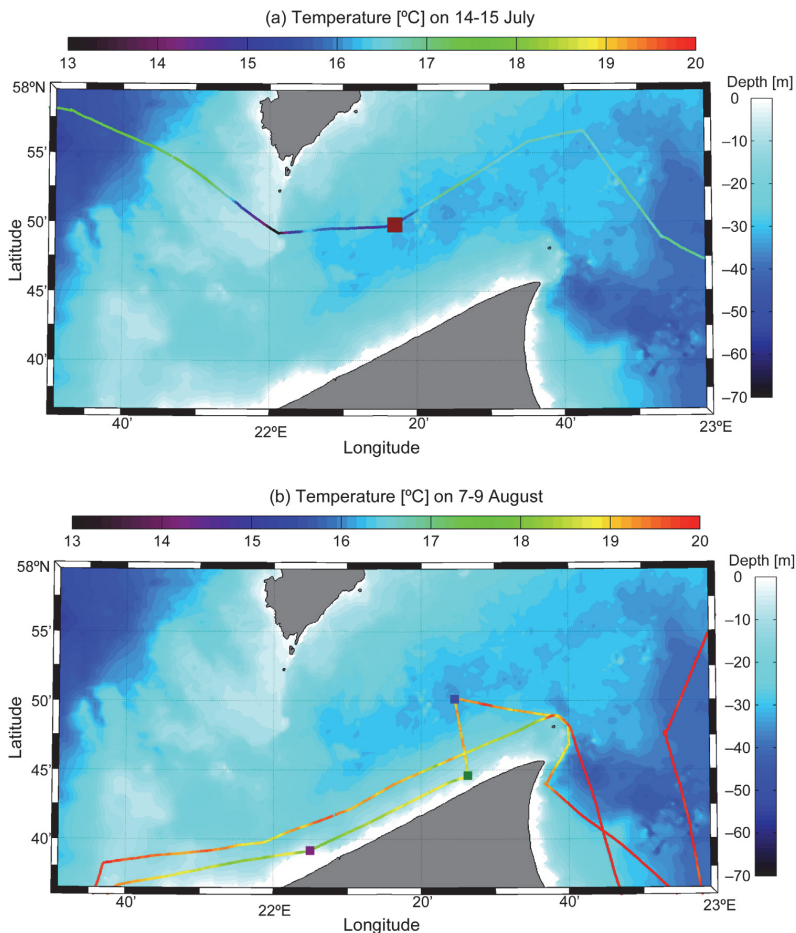

Figure 5 Temperature ([°C]; a, b) and salinity ([g kg^{-1}]; c, d) at 2 m depth acquired by the thermosalinograph on board RV SALME on 14—15 July (a, c) and 7—9 August (b, d). On vertical color bar sea depths [m] are shown.
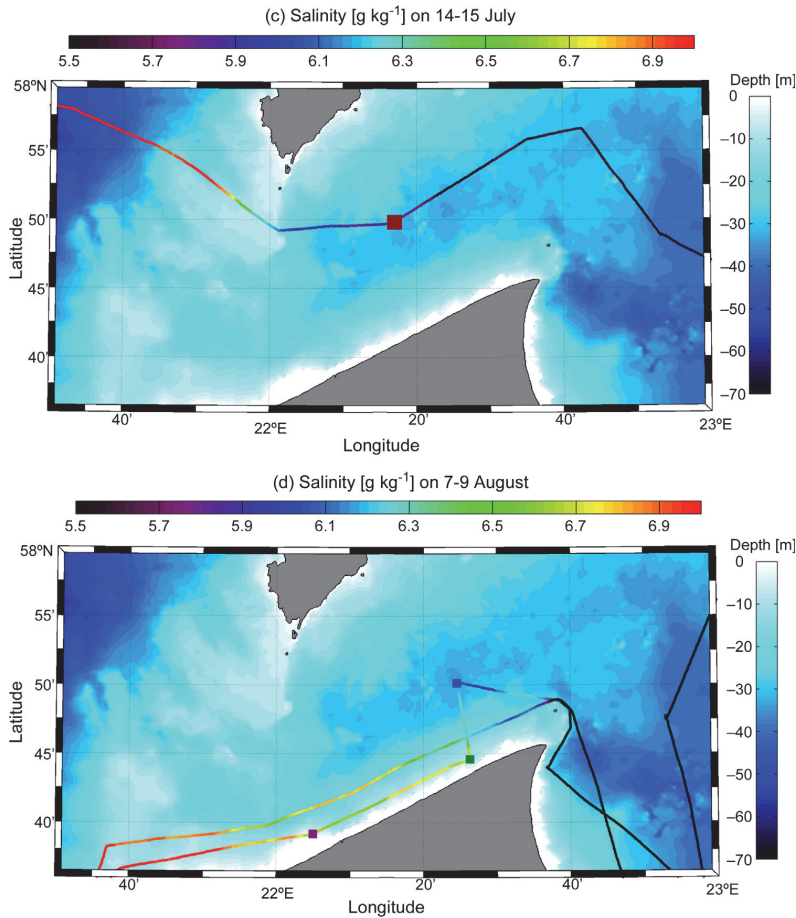
Figure 5 (*Continued*).

warmer than in the thermocline above. The latter indicates that the salt maxima water originates from the warmer layer above.

The similar structure of salt intrusion was found in the central part of the Irbe Strait on 9 August (Fig. 8). At the same time, high saline >6.7 g kg^{-1} and warm water was observed in the upper layer in the southern part of the strait (Figs. 5 and 8). TS-curves suggest that the salt maxima layer observed in the central part of the strait was a mixture of this high saline warm water and thermocline water of the GoR. The possible mechanism that can penetrate the warm and high saline water deeper is downwelling along the southern coast of the Irbe Strait. Indeed, SW wind that generates upwelling along the shore of the Saaremaa Island also causes downwelling along the southern coast of the strait. Moreover, the SW wind likely creates a coastal boundary current along the eastern coast of the Baltic Proper. It can be seen that at the station marked in green in Fig. 8, this warm, salty water has pushed over the fresher water. Thus, it likely caused some vertical mixing there as well.

In an upwelling cell along a boundary, the upwelled water is typically compensated by an onshore flow in the deeper layer. In the present case, upwelling occurred in the strait, which is relatively narrow and shallow. Thus, simultaneously with the upwelling, a downwelling occurred along the opposite coast, and the downwelled waters (originated from the Baltic Proper) rather fast reached the seabed. We suggest that the upwelled water was (at least partly) compensated by this warm and saltier downwelling water in the Irbe Strait. This hypothesis is supported by the TS-curves: one source water for the salt maxima layer observed in the central strait on 9 August (blue curve in Fig. 8) had almost the same TS-characteristics as the warm and saltier water in the southern part of the Irbe Strait (magenta and green curves in Fig. 8). Moreover, the same suggestion can be made on the basis of *AOU* vs. *S* curves (Fig. 8). This saltier and warm water was formed in the Irbe Strait and later spread to the gulf as upwelling—downwelling system relaxed.

Measurements at the coastal stations and buoy station reveal the temporal development of the upper layer
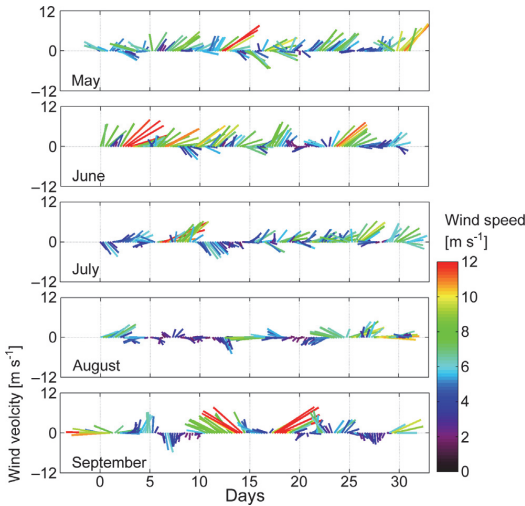
Figure 6 Wind vectors at the Sõrve meteorological station in 2015. The location of the station is shown in Fig. 1 as a magenta circle.

temperature in different parts of the gulf. There were several synoptic events of cooling (at the beginning of August) and warming (at the beginning of July) that simultaneously occurred at all stations (Fig. 9). Those were atmospheric heat flux events. The seasonal temperature increase at Ruhnu and, especially, at the buoy lagged the other two stations until the end of June. This delay was related to the slower warming of the open gulf waters

comparing to the shallow coastal waters. The same tendency was in September, but this time, the slower cooling in the open sea resulted in a higher temperature at the buoy station than at the coastal stations. One can note that the lowest temperatures mostly occurred at Roomassaare in mid-July during a period of two weeks. Upwelling along the north-western coast of the gulf prevailed during this period. The Roomassaare station is not the best location to catch the upwelling in the Irbe Strait but as satellite derived sea surface temperature showed (Fig. 7), at least in some cases, upwelling events occurred in the Irbe Strait and at Roomassaare at the same time. Moreover, the period of upwelling coincided with the period of strongest salt maxima observed at the buoy station (intrusion index in Fig. 3f). This coincidence supports the suggestion that the salt pulses entered the gulf during the simultaneous upwelling in the northwestern gulf (along the shore of the Saaremaa Island) and downwelling along the southern coast of the Irbe Strait.

3.3. Earlier observations

In the previous subchapter, we suggested that the sub-surface saltwater maxima originated from the upper layer of the Baltic Proper and likely entered the gulf via the Irbe Strait. The pre-condition for the sub-surface buoyant salt maxima establishment is a specific density range of the saltwater. The inflowing salty water (or a product of its mixing with the ambient Gulf of Riga water) should be lighter than the deep layer water and denser than the upper layer water in the gulf. The upper layer density (presented as potential density anomaly σ_0) in the Baltic Proper in January—April is in a range of 5.5—6.0 kg m^{-3} (Fig. 10). Water cools down to the temperature of maximum density (2.6—2.7°C) every winter in the Gulf of Riga. Salinity over 6.9 g kg^{-1} (at the temperature of
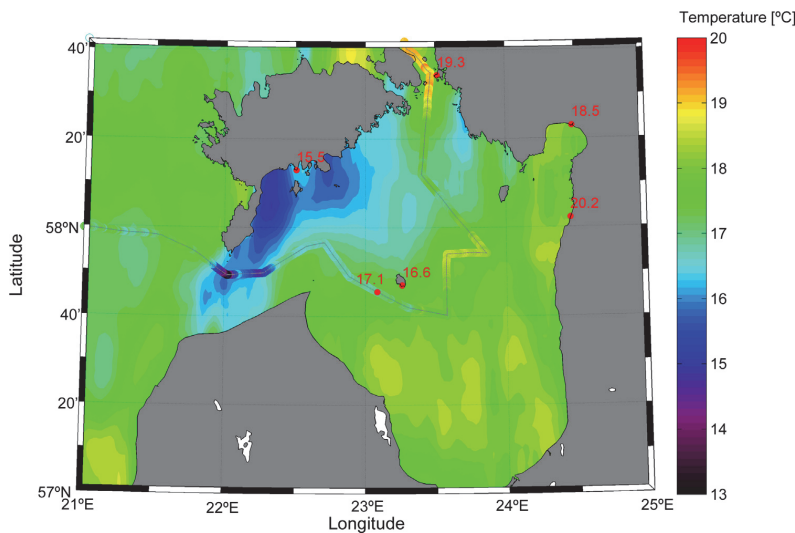

Figure 7 Satellite-derived sea surface temperature; upper layer temperature registered along the RV SALME track by thermo-salinograph, at the buoy station and selected coastal stations on 15 July 2015.
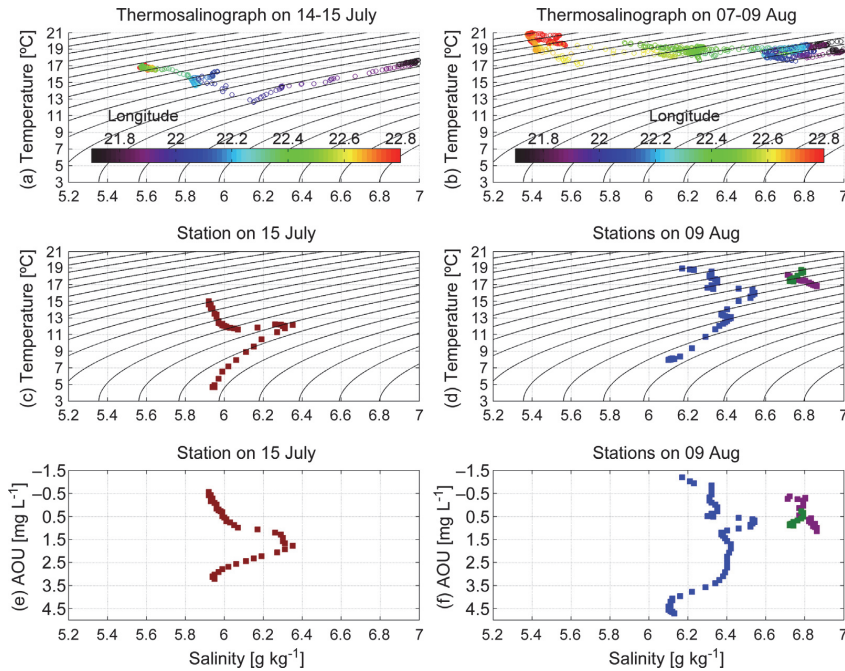
Figure 8 Temperature—salinity (TS) and apparent oxygen utilization (AOU) vs. salinity curves on 14—15 July and 7—9 August. TS-curves along the vessel track acquired by the Salmebox (a, b) and at selected Conductivity-Temperature-Depth (CTD) stations during the two analyzed surveys. Thermosalinograph tracks and locations of CTD stations are shown in Fig. 5 (station dots on the map have same colors as TS dots here). Color bars in the uppermost panel show the longitude.

2.6—2.7°C) would be necessary to reach the density of 5.5 kg m^{-3}. Salinity in the deepest layers of the gulf does not typically exceed 6.5 g kg^{-1} (Raudsepp, 2001). As shown in Fig. 10a, average density anomaly at the 32—38 m depth in
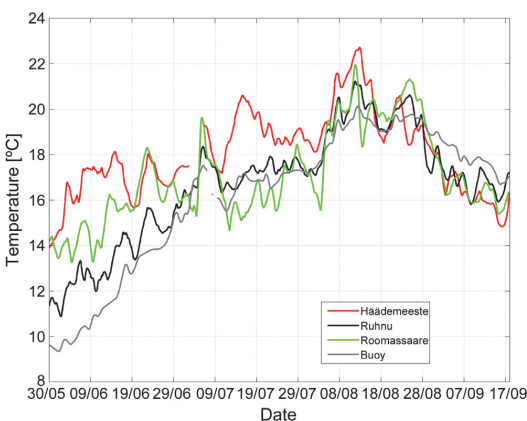

Figure 9 Upper layer water temperature at various locations in the Gulf of Riga. Coastal stations are shown as bright red circles and buoy location as a yellow circle in Fig. 1.

the Gulf of Riga is mostly below 5 kg m^{-3}. Thus, if the Baltic Proper water enters the Gulf of Riga in January—April, it must dive to the near-bottom layer of the gulf and sub-surface maxima as such cannot exist during winters.

As soon as the surface water in the Baltic Proper gets lighter due to the seasonal warming in June, the formation of sub-surface salinity maxima is feasible. In autumn, convection and wind stirring mix the denser deeper layer water and lighter upper layer water thoroughly. As a result, the deep layer temperature increases while salinity and density decrease. Therefore, sub-surface salinity maxima formation in October—November is not feasible anymore, and the dense Baltic Proper water flows to the near-bottom layer of the gulf. The upper layer water in the Baltic Proper tends to be lighter than water in the Gulf of Riga at 32—38 m depth during the timeframe from mid-July to the beginning of September (Fig. 10a). Thus, if the Baltic Proper water flows into the gulf during that time, it likely does not reach the bottom layers of the gulf and rather forms buoyant salt maxima. The temporal variability of the intrusion index, calculated based on the available full-resolution (0.5 m) CTD casts from the years 1993—2014, confirms latter and shows that the saltwater intrusions have been observed from mid-July to mid-September (Fig. 10b).

Comparison of the upper layer density in the Baltic Proper and the Gulf of Riga shows that latter water is always lighter. Even during the autumn-winter cooling period, when the
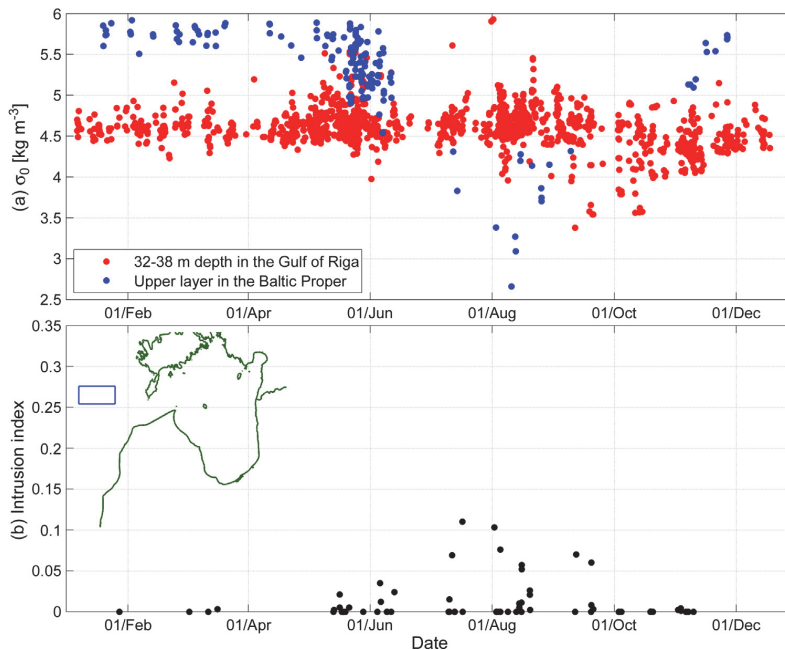
Figure 10   (a) Annual cycle of average potential density anomalies (σ_0; [kg m^{-3}]) in the 0—5 m layer of the Baltic Proper (1979—2014) and at the 32—38 m depth in the Gulf of Riga. (b) Intrusion index in the Gulf of Riga at $\geq$35 m deep stations (1993—2015); only high-resolution profiles were included. The blue box indicates the location of the analyzed profiles from the Baltic Proper. In the Gulf of Riga, all available deep enough measurements were included.

temperature in the Gulf of Riga drops faster than in the Baltic Proper, latter has still heavier upper layer water. This density difference shows that the water coming from the Baltic Proper cannot lie above the Gulf of Riga water.

In conclusion, we suggest that two types of Baltic Proper inflow regimes exist in the gulf. The near-bottom layer salt wedge regime is the only inflow pattern from October to May/June. In summer, from June/July to September, the regime leading to the formation of the buoyant salt intrusion (or saltier water patches) if the inflowing water originates from the upper layer or the regime resulting in the near-bottom salt wedge if the inflowing water originates from the layer beneath the seasonal thermocline can occur.

4. Discussion and conclusions

The year 2015 was special for the Baltic Sea in two senses. First, strong barotropic Major Baltic Inflow (Matthäus et al., 2008) occurred in December 2014 (Mohrholz et al., 2015). Secondly, the winter 2014/2015 was exceptionally mild in the Baltic Sea area, and the Gulf of Riga was almost ice-free in winter (Uotila et al., 2015). However, we do not expect that these two events had a major impact on the thermohaline state of the gulf in summer 2015. It takes years to see the impact of a Major Inflow in the upper layer of the Baltic Proper (Reissmann et al., 2009), which is a salty water source

for the Gulf of Riga. Despite an exceptionally warm winter, the gulf was ventilated down to the bottom layer in the deepest part of the gulf in the Ruhnu Deep (Fig. 11). The mild winter might have an impact on the river discharge (Apsite et al., 2013) and, thereby, to the salinity of the gulf though (Raudsepp, 2001).

High-resolution profiling showed that stratification of the water column during the study period was mainly controlled by the temperature while salinity had only a minor impact. Likewise, the stability of the upper mixed layer was mostly controlled by the temperature. Nevertheless, the vertical stratification in spring is mostly created by the freshwater fluxes, at least in the southern part of the Gulf as suggested by Stipa et al. (1999). It is worth to perform high-resolution profiling in spring, to observe the development of stratification.

Distinctive sub-surface salt maxima were observed in the thermocline in July and August 2015. Due to the lack of data, spatial view on the salt maxima is quite limited. Anyhow, all three available CTD profiles (not shown here) from July to August registered in the Ruhnu Deep revealed the occurrence of salt maxima there. Thus, the maxima can reach the central or southern part of the gulf. It can be expected that the patches of sub-surface salt maxima only occasionally reached or passed the profiling station. In other words, the rapid disappearance of maxima layer observed at the buoy station was not a result of vertical mixing.
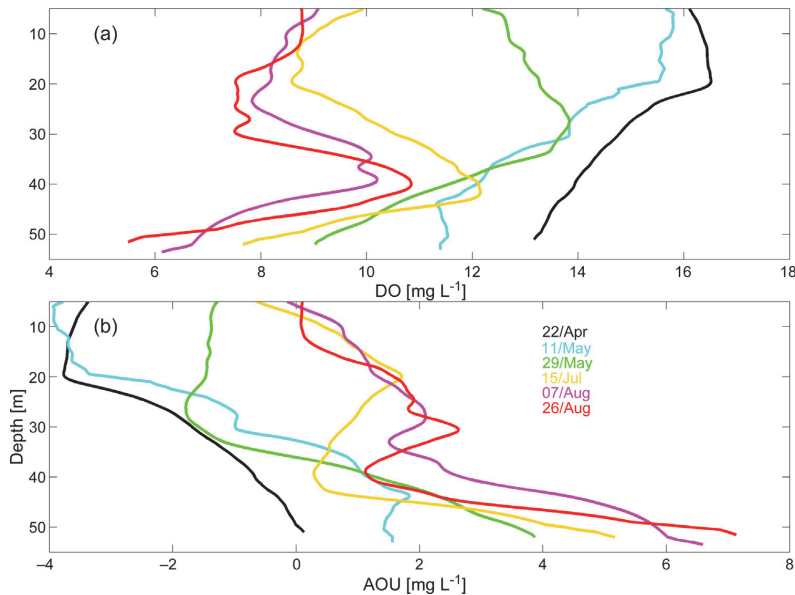
Figure 11 Dissolved oxygen content (a) and apparent oxygen utilization (AOU, b) profiles in the Ruhnu Deep stations in 2015. The location of stations is shown as orange circles in Fig. 1.

Likely, the salt maxima are intrusions of waters of different origin, e.g. as has been observed in the halocline of the Bornholm Basin in the vertical temperature distribution (e.g. Mohrholz et al., 2006). The only evidence of similar salt maxima in the GoR has been reported and measured earlier at two stations in the eastern part of the Irbe Strait by Stipa et al. (1999) on 29 August—1 September 1993. This observational evidence supports our suggestion that the patches of salt maxima enter the gulf via the Irbe Strait.

Episodic current measurements have revealed that the flow regime in the Irbe Strait is two-layered with an inflow in the deeper layer near the southern coast and an outflow along the northern coast (Lilover et al., 1998; Talpsepp, 2005). SW winds evoke upwelling in the Gulf of Riga side of the Irbe Strait along the Saaremaa Island and downwelling along the southern coast of the Irbe Strait. The upwelled Gulf of Riga water is replaced by the waters from the deeper layers of the Irbe Strait, which can be partly the salty and warm downwelling waters. The downwelling water mixes with the ambient Gulf of Riga sub-surface water and the outcome is the sub-surface salt maxima layer. The similar suggestion was drawn by Stipa et al. (1999) as well: downwelling depresses the seasonal pycnocline on the Baltic Proper side of the strait and creates a baroclinic pressure gradient along the strait, which might drive the Baltic Sea surface water, instead of the water below the seasonal pycnocline, into the Gulf of Riga. Stipa et al. (1999) suggested that downwelling occurred in the Baltic Proper along the Latvian coast in 1993 when they registered the salinity maxima in the area. The CTD-stations located closely to each other are to be sampled to check if only the baroclinic pressure gradient is needed (Stipa et al., 1999) for the

maxima layer generation, or also the cross-strait downwelling as we suggested in the present study plays a significant role here.

The salt maxima-favorable coupled upwelling—downwelling situation is evoked by SW winds. Comparison of wind conditions in July—August 2015 with the climatic averages (in July—August 1966—2015) shows that summer 2015 was not a very special year. The favorable SW winds (sector 180—270° was taken into account) occurred 39% of the time in July—August while the climatic occurrence of the wind from the same direction in July—August has been 41%. Likewise, the occurrence of strong SW winds (if only the winds with the speed of >5 m s^{-1} or >10 m s^{-1}) in 2015 was close to climatic average.

The sub-surface salt maxima formation via the Suur Strait cannot be excluded. However Väinameri Archipelago is very shallow (mean depth 5 m) and large area between the open Baltic and GoR. Distance from 20 m isobath in the Baltic Proper through Väinameri to 20 m isobath in the GoR is ca 100 km. Thus, only very strong and long-lasting northerly wind impulse (Otsmann et al., 2001) could cause transport of saltier water via Väinameri Archipelago to the deeper parts of the Gulf of Riga. Temperature—salinity profiles during/after a northerly wind impulse are needed to check the possibility of this pathway.

The existence of fresher sub-surface waters found at the buoy station has also been predicted by numerical modeling (Lips et al., 2016c) in the western part of the gulf as a result of convergence between the low-salinity riverine waters transported from the southern part and waters from the Baltic Proper. The low salinity waters from the southern part of the Gulf of Riga can be transported as far as the buoy

station in the present study and even further to the north due to the prevailing whole-basin anticyclonic gyre with enhanced intensity of currents in the western part of the gulf during the summer period (Lips et al., 2016b).

Buoyant intrusions of inflowing waters are well-known features in the Western Baltic Sea. It is the water that has flown through the Danish Straits to the Baltic and which is not dense (light) enough to reach the bottom layers (to stay in the surface layer) of the Baltic. Buoyant temperature maxima form at the depths of the halocline in the Western Baltic if the baroclinic inflows occur during summer (e.g. Feistel et al., 2004). Note that in the Western Baltic case, the halocline (vertical salinity distribution) stabilizes the water column at the depth range of the temperature maxima while, in the Gulf of Riga case, it is the thermocline (temperature), which compensates the effect of the salinity decrease with the depth. Since the maxima formation is sensible to wind forcing, one might expect that the salt and water balance in the gulf will be impacted by the suggested wind regime changes in the future (Christensen et al., 2015).

Such buoyant inflow regime could be found in many semi-enclosed basins where a sill restricts the water exchange with the open sea with higher salinity/density. Currently, such regime is well known only in fjords (e.g. Belzile et al., 2016). In summer when the seasonal thermocline is present, certain forcing conditions could cause deepening of the upper mixed layer and the inflowing water originating from the surface (or thermocline) layer forms a buoyant salinity maximum in a basin.

The comparison of historical density data in the Gulf of Riga and Baltic Proper showed that the salt water maxima formation is feasible from June to September. Otherwise (in October—May), the Baltic Proper water dives to the near-bottom layer of the gulf and such intrusions do not appear. The seasonality in the water exchange regime was confirmed by an analysis of intrusion index: higher values have occurred from May to September. Thus, likely the maxima layer is a common feature of the gulf in summer and has not been noticed earlier (except at two stations by Stipa et al., 1999 in the Irbe Strait) due to very sparse data, which have been available.

The salinity measurements together with current measurements and high-resolution modeling are needed to estimate the role of sub-surface salinity maxima in the salt balance of the gulf. We checked the outputs of the existing operational models HIROMB-EST (Lagemaa, 2012), which uses the HIROMB-SMHI (Funkquist, 2001) model outcome at the open sea boundary, and the HBM (Berg and Poulsen, 2012). Both models did not capture the salt maxima formation and constantly underestimated salinity, by 0.6 g kg^{-1} on average, at least at the profiling location. It is worth to identify if the incapability of reproducing salt intrusions in the models might lead to a salinity underestimation in the whole gulf.

The AOU vs. salinity curves (Fig. 8) suggested that source water for the salt intrusion had almost saturated oxygen content. This result is not a surprise as the water was originating from the upper layer of the Baltic Proper. The Gulf of Riga has a high production (Seppälä and Balode, 1999) and high oxygen consumption (HELCOM, 2009) due to decomposition of organic material in the near-bottom layer. Lateral advection might be an important source of oxygen for the deep layers in the gulf, especially in summer, when strong stratification impedes vertical mixing. However, if the inflowing saltier water does not reach the deeper bottom layers, the bottom remains isolated from this lateral advection of oxygen. Thus, the oxygen conditions in the near-bottom layer of the gulf strongly depend on the water exchange regime in the Irbe Strait. In summer 2015, the regime resulting in buoyant sub-surface saltwater intrusions prevailed, and the near-bottom layer of the gulf did not receive additional oxygen through the lateral advection. This suggestion can be confirmed by the six dissolved oxygen content and AOU profiles (Fig. 11) acquired from the Ruhnu Deep (Fig. 1) from April to August 2015.

Very high dissolved oxygen values were registered on 22 April. The oversaturation in the upper layer due to the spring bloom was up to 125% or 3.8 mg L^{-1} (shown as AOU negative values in Fig. 11b). Water was saturated in the deep layer indicating that winter convection reached the bottom. Oversaturation remained high in the upper layer, but already 1.4—1.9 mg L^{-1} of oxygen was consumed in the deeper layer by 11 May. A continuous oxygen decline occurred from May to August in the deep layers and by the measurements on 26 August, the oxygen level was 5.5 mg L^{-1} at the temperature and salinity of 3.9°C and 6.0 g kg^{-1}, respectively. The estimated oxygen consumption (based on the AOU) from spring to the end of August had been 7.1 mg L^{-1} in the near-bottom layer. According to the HELCOM (2009), the oxygen decrease might lead to hypoxia in the Gulf of Riga but not every year.

5. Conclusions

- Occasionally very strong salinity maxima were observed in the sub-surface layer.
- The sub-surface salt maxima are intrusions of saline and warm water from the Baltic Proper.
- The potential mechanism of the maxima formation likely is a simultaneous upwelling and downwelling event in the Gulf of Riga side and open sea side of the strait, respectively.
- Due to the buoyant nature of the inflowing water, the near-bottom layer of the Gulf of Riga remains isolated from the lateral flows during summers.
- Latter favors the hypoxia formation in the Gulf of Riga.

Acknowledgments

References

Aigars, J., Poikane, R., Dalsgaard, T., Eglite, E., Jansons, M., 2015. Biogeochemistry of N, P and SI in the Gulf of Riga surface sediments: implications of seasonally changing factors. Cont. Shelf Res. 105, 112—120, http://dx.doi.org/10.1016/j.csr.2015.06.008.

Alenius, P., Tikka, K., Barrera, C., 2014. Gliders for studies of multi-scale variability in the Baltic Sea. In: 6th IEEE/OES Baltic Int. Symp. (BALTIC) — Measuring and Modeling of Multi-Scale Interactions in the Marine Environment, Tallinn, Estonia, 26—29 May 2014, IEEE, 1—6, http://dx.doi.org/10.1109/BALTIC.2014.6887867.

Apsite, E., Rudlapa, I., Latkovska, I., Elferts, D., 2013. Changes in Latvian river discharge regime at the turn of the century. Hydrol. Res. 44 (3), 554—569, http://dx.doi.org/10.2166/nh.2012.007.

Astok, V., Otsmann, M., Suursaar, Ü., 1999. Water exchange as the main physical process in semi-enclosed marine systems: the Gulf of Riga case. Hydrobiologia 393, 11—18, http://dx.doi.org/10.1023/A:1003517110726.

Barda, I., Purina, I., Rimsa, E., Balode, M., 2013. Seasonal dynamics of biomarkers in infaunal clam *Macoma balthica* from the Gulf of Riga (Baltic Sea). J. Mar. Syst., http://dx.doi.org/10.1016/j.jmarsys.2013.05.006.

Belzile, M., Galbraith, P.S., Bourgault, D., 2016. Water renewals in the Saguenay Fjord. J. Geophys. Res. Oceans 121 (1), 638—657, http://dx.doi.org/10.1002/2015JC011085.

Berg, P., Poulsen, J.W., 2012. Implementation details for HBM. DMI Tech. Rep. No. 12-11. DMI, Copenhagen, 147 pp.

Berzinsh, V., 1995. Hydrology. In: Ojaveer, O. (Ed.), Ecosystem of the Gulf of Riga between 1920 and 1990. Estonian Acad. Publ., Tallinn, 7—32.

Christensen, O.-E., Kjellström, E., Zorita, E., 2015. Projected change — atmosphere. In: The BACC II Author Team (Eds.), Second Assessment of Climate Change for the Baltic Sea Basin, Regional Climate Studies. SpringerOpen, Geesthacht, 217—233, http://dx.doi.org/10.1007/978-3-319-16006-1_11.

Eglite, E., Lavrinovic, A., Muller-Karulis, B., Aigars, J., Poikane, R., 2014. Nutrient turnover at the hypoxic boundary: flux measurements and model representation for the bottom water environment of the Gulf of Riga, Baltic Sea. Oceanologia 56 (4), 711—735, http://dx.doi.org/10.5697/oc.56-4.711.

Feistel, R., Nausch, G., Heene, T., Piechura, J., Hagen, E., Sea, B., 2004. Evidence for a warm water inflow into the Baltic Proper in summer 2003. Oceanologia 46 (4), 581—598.

Funkquist, L., 2001. HIROMB, an operational eddy-resolving model for the Baltic Sea. Bull. Maritime Inst. 28 (2), 7—16.

Geyer, W.R., MacCready, P., 2014. The estuarine circulation. Annu. Rev. Fluid Mech. 46, 175—197, http://dx.doi.org/10.1146/annurev-fluid-010313-141302.

HELCOM (Helsinki Commission), 2009. Eutrophication in the Baltic Sea: an integrated thematic assessment of the effects of nutrient enrichment in the Baltic Sea region. In: Baltic Sea Environ. Proc., 115B, Helsinki Commission. 148 pp.

Karstensen, J., Liblik, T., Fischer, J., Bumke, K., Krahmann, G., 2014. Summer upwelling at the Boknis Eck time-series station (1982 to 2012) — a combined glider and wind data analysis. Biogeosciences 11 (13), 3603—3617, http://dx.doi.org/10.5194/bg-11-3603-2014.

Laanearu, J., Lips, U., Lundberg, P., 2000. On the application of hydraulic theory to the deep-water flow through the Irbe Strait. J. Mar. Syst. 25, 323—332.

Lagemaa, P., 2012. Operational forecasting in Estonian marine waters. Tallinn Univ Tech., TUT Press, Tallinn, 130 pp.

Lilover, M.J., Lips, U., Laanearu, J., Liljebladh, B., 1998. Flow regime in the Irbe strait. Aquat. Sci. 60, 253—265.

Lips, U., Kikas, V., Liblik, T., Lips, I., 2016a. Multi-sensor in situ observations to resolve the sub-mesoscale in the stratified Gulf of Finland, Baltic Sea. Ocean Sci. 12 (3), 715—732, http://dx.doi.org/10.5194/os-12-715-2016.

Lips, U., Zhurbas, V., Skudra, M., Väli, G., 2016b. A numerical study of circulation in the Gulf of Riga, Baltic Sea. Part I: Whole-basin gyres and mean currents. Cont. Shelf Res. 112, 1—13, http://dx.doi.org/10.1016/j.csr.2015.11.008.

Lips, U., Zhurbas, V., Skudra, M., Väli, G., 2016c. A numerical study of circulation in the Gulf of Riga, Baltic Sea. Part II: Mesoscale features and freshwater transport pathways. Cont. Shelf Res. 115, 44—52, http://dx.doi.org/10.1016/j.csr.2015.12.018.

Matthäus, W., Nehring, D., Feistel, R., Nausch, G., Mohrholz, V., Lass, H.U., 2008. The inflow of highly saline water into the Baltic Sea. In: Feistel, R., Nausch, G., Wasmund, N. (Eds.), State and Evolution of the Baltic Sea, 1952—2005. Wiley, Hoboken, 265—309.

Mohrholz, V., Dutz, G., Kraus, G., 2006. The impact of exceptional warm summer inflow events on the environmental conditions in the Bornholm Basin. J. Mar. Syst. 60 (3—4), 285—301, http://dx.doi.org/10.1016/j.jmarsys.2005.10.002.

Mohrholz, V., Naumann, M., Nausch, G., Krüger, S., Gräwe, U., 2015. Fresh oxygen for the Baltic Sea—an exceptional saline inflow after a decade of stagnation. J. Mar. Syst. 148, 152—166, http://dx.doi.org/10.1016/j.jmarsys.2015.03.005.

Müller-Karulis, B., Aigars, J., 2011. Modeling the long-term dynamics of nutrients and phytoplankton in the Gulf of Riga. J. Mar. Syst. 87 (3—4), 161—176, http://dx.doi.org/10.1016/j.jmarsys.2011.03.006.

Omstedt, A., Axell, A., 2003. Modeling the variations of salinity and temperature in the large gulfs of the Baltic Sea. Cont. Shelf Res. 23 (3—4), 265—294, http://dx.doi.org/10.1016/S0278-4343(02)00207-8.

Omstedt, A., Elken, J., Lehmann, A., Leppäranta, M., Meier, H.E.M., Myrberg, K., Rutgersson, A., 2014. Progress in physical oceanography of the Baltic Sea during the 2003-2014 period. Prog. Oceanogr. 128, 139—171, http://dx.doi.org/10.1016/j.pocean.2014.08.010.

Otsmann, M., Suursar, Ü., Kullas, T., 2001. The oscillatory nature of the flows in the system of straits and small semienclosed basins of the Baltic Sea. Cont. Shelf Res. 21 (15), 1577—1603, http://dx.doi.org/10.1016/S0278-4343(01)00002-4.

Pitkänen, H., Lehtoranta, J., Räike, A., 2001. Internal nutrient fluxes counteract decreases in external load: the case of the estuarial eastern Gulf of Finland, Baltic Sea. Ambio 30 (4—5), 195—201.

Purokoski, T., Eemeli, A., Nummelin, A., 2013. First long-term deployment of Argo float in Baltic Sea Argo's inaugural operation in shallow, low-salinity water. Sea Technol. 54 (10), 41—44.

Raudsepp, U., 2001. Interannual and seasonal temperature and salinity variations in the Gulf of Riga and corresponding saline water inflow from the Baltic Proper. Hydrol. Res. 32 (2), 135—160.

Reissmann, J.H., Burchard, H., Feistel, R., Hagen, E., Lass, H.-U., Mohrholz, V., Nausch, G., Umlauf, L., Wieczorek, G., 2009. Vertical mixing in the Baltic Sea and consequences for eutrophication—a review. Prog. Oceanogr. 82 (1), 47—80, http://dx.doi.org/10.1016/j.pocean.2007.10.004.

Seinä, A., Palosuo, E., 1996. The classification of the maximum annual extent of ice cover in the Baltic Sea 1720—1995. In: MERI: Report Series of the Finnish Institute of Marine Research, vol. 27. 79—91.

Seppälä, J., Balode, M., 1999. Spatial distribution of phytoplankton in the Gulf of Riga during spring and summer stages. J. Mar. Syst. 23 (1), 51—68, http://dx.doi.org/10.1016/S0924-7963(99)00050-0.

Skudra, M., Lips, U., 2016. Characteristics and inter-annual changes in temperature, salinity and density distribution in the Gulf of Riga. Oceanologia 59 (1),, http://dx.doi.org/10.1016/j.oceano.2016.07.001.

Stipa, T., Tamminen, T., Seppälä, J., 1999. On the creation and maintenance of stratification in the Gulf of Riga. J. Mar. Syst. 23 (1—3), 27—49, http://dx.doi.org/10.1016/S0924-7963(99)00049-4.

Talpsepp, L., 2005. Coherent current oscillations and water exchange in the straits of the Gulf of Riga. Oceanologia 47 (2), 115—127.

Uotila, P., Vihma, T., Haapala, J., 2015. Atmospheric and oceanic conditions and the extremely low Bothnian Bay sea ice extent in 2014/2015. Geophys. Res. Lett. 42 (18), 7740—7749, http://dx.doi.org/10.1002/2015GL064901.

Valle-Levinson, A., 2010. Contemporary issues in Estuarine Physics. Cambridge Univ. Press, Cambridge, 326 pp.

Weiss, R.F., 1970. The solubility of nitrogen, oxygen and argon in water and seawater. Deep-Sea Res. 17 (4), 721—735.

Westerlund, A., Tuomi, L., 2016. Vertical temperature dynamics in the Northern Baltic Sea based on 3D modelling and data from shallow-water Argo floats. J. Mar. Syst. 158, 34—44, http://dx.doi.org/10.1016/j.jmarsys.2016.01.006.

Yurkovskis, A., 2004. Long-term land-based and internal forcing of the nutrient state of the Gulf of Riga (Baltic Sea). J. Mar. Syst. 50 (3—4), 181—197, http://dx.doi.org/10.1016/j.jmarsys.2004.01.004.

ACKNOWLEDGEMENTS

ABSTRACT

The main aim of the thesis was to describe the thermohaline structure and its variability and the main circulation patterns in the Gulf of Riga under different forcing factors. The Gulf of Riga is a sub-basin in the eastern part of the Baltic Sea with a limited water exchange due to the shallow straits that connect it to the open sea and with a substantial amount of freshwater entering the southern part of the gulf.

The present study is based on the long-term CTD data (May-August, 1993-2012) which were analyzed to study inter-annual and long-term changes in temperature, salinity and density in relation to river runoff and atmospheric forcing (e.g. Baltic Sea Index). High-resolution data obtained from the autonomous buoy profiler were used to analyze the vertical thermohaline structure and its features. Finally, the Princeton Ocean Model was applied to the Gulf of Riga in order to study the whole-basin circulation patterns as well as mesoscale features related to the freshwater discharge, currents and thermohaline circulation.

Long-term data revealed that river runoff in spring is a major driving force for the salinity dynamics in the UML and a substantial contributor to enhancing the strength of the stratification later in the year (August). The strongest stratification occurred in years with the highest temperature and river runoff in spring. In comparison to some earlier studies no clear trend was detected regarding the long-term temperature and salinity changes in the gulf.

One of the main scientific questions was related to the whole-basin circulation patterns. The model simulations showed the existence of whole-basin gyres – cyclonic in the cold period of the year and anticyclonic in summer. Observations of lower salinity in the western part of the gulf confirmed the modeled results about the anticyclonic circulation during summer in the Gulf of Riga. Analysis of the mesoscale processes showed the existence of different mesoscale features like eddies and meanders related to the thermohaline circulation and freshwater pathways. The model output showed that Daugava River discharge consists of the freshwater plume with an anticyclonic bulge and the buoyant jet along the eastern coast. A substantial fraction of this freshwater can be involved into the anticyclonic whole-basin circulation in summer seen as reduced salinity along the western coast of the Gulf of Riga.

Autonomous buoy profiler proved the existence of the sub-surface salinity intrusions as well as fresher water patches in the Gulf of Riga. Salinity intrusions, most likely, are formed through simultaneous upwelling and downwelling events along the two opposite coasts of the Irbe Strait. These saline water intrusions can occur only in summer due to the density characteristics between the gulf and the open Baltic Sea. In such case, during summers saline water from the Baltic Proper does not reach the bottom layers of the gulf which might lead to the oxygen depletion in these regions.

Climate change scenarios also confirm the possibility of the increase of oxygen-depleted areas in the Gulf of Riga as they are predicting an increase of water temperature and earlier occurrence of maximum river runoff. In such case, stratification could occur earlier and become stronger in the Gulf of Riga. With the intensification of stratification, the vertical mixing would be reduced even more, and this might lead to the increase of the hypoxic areas in the bottom layers of the Gulf of Riga.

RESÜMEE

Doktoritöö peamiseks eesmärgiks oli Liivi lahe termohaliinse struktuuri ja selle muutlikkuse ning üldtsirkulatsiooni kirjeldamine sõltuvalt erinevatest mõjutavatest teguritest. Liivi laht on Läänemere alam-bassein mere idaosas, mis omab piiratud veevahetust tänu kitsastele ja madalatele väinadele ja suhteliselt suurt magevee juurdevoolu jõgedest lahe lõunaosas.

Doktoritöö aluseks on sondidega kogutud mõõtmiste andmed (mai-august 1993-2012), mille abil on uuritud temperatuuri, soolsuse ja tiheduse jaotuse pikaajalisi muutusi ja aastate-vahelist muutlikkust ning selle sõltuvust jõevee juurdevoolust ja atmosfääri mõjudest (näiteks, Läänemere indeksi muutustest). Kõrge lahutusega mõõtmisi profileeriva poijaamaga on kasutatud vertikaalse termohaliinse struktuuri lühiajalise muutlikkuse ja sellega seotud nähtuste kirjeldamiseks. Numbrilist mudelit POM (*Princeton Ocean Model*) on rakendatud Liivi lahele, et uurida basseini-mastaapi tsirkulatsioonimustreid ja mesomastaapseid nähtusi, mis on seotud magevee juurdevoolu, hoovuste ebastabiilsuse ja termohaliinse tsirkulatsiooniga.

Pikaajaliste andmeridade analüüsi põhjal on leitud, et jõgedest pärinev magevee juurdevool on peamine tegur, mis määrab soolsuse muutlikkuse ülemises segunenud kihis ja mis tugevdab vertikaalset stratifikatsiooni suvel. Tugevaim vertikaalne stratifikatsioon esines aastatel, mil oli kõrge temperatuur ja maksimaalne jõgede vooluhulk kevadel. Erinevalt varasematest uuringutest ei näidanud mõõtmisandmed olulist ühesuunalist soolsuse ja temperatuuri trendi lahes.

Üks peamisi ülesandeid oli seotud lahe üldise tsirkulatsiooni mustritega. Mudelsimulatsioonid näitasid, et basseini-mastaapi tsirkulatsioonimustrites valitseb tsüklonaalne tsirkulatsioon külmal aastaajal ja antitsüklonaalne tsirkulatsioon suvel. Mõõtmiste põhjal määratud madalam soolsus lahe lääneosas suvekuudel toetab mudeliga saadud tulemusi antitsüklonaalse tsirkulatsiooni esinemisest suvel. Mesomastaapsetest protsessidest esinesid pöörised ja hoovuste meandrid, mis olid seotud nii veevahetusega (termohaliinse tsirkulatsiooniga) kui jõevee levikuga lahe pinnakihis. Daugava jõe sissevoolust moodustus jõevee antitsüklonaalne pööris lahe lõunaosas ja piki idarannikut kulgev magedama vee jugahoovus. Oluline osa jõeveest kanti suvel kogu lahte hõlmava antitsüklonaalse tsirkulatsiooniga põhja poole piki lahe läänerannikut.

Veesamba autonoomse profileerijaga kogutud andmetest on tuvastatud pinna-aluste soolsuse maksimumide ja madala soolsusega intrusioonide esinemine Liivi lahes. Soolasema vee intrusioonid moodustusid tõenäoliselt samaaegselt esinevate apvellingu ja daunvellingu tulemusena Irbe väina põhja- ja lõunaosas. Taolised pinna-alused soolase vee intrusioonid saavad tekkida ainult suvekuudel, kui Läänemere avaosa pinnakihi vee tihedus on piisavalt madal. Sellise veevahetuse režiimi puhul ei jõua Läänemere avaosa vesi lahe põhjakihti, mis võib viia hilissuveks hapnikutingimuste halvenemiseni lahe sügavamates piirkondades.

Kliimamuutuste stsenaariumid toetavad samuti Liivi lahe põhjalähedase kihi hapnikutingimuste halvenemise tõenäosust tulevikus, kuna näevad ette vee temperatuuri kasvu ja jõevoolu kevadise maksimumi nihkumist varasemale ajale. Selliste muutuste puhul areneb veesamba stratifikatsioon lahes varem ja on tugevam. Tugevnenud stratifikatsiooni tingimustes on vertikaalne segunemine veel rohkem pärsitud, mis võib viia hüpoksiliste alade laienemisele Liivi lahe põhjas.

ELULOOKIRJELDUS

1. Isikuandmed
   Ees- ja perekonnanimi   Maris Skudra
   Sünniaeg ja -koht   11.02.1986, Riia, Läti
   Kodakondsus   Läti
   E-posti aadress   maris.skudra@msi.ttu.ee

2. Hariduskäik

Õppeasutus (nimetus lõpetamise ajal)	Lõpetamise aeg	Haridus (eriala/kraad)
Läti Ülikool	2011	Keskkonnateadus/MSc
Läti Ülikool	2009	Keskkonnateadus/BSc
Riia Plavnieku Gümnaasium	2005	Keskharidus

3. Keelteoskus (alg-, kesk- või kõrgtase)

Keel	Tase
Läti	Emakeel
Inglise	Kõrgtase
Vene	Kesktase
Saksa, Prantsuse, Eesti	Algtase

4. Teenistuskäik

Töötamise aeg	Tööandja nimetus	Ametikoht
2013 – 2017	TTÜ MSI	Nooremteadur
2007 – …	Veeökoloogia Instituut	Assistent

5. Publikatsioonid Eesti Teadusinfosüsteemi klassifikaatori järgi

   1.1.

- Liblik, Taavi; Skudra, Maris; Lips, Urmas (2016). On the buoyant sub-surface salinity maxima in the Gulf of Riga. Oceanologia, in press, doi: 10.1016/j.oceano.2016.10.001.
- Lips, Urmas; Zhurbas, Victor; Skudra, Maris; Väli, Germo (2016). A numerical study of circulation in the Gulf of Riga, Baltic Sea. Part I: Whole-basin gyres and mean currents. Continental Shelf Research, 112, 1–13, doi: 10.1016/j.csr.2015.11.008.
- Lips, Urmas; Zhurbas, Victor; Skudra, Maris; Väli, Germo (2016). A numerical study of circulation in the Gulf of Riga, Baltic Sea. Part II: Mesoscale features and freshwater transport pathways. Continental Shelf Research, 115(1), 44–52, doi: 10.1016/j.csr.2015.12.018.

- Skudra, Maris; Lips, Urmas (2016). Characteristics and inter-annual changes in temperature, salinity and density distribution in the Gulf of Riga. Oceanologia, in press, doi: 10.1016/j.oceano.2016.07.001.
- Soosaar, Edith; Maljutenko, Ilja; Uiboupin, Rivo; Skudra, Maris; Raudsepp, Urmas (2016). River bulge evolution and dynamics in a non-tidal sea – Daugava River plume in the Gulf of Riga, Baltic Sea. Ocean Science, 12(2), 417-432, doi: 10.5194/os-12-417-2016

3.1.

- Lips, U.; Zhurbas, V.; Skudra, M.; Väli, G. (2014). Features of summertime circulation in the Gulf of Riga (A numerical simulation). *Baltic International Symposium (BALTIC), 2014 IEEE/OES, Tallinn, 27-29 May 2014*. IEEE, 1-9.

CURRICULUM VITAE

1. Personal data
   Name, surname   Maris Skudra
   Date and place of birth   11.02.1986, Riga, Latvia
   E-mail address   maris.skudra@msi.ttu.ee

2. Education

Educational institution	Graduation year	Education (field of study/degree)
University of Latvia	2011	Environmental science/MSc
University of Latvia	2009	Environmental science/BSc
Riga Plavnieku gymnasium	2005	Secondary

3. Language competence/skills (fluent, average, basic skills)

Language	Level
Latvian	Native
English	Fluent
Russian	Average
German, French, Estonian	Basic skills

4. Professional employment

Period	Organization	Position
2013 – 2017	MSI at TUT	Junior researcher
2007 – …	Latvian Institute of Aquatic Ecology	Research assistant

5. Publications according ETIS

   1.1.

- Liblik, Taavi; Skudra, Maris; Lips, Urmas (2016). On the buoyant sub-surface salinity maxima in the Gulf of Riga. Oceanologia, in press, doi: 10.1016/j.oceano.2016.10.001.
- Lips, Urmas; Zhurbas, Victor; Skudra, Maris; Väli, Germo (2016). A numerical study of circulation in the Gulf of Riga, Baltic Sea. Part I: Whole-basin gyres and mean currents. Continental Shelf Research, 112, 1–13, doi: 10.1016/j.csr.2015.11.008.
- Lips, Urmas; Zhurbas, Victor; Skudra, Maris; Väli, Germo (2016). A numerical study of circulation in the Gulf of Riga, Baltic Sea. Part II:

Mesoscale features and freshwater transport pathways. Continental Shelf Research, 115(1), 44–52, doi: 10.1016/j.csr.2015.12.018.

- Skudra, Maris; Lips, Urmas (2016). Characteristics and inter-annual changes in temperature, salinity and density distribution in the Gulf of Riga. Oceanologia, in press, doi: 10.1016/j.oceano.2016.07.001.
- Soosaar, Edith; Maljutenko, Ilja; Uiboupin, Rivo; Skudra, Maris; Raudsepp, Urmas (2016). River bulge evolution and dynamics in a non-tidal sea – Daugava River plume in the Gulf of Riga, Baltic Sea. Ocean Science, 12(2), 417-432, doi: 10.5194/os-12-417-2016

3.1.

- Lips, U.; Zhurbas, V.; Skudra, M.; Väli, G. (2014). Features of summertime circulation in the Gulf of Riga (A numerical simulation). *Baltic International Symposium (BALTIC), 2014 IEEE/OES, Tallinn, 27-29 May 2014*. IEEE, 1-9.

DISSERTATIONS DEFENDED AT
TALLINN UNIVERSITY OF TECHNOLOGY ON
NATURAL AND EXACT SCIENCES

1. **Olav Kongas**. Nonlinear Dynamics in Modeling Cardiac Arrhytmias. 1998.
2. **Kalju Vanatalu**. Optimization of Processes of Microbial Biosynthesis of Isotopically Labeled Biomolecules and Their Complexes. 1999.
3. **Ahto Buldas**. An Algebraic Approach to the Structure of Graphs. 1999.
4. **Monika Drews**. A Metabolic Study of Insect Cells in Batch and Continuous Culture: Application of Chemostat and Turbidostat to the Production of Recombinant Proteins. 1999.
5. **Eola Valdre**. Endothelial-Specific Regulation of Vessel Formation: Role of Receptor Tyrosine Kinases. 2000.
6. **Kalju Lott**. Doping and Defect Thermodynamic Equilibrium in ZnS. 2000.
7. **Reet Koljak**. Novel Fatty Acid Dioxygenases from the Corals *Plexaura homomalla* and *Gersemia fruticosa*. 2001.
8. **Anne Paju**. Asymmetric oxidation of Prochiral and Racemic Ketones by Using Sharpless Catalyst. 2001.
9. **Marko Vendelin**. Cardiac Mechanoenergetics *in silico*. 2001.
10. **Pearu Peterson**. Multi-Soliton Interactions and the Inverse Problem of Wave Crest. 2001.
11. **Anne Menert**. Microcalorimetry of Anaerobic Digestion. 2001.
12. **Toomas Tiivel**. The Role of the Mitochondrial Outer Membrane in *in vivo* Regulation of Respiration in Normal Heart and Skeletal Muscle Cell. 2002.
13. **Olle Hints**. Ordovician Scolecodonts of Estonia and Neighbouring Areas: Taxonomy, Distribution, Palaeoecology, and Application. 2002.
14. **Jaak Nõlvak**. Chitinozoan Biostratigrapy in the Ordovician of Baltoscandia. 2002.
15. **Liivi Kluge**. On Algebraic Structure of Pre-Operad. 2002.
16. **Jaanus Lass**. Biosignal Interpretation: Study of Cardiac Arrhytmias and Electromagnetic Field Effects on Human Nervous System. 2002.
17. **Janek Peterson**. Synthesis, Structural Characterization and Modification of PAMAM Dendrimers. 2002.
18. **Merike Vaher**. Room Temperature Ionic Liquids as Background Electrolyte Additives in Capillary Electrophoresis. 2002.
19. **Valdek Mikli**. Electron Microscopy and Image Analysis Study of Powdered Hardmetal Materials and Optoelectronic Thin Films. 2003.
20. **Mart Viljus**. The Microstructure and Properties of Fine-Grained Cermets. 2003.
21. **Signe Kask**. Identification and Characterization of Dairy-Related *Lactobacillus*. 2003.
22. **Tiiu-Mai Laht**. Influence of Microstructure of the Curd on Enzymatic and Microbiological Processes in Swiss-Type Cheese. 2003.
23. **Anne Kuusksalu**. 2–5A Synthetase in the Marine Sponge *Geodia cydonium*. 2003.
24. **Sergei Bereznev**. Solar Cells Based on Polycristalline Copper-Indium Chalcogenides and Conductive Polymers. 2003.

25. **Kadri Kriis**. Asymmetric Synthesis of C_2-Symmetric Bimorpholines and Their Application as Chiral Ligands in the Transfer Hydrogenation of Aromatic Ketones. 2004.

26. **Jekaterina Reut**. Polypyrrole Coatings on Conducting and Insulating Substracts. 2004.

27. **Sven Nõmm**. Realization and Identification of Discrete-Time Nonlinear Systems. 2004.

28. **Olga Kijatkina**. Deposition of Copper Indium Disulphide Films by Chemical Spray Pyrolysis. 2004.

29. **Gert Tamberg**. On Sampling Operators Defined by Rogosinski, Hann and Blackman Windows. 2004.

30. **Monika Übner**. Interaction of Humic Substances with Metal Cations. 2004.

31. **Kaarel Adamberg**. Growth Characteristics of Non-Starter Lactic Acid Bacteria from Cheese. 2004.

32. **Imre Vallikivi**. Lipase-Catalysed Reactions of Prostaglandins. 2004.

33. **Merike Peld**. Substituted Apatites as Sorbents for Heavy Metals. 2005.

34. **Vitali Syritski**. Study of Synthesis and Redox Switching of Polypyrrole and Poly(3,4-ethylenedioxythiophene) by Using *in-situ* Techniques. 2004.

35. **Lee Põllumaa**. Evaluation of Ecotoxicological Effects Related to Oil Shale Industry. 2004.

36. **Riina Aav**. Synthesis of 9,11-Secosterols Intermediates. 2005.

37. **Andres Braunbrück**. Wave Interaction in Weakly Inhomogeneous Materials. 2005.

38. **Robert Kitt**. Generalised Scale-Invariance in Financial Time Series. 2005.

39. **Juss Pavelson**. Mesoscale Physical Processes and the Related Impact on the Summer Nutrient Fields and Phytoplankton Blooms in the Western Gulf of Finland. 2005.

40. **Olari Ilison**. Solitons and Solitary Waves in Media with Higher Order Dispersive and Nonlinear Effects. 2005.

41. **Maksim Säkki**. Intermittency and Long-Range Structurization of Heart Rate. 2005.

42. **Enli Kiipli**. Modelling Seawater Chemistry of the East Baltic Basin in the Late Ordovician–Early Silurian. 2005.

43. **Igor Golovtsov**. Modification of Conductive Properties and Processability of Polyparaphenylene, Polypyrrole and polyaniline. 2005.

44. **Katrin Laos**. Interaction Between Furcellaran and the Globular Proteins (Bovine Serum Albumin β-Lactoglobulin). 2005.

45. **Arvo Mere**. Structural and Electrical Properties of Spray Deposited Copper Indium Disulphide Films for Solar Cells. 2006.

46. **Sille Ehala**. Development and Application of Various On- and Off-Line Analytical Methods for the Analysis of Bioactive Compounds. 2006.

47. **Maria Kulp**. Capillary Electrophoretic Monitoring of Biochemical Reaction Kinetics. 2006.

48. **Anu Aaspõllu.** Proteinases from *Vipera lebetina* Snake Venom Affecting Hemostasis. 2006.

49. **Lyudmila Chekulayeva**. Photosensitized Inactivation of Tumor Cells by Porphyrins and Chlorins. 2006.

50. **Merle Uudsemaa**. Quantum-Chemical Modeling of Solvated First Row Transition Metal Ions. 2006.

51. **Tagli Pitsi**. Nutrition Situation of Pre-School Children in Estonia from 1995 to 2004. 2006.

52. **Angela Ivask**. Luminescent Recombinant Sensor Bacteria for the Analysis of Bioavailable Heavy Metals. 2006.

53. **Tiina Lõugas**. Study on Physico-Chemical Properties and Some Bioactive Compounds of Sea Buckthorn (*Hippophae rhamnoides* L.). 2006.

54. **Kaja Kasemets**. Effect of Changing Environmental Conditions on the Fermentative Growth of *Saccharomyces cerevisae* S288C: Auxo-accelerostat Study. 2006.

55. **Ildar Nisamedtinov**. Application of ^{13}C and Fluorescence Labeling in Metabolic Studies of *Saccharomyces* spp. 2006.

56. **Alar Leibak**. On Additive Generalisation of Voronoï's Theory of Perfect Forms over Algebraic Number Fields. 2006.

57. **Andri Jagomägi**. Photoluminescence of Chalcopyrite Tellurides. 2006.

58. **Tõnu Martma**. Application of Carbon Isotopes to the Study of the Ordovician and Silurian of the Baltic. 2006.

59. **Marit Kauk**. Chemical Composition of $CuInSe_2$ Monograin Powders for Solar Cell Application. 2006.

60. **Julia Kois**. Electrochemical Deposition of $CuInSe_2$ Thin Films for Photovoltaic Applications. 2006.

61. **Ilona Oja Açik**. Sol-Gel Deposition of Titanium Dioxide Films. 2007.

62. **Tiia Anmann**. Integrated and Organized Cellular Bioenergetic Systems in Heart and Brain. 2007.

63. **Katrin Trummal**. Purification, Characterization and Specificity Studies of Metalloproteinases from *Vipera lebetina* Snake Venom. 2007.

64. **Gennadi Lessin**. Biochemical Definition of Coastal Zone Using Numerical Modeling and Measurement Data. 2007.

65. **Enno Pais**. Inverse problems to determine non-homogeneous degenerate memory kernels in heat flow. 2007.

66. **Maria Borissova**. Capillary Electrophoresis on Alkylimidazolium Salts. 2007.

67. **Karin Valmsen**. Prostaglandin Synthesis in the Coral *Plexaura homomalla*: Control of Prostaglandin Stereochemistry at Carbon 15 by Cyclooxygenases. 2007.

68. **Kristjan Piirimäe**. Long-Term Changes of Nutrient Fluxes in the Drainage Basin of the Gulf of Finland – Application of the PolFlow Model. 2007.

69. **Tatjana Dedova**. Chemical Spray Pyrolysis Deposition of Zinc Sulfide Thin Films and Zinc Oxide Nanostructured Layers. 2007.

70. **Katrin Tomson**. Production of Labelled Recombinant Proteins in Fed-Batch Systems in *Escherichia coli*. 2007.

71. **Cecilia Sarmiento**. Suppressors of RNA Silencing in Plants. 2008.

72. **Vilja Mardla**. Inhibition of Platelet Aggregation with Combination of Antiplatelet Agents. 2008.

73. **Maie Bachmann**. Effect of Modulated Microwave Radiation on Human Resting Electroencephalographic Signal. 2008.

74. **Dan Hüvonen**. Terahertz Spectroscopy of Low-Dimensional Spin Systems. 2008.

75. **Ly Villo**. Stereoselective Chemoenzymatic Synthesis of Deoxy Sugar Esters Involving *Candida antarctica* Lipase B. 2008.

76. **Johan Anton**. Technology of Integrated Photoelasticity for Residual Stress Measurement in Glass Articles of Axisymmetric Shape. 2008.

77. **Olga Volobujeva**. SEM Study of Selenization of Different Thin Metallic Films. 2008.

78. **Artur Jõgi**. Synthesis of 4'-Substituted 2,3'-dideoxynucleoside Analogues. 2008.

79. **Mario Kadastik**. Doubly Charged Higgs Boson Decays and Implications on Neutrino Physics. 2008.

80. **Fernando Pérez-Caballero**. Carbon Aerogels from 5-Methylresorcinol-Formaldehyde Gels. 2008.

81. **Sirje Vaask**. The Comparability, Reproducibility and Validity of Estonian Food Consumption Surveys. 2008.

82. **Anna Menaker**. Electrosynthesized Conducting Polymers, Polypyrrole and Poly(3,4-ethylenedioxythiophene), for Molecular Imprinting. 2009.

83. **Lauri Ilison**. Solitons and Solitary Waves in Hierarchical Korteweg-de Vries Type Systems. 2009.

84. **Kaia Ernits**. Study of In_2S_3 and ZnS Thin Films Deposited by Ultrasonic Spray Pyrolysis and Chemical Deposition. 2009.

85. **Veljo Sinivee**. Portable Spectrometer for Ionizing Radiation "Gammamapper". 2009.

86. **Jüri Virkepu**. On Lagrange Formalism for Lie Theory and Operadic Harmonic Oscillator in Low Dimensions. 2009.

87. **Marko Piirsoo**. Deciphering Molecular Basis of Schwann Cell Development. 2009.

88. **Kati Helmja**. Determination of Phenolic Compounds and Their Antioxidative Capability in Plant Extracts. 2010.

89. **Merike Sõmera**. Sobemoviruses: Genomic Organization, Potential for Recombination and Necessity of P1 in Systemic Infection. 2010.

90. **Kristjan Laes**. Preparation and Impedance Spectroscopy of Hybrid Structures Based on $CuIn_3Se_5$ Photoabsorber. 2010.

91. **Kristin Lippur**. Asymmetric Synthesis of 2,2'-Bimorpholine and its 5,5'-Substituted Derivatives. 2010.

92. **Merike Luman**. Dialysis Dose and Nutrition Assessment by an Optical Method. 2010.

93. **Mihhail Berezovski**. Numerical Simulation of Wave Propagation in Heterogeneous and Microstructured Materials. 2010.

94. **Tamara Aid-Pavlidis**. Structure and Regulation of BDNF Gene. 2010.

95. **Olga Bragina**. The Role of Sonic Hedgehog Pathway in Neuro- and Tumorigenesis. 2010.

96. **Merle Randrüüt**. Wave Propagation in Microstructured Solids: Solitary and Periodic Waves. 2010.

97. **Marju Laars**. Asymmetric Organocatalytic Michael and Aldol Reactions Mediated by Cyclic Amines. 2010.

98. **Maarja Grossberg**. Optical Properties of Multinary Semiconductor Compounds for Photovoltaic Applications. 2010.

99. **Alla Maloverjan**. Vertebrate Homologues of Drosophila Fused Kinase and Their Role in Sonic Hedgehog Signalling Pathway. 2010.

100. **Priit Pruunsild**. Neuronal Activity-Dependent Transcription Factors and Regulation of Human *BDNF* Gene. 2010.

101. **Tatjana Knjazeva**. New Approaches in Capillary Electrophoresis for Separation and Study of Proteins. 2011.

102. **Atanas Katerski**. Chemical Composition of Sprayed Copper Indium Disulfide Films for Nanostructured Solar Cells. 2011.

103. **Kristi Timmo.** Formation of Properties of $CuInSe_2$ and $Cu_2ZnSn(S,Se)_4$ Monograin Powders Synthesized in Molten KI. 2011.

104. **Kert Tamm**. Wave Propagation and Interaction in Mindlin-Type Microstructured Solids: Numerical Simulation. 2011.

105. **Adrian Popp**. Ordovician Proetid Trilobites in Baltoscandia and Germany. 2011.

106. **Ove Pärn**. Sea Ice Deformation Events in the Gulf of Finland and This Impact on Shipping. 2011.

107. **Germo Väli**. Numerical Experiments on Matter Transport in the Baltic Sea. 2011.

108. **Andrus Seiman**. Point-of-Care Analyser Based on Capillary Electrophoresis. 2011.

109. **Olga Katargina**. Tick-Borne Pathogens Circulating in Estonia (Tick-Borne Encephalitis Virus, *Anaplasma phagocytophilum*, *Babesia* Species): Their Prevalence and Genetic Characterization. 2011.

110. **Ingrid Sumeri**. The Study of Probiotic Bacteria in Human Gastrointestinal Tract Simulator. 2011.

111. **Kairit Zovo**. Functional Characterization of Cellular Copper Proteome. 2011.

112. **Natalja Makarytsheva**. Analysis of Organic Species in Sediments and Soil by High Performance Separation Methods. 2011.

113. **Monika Mortimer**. Evaluation of the Biological Effects of Engineered Nanoparticles on Unicellular Pro- and Eukaryotic Organisms. 2011.

114. **Kersti Tepp**. Molecular System Bioenergetics of Cardiac Cells: Quantitative Analysis of Structure-Function Relationship. 2011.

115. **Anna-Liisa Peikolainen**. Organic Aerogels Based on 5-Methylresorcinol. 2011.

116. **Leeli Amon**. Palaeoecological Reconstruction of Late-Glacial Vegetation Dynamics in Eastern Baltic Area: A View Based on Plant Macrofossil Analysis. 2011.

117. **Tanel Peets**. Dispersion Analysis of Wave Motion in Microstructured Solids. 2011.

118. **Liina Kaupmees**. Selenization of Molybdenum as Contact Material in Solar Cells. 2011.

119. **Allan Olspert**. Properties of VPg and Coat Protein of Sobemoviruses. 2011.

120. **Kadri Koppel**. Food Category Appraisal Using Sensory Methods. 2011.

121. **Jelena Gorbatšova**. Development of Methods for CE Analysis of Plant Phenolics and Vitamins. 2011.

122. **Karin Viipsi**. Impact of EDTA and Humic Substances on the Removal of Cd and Zn from Aqueous Solutions by Apatite. 2012.

123. **David Schryer**. Metabolic Flux Analysis of Compartmentalized Systems Using Dynamic Isotopologue Modeling. 2012.

124. **Ardo Illaste**. Analysis of Molecular Movements in Cardiac Myocytes. 2012.

125. **Indrek Reile**. 3-Alkylcyclopentane-1,2-Diones in Asymmetric Oxidation and Alkylation Reactions. 2012.

126. **Tatjana Tamberg**. Some Classes of Finite 2-Groups and Their Endomorphism Semigroups. 2012.

127. **Taavi Liblik**. Variability of Thermohaline Structure in the Gulf of Finland in Summer. 2012.

128. **Priidik Lagemaa**. Operational Forecasting in Estonian Marine Waters. 2012.

129. **Andrei Errapart**. Photoelastic Tomography in Linear and Non-linear Approximation. 2012.

130. **Külliki Krabbi**. Biochemical Diagnosis of Classical Galactosemia and Mucopolysaccharidoses in Estonia. 2012.

131. **Kristel Kaseleht**. Identification of Aroma Compounds in Food using SPME-GC/MS and GC-Olfactometry. 2012.

132. **Kristel Kodar**. Immunoglobulin G Glycosylation Profiling in Patients with Gastric Cancer. 2012.

133. **Kai Rosin**. Solar Radiation and Wind as Agents of the Formation of the Radiation Regime in Water Bodies. 2012.

134. **Ann Tiiman**. Interactions of Alzheimer's Amyloid-Beta Peptides with Zn(II) and Cu(II) Ions. 2012.

135. **Olga Gavrilova**. Application and Elaboration of Accounting Approaches for Sustainable Development. 2012.

136. **Olesja Bondarenko**. Development of Bacterial Biosensors and Human Stem Cell-Based *In Vitro* Assays for the Toxicological Profiling of Synthetic Nanoparticles. 2012.

137. **Katri Muska**. Study of Composition and Thermal Treatments of Quaternary Compounds for Monograin Layer Solar Cells. 2012.

138. **Ranno Nahku**. Validation of Critical Factors for the Quantitative Characterization of Bacterial Physiology in Accelerostat Cultures. 2012.

139. **Petri-Jaan Lahtvee**. Quantitative Omics-level Analysis of Growth Rate Dependent Energy Metabolism in *Lactococcus lactis*. 2012.

140. **Kerti Orumets**. Molecular Mechanisms Controlling Intracellular Glutathione Levels in Baker's Yeast *Saccharomyces cerevisiae* and its Random Mutagenized Glutathione Over-Accumulating Isolate. 2012.

141. **Loreida Timberg**. Spice-Cured Sprats Ripening, Sensory Parameters Development, and Quality Indicators. 2012.

142. **Anna Mihhalevski**. Rye Sourdough Fermentation and Bread Stability. 2012.

143. **Liisa Arike**. Quantitative Proteomics of *Escherichia coli*: From Relative to Absolute Scale. 2012.

144. **Kairi Otto**. Deposition of In_2S_3 Thin Films by Chemical Spray Pyrolysis. 2012.

145. **Mari Sepp**. Functions of the Basic Helix-Loop-Helix Transcription Factor TCF4 in Health and Disease. 2012.

146. **Anna Suhhova**. Detection of the Effect of Weak Stressors on Human Resting Electroencephalographic Signal. 2012.

147. **Aram Kazarjan**. Development and Production of Extruded Food and Feed Products Containing Probiotic Microorganisms. 2012.

148. **Rivo Uiboupin**. Application of Remote Sensing Methods for the Investigation of Spatio-Temporal Variability of Sea Surface Temperature and Chlorophyll Fields in the Gulf of Finland. 2013.

149. **Tiina Kriščiunaite**. A Study of Milk Coagulability. 2013.

150. **Tuuli Levandi**. Comparative Study of Cereal Varieties by Analytical Separation Methods and Chemometrics. 2013.

151. **Natalja Kabanova**. Development of a Microcalorimetric Method for the Study of Fermentation Processes. 2013.

152. **Himani Khanduri**. Magnetic Properties of Functional Oxides. 2013.

153. **Julia Smirnova**. Investigation of Properties and Reaction Mechanisms of Redox-Active Proteins by ESI MS. 2013.

154. **Mervi Sepp**. Estimation of Diffusion Restrictions in Cardiomyocytes Using Kinetic Measurements. 2013.

155. **Kersti Jääger**. Differentiation and Heterogeneity of Mesenchymal Stem Cells. 2013.

156. **Victor Alari**. Multi-Scale Wind Wave Modeling in the Baltic Sea. 2013.

157. **Taavi Päll**. Studies of CD44 Hyaluronan Binding Domain as Novel Angiogenesis Inhibitor. 2013.

158. **Allan Niidu**. Synthesis of Cyclopentane and Tetrahydrofuran Derivatives. 2013.

159. **Julia Geller**. Detection and Genetic Characterization of *Borrelia* Species Circulating in Tick Population in Estonia. 2013.

160. **Irina Stulova**. The Effects of Milk Composition and Treatment on the Growth of Lactic Acid Bacteria. 2013.

161. **Jana Holmar**. Optical Method for Uric Acid Removal Assessment During Dialysis. 2013.

162. **Kerti Ausmees**. Synthesis of Heterobicyclo[3.2.0]heptane Derivatives *via* Multicomponent Cascade Reaction. 2013.

163. **Minna Varikmaa**. Structural and Functional Studies of Mitochondrial Respiration Regulation in Muscle Cells. 2013.

164. **Indrek Koppel**. Transcriptional Mechanisms of BDNF Gene Regulation. 2014.

165. **Kristjan Pilt**. Optical Pulse Wave Signal Analysis for Determination of Early Arterial Ageing in Diabetic Patients. 2014.

166. **Andres Anier**. Estimation of the Complexity of the Electroencephalogram for Brain Monitoring in Intensive Care. 2014.

167. **Toivo Kallaste**. Pyroclastic Sanidine in the Lower Palaeozoic Bentonites – A Tool for Regional Geological Correlations. 2014.

168. **Erki Kärber**. Properties of ZnO-nanorod/In_2S_3/$CuInS_2$ Solar Cell and the Constituent Layers Deposited by Chemical Spray Method. 2014.

169. **Julia Lehner**. Formation of Cu_2ZnSnS_4 and $Cu_2ZnSnSe_4$ by Chalcogenisation of Electrochemically Deposited Precursor Layers. 2014.

170. **Peep Pitk**. Protein- and Lipid-rich Solid Slaughterhouse Waste Anaerobic Co-digestion: Resource Analysis and Process Optimization. 2014.

171. **Kaspar Valgepea**. Absolute Quantitative Multi-omics Characterization of Specific Growth Rate-dependent Metabolism of *Escherichia coli*. 2014.

172. **Artur Noole**. Asymmetric Organocatalytic Synthesis of 3,3'-Disubstituted Oxindoles. 2014.

173. **Robert Tsanev**. Identification and Structure-Functional Characterisation of the Gene Transcriptional Repressor Domain of Human Gli Proteins. 2014.

174. **Dmitri Kartofelev**. Nonlinear Sound Generation Mechanisms in Musical Acoustic. 2014.

175. **Sigrid Hade**. GIS Applications in the Studies of the Palaeozoic Graptolite Argillite and Landscape Change. 2014.

176. **Agne Velthut-Meikas**. Ovarian Follicle as the Environment of Oocyte Maturation: The Role of Granulosa Cells and Follicular Fluid at Pre-Ovulatory Development. 2014.

177. **Kristel Hälvin**. Determination of B-group Vitamins in Food Using an LC-MS Stable Isotope Dilution Assay. 2014.

178. **Mailis Päri**. Characterization of the Oligoadenylate Synthetase Subgroup from Phylum Porifera. 2014.

179. **Jekaterina Kazantseva**. Alternative Splicing of *TAF4*: A Dynamic Switch between Distinct Cell Functions. 2014.

180. **Jaanus Suurväli**. Regulator of G Protein Signalling 16 (RGS16): Functions in Immunity and Genomic Location in an Ancient MHC-Related Evolutionarily Conserved Synteny Group. 2014.

181. **Ene Viiard**. Diversity and Stability of Lactic Acid Bacteria During Rye Sourdough Propagation. 2014.

182. **Kristella Hansen**. Prostaglandin Synthesis in Marine Arthropods and Red Algae. 2014.

183. **Helike Lõhelaid**. Allene Oxide Synthase-lipoxygenase Pathway in Coral Stress Response. 2015.

184. **Normunds Stivrinš**. Postglacial Environmental Conditions, Vegetation Succession and Human Impact in Latvia. 2015.

185. **Mary-Liis Kütt**. Identification and Characterization of Bioactive Peptides with Antimicrobial and Immunoregulating Properties Derived from Bovine Colostrum and Milk. 2015.

186. **Kazbulat Šogenov**. Petrophysical Models of the CO_2 Plume at Prospective Storage Sites in the Baltic Basin. 2015.

187. **Taavi Raadik**. Application of Modulation Spectroscopy Methods in Photovoltaic Materials Research. 2015.

188. **Reio Põder**. Study of Oxygen Vacancy Dynamics in Sc-doped Ceria with NMR Techniques. 2015.

189. **Sven Siir**. Internal Geochemical Stratification of Bentonites (Altered Volcanic Ash Beds) and its Interpretation. 2015.

190. **Kaur Jaanson**. Novel Transgenic Models Based on Bacterial Artificial Chromosomes for Studying BDNF Gene Regulation. 2015.

191. **Niina Karro**. Analysis of ADP Compartmentation in Cardiomyocytes and Its Role in Protection Against Mitochondrial Permeability Transition Pore Opening. 2015.

192. **Piret Laht**. B-plexins Regulate the Maturation of Neurons Through Microtubule Dynamics. 2015.

193. **Sergei Žari**. Organocatalytic Asymmetric Addition to Unsaturated 1,4-Dicarbonyl Compounds. 2015.

194. **Natalja Buhhalko**. Processes Influencing the Spatio-temporal Dynamics of Nutrients and Phytoplankton in Summer in the Gulf of Finland, Baltic Sea. 2015.

195. **Natalia Maticiuc**. Mechanism of Changes in the Properties of Chemically Deposited CdS Thin Films Induced by Thermal Annealing. 2015.

196. **Mario Öeren**. Computational Study of Cyclohexylhemicucurbiturils. 2015.

197. **Mari Kalda**. Mechanoenergetics of a Single Cardiomyocyte. 2015.

198. **Ieva Grudzinska**. Diatom Stratigraphy and Relative Sea Level Changes of the Eastern Baltic Sea over the Holocene. 2015.

199. **Anna Kazantseva**. Alternative Splicing in Health and Disease. 2015.

200. **Jana Kazarjan**. Investigation of Endogenous Antioxidants and Their Synthetic Analogues by Capillary Electrophoresis. 2016.

201. **Maria Safonova**. SnS Thin Films Deposition by Chemical Solution Method and Characterization. 2016.

202. **Jekaterina Mazina**. Detection of Psycho- and Bioactive Drugs in Different Sample Matrices by Fluorescence Spectroscopy and Capillary Electrophoresis. 2016.

203. **Karin Rosenstein**. Genes Regulated by Estrogen and Progesterone in Human Endometrium. 2016.

204. **Aleksei Tretjakov**. A Macromolecular Imprinting Approach to Design Synthetic Receptors for Label-Free Biosensing Applications. 2016.

205. **Mati Danilson**. Temperature Dependent Electrical Properties of Kesterite Monograin Layer Solar Cells. 2016.

206. **Kaspar Kevvai**. Applications of ^{15}N-labeled Yeast Hydrolysates in Metabolic Studies of *Lactococcus lactis* and *Saccharomyces Cerevisiae*. 2016.

207. **Kadri Aller**. Development and Applications of Chemically Defined Media for Lactic Acid Bacteria. 2016.

208. **Gert Preegel**. Cyclopentane-1,2-dione and Cyclopent-2-en-1-one in Asymmetric Organocatalytic Reactions. 2016.

209. **Jekaterina Služenikina**. Applications of Marine Scatterometer Winds and Quality Aspects of their Assimilation into Numerical Weather Prediction Model HIRLAM. 2016.

210. **Erkki Kask**. Study of Kesterite Solar Cell Absorbers by Capacitance Spectroscopy Methods. 2016.

211. **Jürgen Arund**. Major Chromophores and Fluorophores in the Spent Dialysate as Cornerstones for Optical Monitoring of Kidney Replacement Therapy. 2016.

212. **Andrei Šamarin**. Hybrid PET/MR Imaging of Bone Metabolism and Morphology. 2016.

213. **Kairi Kasemets**. Inverse Problems for Parabolic Integro-Differential Equations with Instant and Integral Conditions. 2016.

214. **Edith Soosaar**. An Evolution of Freshwater Bulge in Laboratory Scale Experiments and Natural Conditions. 2016.

215. **Peeter Laas**. Spatiotemporal Niche-Partitioning of Bacterioplankton Community across Environmental Gradients in the Baltic Sea. 2016.

216. **Margus Voolma**. Geochemistry of Organic-Rich Metalliferous Oil Shale/Black Shale of Jordan and Estonia. 2016.

217. **Karin Ojamäe**. The Ecology and Photobiology of Mixotrophic Alveolates in the Baltic Sea. 2016.

218. **Anne Pink**. The Role of CD44 in the Control of Endothelial Cell Proliferation and Angiogenesis. 2016.

219. **Kristiina Kreek**. Metal-Doped Aerogels Based on Resorcinol Derivatives. 2016.

220. **Kaia Kukk**. Expression of Human Prostaglandin H Synthases in the Yeast Pichia pastoris. 2016.

221. **Martin Laasmaa**. Revealing Aspects of Cardiac Function from Fluorescence and Electrophysiological Recordings. 2016.

222. **Eeva-Gerda Kobrin**. Development of Point of Care Applications for Capillary Electrophoresis. 2016.

223. **Villu Kikas**. Physical Processes Controlling the Surface Layer Dynamics in the Stratified Gulf of Finland: An Application of Ferrybox Technology. 2016.